DEVELOPMENT AND EXPERIMENTAL VALIDATION OF SIMULATION OF HYDRONIC SNOW MELTING SYSTEMS FOR BRIDGES

By

XIAOBING LIU

Master of Science

Tongji University

Shanghai, China

1998

Submitted to the Faculty of the
Graduate College of the
Oklahoma State University
in partial fulfillment of
the requirements for
the Degree of
DOCTOR OF PHILOSOPHY
May, 2005

DEVELOPMENT AND EXPERIMENTAL VALIDATION OF SIMULATION OF HYDRONIC SNOW MELTING SYSTEMS FOR BRIDGES

Dissertation Approved:

Dr. Jeffrey D. Spitler

Dissertation Adviser

Dr. Daniel E. Fisher

Dr. Khaled A. Sallam

Dr. James R. Whiteley

Dr. A. Gordon Emslie

Dean of the Graduate College

ACKNOWLEDGEMENTS

I would like to dedicate this dissertation to my father, Changming Liu. He was a great man and he will live in my heart forever.

I would like to thank all my families in China for their endless love and continuous support. To make them happy is one of the major drives of my life.

I would like to thank my dear wife, Dongyi Xiao. It is she who accompanies me day and night, encourages me to continue, and supports me in all kinds of ways. Without her love, I cannot get many things so far. I would also like to thank my daughter, Rena, who is only seven months old now. She brings so much joy in my life. Only seeing her picture on my computer can make me regain strength to keep working.

I would sincerely appreciate my advisor, Dr. Jeffrey D. Spitler, for his continuous support, constructive guidance, excellent leadership, and undying understanding. From him, I learned many things not only in research but also in life.

My sincere appreciation also extends to the members of my doctoral committee: Drs. Daniel E. Fisher, Khaled A. Sallam, and James R. Whiteley for their ideas and suggestions that helped me improve this dissertation.

Dr. Marvin Smith and his team in the Division of Engineering Technology at Oklahoma State University did an excellent job in building the experimental snow melting system and the corresponding data acquisition system. Their measured data during snow events are used extensively throughout this work. Dr. Simon J. Rees, currently senior research fellow in the Institute of Energy and Sustainable Development at De Montfort University, UK, developed a sophisticated model for the snow melting process. Andrew D. Chiasson, currently research associate at the Geo-Heat Center at Oregon Institute of Technology, developed a 2-D finite difference model for the heated pavement. Based on their work, the model for snow melting process on a hydronically-heated slab was developed in this study.

I would also like to thank my colleagues in the Building and Environment Thermal Systems Research Group at Oklahoma State University for their ideas, help, and friendship. Here, I only list a few: Chanvit Chantrasrisalai, Calvin Iu, Weixiu Kong, Zheng Deng, Hui Jin, Xia Xiao, and Ben Alexander.

Support from Federal Highway Administration (FHWA) under grant number DTFH61-99-X-00067 for this work is gratefully acknowledged.

TABLE OF CONTENTS

LIST OF TABLES

LIST OF FIGURES

NOMENCLATURE

c_p	specific heat, Btu/(lb-^{o}F) or J/(kg-^{o}C)
H	height, ft or m
h_c	convection heat transfer coefficient, Btu/(h-ft^2) or W/m^2
h_d	mass transfer coefficient, lb_m/ ft^2-s or kg/ m^2-s
h_{fg}	latent heat of vaporization of water, Btu/lb_m or J/kg
h_{if}	latent heat of fusion of water, Btu/lb_m or J/kg
I	total horizontal incident solar radiation, Btu/(h-ft^2) or W/m^2
k	thermal conductivity, Btu/(h-ft-^{o}F) or W/(m-K)
Le	Lewis number
m''	mass per unit area, lb_m /ft^2 or kg/m^2
$\dot{m}''$	mass flow rate per unit area, lb_m /(s-ft^2) or kg/(s-m^2)
q''	heat flux, Btu/(h-ft^2) or W/m^2
t	temperature, ^{o}F or ^{o}C
T	temperature, K
w	humidity ratio, lb_m/ lb_m or kg/kg dry air

Greek symbols

α	solar absorptance of pavement

ε	emissivity coefficient
θ	time
$d\theta$	time step, s
ρ	density, lb_m/ft^3 or kg/m^3
σ	Stephan-Boltzmann constant

Subscript and superscripts

air	ambient air
evap/cond	evaporation/condensation
cond_slab	conductive heat transfer from slab
cond_snow	conductive heat transfer in dry snow
conv	convective heat transfer
pv	pavement
rad_LW	longwave radiation
solar	solar radiation
snow	dry snow

CHAPTER 1. INTRODUCTION

Driving on an icy/snowy road is very dangerous. Many hazardous accidents are associated with the icy/snowy road conditions. In the road system, bridges are the points where icy conditions most frequently occur. The reason is that bridges are usually elevated and exposed to the ambient air, and therefore tend to cool more quickly than roads, which are warmed by the earth underneath. It can often be observed that icy conditions occur on bridges while the adjacent roads are still clear from ice or snow. The sudden transition from ice-free to icy surface is dangerous for driving. Therefore, preventing ice formation and snow accumulation on bridge surface is of high priority to improve the safety of driving.

Many efforts to prevent bridge decks from icing have been made in the past years and alternatives are still being researched. Among numerous approaches, spreading salt and/or sand or other gritty material on the bridge surface is the most conventional and popular way due to the low cost. However, ice will not be melted by the most popularly used salt (sodium chloride) if the temperature falls below 25˚F (-3.9˚C). In addition, the use of salt results in corrosion of the paint, structural steel, and reinforcing steel embedded in concrete of bridge deck, and eventually will necessitate the rehabilitation or replacement of the bridge deck.

To avoid these problems, using a heating system to melt snow and prevent bridge icing has been proposed in the past decades as an alternative to spreading salt. By eliminating the application of de-icing salt, the heating system can drastically reduce the corrosion of bridges and provide greater safety for pedestrians and vehicles. The available technologies for bridge heating generally fall into three groups: hydronic, heat pipe, and electrical.

Hydronic systems use a circulating pump to circulate heated fluid through pipes embedded near the upper surface of the pavement. Heat is transferred from the heat carrier fluid to the pavement and warms the surface by conduction. A variety of fluids, including brine, oils, and glycol-water, are suitable as heat carrier fluids in hydronic heating systems (ASHRAE 1999). Freeze protection is essential since most systems will be operated intermittently in subfreezing weather. The pipe material in the deck is usually either cross-linked or high-density polyethylene. The pipe can often be arranged so that it can be simply clipped to the steel reinforcement prior to pouring the concrete.

Heat pipe (thermal siphon) systems circulate working fluid spontaneously without using external circulating power. The working fluid is heated to evaporate at the bottom of the heat pipe (evaporator portion), and then the vapor travels upward into the condenser portion of the heat pipes installed in the bridge deck, where it is condensed and transfers heat to the bridge. In order for the condensed liquid to flow by gravity back down into the evaporator to complete the cycle, the condenser portion of the heat pipes must be installed with a slight slope and the inside of each heat pipe must be carefully

cleaned. These rigorous requirements result in a high installation cost, which could offset the benefit from the spontaneous circulation. Various working fluids, including ammonia and Freons, have been tried in heat pipe systems (Nydahl et al. 1984, Hoppe 2000). However, delivering required heat intensity uniformly on the bridge surface is always a challenge to heat pipe systems because the heat transfer rate of the heat pipes, which contain two-phase fluid with varying quality, tends to change significantly along the pipe and during the heating operation.

Electrical systems use electricity as heat source and usually heat the bridge with embedded electric cables. Mineral insulated (MI) cables are most popularly used because of the good thermal conductivity of its electrical insulation. The heat output of the electrical system is determined by the resistance of the installed electric cables and the imposed voltage.

Among the three available heating technologies, hydronic heating is the most promising candidate to be practically applied for the applications of bridge snow melting. This is due to certain inherent advantages compared to other systems. In contrast to the heat pipe systems, the hydronic systems circulate heated fluid with a circulating pump instead of the spontaneous movement of the vapor and the condensed liquid. Therefore, neither carefully constructed slope of the piping nor extremely clean pipes are required. What is more important is that heat flux can be more reliably delivered to the bridge surface by the hydronic systems. Compared to electrical systems, hydronic systems are much more flexible in the selection of heat source. It can be an oil or gas boiler, electrical

heater, or even some waste heat, such as by-product heat of industry process or geothermal return water of district heating system (Boyd 2003). It is also possible that the heat used in the hydronic heating system is extracted from ground or ground water using the ground source heat pump (GSHP). Such systems generally have higher energy efficiency than boilers or electrical heaters.

However, the higher initial costs and the lack of reliable design guidelines are hurdles for implementation of this technology. Reducing the initial cost of the hydronic snow melting system, which is dominated by the installation cost of the hydronic piping and heating equipment, relies on the emergence of low cost but good performance pipe material, cost effective piping installation technology, and inexpensive heat sources. One approach to make the hydronic snow melting system economically feasible is to reduce the life cycle cost of the system by optimizing the design. There are some challenges for achieving an optimal system that can achieve desired snow-melting performance with minimum life cycle costs. First, many design parameters are interacting (i.e. heating capacity, pipe layout, and control strategy) and the various combinations of the design parameters can lead to significant difference in the performance and cost of the system. Therefore, it is necessary to evaluate various combinations of the design parameters in terms of resulting life cycle cost and snow-melting performance. Second, the weather conditions of snowstorms vary widely and typical weather year data is not available for the design of snow melting systems. It is therefore desired to evaluate a design over multi-year period. It is also a necessity for the design of the hydronic snow melting systems that utilize GSHP as heat source since the long-term performance of GSHP is

significantly impacted by the history of the heat extraction/rejection. Computer simulation of the system is the only feasible way to fulfill all these requirements for optimizing the design. The approaches for reducing the system cost, challenges and solution for optimal design of the hydronic snow melting systems are illustrated in Figure 1-1.

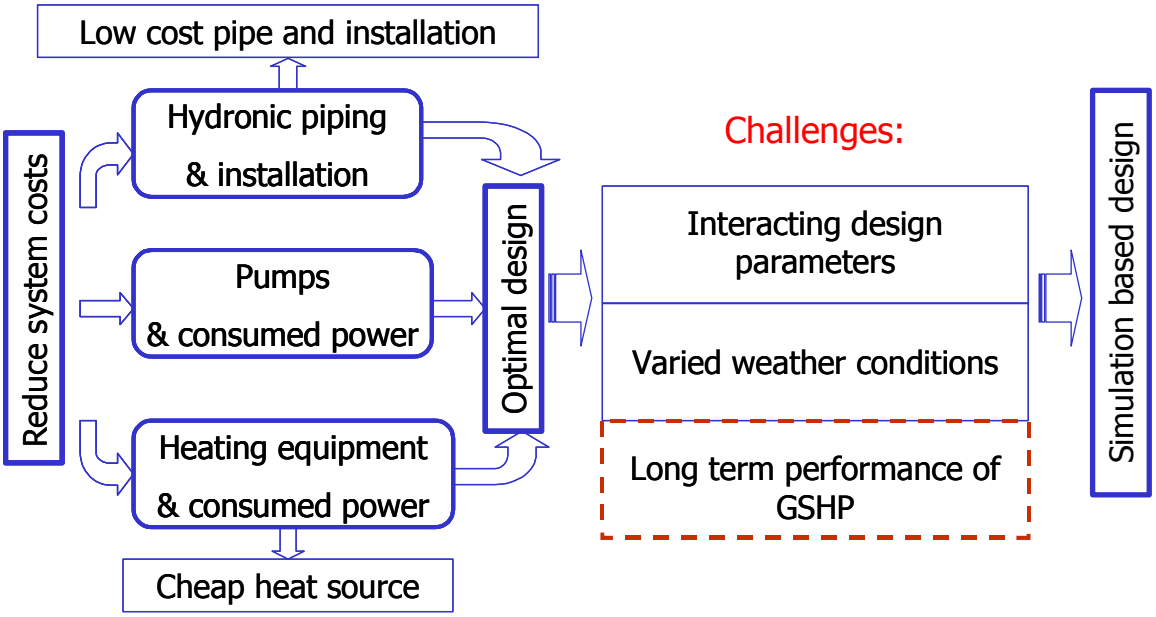

Figure 1-1 The approaches for reducing the system cost, challenges and solution for optimal design of the hydronic snow melting systems.

This thesis will focus on the development of a computer simulation program of the hydronic snow melting system and its application in the design. In Chapter 2, a literature review will be given on design and modeling of hydronic snow melting systems. The objectives of this thesis will be presented in Chapter 3. In Chapter 4, a numerical model of the hydronically-heated slab and the snow melting process taking place on its surface will be described in detail. The experimental validation of the model

will also be covered in this chapter. In Chapter 5, the implementation of a computer simulation program for the hydronic snow melting systems that utilize GSHP as heat source will be described along with the experimental validation of the system simulation results. In Chapter 6, impacts of design and control parameters on the required heating capacity for achieving specified snow melting performance will be investigated through a parametric study based on system simulations. In Chapter 7, a summary of the completed and proposed work will be given.

CHAPTER 2. LITERATURE REVIEW

In this chapter, a review of existing models of hydronic snow melting systems will be presented. In addition, the available approaches for determining the system heating capacity will be reviewed along with some other issues in the design of hydronic bridge snow melting systems.

2.1. Modeling Hydronic Snow Melting Systems

Hydronic heating is one of the three available heating-based snow-melting technologies. Heated fluid is circulated through the hydronic piping embedded in the slab to melt snow and ice on the slab surface. The modeling work described here focuses only on the hydronically-heated slab and the snow melting process occurring on its surface. It involves solving two problems: one is the heat diffusion inside the hydronically-heated slab, and the other is the mass and heat transfer between the slab surface and the environment. Since, from the modeling point of view, there is no difference whether the system is heated with electric cable or hydronic piping, most of the models reviewed can be applied for both cases. The previously developed models can be divided into two categories: steady state and transient.

2.1.1. Steady State Models

Steady state models assume the snow melting system is in steady state and therefore the transients due to intermittent heating operation and varied weather conditions are not accounted for.

2.1.1.1. Chapman (1952) – One-dimensional Steady State Analysis

Chapman, et al. (1952a) described a one-dimensional steady state analysis of heating-based snow melting systems. He stated that the required heat output at a snow-melting surface depended on the sum of five terms, which were heat of fusion, sensible heat for increasing the snow temperature to melting point, heat of vaporization, heat transfer by radiation and convection, and back loss to the ground. Furthermore, any snow accumulation on the surface acted to partially insulate the surface from heat loss and evaporation. To conveniently account for the insulating effect of snow, Chapman (1952b) used the concept of effective or equivalent snow-covered area, which is perfectly insulated and from which no evaporation occurs. He also defined a dimensionless snow free area ratio (A_r), which is the ratio of the effective or equivalent snow free area to the total area of a surface, to correct the surface heat flux due to evaporation and radiative and convective heat transfer. Thus, the required heat output at a snow-melting surface was expressed as:

$$q_o = q_s + q_m + A_r (q_h + q_e) \tag{2-1}$$

where,

q_o : total required heat flux, Btu/hr-ft^2 (W/m^2)

q_s : sensible heat flux to raise the temperature of the snow from that of the air to the melting point Btu/hr-ft^2 (W/m^2)

A_r : equivalent snow-free area ratio, dimensionless

q_m : latent heat flux for melting snow, Btu/hr-ft^2 (W/m^2)

q_h : combined convective and radiative heat flux, Btu/hr-ft^2 (W/m^2)

q_e : heat flux for evaporating water on the surface, Btu/hr-ft^2 (W/m^2)

The sensible heat flux is the flux required to raise the temperature of the snow from that of the air to the melting point. It was expressed as:

$$q_s = \rho s c_i (t_f - t_a) \tag{2-2a}$$

where,

ρ : density of liquid water: 5.2 lb/ ft^2-in or 1.0 kg/ m^2-mm

s : snowfall rate water equivalent, inches/hr (mm/s)

c_i : specific heat of ice: 0.5 Btu/lb-°F or 2100 J/ kg-°C

t_f : water film temperature, °F (°C)

t_a : ambient temperature, °F (°C)

The latent heat flux for melting snow was calculated based on heat of fusion, density of snow and snowfall rate:

$$q_m = \rho s h_{if} \tag{2-2b}$$

where,

h_{if} : heat of fusion: 143.4 Btu/lb or 3.3×10^5 J/ kg

The heat flux for evaporating water on the surface was computed with following equation:

$$q_e = (aV + b)(P_{wv} - P_{av})h_{fg} \quad \text{(2-2c)}$$

where,

a : constant: 0.0201 hr^2/mile-ft or 530.84 s^2/m^2

b : constant: 0.055 hr/ ft or 649.61 s/m

V : wind speed, mph (m/s)

P_{av} : partial pressure of water vapor in ambient air, in. Hg (Pa)

P_{wv} : partial pressure of water vapor in saturated air film on surface, in. Hg (Pa)

h_{fg} : heat of vaporization of water, Btu/lb (J/kg)

The combined convective and radiative heat flux on the snow-free (wet) surface was determined with the following equation:

$$q_h = c(aV + b)(t_f - t_a) \quad \text{(2-2d)}$$

where,

c : constant: 11.4 Btu/hr^2-ft-°F or 0.005476 W/m-s-K

The calculation assumed uniform water film temperature (t_f) over the entire surface. Hence, the effect of heating element location on the pavement surface

temperature, and in turn, the variation of the heat intensity at the surface, were not taken into account in the calculation.

The equivalent snow free area ratio (A_r) in Equation (2-1) actually represents an insulating factor, which is used to account for the insulating effect of dry snow (Chapman and Katunich 1956). Therefore, it is different from the visually observed snow cover degree over the heated surface, which is usually used to evaluate the snow melting performance. For instance, A_r will be equal to one if the surface is covered with slush, which is snow that is fully saturated with water and thus does not have the insulating effect of dry snow. However, a slush-covered surface is slippery and can freeze quickly because the slush contains icy crystals and its temperature is at the freezing point. Therefore, a surface covered with slush should not be considered as snow-free from the point of view of snow melting performance.

2.1.1.2. Schnurr and Rogers (1970) – 2-D Finite Difference Model

Schnurr and Rogers (1970) developed a two-dimensional finite difference model of the hydronically-heated slab. In contrast to previous studies, this model accounted for the variation of surface temperature resulting from the discrete layout of hydronic piping. It assumed steady state heat transfer in the slab, uniform pipe surface temperature, and a snow-free surface. The equations provided by Chapman were used to calculate the surface heat flux. Because of symmetry and small temperature difference between adjacent pipes, the solution domain was reduced to half of the pipe spacing as shown in Figure 2-1. A square grid system with spacing of ¼ of the pipe outside diameter was used in the solution domain. The required pipe surface temperature to maintain specified

surface conditions was determined in an iterative manner. Although this model accounted for the discrete layout of the hydronic piping, it was limited to steady state conditions and snow-free surfaces.

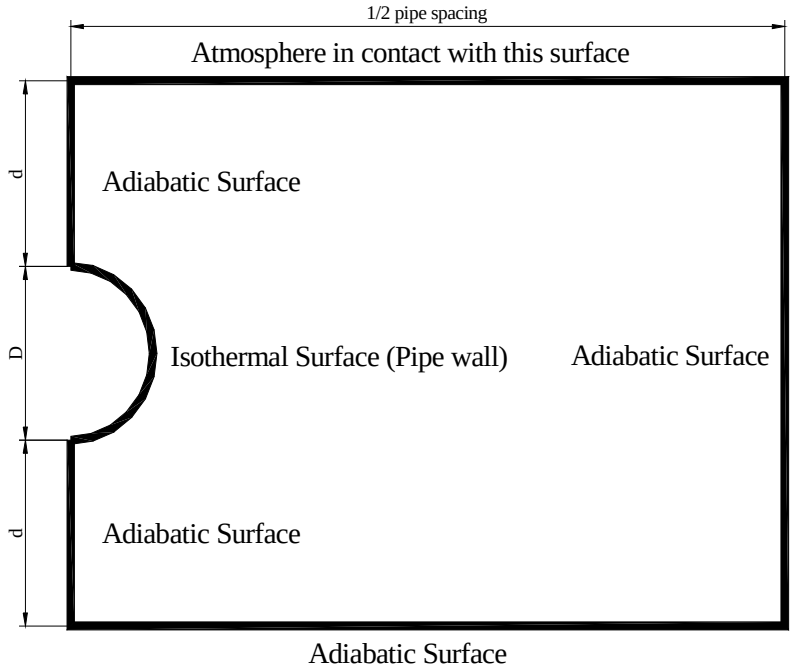

Figure 2-1 The model domain and boundary conditions.

2.1.1.3. Kilkis (1994) – A Simplified Model

Kilkis (1994b) developed a steady state model of the hydronically-heated slab based on his composite fin model (Kilkis, 1992). Different from the model developed by Schnurr and Rogers (1970), this model allowed for various surface conditions (e.g. snow free or partially covered with snow).

In a companion paper, Kilkis (1994a) described the equations used to calculate the surface heat flux. The author calculated the convection loss (q_c) with an empirical

correlation given by Equation (2-3), which was proposed by Williams (1976) for a 16-ft^2 snow-melting surface:

$$q_c = (aV + b)(t_f - t_a) \tag{2-3}$$

where,

a = constant: 0.14 Btu / mile-ft^2-°F or 1.78 J/ m^3-°C

b = constant: 0.39 Btu/ hr-ft^2-°F or 2.21 W/m^2-°C

The author mentioned that since the wind speeds from meteorological data were generally recorded at 33 ft (10 m) and in open fields, they should be adjusted with respect to surrounding terrain and the height of the snow-melting surface.

The radiation loss (q_r) was computed differently according to the sky condition. For cloudy sky, an equation provided by Williams (1976) was used; for clear sky, an empirical equation developed by Williamson (1967) was employed.

The evaporation heat flux was calculated in terms of the convective heat loss by following equations:

$$q_e = \frac{q_c}{R} \cdot \frac{P_{wv} - P_{av}}{t_f - t_a} \tag{2-4}$$

and

$$R = \frac{P_a}{c} \tag{2-5}$$

where,

P_a : atmospheric pressure, in. Hg (Pa)

c : constant: 2990 °F or 1643 °C

Using this model, the maximum/minimum surface temperature of the slab and the required mean fluid temperature could be predicted for given weather conditions, expected snow melting performance (the value of A_r), and the layout of the hydronic piping. However, this model was limited to steady state condition.

2.1.2. Transient Models

Several models that took into account the transient conduction heat transfer in the slab were developed based upon the steady state model of Schnurr and Rogers (1970). Other models developed recently went further to account for the varying surface conditions on a snow-melting surface during a storm event.

2.1.2.1. Leal and Miller (1972) – Two Dimensional Finite Difference Model

Leal and Miller (1972) extended the two-dimensional steady state model developed by Schnurr and Rogers (1970) by accounting for the transient conduction heat transfer in the slab. However, the extended model assumed linear relationship between the heat flux and temperature at the top surface of the slab. Obviously, this assumption is not valid for a surface where melting of snow, a phase change process, is involved.

2.1.2.2. Schnurr and Falk (1973) – Two Dimensional Finite Difference Model

Schnurr and Falk (1973) presented another extension of the model developed by Schnurr and Rogers (1970). In their model, the transient conduction heat transfer in the

slab was solved with a fully explicit finite difference method. This model assumed that snow would be melted instantaneously whenever it fell on the heated slab and therefore no snow accumulated on the slab surface. As a result, it was unable to accurately predict the snow melting process when the slab was covered partially or fully with snow.

2.1.2.3. Chiasson, et al. (2000a) – Two Dimensional Finite Difference Model

Chiasson, et al. (2000a) described a model of a hydronically-heated slab. With respect to solving the heat diffusion problem inside the slab, this model is very similar to that developed by Schnurr and Falk (1973). The only difference is that the grid size was specified by default as the radius of the pipes embedded in the slab.

Compared with other models reviewed previously, this model employed different algorithms to calculate the heat flux on the boundaries of the solution domain. Solar radiation was included in the heat balance at the top surface of the slab and radiative (thermal) heat flux was evaluated separately from the convective heat flux. In the calculation of the radiative (thermal) heat flux, the sky temperature (T_{sky}) was computed from the correlation given by Bliss (1961), which relates T_{sky} only to the dew point and dry bulb temperatures of the ambient air without considering the significant effect of cloud cover. It is thus theoretically only valid for clear sky condition. The convection heat transfer coefficient was taken as the maximum between the free and forced convection coefficient.

Another significant difference between this model and other previously reviewed models is that the boundary condition at the pipe wall was specified as flux-type

(Neumann boundary condition) instead of uniform temperature. The heat flux was that transferred from the heated fluid by convection.

In this model, the heat flux due to melting snow (q''_{melt}) was determined using both heat and mass balance on each top surface cell. Therefore, the mass of snow on the each surface cell can be tracked. The mass of snow that can be melted in a time step was the smaller of the maximum possible snow-melting rate at this time step ($\dot{m}''_{melt\_MAX}$), which is given by Equation (2-6); and that determined from the surface heat balance ($\dot{m}''_{melt\_HB}$), which is given by Equation (2-7).

$$\dot{m}''_{melt\_MAX} = \frac{m''_{ice\_accumulated}}{\Delta\theta} + (\dot{m}''_{snow} + \dot{m}''_{FreezingRain}) \qquad (2\text{-}6)$$

where,

$m''_{ice\_accumulated}$: mass of ice accumulated in the previous simulation time steps, lb/ft^2 (kg/m^2)

$(\dot{m}''_{snow} + \dot{m}''_{FreezingRain})$: sum of the freezing rainfall and snowfall rate in current simulation time step, lb/(s-ft^2) or kg/(s-m^2)

$\Delta\theta$: size of simulation time step, s

$$\dot{m}''_{melt\_HB} = \frac{q''_{solar} + q''_{thermal} + q''_{convection} + q''_{sensible} + q''_{evaporation} + q''_{cond,ice}}{h_{if}} \qquad (2\text{-}7)$$

where,

$q''_{cond,ice}$: conductive heat flux at the slab surface, Btu/hr- ft^2 (W/m^2)

h_{if} : latent heat of fusion of ice, Btu/lb (J/kg)

Although this model kept track of mass of snow on each surface cell, it didn't take into account the insulating effect of snow since snow was treated as equivalent ice in this model.

A "time marching" method was used in this model to calculate the transient conduction heat transfer in the slab. It used the temperature at each node of the solution domain at the end of last time step and the weather conditions during the current time step to evaluate the heat fluxes occurring at the surface during this time step. This method is acceptable if there is no significant change of the temperatures within a single time step. However, it is not applicable for the case when snow is falling on a warm surface because the melting of snow can rapidly drive the surface temperature to near the freezing point. The rapid reduction of surface temperature will significantly reduce the heat loss from the surface and increase the conductive heat flux due to the resulting greater temperature gradient at the slab surface, and it is therefore favorable for melting snow. Neglecting this fact will result in unrealistic simulation results with un-melted snow present on the surface, and at the same time, the surface temperature is several degrees higher than the freezing point.

Like most of the models reviewed before, this model was not validated with experimental data collected under snow melting condition. However, it was validated under the conditions when the slab was dry.

2.1.2.4. Rees, et al. (2002) – Finite Volume Model

Rees et al. (2002) developed a two-dimensional transient model for analyzing the performance of the heating-based snow melting systems that use hydronic piping or electric cable as heating element. The solution domain was similar to that used in the finite difference models reviewed previously (Figure 2-1) except that a block structured boundary fitted grid was used to deal with the complex geometries (round tube in square slab) as shown in Figure 2-2. The two-dimensional and transient conduction heat transfer in the slab was calculated using the finite volume method with a general elliptical multi-block solver (GEMS2D) developed by Rees (2002). Only constant temperature or heat flux can be specified as the boundary condition at the tube surface.

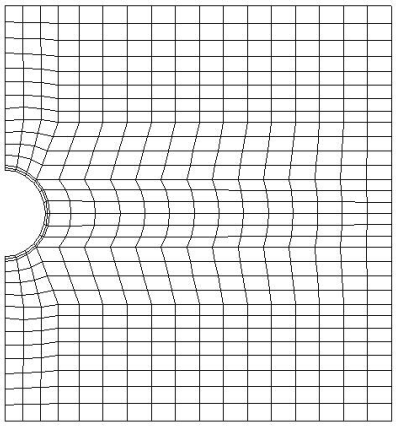

(From Rees, et al. 2002)

Figure 2-2 Grid generated for a slab containing a pipe (4 blocks).

The most important improvement that distinguishes this model from all the other previously developed models is that this model accounted for various surface conditions occurring on a heated surface during a storm event. The following seven surface

conditions were defined and corresponding sub-models of each condition were implemented in a boundary condition model.

Dry: The surface is free of liquid and ice. The surface temperature may be above or below freezing.

Wet: The surface is above freezing and has some liquid retained on it, but no ice.

Dry Snow: The surface has freshly fallen snow on it but no liquid. The snow can be regarded as a porous matrix of ice. The surface temperature is below freezing so that snow is not currently being melted.

Slush: The surface contains ice in the form of snow crystals that are fully saturated with water. Water penetrates the ice to the upper surface. The surface temperature is at freezing point.

Snow and Slush: The surface contains snow that is partly melted. The lower part of the snow is saturated with water and the upper is as dry snow. This is the general melting snow condition and the surface temperature is at freezing point.

Solid Ice: The ice on the surface is in solid form rather than porous like snow – i.e. as liquid that has frozen solid. The surface temperature must be below freezing.

Solid Ice and water: The surface consists of solid ice and water. This can occur when rain falls on solid ice or when the solid ice is being melted. Melting can be from below or above. The surface temperature is at freezing.

Among the seven conditions, the **Snow and Slush** is the most complicated case. To model snow melting process in such case, three nodes were employed as indicated in

Figure 2-3: one at the top surface of the snow layer, one in the center of the snow layer and one at the saturated (slush) layer. Since the snow layer was treated as quasi one-dimensional, no lateral heat transfer effects within the snow layer are considered. The convection and radiation transfer was limited to the top node. Conduction heat transfer can go from the slab surface and through the slush and snow layer. The evaporation was neglected in this case because of the dry snow layer. Solar radiation was ignored in the model.

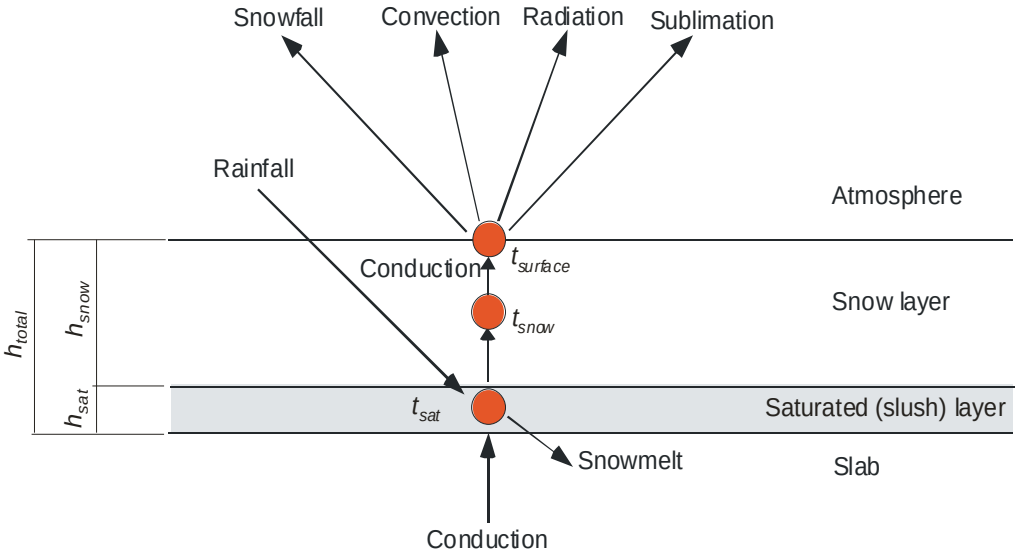

(From Rees, et al. 2002)

Figure 2-3 Schematic representation of heat transfer in the two nodes snowmelt model.

The sub-model of the **Snow and Slush** condition was formed by five primary equations – a mass balance for the solid ice, a mass balance for liquid water, and a heat balance on each of the three nodes. Here, the "ice" refers to the ice crystals contained in the porous structure of snow.

(1) Mass balance on the ice

The rate of change of the mass of ice crystals is determined by the mass of snowfall and the melted snow:

$$\frac{dm_{ice}}{d\theta} = \dot{m}''_{snowfall} - \dot{m}''_{melt} \tag{2-8}$$

where,

m_{ice} : mass of ice crystals per unit area, lbm/ft^2 or kg/m^2

θ : time, hr or s

$\dot{m}''_{snowfall}$: snowfall rate in mass per unit area, lbm/(hr-ft^2) or kg/(s-m^2)

$\dot{m}''_{melt}$: snowmelt rate in mass per unit area, lbm/(hr-ft^2) or kg/(s-m^2)

(2) Mass balance on the liquid water

The mass of liquid water is determined by the mass of melted snow, rainfall and the water drained off the surface:

$$\frac{dm_l}{d\theta} = \dot{m}''_{melt} + \dot{m}''_{rain} - \dot{m}''_{runoff} \tag{2-9}$$

where,

m_l : mass of liquid water per unit area in the slush layer, lbm/ft^2 or kg/m^2

$\dot{m}''_{rain}$: rainfall rate in mass per unit area, lbm/(hr-ft^2) or kg/(s-m^2)

$\dot{m}''_{runoff}$: rate of runoff in mass per unit area, lbm/(hr-ft^2) or kg/(s-m^2)

A simple heuristic approach was taken to estimate the amount of runoff. In order to approximate the effect of water being retained in the snow due to capillary action, the

runoff was limited to 10% of the melt rate until the saturated layer is 2 inch (5 cm) thick. The runoff rate was increased to the melt rate after this point in order to prevent more water being retained.

(3) Energy balance on the surface of snow layer

The sublimation and evaporation heat fluxes on the dry snow surface were neglected. The snow surface temperature was calculated from a heat balance on the surface node:

$$q''_{convection} + q''_{radiation} = k_{snow} \frac{(t_{snow} - t_{surface,snow})}{0.5 h_{snow}} \tag{2-10}$$

where,

$q''_{convection}$: convective heat flux on the surface of snow layer, Btu/(hr-ft^2), or W/(m^2)

$q''_{radiation}$: radiative heat flux on the surface of snow layer, Btu/(hr-ft^2), or W/(m^2)

k_{snow} : thermal conductivity of the snow, Btu/(hr-ft-F), or W/(m-K)

$t_{surface,snow}$: temperature at the upper surface of snow layer, °F or °C

t_{snow} : temperature at the center of snow layer, °F or °C

h_{snow} : thickness of snow layer, ft or m

(4) Energy balance in the center of snow layer

The derivative of the middle node temperature (t_{snow}) with respect to time is determined by the following equation:

$$m_{snow}c_p \frac{dt_{snow}}{d\theta} = k_{snow} \frac{(t_{slush} - t_{snow})}{0.5h_{snow}} - q''_{snowfall} - k_{snow} \frac{(t_{snow} - t_{surface,snow})}{0.5h_{snow}} \quad (2\text{-}11)$$

where,

m_{snow} : mass of dry snow per unit area in the slush layer, lbm/ft^2 or kg/m^2

t_{slush} : temperature of the slush layer, °F or °C

$q''_{snowfall}$: heat flux to raise the temperature of snowfall from that of ambient to that at the center of snow layer, Btu/(hr-ft^2), or W/(m^2)

(5) Energy balance in slush layer

The energy balance at the slush node presumes that the liquid/ice mixture was in thermodynamic equilibrium and therefore the temperature was uniform at melting point t_{melt}. Then, the energy balance was given by:

$$\dot{m}''_{melt}h_{if} = q''_{conduction,slab} + q''_{rainfall} - k_{snow} \frac{(t_{slush} - t_{snow})}{0.5h_{snow}} \quad (2\text{-}12)$$

where,

h_{if} : fusion heat of snow, Btu/(hr-ft-F), or W/(m-K).

$q''_{conduction,slab}$: conduction heat flux from the slab to the slush layer, Btu/(hr-ft^2), or W/(m^2). It was calculated with the finite volume solver.

$q''_{rainfall}$: heat flux to raise the temperature of rainfall from that of ambient to that of slush layer, Btu/(hr-ft^2), or W/(m^2).

The thickness of the snow layer (h_{snow}) was found by subtracting the height of the slush layer (h_{sat}) from the total height of the snow and slush layers (h_{total}, see Figure 2-3). h_{total} and h_{sat} were determined with following equations, respectively:

$$h_{total} = \frac{m_{ice}}{\rho_{ice}(1 - n_{eff})} \tag{2-13}$$

where,

h_{total} : total thickness of the snow and saturated layers, ft or m

n_{eff} : effective porosity of the ice matrix for both layers, dimensionless

ρ_{ice} : density of ice, lbm/ft^3 or kg/m^3

$$h_{sat} = \frac{m_l}{\rho_l n_{eff}} \tag{2-14}$$

where,

ρ_l : density of liquid water, lbm/ft^3 or kg/m^3

The mass of the dry snow (m_{snow}) was then calculated using:

$$m_{snow} = \rho_{ice} h_{snow}(1 - n_{eff}) \tag{2-15}$$

The correlations and algorithms used in this model for calculating the convection, radiation, and evaporation heat transfer are the same as those in Ramsey, et al. (1999).

Solving all of the equations in a sub-model in the boundary condition model generally involves nested iterations, which is already very time consuming. However, there was another iteration loop coupling the boundary condition model to the finite volume solver to find the converged solution of the heat flux (temperature gradient) and the slab surface temperature. This iteration process required quite a lot of computational effort because of the highly nonlinear relationship between the heat flux and temperature at the slab surface during the snow melting process. Furthermore, an additional iteration loop may be necessary to determine the average temperature of the heat carrier fluid if the inlet fluid temperature is given as an input to this model, which is the case in the simulation of the whole snow melting system. This iterative nature and complex computation of this model make it too computationally intensive to be practical as a component model in multi-year system simulations of a snow melting system.

On the other hand, it is questionable whether the computational efforts required by this model pay off in the sense of increased accuracy. First, because of the very low thermal conductivity of dry snow (0.03 W/m-K, or 0.02 Btu/hr-ft-F for the freshly fallen snow), the surface heat loss is generally small and not very sensitive to the thickness and temperature of the dry snow layer. Second, the heuristic approach for determining the runoff rate ($\dot{m}''_{runoff}$) and the assumption of the effective porosity (n_{eff}) used in the model leads to some uncertainties in distinguishing the snow and slush layer, which is much

more critical in determining the surface heat flux since a slush layer does not have the insulating effect of a snow layer. Third, the permeation of snowmelt into the slab, which is usually constructed with concrete, was not considered in the model, but it certainly affects the mass balance of liquid water on the slab surface and the thermal conductivity of the slab. It is therefore highly desirable to further understand the physics of the snow melting process on the slab and investigate numerical methods for modeling the heat and mass transfer in order to achieve a more computationally efficient model while retaining reasonable accuracy for the purpose of the system simulations.

2.1.3. Summary

The previously developed models can be divided into two categories: steady state and transient. The steady state models (Schnurr and Rogers 1970; Kilkis 1994) cannot take into account the transient effects due to intermittent heating operation and varied weather conditions. The transient models developed in 1970's (Leal and Miller 1972; Schnurr and Falk 1973) did not consider the accumulation of un-melted snow on the surface, and therefore, they were not able to predict the surface conditions in the cases that the snow could not be instantaneously melted. Chiasson (1999) presented a two dimensional transient model with consideration of the accumulation of the un-melted snow, but the coupling between the surface temperature and heat flux during the snow melting process was not properly handled and the insulating effect of the snow was not properly accounted for. The model developed by Rees et al. (2002) kept track of the temperature and mass of snow, ice, and water on each surface cell, and hence, was able to

predict the surface condition during entire snow event for a given heat supply. However, due to the considerable computation time resulting from the iterative nature of the algorithm and complexity of the calculations, this model is not fast enough to be used in simulations over a multi-year period (e.g. life time of the project) in an acceptable time, which is desired for the simulation-based design. Therefore, it is highly desirable to develop a more computationally efficient model while retaining reasonable accuracy for the purpose of the system simulations.

2.2. Design of Snow Melting Systems

To design a snow melting system, the most important task is to properly determine the heating capacity of the system. Sufficient heat must be provided to effectively melt snow, but at the same time, the system should not be oversized to unnecessarily increase the cost of an already expensive installation. Existing algorithms for determining the heating capacity of the snow melting system will be reviewed in this section. Since expected snow melting performance (design objective) will significantly affect the heating requirement, a review of the design objectives will be given at first.

2.2.1. Design Objective

The objective of a snow melting system design is to achieve a certain specified snow melting performance. The snow melting performance can be classified according to the permissible amount of snow accumulation and how rapidly it can be melted. The

snow free area ratio (A_r), which is defined as the ratio of snow free area of a surface to its total area (ASHRAE HOA 1999), is one measure of the snow melting performance. A fractional snow free area ratio indicates the presences of 'stripes' of snow on the surface, as shown in Figure 2-4. Therefore, A_r is widely used to evaluate the snow-melting performance (Chapman 1956; Kilkis 1994; ASHRAE HOA 1999).

Figure 2-4 Picture showing 'stripes' of snow on a heated bridge surface.

Chapman (1956) presented definitions of snow-melting performance class as following:

- **Class 1 (residential):** During the snowfall, it is permitted that the entire surface is covered with snow **(A_r =0)**. After the snowfall, the system is expected to melt the accumulated snow.
- **Class 2 (commercial):** During the snowfall, 50% of the surface is allowed to be covered with snow **(A_r =0.5)**.
- **Class 3 (industrial):** During the snowfall, the entire surface is kept free from snow accumulation **(A_r =1)**.

In the terminology of the Heated Bridge Technology (HBT) report (Minsk 1999), there are only two design objectives: "Snowfree" and "Anti-ice". The objective of a

"Snowfree" system is to keep the surface clear of snow and ice (bare pavement) under all precipitation conditions. On the other hand, the objective of an "Anti-ice" system is to prevent bonding of ice and compacted snow to the deck during and after snowstorm. A snowplow is usually required for this kind of bridge heating system to clear the snow on the bridge. The Heated Bridge Technology (HBT) report does not mentioned whether such an "Anti-ice" system should be able to prevent preferential icing on the bridge surface. In one project of the HBT program in Texas, the heating system was used to maintain a similar condition between the bridge and the adjacent roadway (Minsk, 1999), which implies prevention of preferential icing on the bridge surface.

In Japan, the design objective of the bridge heating system was considered by some researchers as being able to melt the snow on bridge earlier than the snow on the normal road (Yoshitake, et al. 1997). For systems with this (low) level of design objective, the heat stored in the ground is usually directly used as heat source. The heat is provided either from the ground water or by ground loop heat exchanger.

The determination of the design objective should take into account the climate of a specified site. Minsk (1999) stated that the application of heated bridge technologies could be economically and technically feasible only in a temperate region. Actually, all the bridges in the HBT program are in temperate climates and the design objectives are all snow-free, except the bridge in Texas. A researcher in Canada reported that snow-melting systems operated in cold climates were seldom designed to maintain completely

bare pavements during snowstorms due to the large amounts of heat required (Williams, 1976).

No literature was found concerning the relationship between bridge surface conditions and transportation safety. However, Chapman (1956) stated that the friction coefficient for rubber tires on highway with new concrete was taken as 0.9 when the concrete was wet, and 0.2 for packed snow. The author mentioned that a minimum friction coefficient of 0.4 was required for safe driving. Williams (1976) also stated that a heated area with average snow coverage of 50% appeared to be reasonable for most traffic conditions. A study published recently by the Society of Accident Re-constructionists (SOAR) provided the friction values of car tires involved in collisions on various snow/ice covered surface conditions (Hunter 1998). Table 2-1 is a summary of the friction values of car tires on road with various surface conditions. One obvious conclusion can be drawn from the table is that a road surface covered with “heavy frost” or “black ice” could be as slippery as when it is covered with snow. As a result, a bridge snow melting system should also be able to prevent the formation of “heavy frost” or “black ice” on the surface in order to maintain safe driving conditions.

TABLE 2-1 Friction Values of Car Tires on Road with Various Surface Conditions

Classification	Description	Friction Available
Dry Asphalt	This value is commonly used as the reference value for rubber tires on dry asphalt. Concrete is typically lower.	0.68 to 0.85 Average value of 0.72
Partial Frost	Light or partial coating of frost on the road surface. Visible to the driver as intermittent frosting appearance.	Partial Frost had a resistance level similar to the lower range of wet asphalt. Average value of 0.63
Frost	General white coating covering entire lane. Visible to the driver and completely recognizable as frost.	Frost was .10 less than Partial Frost. Average value of 0.53.
Heavy Frost	Almost ice conditions. Heavy white coating and very visible to the driver	Heavy Frost had a value close to the higher ranges of ice. Average of a 0.39.
Tracked Snow	Snow compacted by vehicles.	The test results varied in range. Average was a 0.35
Untracked Snow	Snow not compacted by prior vehicles.	The individual readings were similar to Tracked Snow. Average of 0.35
Snow & Ice	Generally known by motorists as compact snow and ice, or "hard pack".	Snow and Ice was nearly identical to the frictional resistance found for Black Ice, 0.25 to a high of 0.41 Average of 0.32
Black Ice	Icy layer generally covering asphalt, difficult to see by the average driver. Often found on overpasses and elevated structures.	The ranges for Black Ice varied from a low of 0.25 to a high of 0.41 Average of 0.32
Sunny Ice	Ice that has been exposed to the heating rays of the sun. A water layer was not generally observed.	Sunny Ice yielded low readings, Average of 0.24.
Wet Ice	Ice covered with a layer of water. Generally seen when the temperatures reach 32 to 33 degrees, or near the melting point.	Wet Ice, similar to sunny ice, Average of 0.24.
Glare Ice	Ice that was the smoothest surface observed. Similar to wet ice except the water layer was not observed. looks like glass.	The lowest value measured was Glare Ice. Average of 0.19.

(Obtained from http://www.enteract.com/~icebike/Articles/howslippery.htm)

2.2.2. Determining Heating Capacity of Snow Melting Systems

As previously reviewed, Chapman (1952a; 1952b) proposed a steady state energy balance equation [Equation (2-1)] to determine the required heat for snow melting. He also provided a set of equations [Equation (2-2a) to (2-2d)] to evaluate each heat flux term in the energy balance equation. Chapman asserted that the design energy output should be based on a frequency distribution of the heat requirements. He stressed that it was not correct to separately select the design condition for air temperature, snowfall rate, wind speed and atmospheric vapor pressure. The suggested procedure was to calculate the actual load hourly and make a frequency distribution, and then set the design capacity by selecting a capacity that will be adequate for a given number of hours of snowfall annually, which is usually stated as percent of annual snowfall.

Williams (1973) developed formulas for estimating heating requirements from snow melting tests carried out during three winters at Ottawa, Canada. By comparing the heating requirements during snowfall and after snowfall, a conclusion was drawn that more heat was required to maintain an ice-free surface immediately after a snowstorm than that required during the storm. He inferred that this would be true for snow-melting systems operating in cold climates. Hence, the heating requirements could be estimated by calculating the rate of surface heat loss from bare wet pavements by using weather data obtained from representative or design storms. In the same article, Williams reported that adjustment of the convective heat transfer coefficient was necessary for the size of the heated area, the exposure to the wind, and the height at which wind speeds were

measured. He also mentioned that cloud conditions needed to be taken into account when calculating the longwave radiation heat transfer.

Kilkis (1994a) proposed an algorithm that to determine the design heat requirement without the elaborate frequency analysis described by Chapman (1952b). He defined a "Coincident Air Temperature" with Equation (2-16), which corresponded to the maximum snow-melting load intensity at the design rate of snowfall for a given performance class and location.

$$t_c = t_b + \frac{(t_{ref} - t_b)}{(0.1 + 1.2 \cdot C_{performance})} \tag{2-16}$$

where,

t_c : snowfall coincident design air temperature, °F (°C)

t_b : design outdoor temperature, °F (°C)

t_{ref} : reference temperature, 33°F or 0.56°C

$C_{performance}$: snow-melting performance class, dimensionless; ($C_{performance}$ = 1,2,3 corresponding to the snow-melting performance class described before)

An expression was developed as following to determine the design rate of snowfall (*s'*):

$$s' = (\frac{SF}{24} \cdot C) \cdot \frac{\rho_s}{\rho_w} \tag{2-17}$$

where,

s' : design rate of snowfall equivalent water, in. (H_2O)/hr or mm(H_2O)/hr

SF : maximum amount of snowfall recorded at a given location in 24 hours, in. /24hr or mm/24hr

ρ_s : density of snow, lb/ft^3 (kg/m^3)

ρ_w : density of water, 62.4 lb/ft^3 or 1000 kg/m^3

The heating requirements in the three phases (before snow, during snow, and after snow) of the snow melting operation were calculated respectively with a simple steady state model developed by the author (Kilkis, 1994b), which has been reviewed in the first section of this chapter. Finally, the design heating capacity was determined by the maximum of the three heating requirements.

ASHAE (a predecessor organization to ASHRAE) first issued an entire chapter on snow melting in the 1959 edition of the *ASHAE Guide*. After that, further research was not undertaken until 1995 when ASHRAE Research Project 926 was authorized, which aimed to update the guidelines for snow melting systems.

A conclusion stated in the final report of ASHRAE RP-926 (Ramsey, et al. 1999) is that there was no acceptable simplified approach identified to determine the heating requirement of snow melting systems for locations with limited meteorological data. As a result, the heating requirement calculation in the 1999 *ASHRAE Handbook—HVAC Applications* still followed the frequency analysis method described by Chapman. The weather data were taken for the years 1982 through 1993 of 46 cities in US.

The algorithm described in the handbook was based on the steady state energy balance equation provided by Chapman [Equation (2-1)]. However, the equations for calculating each heat flux term have been updated. The convective heat transfer rate was evaluated using the correlations described by Incropera and Dewitt (1996) for the turbulent convection heat transfer coefficient of a horizontal surface. The radiation loss was evaluated using an effective sky temperature (Ramsey, et al. 1999) that was based on the dry-bulb air temperature, relative humidity, and sky cover fraction. The analogy between mass and heat transfer was used to determine the water vapor mass transfer coefficient. A detailed discussion of the analogy is given in Chapter 5 of the 1997 *ASHRAE Handbook—Fundamentals*. The convection and evaporation losses were functions of the wind speed and the characteristic dimension of the slab. Detailed description of these equations was given in the same *ASHRAE Handbook—HVAC Applications* and Ramsey, et al. (1999).

2.2.3. Summary

The existing approaches for determining the heating capacity of a snow melting system are based on the one-dimensional steady state analysis proposed by Chapman (1952a and 1952b). The differences among these approaches lie in the methods of selecting design conditions and calculating each heat flux term involved in the surface heat balance. In Kilkis' approach (1994a), the effect of piping parameters on the required

heating capacity was taken into account by using a simplified steady state snow-melting model (1994b).

However, in a steady state calculation, neither the history of the storm nor the dynamic response of the heated slab can be considered. As previously stated, the design heat flux can never be achieved at the surface instantaneously due to the time constant of the system, which implies that the surface may not reach the design conditions promptly as required. Spitler, et al. (2001) reported that, to maintain same surface condition, the heating loads calculated with the transient model developed by the authors might be several times as high as the steady state heating requirements. Therefore, it is highly desirable to update the current approach of snow melting load calculation by applying transient analysis of the snow melting system.

CHAPTER 3. DEFINITION OF THE PROBLEMS AND OBJECTIVES

System simulation is an important prerequisite to achieving an optimal design of hydronic snow melting systems. It must be able to accurately predict the system response to a wide variety of weather conditions. This requires reliable models for the components of the system, including the hydronically-heated slab, circulating pump, controller, and heating equipment. While many of these components are typical HVAC system components and their models have been developed by previous researchers (Clark 1985; Brandemuehl 1992; Yavuzturk and Spitler 1999; Jin and Spitler 2002), the model of the snow-melting process on a hydronically-heated slab is still under development. As a result, current guidance in the ASHRAE handbook (ASHRAE HOA 2003) for the design of hydronic snow melting systems is based on a simple, rough approach. It assumes one-dimensional steady-state heat transfer at the snow-melting surface (Ramsey, et al. 1999). Therefore, many important factors (i.e. transient heat transfer, piping layout and control strategy) that can significantly affect the snow melting performance and system life cycle cost are not taken into account. It is highly desirable to comprehensively consider all of these factors and update the current design guidance by using 2-dimensional and transient simulation of the hydronic snow melting system. As a result, the objectives of current research are:

(1). Modeling the 2-dimensional and transient snow melting process on a hydronically heated slab. The model will be validated against experimental data.

(2). Implementing a system simulation program for the hydronic snow melting systems. The system simulation will be validated against experimental data.

(3). Update the design guidance of the hydronic snow melting systems.

3.1. Modeling Snow Melting on a Hydronically-Heated Slab

The first objective of current research is to develop a model for the snow melting process on a hydronically-heated slab that can be used in the simulation of hydronic snow melting systems. Due to the large thermal mass of the slab, widely varying weather conditions, and intermittent operation of the heating system, the bridge deck slab rarely reaches steady state. Therefore, the model should be able to account for the transient heat transfer in the slab and variations in slab surface conditions. In addition, the layout of the embedded pipe network significantly affects the distribution of heat flux on the slab surface, and in turn, the snow melting performance. It is thus necessary to take into account this two-dimensional effect in the model. Also, the model should be computationally efficient since it will be used in system simulations that cover multi-year periods. Given entering fluid temperature, fluid mass flow rate, and weather data, this model should be able to predict slab temperature and degree of snow cover on the slab surface along with the exiting fluid temperature.

The predictions of this model will be validated against measured data from an experimental hydronically-heated bridge deck. To provide accurate information to the model, parameters of the pavement slab, such as thermal properties and surface solar absorptance, will be determined accurately. In addition, the atmospheric longwave radiation and snowfall rate, which are important inputs to the model but usually either crudely estimated or not available in general weather data products, will be measured at the site of the experimental bridge deck.

3.2. Simulation of Hydronic Snow Melting Systems

The second objective of the current research is to develop a simulation program for hydronic snow melting systems. For systems utilizing different heat sources, the complexity of system simulation is varied. For instance, the simulation will be very simple if an electrical heater is used as heat source since the output of the heater depends only on the voltage imposed on it. However, the simulation will be more complicated in the case of a GSHP used as the heat source because the performance of GSHP will degrade due to continuous heating operation. It is therefore necessary to model the GSHP and perform system simulation over the lifetime of the system (i.e. 20 years) to examine whether the GSHP is adequately sized. Thus, the simulation program should have the flexibility to simulate hydronic systems with various configurations. Component based simulation environments, such as HVACSIM+ (Clark 1985) and TRNSYS (SEL 1996), provide this flexibility. Under such simulation environments, a system simulation can be

built up by connecting the models of the system components properly. The numerical solver of the simulation environment solves the resulting differential and algebraic equations that represent the behavior of the system.

3.3. Heating Capacity of Hydronic Snow Melting Systems

The third objective of the current research is to update the guidance for required heating capacity of a hydronic snow melting system. To evaluate the impacts of transient, two-dimensional and solar effects on the required heating capacity to achieve certain snow melting performance, simulation of the hydronic snow melting system will be utilized, which employs the transient and two-dimensional model for the snow melting process on a hydronically-heated slab and uses multiple years of real weather data.

A parametric study will be conducted to investigate the impact of various design parameters and control strategies on system snow melting performance and required heating capacity.

Although the required heating capacity can be determined through system simulation, it is desirable to generate a set of tables distilled from the simulation results so that the designer can conveniently select the proper heating capacity for a snow melting system from the tabulated data.

CHAPTER 4. DEVELOPMENT AND EXPERIMENTAL VALIDATION OF A NUMERICAL MODEL FOR HYDRONICALLY-HEATED SLAB IN SNOW MELTING CONDITIONS

Modeling the process of snow melting on the hydronically-heated slab is complicated by a number of factors:

- Heat and mass transfer mechanisms involved in the snow melting process are complex and require treatment of phase change phenomena.
- Snow is a porous material composed of ice crystals, air, and water vapor. The physical properties of snow are not constant, but functions of the primary characteristics, such as density, grain shape, temperature, etc. (Jordan 1999).
- The surface condition during the snow melting process can vary not only temporally due to the variation of weather conditions, but also spatially at a particular moment because of the discrete arrangement of the heat sources (see Figure 4-1).
- Because any type of pavement has significant thermal mass, transient treatment is required.

- Weather conditions in storm events are highly changeable. Any model has to deal with variable precipitation, temperature, humidity, wind speed and solar radiation.

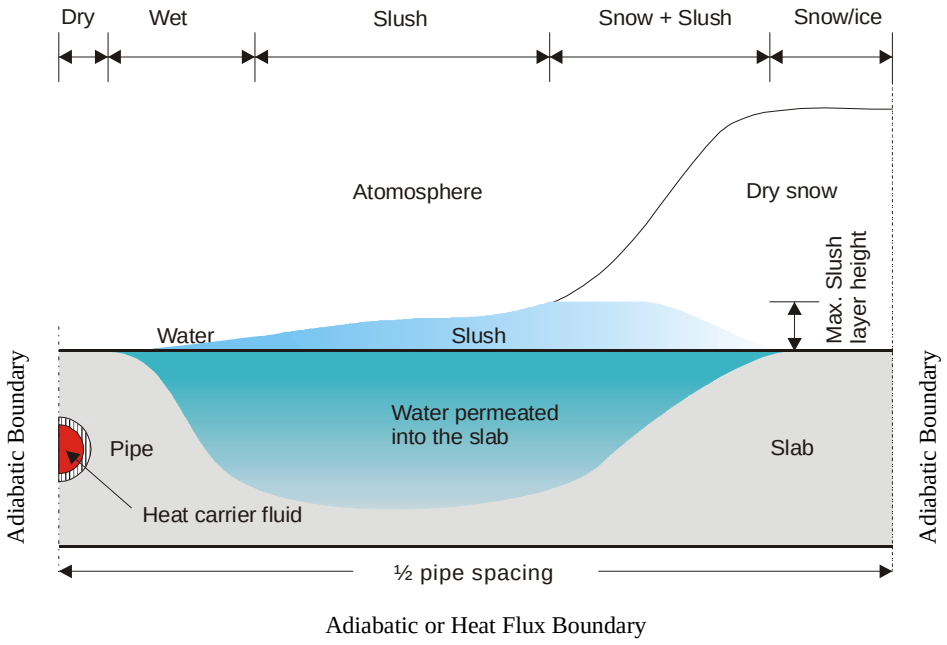

Figure 4-1 Variation of surface condition on a hydronically-heated slab in snow melting process.

A number of models for snow melting on hydronically-heated pavements have been previously presented. In the models developed by Schnurr and Rogers (1970), Kilkis (1994) and Ramsey, et al. (1999), steady state conditions were assumed. Such models have been used in the design process by calculating the required heat flux to instantaneously melt all snow precipitation. Such models are not suitable for simulations of actual performance, where snow may accumulate on all or part of the surface.

The transient models developed in the 1970's (Leal and Miller 1972; Schnurr and Falk 1973) did not consider the accumulation of un-melted snow on the surface. Chiasson, et al. (2000) presented a two dimensional transient model with consideration of the accumulation of un-melted snow, but without accounting for its insulating effect.

The model developed by Rees, et al. (2002) kept track of the temperature and mass of snow, ice, and water and modeled the snow melting process elaborately. However, due to the considerable computation time resulting from the implicit nature of the algorithm and complexity of the calculations, this model is not computationally efficient enough for multi-year system simulations with hourly data. While the model developed by Rees, et al. was partly validated with limited laboratory tests (Hockersmith 2002; Espin 2003), no experimental validation is reported for other models.

In this chapter, the development of a numerical model of snow melting on a heated pavement slab will be described. The validation of this model using experimental data from a typical snow event will also be presented.

4.1. Model Development

Of principal interest in evaluating the performance of snow melting systems is the ability of the system to minimize the amount of time the pavement is covered with snow, ice and frost during the duration of a snowstorm event or other pavement freezing conditions. The transient nature of weather conditions during a storm and the dynamic

behavior of the pavement and hydronic system necessitate the pavement thermal state and surface conditions to be simulated for some period before the onset of precipitation. Accordingly, it is necessary for the model to deal with boundary conditions representative of a wide variety of weather conditions, not just those found during snow precipitation.

In order to calculate current conditions on any part of the pavement it is not only necessary to consider current precipitation – its temperature, rate and whether it is water or snow – but also the prior condition of the surface and heat flux conducted through the slab. For example, if snow precipitation falls onto a dry pavement surface at sub-freezing temperatures (e.g. at the start of snow fall when the system has been off) fluxes from the heating system contribute to sensible heating of the snow and no melting may occur. However, if heating fluxes are higher or the pavement slab temperature has been raised to freezing point, current snow precipitation may be melted 'instantaneously' (i.e. within a given time step) and the surface condition can be identified as 'wet'. Similarly, if the rate of precipitation later rises sufficiently, the heating fluxes may be enough to continue melting some of the snow but at a rate lower than that of the precipitation resulting in a build-up of snow.

Several consequences can be noted. Firstly, knowledge of the current heating flux and surface temperature are not sufficient to define the current surface conditions. Furthermore, the boundary conditions are very non-linear in that a number of conditions may exist when the pavement surface temperature is at freezing point. It is consequently

necessary to consider previous thermal and surface conditions in order to predict current conditions. These difficulties are dealt with by taking a rules-based approach to defining surface conditions and formulating the heat and mass balance with the appropriate terms. This can be done by considering the surface temperature, mass of ice present, heating flux, and weather boundary conditions. Weather boundary conditions used in the model have been restricted to those found in standard weather records (data files), which include: rate and type of precipitation (rain, snow or hail); ambient wet and dry bulb temperature; wind speed and solar fluxes.

The ‘snow melting model’ can be considered as an algorithm or procedure where different surface heat transfer sub-models are applied. The resulting heat balance is then used to calculate the rate of melting which is in turn used in simple integration to find the current mass per unit area of ice present. The procedure for identifying surface conditions and applying various ‘sub-models’ for is shown in Figure 4-2.

Heat balances can be easily defined to allow calculation of surface temperatures in common weather conditions where the surface is either dry or wet. The models that have been applied in these cases are very similar to those of Ramsey et al. (1999). Further details are given in Rees et al. (2002). Of principal interest here are the models of the melting processes so that their presentation is concentrated on in the following sections after first discussing classification and definition of surface conditions.

4.1.1. Classification and Definition of Surface Conditions

Following the classification described by Rees, *et al.* (2002), seven surface conditions are identified. The classification and definition of the seven surface conditions are summarized in Table 4-1:

TABLE 4-1 Classification and Definition of Surface Conditions

Surface condition	Definition
Hoarfrost	The surface is covered with frost, which is due to sublimation of water vapor in the ambient air on a cold surface. The pavement surface temperature must be below freezing.
Dry	The surface is free of liquid and ice. The pavement surface temperature may be above or below freezing.
Wet	The surface temperature is above freezing and has some liquid water retained on it, but no ice. The liquid water can come from rainfall, condensed vapor, or the melted snow.
Dry snow	The surface is covered with dry snow without liquid. The snow can be regarded as a porous matrix of ice. The pavement surface temperature is below freezing so that snow is not currently being melted.
Slush only	The surface contains ice crystals that are fully saturated with water. Water penetrates the porous matrix of ice from bottom to the upper surface. The pavement surface temperature is at freezing point.
Snow and slush	The surface contains snow that is partly melted. The lower part of the snow is saturated with water and the upper is as dry snow. The pavement surface temperature is at freezing point.
Solid ice	The ice on the surface is in solid form rather than porous like snow. The pavement surface temperature must be below freezing.

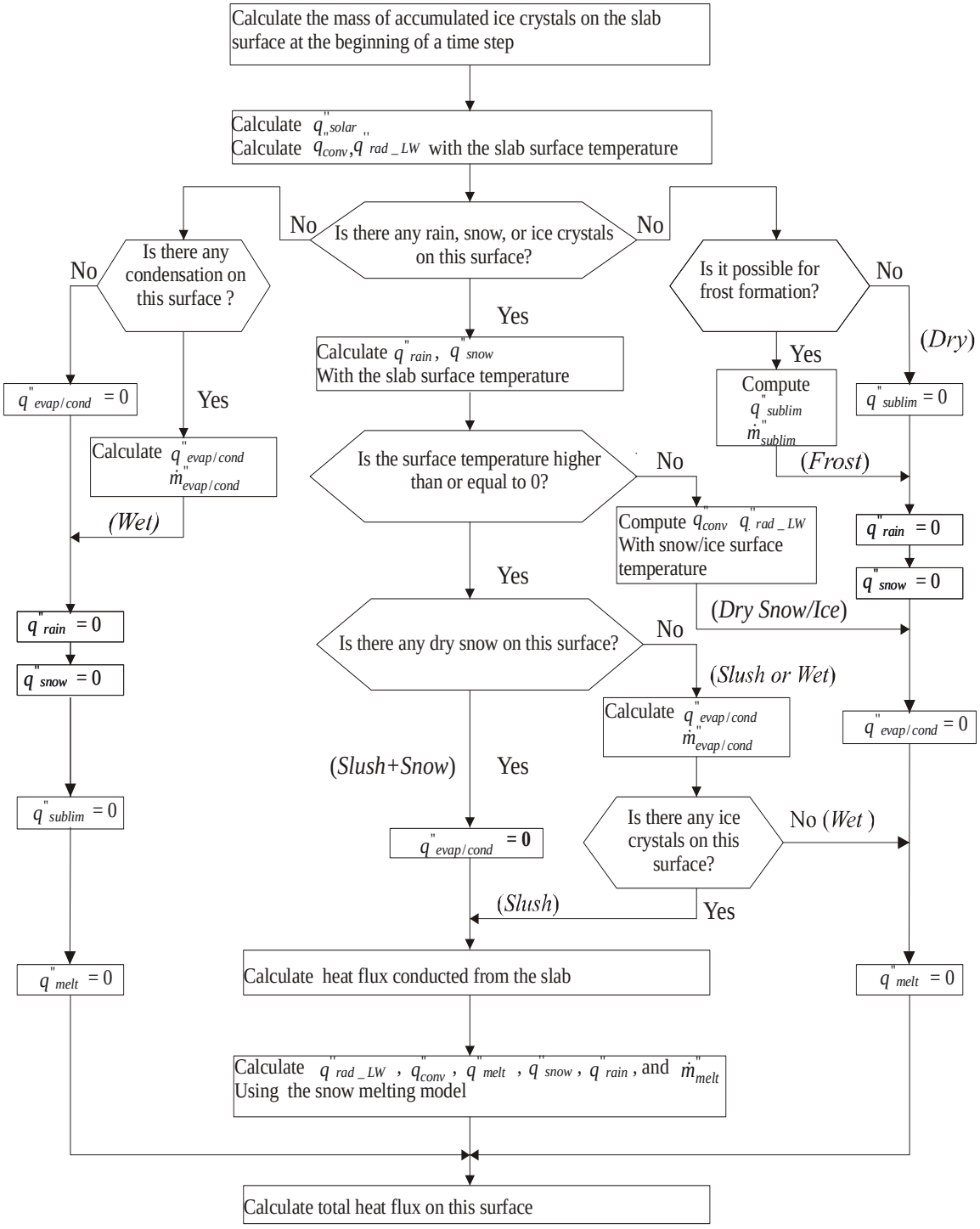

Figure 4-2 Flow chart of the snow melting calculation algorithm.

4.1.2. Snow Melting Model

Snow is a porous material composed of ice crystals, air, and water vapor. When melting from the lower (pavement) surface, some of the snowmelt is transported upwards through the snow by capillary action (Aoki, et al. 1987). While the snow at the bottom is saturated with liquid water, a layer of dry snow may exist above. The saturated and non-saturated layers are usually termed as ‘slush’ and ‘dry snow’, respectively. The snow-covered surface can be considered as combinations of these layers. In sub-freezing conditions where the slab surface is dry, the snow matrix can be conceived of as just ‘dry snow’. When melting occurs and the lower portions of the snow cover are saturated, this is denoted as ‘snow and slush’. In later stages of the snow melting process the depth of snow may be reduced so that there exists a relatively thin layer of fully saturated snow and liquid in approximate equilibrium, which is termed as ‘slush only’ condition.

In this model, the snow melting process under the ‘snow and slush’ condition is modeled with two nodes to allow calculation of conduction heat transfer in the dry snow layer (the insulating effect of the dry snow is significant). The snow melting process under the ‘slush only’ condition is modeled with only one node, which is in the center of slush layer. The heat transfer under ‘snow and slush’ and ‘slush only’ conditions are represented schematically in Figure 4-3 (a) and (b).

A number of assumptions are made in this model. These include the following:

- The dry snow layer is homogeneous.

- The slush layer is isothermal.
- Melting of snow occurs only at the pavement surface and absorbed solar radiation contributes directly to melting in the lower layer.
- While snowfall is accounted for at the dry snow layer, rainfall occurring after a snow layer has formed is accounted for directly at the slush layer
- Ice and liquid exist simultaneously in the slush layer.
- The snow melting process is treated as a one-dimensional process and therefore the lateral heat and mass transfer between the adjacent snow and slush are not accounted for.

Distinguishing whether a surface is covered with 'slush only' or 'slush and snow' is important in this approach and it is necessary to define a set of criteria that can be applied as a rule in the model algorithm. Experimental investigations (Coléou, et al. 1999; Jordan, et al. 1999; Hockersmith 2002) have shown that, due to capillary forces, water will rise to an equilibrium height in about 10 seconds if there is enough water at the bottom of the snow cover. It was also reported that the capillary rise level was dependent on the snow characteristics (e.g. porosity and grain size). The height of capillary rise of water in freshly fallen snow (density is 7.3 lb_m/ft^3 or 117 kg/m3) was reported by Jordan, et al. (1999) to be approximately 1" (2.5 cm). Given the two layer conceptual model used in this work, the total height of the snow/ice matrix can be estimated from the layer's mass. The existence of a 'slush only' condition can then be tested by comparing the predicted mass of the snow/ice with a mass equivalent to a 1" (2.5 cm) layer of slush.

Rees, et al. (2002) were able to estimate the total snow and saturated depth explicitly as both liquid and ice mass balances were calculated.

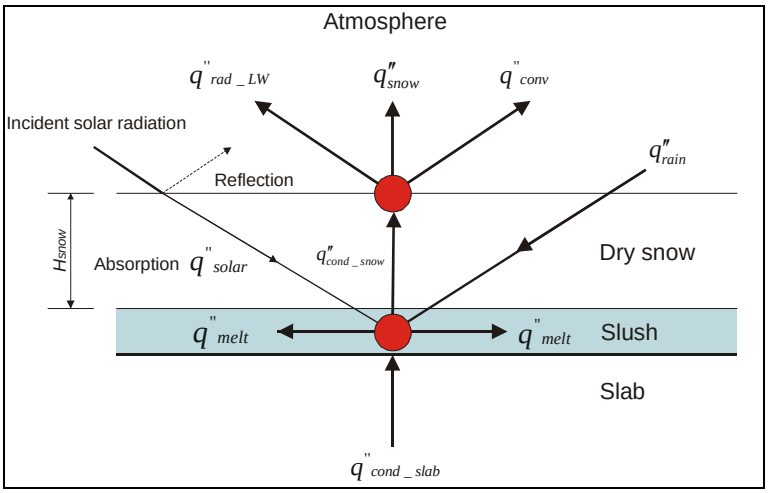

(a)

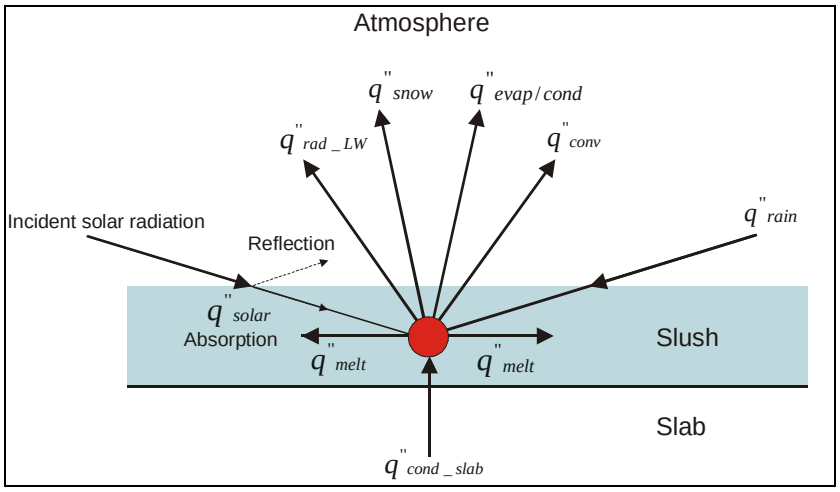

(b)

Figure 4-3 Schematic representation of heat transfer in (a): two-node "snow and slush" model; (b): one-node "slush only" model.

This snow-melting model is formulated by considering a mass balance for the ice crystals in both the dry snow and slush, a heat balance on the dry snow surface, and a

heat balance in the slush layer. The mass balance for the ice crystals in both the dry snow and slush (m''_{ice}) is given by:

$$\frac{dm''_{ice}}{d\theta} = \dot{m}''_{snowfall} - \dot{m}''_{melt} \tag{4-1}$$

where,

$\dot{m}''_{snowfall}$: snowfall rate, $lb_m/s\text{-}ft^2$ or $kg/s\text{-}m^2$

$\dot{m}''_{melt}$: snow-melting rate, $lb_m/s\text{-}ft^2$ or $kg/s\text{-}m^2$

The heat balance in the slush layer is given by:

$$\dot{m}''_{melt} \cdot h_{if} = q''_{cond\_slab} + q''_{solar} + q''_{rainfall} - q''_{cond\_snow} \tag{4-2}$$

where,

h_{if} : latent heat of fusion of water, Btu/lb_m or J/kg

q''_{cond_slab} : conduction heat flux from slab into slush layer, $Btu/h\text{-}ft^2$ or W/m^2

q''_{cond_snow} : conduction heat flux through snow layer, $Btu/h\text{-}ft^2$ or W/m^2

Heat is transferred from the dry snow layer to the slush layer by conduction (q''_{cond_snow}), so that, ignoring evaporation, the heat balance on the dry snow upper surface is given by:

$$q''_{cond\_snow} = q''_{conv} + q''_{rad\_LW} + q''_{snowfall} \tag{4-3}$$

The dry snow layer is assumed to be homogeneous and a linear temperature gradient applied so that the conduction heat transfer rate is given by:

$$q''_{cond\_snow} = \frac{k_{snow}}{H_{snow}}(t_{snow\_bottom} - t_{snow\_top}) \quad (4\text{-}4)$$

In the above equation, the effective thermal conductance of the dry snow (k_{snow}) is related to the density of the dry snow (ρ_{snow}) using the relation defined by Yen (1981)[1] as $k_{snow} = 2.22362\rho_{snow}^{1.885}$. The bottom surface temperature of the dry snow (t_{snow_bottom}) is the temperature of the slush layer, i.e. the freezing point. The thickness of the dry snow layer (H_{snow}) is found from the layer's mass, assuming a constant snow density: $H_{snow} = (m''_{ice} - m''_{slush})/\rho_{snow}$ where m''_{slush} is the mass of ice crystals in a slush layer with the maximum depth of 1" (2.5 cm).

The convective heat flux (q''_{conv}) and longwave radiative heat flux (q''_{rad_LW}) are given by Equation (4-5) and (4-6), respectively:

$$q''_{conv} = h_c(t_{snow\_top} - t_{air}) \quad (4\text{-}5)$$

$$q''_{rad\_LW} = \varepsilon\sigma(T^4_{snow\_top} - T^4_{sky}) \quad (4\text{-}6)$$

The convection heat transfer coefficient (h_c) is taken as the maximum between the free and forced convection coefficients, which is calculated from the Nusselt Number (Nu). For free convection heat transfer, Nu is a function of the Rayleigh Number (Ra), and it is calculated with the correlations described by Incropera and DeWitt (1996) for

[1] In this equation, ρ_{snow} is in the unit of Mg/m^3 and k_{snow} is in the unit of W/m-C.

free convection from the upper surface of a heated plate or the lower surface of a cooled plate:

$$Nu = 0.54Ra^{\frac{1}{4}} \qquad (10^4 < \text{Ra} < 10^7 - \text{laminar flow}) \qquad (4\text{-}7)$$

$$Nu = 0.15Ra^{\frac{1}{3}} \qquad (10^7 > \text{Ra} > 10^{11} - \text{turbulent flow}) \qquad (4\text{-}8)$$

For forced convection heat transfer, Nu is a function of the Reynolds Number (Re), and it is calculated with the empirical relations described by Incropera and DeWitt (1996) as shown following:

$$Nu = 0.664\,\text{Re}^{\frac{1}{2}}\,\text{Pr}^{\frac{1}{3}} \quad \text{(laminar flow)} \qquad (4\text{-}9)$$

$$Nu = 0.037\,\text{Re}^{\frac{4}{5}}\,\text{Pr}^{\frac{1}{3}} \quad \text{(mixed and turbulent flow)} \qquad (4\text{-}10)$$

The convection coefficient (h_c) is then computed by following equation:

$$h_c = \frac{Nu \cdot K}{L} \qquad (4\text{-}11)$$

where,

k: thermal conductivity of air at pavement node - air film temperature, Btu/(h-ft-^{o}F) or W/(m-K)

L: characteristic length of the slab, ft or m

There are many models for the sky temperature (T_{sky}) available in the published literature (Clark and Allen 1978; Martin and Berdahl 1984; Brown 1997; Ramsey, et al. 1999; Crawford and Duchon 1999). The model proposed by Ramsey, et al. was used in

previous snow melting load calculation procedures (Ramsey, et al. 1999; Rees, et al. 2002). However, as discussed later in section 4.2.2.3, the algorithm proposed by Martin and Berdahl (1984) performs better than the model of Ramsey, et al. in matching the measured sky temperature. It is therefore recommended for the calculation of the sky temperature.

The algorithm proposed by Martin and Berdahl is based on a simple empirical and theoretical model of clouds, together with a correlation between clear sky emissivity and the surface dew point temperature. The monthly average clear sky emissivity (ε_{clear}) is obtained by the following relationship:

$$\varepsilon_{clear} = 0.711 + 0.56(\frac{t_{dp}}{100}) + 0.73(\frac{t_{dp}}{100})^2 + 0.013\cos[2\pi\frac{\theta_h}{24}] + 0.00012(P - 1000) \quad (4\text{-}12)$$

where,

t_{dp}: dew point temperature, °F or °C;

θ_h: hour of the day;

P: station pressure in millibar.

The cloudy sky emissivity (ε_{cloud}) is computed using Equation (4-13), which includes contributions from several cloud layers labeled with the index *i*.

$$\varepsilon_{cloud} = \varepsilon_{clear} + (1 - \varepsilon_{clear})\sum_i n_i \varepsilon_{c,i} \Gamma_i \quad (4\text{-}13)$$

where,

n_i: fractional area of the sky covered by clouds at i^{th} level;

$\varepsilon_{c,i}$: hemispherical emissivity of cloud at i^{th} level;

Γ_i: cloud factor at i^{th} level, which is a factor depending on the cloud base temperature.

The cloud fraction and the height of cloud bases at low, medium, and high levels are usually available in the local climatological data product of National Climatic Data Center (NCDC). Low and mid-level clouds tend to be opaque ($\varepsilon_{c,i} \approx 1.0$), while the emissivity of high-altitude cloud is recommended by the authors to be 0.4. The cloud factor Γ_i is calculated using the following equation:

$$\Gamma_i = e^{-h_i / h_0} \tag{4-14}$$

where,

h_i: base height of cloud at i^{th} level, mile or km;

h_0: constant 5.1 mile or 8.2 km.

The sky temperature (T_{sky}) is finally determined by:

$$T_{sky} = T_{air} \varepsilon_{cloud}^{1/4} \tag{4-15}$$

The uncertainty of the sky temperature calculated using the above algorithm and the Typical Meteorological Year (TMY) weather data was estimated as ±4.1 ºF (±2.3 ºC) by comparing with the measured data (Martin and Berdahl 1984).

Precipitation of rain or snow and the associated sensible heat flux are dealt with slightly differently. Snow precipitation is attributed to the upper snow layer and rain to

the lower node (rain is thought of as penetrating the snow and arriving in the saturated layer). Precipitation is assumed to arrive at the current ambient temperature and reach equilibrium with the snow or slush node. A sensible heat flux is associated with this temperature change. The sensible heat flux of snow ($q''_{snowfall}$ in Equation 4-3) is given by:

$$q''_{snowfall} = \dot{m}''_{snowfall} \cdot c_{p\_snowfall} \cdot (t_{snow\_top} - t_{air}) \quad (4\text{-}16)$$

Similarly, the sensible heat flux associated with rain precipitation ($q''_{rainfall}$ in Equation 4-2) is given by:

$$q''_{rainfall} = \dot{m}''_{rainfall} \cdot c_{p\_rainfall} \cdot (t_{air} - t_{snow\_bottom}) \quad (4\text{-}17)$$

The solar radiation absorbed by the slab (q''_{solar}) is determined by the product of the total horizontal incident solar radiation[2] (I) and the solar absorptance (α) as shown in Equation (4-18):

$$q''_{solar} = \alpha \cdot I \quad (4\text{-}18)$$

The surface solar absorptance (α) is the balance of the surface albedo, which will vary under different surface conditions. Research conducted by Levinson and Akbari (2001) at LBNL showed that the mature solar absorptance of concrete mixes could range from 0.23 to 0.59 (mean 0.41). Wetting strongly increases the solar absorptance of concretes (mean increase 0.23). The solar absorptance of snow is generally a minimum

[2] The sum of the direct and diffuse solar radiation incident upon the horizontal slab surface – data that is commonly available from standard weather data records

after a fresh snowfall and increases with time due to growth in grain sizes, melt water near the snow surface and the accumulation of dust and debris on the snow surface. Values for solar absorptance can range from less than 0.2 for freshly fallen snow to as much as 0.6 for melting, late-season, ripe snow (CECW-EH 1998). In this model, the solar absorptance at dry condition (α_{dry}) is a required parameter and the variation of solar absorptance at different surface conditions is considered. For wet surface, the solar absorptance (α_{wet}) will be increased by 0.23 according to Levinson and Akbari (2001); for snow surface, the solar absorptance (α_{snow}) will be 0.2; for surface covered only with slush, the solar absorptance (α_{slush}) is approximated by linear interpolation between the values of wet and dry snow surface according to the accumulated mass flux of ice crystals in the snow (m''_{ice}).

If the surface is only covered with a layer of slush (Figure 4-3 b) the heat balance at the single node of the slush layer is given by:

$$\dot{m}''_{melt} \cdot h_{if} = q''_{cond\_slab} + q''_{solar} + q''_{rainfall} - q''_{conv} - q''_{rad\_LW} - q''_{snowfall} - q''_{evap/cond} \qquad (4\text{-}19)$$

In above equation, $q''_{rainfall}$, q''_{conv}, q''_{rad_LW}, $q''_{snowfall}$, and $q''_{evap/cond}$ are evaluated with the ambient temperature and the slush temperature, which is at the freezing point of water. The heat flux for evaporating water or from condensed water vapor ($q''_{evap/cond}$) is given by:

$$q''_{evap/cond} = h_{fg} \cdot h_d \cdot (w_{air} - w_{pv}) \qquad (4\text{-}20)$$

where,

h_{fg} : heat of vaporization of water, Btu/lb or J/kg

w_{air} : humidity ratio of the ambient air, lb_m/ lb_m or kg/kg dry air

w_{pv} : humidity ratio of saturated air at slush surface, lb_m/ lb_m or kg/kg dry air

h_d : mass transfer coefficient, lb_m/ ft^2-s or kg/ m^2-s

4.1.3. Model Implementation

There may be a number of ways in which the surface boundary conditions can be coupled with models of conduction heat transfer in the subsurface. Here, a two-dimensional finite difference model has been used to calculate conduction heat transfer. This is an explicit method that uses a large number of time steps per hourly interval in the weather data (details are given in Chiasson, *et al*., 2000). As the system consists of equally spaced parallel pipes in short hydronic circuits, a two-dimensional representation is deemed a sufficient representation of the whole pavement. Symmetry allows the mesh to represent half the pipe spacing in width – as indicated in Figure 4-1.

The heat and mass balance equations are solved by a successive substitution method to find the node temperatures, melting rate and current mass of ice. The heat balance equations can be solved by using the flux conducted through the slab (q''_{cond_slab}) calculated at the previous time step. The fluxes at the slab surface calculated at the current time step are then used to set a Neumann boundary condition in the finite

difference model. This explicit approach works well with realistic heat fluxes and small time step size.

The model of surface conditions described here is strictly one-dimensional in that lateral heat transfer in the snow/ice layer is not considered. However, by coupling one instance of the nodal snow melting model with each surface node of the two-dimensional finite difference grid, the surface model is quasi two-dimensional. In this way the lateral variations in conditions, as indicated in Figure 4-1, can be modeled and the proportion of snow free area can be calculated.

The bridge deck model was implemented as a component of a bridge heating system model and the simulation performed using the differential algebraic equation solver of HVACSIM+ (Clark 1985). Given system fluid temperature, mass flow rate, and weather data, this model can predict the surface conditions and temperatures over the heated surface along with the exiting fluid temperature.

4.2. Experimental Validation

In this section, an experimental hydronic bridge snow melting system and measurements of several crucial parameters will be introduced and the experimental validation results of the model will be presented.

4.2.1. Experimental Hydronic Bridge Snow Melting System

An experimental hydronic bridge snow melting has been built at Oklahoma State University (Smith 1999-2002). It provides a means of collecting experimental data for the purposes of model validation under various operating conditions. The experimental bridge deck is 60 ft (18.3 m) in length and 20 ft (6.1 m) in width (2 lanes wide). The embedded hydronic tubing is ¾" (19 mm) diameter cross-linked polyethylene pipe on 1 ft (0.3 m) centers at a depth of 3.5" (89 mm). An aqueous solution of propylene glycol at 39% concentration by mass is used as the heat carrier fluid circulated in the embedded pipe network.

A ground coupled heat pump system was used to heat the propylene glycol solution and the maximum possible entering fluid temperature to the bridge deck hydronic heating system is about 130 °F (54 °C). The heating system is controlled to maintain the average bridge surface temperature at 40 °F (4.4°C) when there is a risk of icing or snowfall.

Sixty thermistors are embedded at different locations inside the pavement slab to measure the pipe wall and pavement surface temperatures. In addition, the leaving and entering fluid temperatures and the volume flow rate are measured with thermistor probes and flow meter respectively. The estimated uncertainties of the temperature and flow rate measurements are ±0.18 °F (±0.1 °C) and ±3%, respectively (Holloway 2000).

Surface conditions are often considered in design calculations in terms of the fraction of the surface that is clear of snow. This is commonly denoted 'snow free area ratio' or 'A_r' (ASHRAE 2003). Hence a snow free condition is indicated by a snow free area ratio of one, and a snow-covered surface as a value of zero. Patches of snow between pipe locations (striping) correspond to intermediate values. In this experimental work, this snow free area ratio has been estimated by examining images of the bridge surface taken during the snow event by a digital video system.

4.2.2. Model Data

To perform simulation using this model, it is required to provide weather data and the parameters that describe the simulated slab. The weather data used in the validation exercise, except the snowfall rate, are obtained from the Oklahoma Mesonet, which is a network of weather stations throughout Oklahoma (Elliot et al. 1994). The local Mesonet weather station is approximately 1 mile (1.6 km) from the experimental bridge site. Measurements of several crucial parameters of the experimental bridge deck and weather data have been conducted to provide accurate information to the model. This will be discussed in the following sections.

4.2.2.1. Effective Thermal Properties of Pavement

The thermal conductivity, specific heat, and density of the pavement are important parameters that can significantly impact the heat diffusion inside the pavement.

Although these properties of the concrete that is used to build the pavement can be accurately measured, they cannot be used directly as parameters of the pavement because the pavement is composed of not only concrete but also pipes and steel bars, to which the pipes are tied. In this validation work, the effective properties of the pavement are estimated by volume-weighted average of the properties of its component. In the experimental bridge deck, the concrete, rebar, and pipes occupy 99%, 0.8%, and 0.2% of the total volume of the pavement respectively.

The pavement of the experimental bridge deck is built with the limestone concrete. The properties of the concrete at three levels of moisture content conditions (oven dry, normally dry, and saturated) and the corresponding volume-weighted averages are summarized in Table 4-2. The thermal conductivity of the concrete at normally dry condition is measured with the guarded hot plate method (Smith 2000), while data at oven dry and saturated moist conditions are adopted from ASME (1978) for the limestone concrete. The specific heats of the concrete at the three levels of moisture content conditions are measured with a method similar to that described by the U.S. Army Corps of Engineers Specification (1973). The densities of the concrete at the three levels of moisture content conditions are determined by the ratio of the weight of a sample of the concrete to its volume.

As shown in Table 4-2, the volume-weighted average value of thermal conductivity is significantly higher than that of the concrete, although the differences will decrease as the moisture content increases. It is due to the high thermal conductivity of

steel (26.2 Btu/hr-ft-ºF or 45.3 W/m-K), which is about 28 times of that of concrete (0.9 Btu/hr-ft-ºF or 1.6 W/m-K). On the other hand, the volume-weighted average does not considerably change the values of specific heat and density.

TABLE 4-2 Pavement Thermal Properties at Various Moisture Content Conditions

Property	Condition	Concrete	Volume-weighted average
Thermal conductivity [Btu/hr-ft-F] / [W/m-K]	Oven dry	0.8 / 1.4[(a)]	1.0 / 1.8
	Normally dry	0.9 / 1.6[(b)]	1.2 / 2.0
	Saturated	1.3 / 2.2[(a)]	1.5 / 2.6
Specific heat [Btu/lb-F] / [J/kg-K]	Oven dry	0.203 / 851	0.211 / 881
	Normally dry	0.215 / 898	0.222 / 928
	Saturated	0.248 / 1037	0.255 / 1065
Density [lb/ ft^3] / [kg/m^3]	Oven dry	143/ 2290	146 / 2341
	Normally dry	145 / 2324	148 / 2375
	Saturated	152 / 2430	155 / 2480

Note:
(a): measured with the guarded hot plate method (Smith 2000);
(b): adopted from ASME (1978) for limestone concrete.

The method of using the volume-weighted average to account for the effect of embedded rebar is only a rough approximation. In addition, the thermal conductivity of limestone concrete at saturated condition is adopted from the published data, which may be different from the actual value of the concrete used in the bridge deck. In order to examine whether the volume-weighted averages are proper parameters for the bridge deck, an initial test of the model predictions has been conducted. The selected initial test period was 28 hours after a 5-hour freezing rainfall event. The ice on the bridge surface was melted by the sunshine 9 hours before the initial test period and therefore the concrete was very close to saturated. The bridge was heated from 21:30 through 9:30 in the next morning. There is not any precipitation during this period. The test is conducted by providing locally measured weather data, entering fluid temperature, and flow rate as

inputs to the model and comparing the predicted average bridge surface temperature, exiting fluid temperature with the measured data. The properties of the concrete and the volume-weighted averages at saturated condition, and the properties of the concrete at normally dry condition have been tried as parameters of the model. Comparisons between measured and model predicted average surface temperatures and exiting fluid temperatures are shown in Figure 4-4 (a) and (b), respectively. As illustrated by the figures, the volume-weighted averages of the properties at saturated condition lead to best match between the measured data and model predictions. Therefore, they will be used in the following validation work when the concrete is saturated.

4.2.2.2. Solar Absorptance

The solar absorptance of the bridge deck at dry condition (α_{dry}) was obtained from the measurements of a Kipp & Zonen CNR 1 four-component net radiometer on the experimental bridge deck. The solar absorptance was calculated as the balance of the surface reflectance, which can be determined by the ratio of the solar radiation measured by the downward pyranometer to that measured by the upward pyranometer.

$$\alpha = 1 - E_{lowr} / E_{upper} \tag{4-21}$$

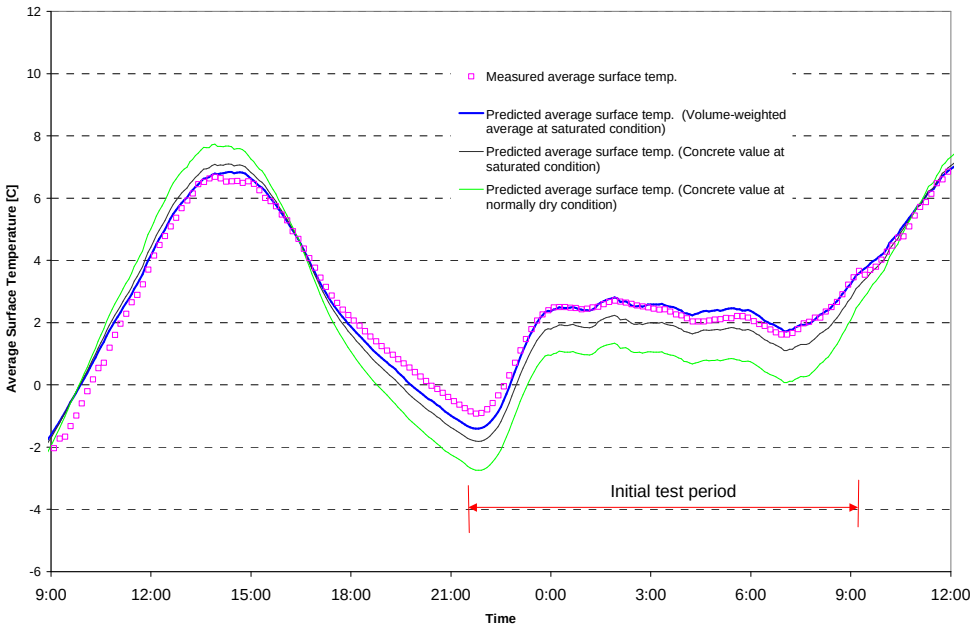

(a)

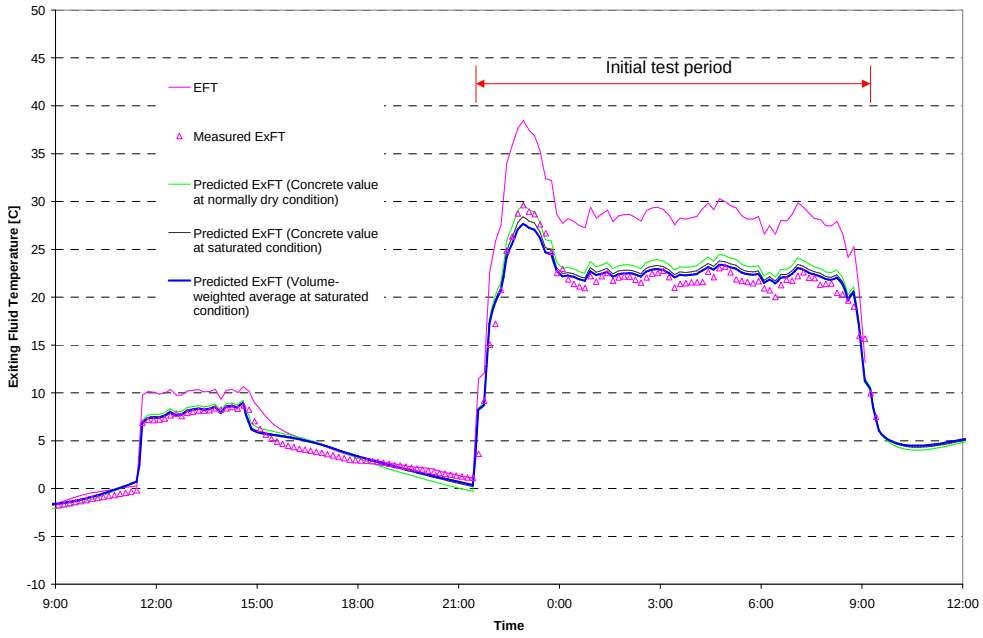

(b)

Figure 4-4 Initial test results (a): comparison of average surface temperature; (b): comparison of exiting fluid temperature.

As shown in Figure 4-5, the majority of solar absorptance measurements are within the range from 0.60 to 0.62 when the solar incidence angle (ϕ) is less than 70°. The measurements of solar absorptance decrease dramatically when the solar incidence angle is greater than 70°. The scattered points of the solar absorptance measurements were due to the movement of cloud. This solar incidence angle dependence of the solar absorptance has been considered in the model with a polynomial correlation regressed from the measured data.

$$\alpha = 0.62 \times (1.0227 - 1.7 \times 10^{-3} \phi + 8 \times 10^{-6} \phi^2 + 4 \times 10^{-7} \phi^3 - 6 \times 10^{-9} \phi^4) \quad (4\text{-}22)$$

According to the specification of the Kipp & Zonen CM3 pyranometer (Kipp & Zonen 2000), the uncertainty of solar radiation measurement is mainly from the following four aspects:

- Non-linearity: ±2.5% (0-1000 W/m^2)
- Spectral selectivity: ±5% (350-1500 nm)
- Temperature dependence of sensitivity: ±6% (-10 to +40ºC)
- Tilt response: ±2%

Assuming the above four uncertainties are independent, the uncertainty of solar radiation measurement may be estimated as ±8% by adding the individual uncertainties in quadratur. If the uncertainties of the downward and upward pyranometers are independent, the uncertainty of the calculated solar absorptance will be the quadratic sum of the fractional uncertainties of the numerator and denominator in Equation (4-21)

(Taylor 1997). Thus, the uncertainty of the calculated solar absorptance is determined as ±11%.

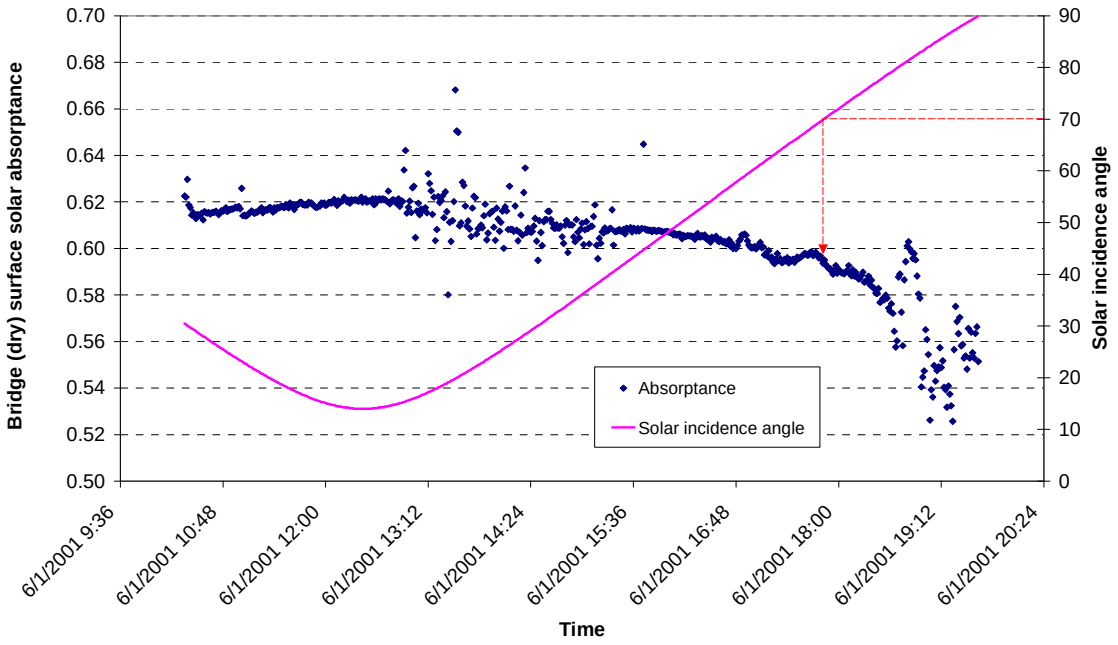

Figure 4-5 Measurements of surface solar absorptance of the experimental bridge deck.

4.2.2.3. Sky Temperature

Sky temperature (T_{sky}) is an effective temperature of the sky, which is usually treated as a black body. In this model, T_{sky} is used to calculate the longwave radiative heat flux on the slab surface (q''_{rad_LW}). Although there are several models available in literature that can calculate the sky temperature, significant difference exists among the predictions of these models. To select the best model, measurements of the longwave radiation from sky are conducted on the experimental bridge deck with a Kipp & Zonen CNR 1 four-component net radiometer during various seasons and sky conditions.

Predictions of a few sky temperature models (Clark and Allen 1978; Martin and Berdahl 1984; Brown 1997; Ramset, et al. 1999; Crawford and Duchon 1999) that account for the effect of cloud cover have been compared with the measured data. The comparison results show that the model proposed by Martin and Berdahl (1984) most closely matches the measured data. A comparison between the predictions from Martin and Berdahl's model and that proposed by Ramsey, et al. (1999), which has been used in the previous snow melting models (Ramsey, et al. 1999; Rees, et al. 2002), is shown in Figure 4-6. As can be seen clearly, although the model proposed by Ramsey, et al. (1999) can favorably match the experimental data under both clear sky and precipitation conditions, it significantly underestimates the sky temperature under cloudy sky condition. It is due to the coarse approximation of the cloud temperature used in this model (Ramsey, et al. 1999).

Cloud cover information is a crucial parameter to predict of the sky temperature. As can be seen in Figure 4-6, cloud cover can significantly reduce the difference between the air and sky temperature. In this study, the cloud cover information is obtained from the National Virtual Data System (NVDS 2002). Since the data were observed at a regional airport, which is about 3.4 mile (5.4 km) away from the experimental bridge deck, there may be some differences between the data and actual cloud cover condition in the bridge site. It may partially explain the significant discrepancies between the measured sky temperatures and the predictions from all the models during the period from 12/22/2002 12:00 pm to 12/23/2002 12:00 am.

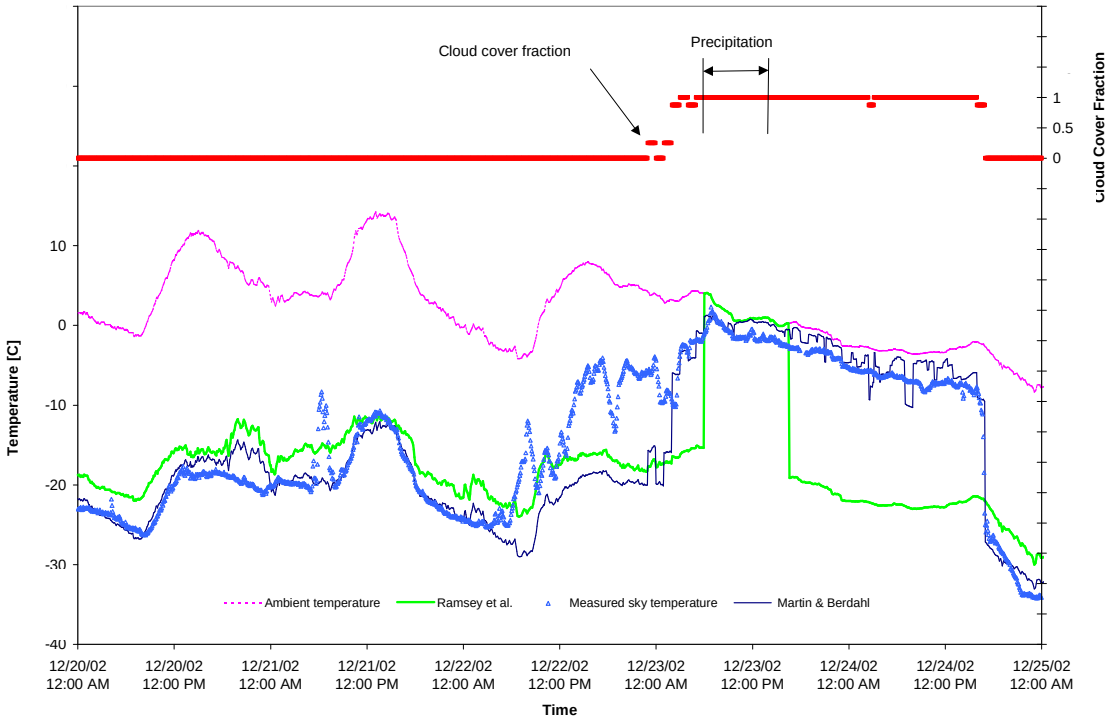

Figure 4-6 Comparison of model predicted and measured sky temperature.

4.2.2.4. Snowfall Rate

The snowfall rate is a critical input to the bridge model. However, it is usually either crudely estimated or not available in weather data. In this study, the time-varying snowfall rate was measured with a modified heated tipping bucket rain gauge. The tipping bucket rain gauge is comprised of a cone for collecting rainfall or snowmelt and two specially designed buckets, which will tip when the weight of 0.01" (0.25 mm) of water falls into one of them. The original rain collector heater was only designed to protect the internal components of the rain gauge from freezing and not able to melt the snow collected in the collector fast enough to get an accurate snowfall rate measurement. As a result, this rain gauge has been modified by wrapping a self-regulated electrical

cable around the inside surface of the collector to warm its entire surface, so that snow can be melted quickly after it strikes the collector surface. This modified rain gauge has been calibrated and the uncertainty is less than ±10%. Figure 4-7 shows the measured precipitation rate during the snow event on December 23, 2002. As shown in the figure, the event started with rainfall at about 6:00 in the morning, and then, it began to snow at 9:00 am and the snowfall ceased at about 4:30 pm. Total amount of precipitation in equivalent water is 1.1 " (29 mm) during the whole event. Since the rain gauge cannot differentiate between snow and rain by itself, the snow and the rain were distinguished by visual observation.

The incident solar radiation during the snow event is also shown in Figure 4-7. It can be seen clearly that there is considerable solar radiation (about 63 Btu/h-ft^2 or 200 W/m^2) when light snow is falling although heavy snowfall can significantly reduce the amount of the incident solar radiation. Considering that the surface solar absorptance may vary from 0.2 (covered dry snow) to 0.8 (wetted by the snowmelt), the heat gain from solar radiation in this case can be in the range of 12 to 48 Btu/h-ft^2 (40 to 160 W/m^2). Given that the typical value of required heat flux to maintain a snow free surface is from 90 to 180 Btu/h-ft^2 (300 to 600 W/m^2) (ASHRAE 2003), this amount of energy could make a significant difference in the snow melting process. It is for this reason that the variation of solar absorptance at different surface conditions has been considered in this model.

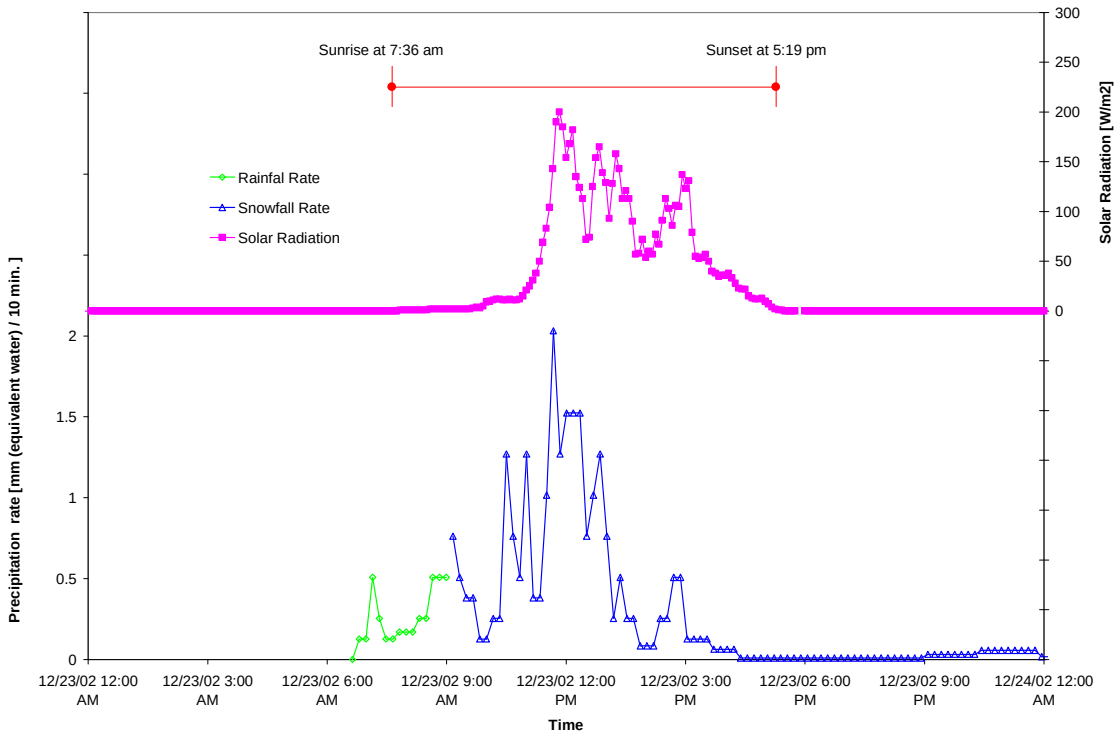

Figure 4-7 Measured precipitation rate and solar radiation during the snow event on Dec. 23, 2002.

4.2.3. Validation Results

In designing and evaluating snow melting performance it is the calculation of surface temperatures and surface conditions (indicated by snow free area ratio) at any given time that is of prime concern. (System performance is often defined in terms of the number of hours the surface can be kept clear of snow *vs.* total hours of snowfall.) The ability to predict surface temperatures is not only of direct relevance to prediction of surface conditions, but is also of interest if one is concerned with modeling the whole heating system and its control systems. Similarly, heating system fluid temperatures/fluxes are of interest if the whole system is to be modeled and energy

efficiency considered. Accordingly, it is the prediction of snow free area, surface and fluid temperature that are examined in evaluating the model.

The validation exercise has been conducted by providing weather data, entering fluid temperature, and flow rate as inputs to the model and comparing the predicted average bridge surface temperature, exiting fluid temperature, and the degree of snow cover with the corresponding measured values. The data used were recorded during the snowstorm event on December 23, 2002, which is representative of a heavy snowstorm. Besides the initial dry condition, four different surface conditions occur:

1. Wet: rainfall from 6am for 3 hours, surface above freezing temperature
2. Slush and snow: complete snow cover for 4 hours. The heating system is started after 1 hour.
3. Wet, slush, and slush and snow: various conditions as stripes appear during partial snow clearance
4. Wet: snow clear but surface wetted by melt water

The effective pavement thermal properties at saturated condition (as given in Table 4-2) are used in the simulation since the snowfall followed with 3 hours of rainfall (see Figure 4-6). In addition, to eliminate error resulting from estimation of the sky temperature, measured sky temperatures are used as one of the inputs to the model. To initialize the slab temperature, the simulation period started three days prior to the snow event and corresponding weather data are used in the initial period of the simulation.

Figure 4-8 shows predictions of surface temperature during the storm. The temperatures shown are those calculated at positions directly above the heated pipe, and exactly midway between the pipes. As shown in the figure, the surface temperature remains at 32 ˚F (0 ˚C) at the point midway between the pipes before the entire surface is clear of snow and becomes wet. The maximum surface temperature occurs directly above the pipe location and rises quickly – the average being correspondingly between these limits. Experimental data are not shown in this figure since surface temperatures were measured 3/8" (10 mm) below the surface in practice. Further comparisons are made using the temperatures calculated at the corresponding depth.

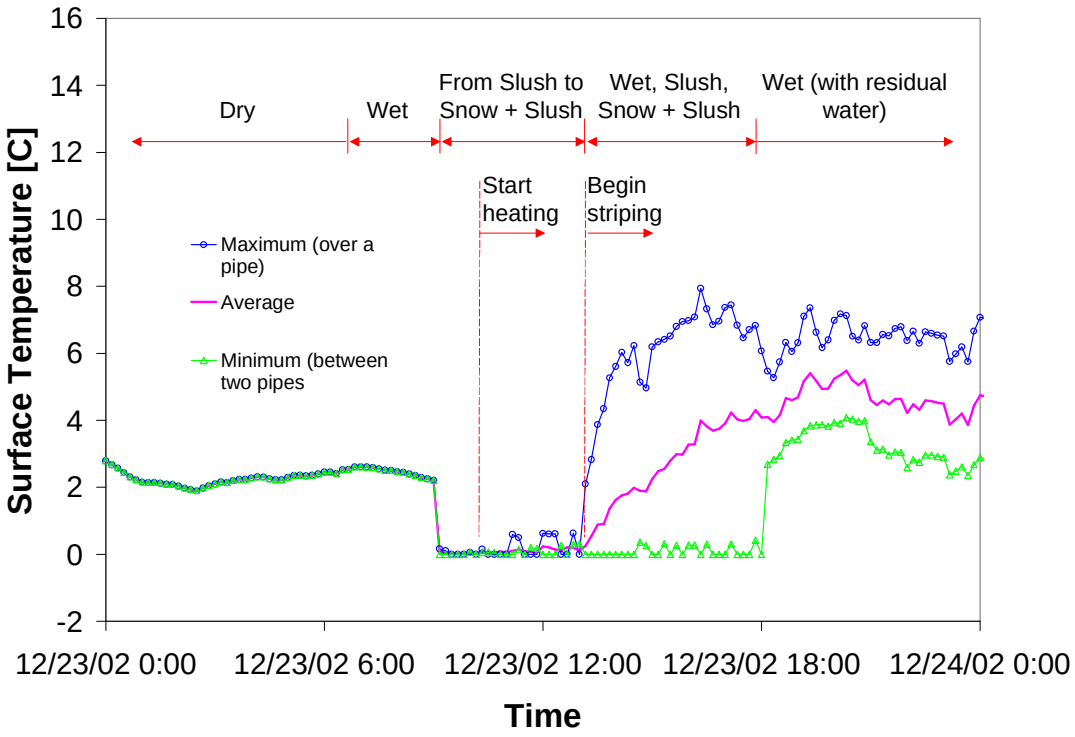

Figure 4-8 Variation of the calculated maximum, average, and minimum temperature at the pavement surface.

4.2.3.1. Surface Temperatures

Measured and predicted bridge average surface temperatures during the snow event are compared in Figure 4-9. Precipitation type and surface conditions during the storm are also indicated on this figure. The average near-surface temperature (10 mm below surface) drops immediately from approximately 35.6 °F (2.0 °C) at the beginning of snowfall and remains at about 33.3 °F (0.7 °C) until the heating system is started at 10:00 am. From this time, the bridge average surface temperature rises slightly as heat fluxes from the pipes increase. Although no snow-free areas (striping) are detected, melting starts from the lower surface of the snow layer during this period. These temperatures appear slightly above freezing point as the sensors are slightly below the top surface, as noted above, and heat fluxes are upwards.

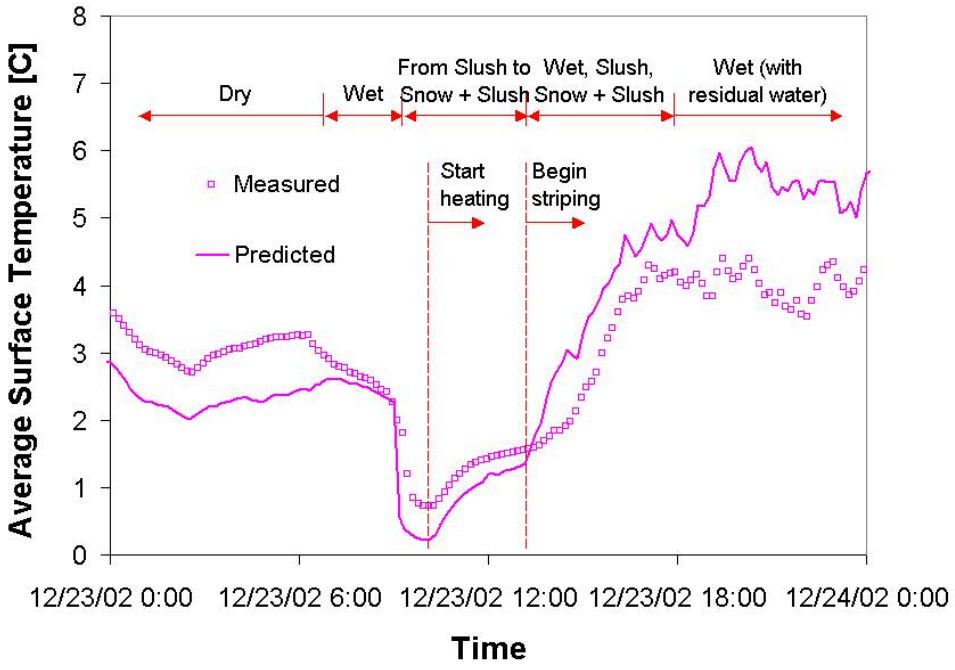

Figure 4-9 Comparison of measured and predicted bridge average surface temperature. Surface temperatures shown are from sensors 10mm below the top surface and at corresponding points in the model.

Snow starts to clear from the surface at approximately 12.30 pm. This is illustrated in the first of the images shown in Figure 4-10 taken at 12.38 pm when the snow free area is estimated as 0.05 (5% of the surface clear). Average temperatures then rise as part of the surface is cleared of snow – the average temperature being that of portions of wet, slush and snow covered regions. As more snow clears the rate of average surface temperature rise increases. Snow is found to have cleared completely at approximately 5 pm.

During initial dry conditions, the surface temperature is determined by the heat balance between the convective and longwave radiative heat fluxes on the surface. Differences between measured and predicted surface temperatures are 1.3 °F (0.7 °C)[3] in this period. Uncertainties of relevance in the modeling of these conditions are the values of surface properties and convection coefficients. Experimental uncertainties of concern are the measurement of surface temperatures and weather conditions. Of the weather measurements probably it is the local wind speed that is most likely to vary from measurements at the weather station. Previous measurements of surface properties and sky temperatures using the net radiometer limit the uncertainty in radiant fluxes so that the chief concern is the uncertainty of the convective fluxes. Calculation of convective fluxes may be in error due the limitations of the applicability of correlations derived for flat plates to the bridge geometry (the bridge is significantly exposed on three sides).

[3] Differences between measured and predicted temperatures are RMS values over the period discussed.

Initial snowfall + 3 hours, 38 minutes

Observed SFAR: 0.05; Predicted SFAR: 0

Initial snowfall + 5 hours, 8 minutes

Observed SFAR: 0.4; Predicted SFAR: 0.3

Initial snowfall + 6 hours, 8 minutes

Observed SFAR: 0.6; Predicted SFAR: 0.5

Initial snowfall + 8 hours, 8 minutes

Observed SFAR: 1; Predicted SFAR: 0.8

Later drifting of snow onto the heated area.

Figure 4-10 Images of bridge surface condition taken by a digital camera along with estimates of snow free area ratio. The last image shows drifted snow on the heated surface after snowfall.

Differences in surface temperature predictions during ‘wet’ conditions are limited to 0.4 °F (0.2 °C). In these wet conditions the surface is driven close to the ambient temperature because of the direct contact of the rainfall, which is assumed to be at the ambient temperature.

At the beginning of snowfall, the surface was observed to be in the slush condition because the snowflakes falling on the bridge were saturated immediately with the residual water on the bridge surface. As the mass balance of the water is not calculated but is assumed to run off at each time step, the sensible heat of residual water is not considered in following time steps. This may account for the drop in temperature predicted at the start of snowfall being more rapid than that measured, and the average surface temperature being 0.9 °F (0.5 °C) lower than measured data. These errors become less significant as snow melting progresses.

As melting has progressed so that stripes appear and as the measured and predicted snow free area ratio increases until snow clearance is achieved, surface temperatures are over-predicted and differences increase to 1.4 °F (0.8 °C). In addition to the noted uncertainties in the value of convection coefficients, the most significant experimental uncertainty is in the measurement of snowfall rate, which is estimated as ±10%. The effects of this uncertainty are discussed in the following section. Surface temperatures are also over predicted in the later period when the surface is clear of all ice but remains wet. Differences between measured and predicted average surface temperatures increase to 2.7 °F (1.5 °C). This is thought to be due to the fact that the model assumes all water runs-off immediately whereas evaporation of residual water will in fact absorb some heat from the slab. Furthermore, it has been observed that some snow drifted from unheated surrounding regions to the heated portion of the bridge deck (see Figure 4-10).

As a check on the effects of residual water on the surface temperature calculation, a modified weather data has been created with a “fictitious” rainfall of 0.5 mm/hr that keeps the surface wet from the ending time of the measured snowfall to the time when the surface is completely dry. This causes the model to calculate the heat loss due to evaporation on the bridge surface. Figure 4-11 shows a comparison between predicted average surface temperatures with and without the fictitious rainfall. As shown in this figure, the added fictitious rainfall leads to significant improvement in the prediction of the average surface temperature. The RMS error between the measured and predicted temperature in this time period is reduced from 2.6 °C to 1.5 °C. Since it is assumed in this model that the rainfall quickly run off the bridge surface and only a thin film of water will exist on the bridge surface, the rate of the fictitious rainfall does not make a significant difference in the simulation results.

The time required to completely dry the bridge surface depends on the weather condition after snowfall, drainage condition of the bridge surface, etc. Therefore, it is not now possible to give a general rule for the lasting period of the fictitious rainfall and no change to the model has been made. With additional experimental testing, it might be possible to give a reasonable fixed period of time, post-snowfall, for which the surface could be kept wet in the model.

The rest of the difference is thought due to the snow drifted from unheated surrounding regions to the heated portion of the bridge deck (see Figure 4-10). Further

research may be needed to estimate the amount of the drifted snow and take account it into the model.

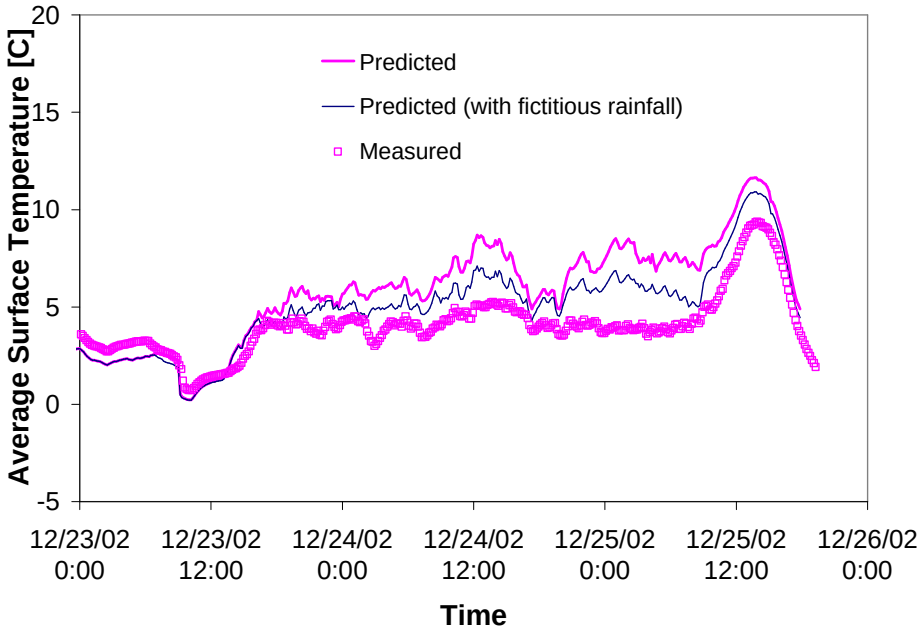

Figure 4-11 Comparison between predicted average surface temperatures with and without adding the fictitious rainfall, which has a constant rate of 0.5 mm /hr.

4.2.3.2. Surface Conditions

Figure 4-10 shows some of the digital images of the bridge surface during the snow melting process from which snow-free area ratios (A_r) have been estimated. The variation of snow free area ratio during the snow event is shown in Figure 4-12 along with the rate of precipitation. As previously stated, the snow free area ratio was estimated by examining images of the bridge surface taken during the snow event by a digital video system. Although the two extreme surface conditions: fully snow-covered (A_r = 0) and

completely snow-free (A_r = 1) can be clearly identified from the images, there are some uncertainties in estimating the snow free area ratio when the surface condition is in the middle of the two extremes. It is estimated that the uncertainty is less than ±0.1, which has been indicated in Figure 4-12 by error bars.

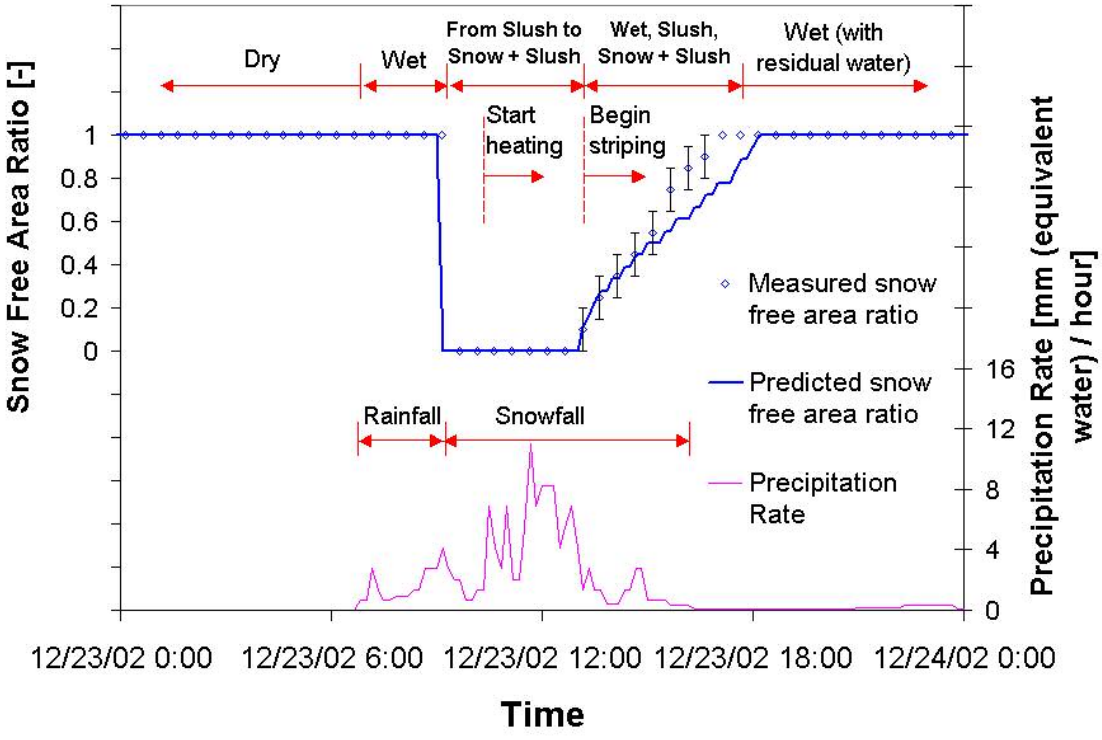

Figure 4-12 Comparison of measured and predicted snow free area ratio along with the precipitation rate.

It has been noted above that during the initial hour of snowfall the surface temperatures drop quickly and some melting occurs as the pavement top surface is initially above freezing point. As the rate of precipitation rapidly increases the surface becomes completely snow covered (A_r = 0). The model provides indications of surface condition by various flags shown in the output. This, in addition to the trends in surface

temperature and snow free area ratio, shows that the correct sequence of changes in surface condition are predicted: the sequence of conditions being dry; wet; slush; snow and slush; partial clearance; complete snow clearance. The model is limited in its ability to predict the final wet condition (after melting but without rain) due to water being assumed to run off immediately – this has been noted above.

One of the prime concerns, when using the model to study safety and control of the system, is the onset and completion of snow clearance. This is indicated by the snow-free area ratio raising above 0.0 and progressing towards 1.0. The result shown in Figure 4-12 shows that the onset of snow cover and start of snow clearance (striping) are matched to the measurements to within one half hour[4]. Predictions of snow-free area ratio are very close to those measured in the range 0.0-0.5. There are more noticeable differences in the range 0.5-1.0 so that the final point of snow clearance is predicted one and half hour later than that observed. The model, being quasi-2D, does not allow consideration of lateral heat transfer in the snow and slush layer. It is possible that lateral heat transfer is taking place as the stripes become more pronounced at this stage and melting accelerated.

In the prediction of surface conditions, the main experimental uncertainty is in the measurement of snowfall rate as the accuracy of the tipping bucket gauge is limited to

[4] The values from the calculations do not change smoothly as there are a modest number of cells across the surface (18) and it may require a number of time steps before certain cells become snow free. The proportion of snow free cells consequently does not change smoothly.

±10%. Figure 4-13 shows a sensitivity analysis with the snowfall rate assumed 10% higher than measured and 10% lower than that recorded. Increasing the snowfall rate by 10% will reduce the discrepancies between the predicted and measured average surface temperature by 0.9 °F (0.5 °C) but also result in about one more hour time lag in predicting the variation of snow-free area ratio. Decreasing the snowfall rate by 10% has the effect of more accurately predicting complete snow clearance but bringing forward the predicted start of snow clearance. The rate of snow clearance is very similar in each case. This can be expected since this is essentially limited, at this point in the storm, by the heat input to the bridge. It is reasonable to say then that the predictions of snow-free area ratio fall within the bounds of experimental error. The accuracy shown would be satisfactory for system design and performance evaluation tasks.

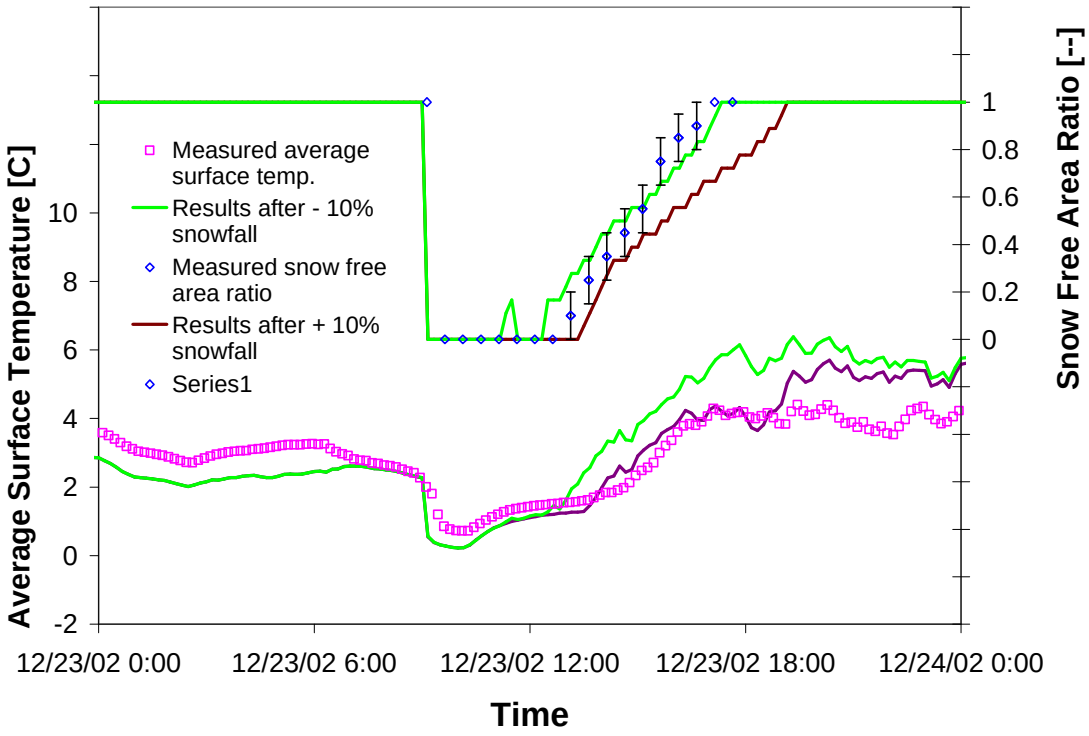

Figure 4-13 Effect of snowfall rate on the model predictions of snow-free area ratio and average surface temperature.

4.2.3.3. Fluid Temperature

The model has been implemented so that the heat source is specified in terms of a specified fluid inlet temperature and mass flow rate. This is the most convenient formulation for the simulation of the whole hydronic system along with the heated bridge deck. Since the heat provided to the slab is indicated by the difference between the inlet and outlet fluid temperature, the prediction of the outlet fluid temperature is important to the validation exercise.

Figure 4-14 shows the comparison between the predicted and measured outlet fluid temperatures. The inlet fluid temperature is also included in the figure to indicate the overall heat balance. The control system is designed to maintain the average bridge surface temperature at 40 °F (4.4 °C) during the storm. The system output is modulated by switching the heat pump on and off intermittently. The intermittent operation of the system can be observed in this figure at the point where the surface is completely clear of snow and surface temperatures rises. Figure 4-14 demonstrates that the predicted exiting fluid temperatures match the measured data satisfactorily, except for some discrepancies at the beginning of the heating operation. The discrepancies are thought due to the coarse approximation of the round tube by the rectangular grid system applied in the finite difference solution domain (Chiasson, *et al*. 2000). The RMS error during the entire heating operation is 1.4 °F (0.8 °C). Given the difference between the fluid temperatures

during the heating operation is approximately 18 °F (10 °C), this corresponds to an 8% over-prediction of the overall heat transfer.

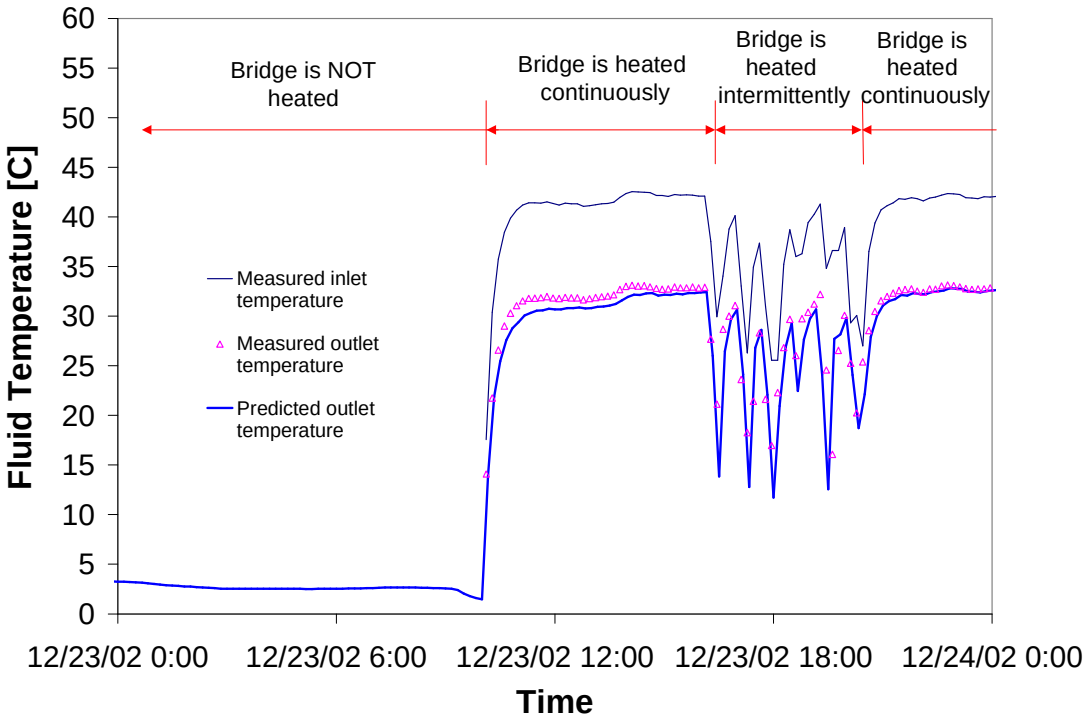

Figure 4-14 Comparison between measured and predicted bridge exiting fluid temperature.

4.3. Conclusions

A model of the transient snow melting process occurring on heated pavement surfaces has been developed. This model has been used, along with a two-dimensional finite difference representation of a hydronically heated concrete pavement, to simulate the operation of a bridge deck de-icing system under winter storm conditions. Given system heat fluxes and weather data, this model can predict the surface conditions and temperatures over the heated surface including the degree of snow cover. This model is

computationally efficient while retaining sufficient accuracy and therefore can be used in the design and optimization of the hydronic snow melting system, which may require multi-year simulations of the system.

The predictions of this model have been validated with corresponding measured data of an experimental hydronic bridge snow melting system for several snow events. Measurements of several crucial parameters of the experimental bridge deck and weather data have been conducted to provide accurate information to the model. Validation results show that the model predictions favorably match the corresponding measured data and it can be used to successfully estimate the surface conditions during the snow melting process.

The model developed in this chapter may be used in conjunction with weather forecasting models to predict when icy conditions may occur on bridges. This may be used in a range of applications including planning of conventional snow and ice removal operations and control of other types of anti-icing applications.

CHAPTER 5. SIMULATION OF GSHP BASED HYDRONIC SNOW MELTING SYSTEMS

Ground source heat pump (GSHP) systems use the ground as a heat source to extract heat for heating applications and as a heat sink to reject heat for cooling applications. This kind of system usually offers higher energy efficiency than other heating equipment, such as boilers and electrical heaters. As a result, it has been proposed as a heat source for hydronic snow melting system in a recent research project funded by Federal Highway Administration (FHWA) (Spitler, et al. 1999). Figure 5-1 shows a conceptual diagram of such a system. This system consists of hydronic tubing embedded in the bridge deck with heated fluid circulated from a number of water-to-water heat pumps that, in turn, extract heat from the ground via vertical U-tube borehole heat exchangers. In summer, the solar radiation could be collected with the deck and stored in the ground to replenish the energy extracted during winter. The system is controlled so that it can automatically start up the system depending on the predicted arrival time of freezing weather conditions at the bridge site, and then control the heat pump operation to keep the bridge surface temperature in the desired range.

There are several challenges in designing such systems. First, the long-term changes in performance of the ground heat exchangers need to be considered. It is usually necessary to model the performance of the ground heat exchangers over the lifetime of

the project in order to ensure an adequate design. It is accordingly necessary to consider, not static design conditions, but the time varying nature of heating loads over these periods. Similarly, the large thermal mass of the bridge deck and the widely varied weather conditions require that transient performance of a snow melting system be considered. Proper consideration of these complexities requires some reliance on system simulation in the design process.

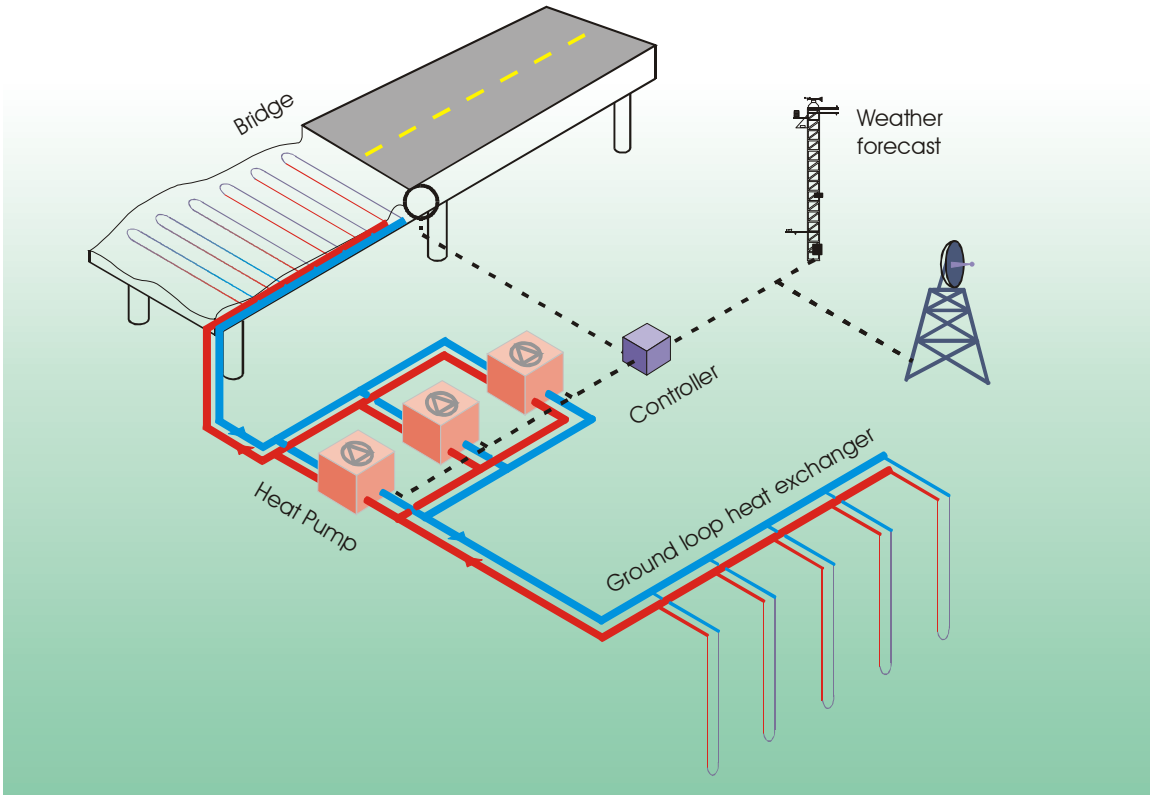

Figure 5-1 Conceptual diagram of the GSHP based hydronic bridge snow melting system. (From progress report of the Oklahoma State University Geothermal Smart Bridge Project)

In this chapter, the implementation of a simulation program for the GSHP based hydronic snow melting system will be discussed along with the experimental validation of the simulation results.

5.1. Component Models of the System Simulation

In order to simulate the GSHP based hydronic snow melting system it is necessary to model the following system components:

- Hydronically-heated slab, which is the pavement of the bridge deck
- Ground-loop heat exchanger
- Water-to-water heat pump
- System controller
- Circulating pump

The model of the hydronically-heated slab has been described in detail in Chapter 4; therefore, only models of the ground loop heat exchanger, water-to-water heat pump, system controller, and circulating pump will be presented in this section. More detailed documentation of each component model is given in Appendix A.

5.1.1. Ground Loop Heat Exchanger

Vertical ground loop heat exchangers are used in the GSHP based snow-melting system. This type of ground loop heat exchanger consists of a single borehole or a group of boreholes. A loop of pipe with a 'U' bend at the bottom (usually called U-tube) is inserted in each borehole. The borehole is either back-filled or, more commonly, grouted over its full depth. Grouting is normally required to prevent contamination of the ground water and give better thermal contact between the pipe and the ground.

The model of the ground loop heat exchanger (GLHE) used in the simulation is an updated version of that originally developed by Yavuzturk and Spitler (1999b). It is based on dimensionless, time-dependent temperature response factors known as "g-functions", which represent the temperature response at borehole wall to a single step heat pulse. The g-functions originally calculated by Eskilson (1987) are only valid on large time scale (usually more than a month) and therefore called long-term g-functions. Yavuzturk and Spitler (1999a) extended the g-functions to shorter time scale (less than a hour), which are referred as short-term g-functions. The g-functions for various borehole field geometries are different and need to be pre-calculated with special computer programs (Eskilson 1987; Yavuzturk and Spitler 1999a). The pre-calculated g-functions are used as parameters of the GLHE model.

To improve the computational efficiency, the original model has been updated by revising the solution-solving method and incorporating a hierarchical load aggregation algorithm. These revisions will be discussed below.

5.1.1.1. Explicit Solution

The g-function based GLHE model is formed with three coupled equations, which are used to determine the ground load, outlet fluid temperature, and average fluid temperature, respectively.

The normalized ground load (QN), which is the heat rejection/extraction intensity on the ground loop heat exchanger, is given by Equation (5-1):

$$QN_n = \frac{\dot{m} \cdot C_{fluid} \cdot (t_{fluid\_out} - t_{fluid\_in})}{H \cdot N_{borehole}} \tag{5-1}$$

where,

QN_n : normalized ground load at the n^{th} time step, Btu/ (hr-ft) or (W/m)

$\dot{m}$: fluid mass flow rate in GLHE, lb/s or (kg/s)

C_{fluid} : specific heat of heat carrier fluid in GLHE, Btu/(lb-°F) (J/kg-°C)

H : borehole depth, ft (m)

t_{fluid_out} : fluid temperature at the outlet of GLHE, °F (°C)

t_{fluid_in} : fluid temperature at the inlet of GLHE, °F (°C)

$N_{borehole}$: number of boreholes of the GLHE

The outlet fluid temperature is computed from average fluid temperature (t_{fluid_avg}) using Equation (5-2):

$$t_{fluid\_out} = t_{fluid\_avg} + \frac{QN_n \cdot H \cdot N_{borehole}}{2 \cdot \dot{m} \cdot C_{fluid}} \tag{5-2}$$

The average fluid temperature (t_{fluid_avg}) is calculated in two steps. The first step is to calculate the average borehole wall temperature by decomposing the ground load into a series of step heat rejection/extraction pulses, and superimposing the responses of the average borehole wall temperature to each step pulse. The second step is to calculate the average fluid temperature from the average borehole wall temperature and the borehole resistance. As a result, the average fluid temperature (t_{fluid_avg}) at the end of the n^{th} time step is given by Equation (5-3):

$$t_{fluid\_avg} = t_{ground} - \sum_{i=1}^{n} \frac{(QN_i - QN_{i-1})}{2 \cdot \pi \cdot k} g\left(\frac{\theta_n - \theta_{i-1}}{\theta_s}, \frac{r_b}{H}\right) - QN_n \cdot R_{borehole} \tag{5-3}$$

where,

t_{ground} : undisturbed ground temperature, °F (°C)

θ : time, (s)

θ_s : time constant, which is defined by $t_s = \frac{H^2}{9\alpha}$, (s). α is the diffusivity of the ground.

r_b : borehole radius, ft (m)

k : ground thermal conductivity, Btu/ (hr-ft-°F) or (W/m-°C)

$R_{borehole}$: borehole thermal resistance, °F/(Btu/hr-ft) or K/(W-m)

The solutions of t_{fluid_out}, QN_n and t_{fluid_avg} were solved in an iterative manner in the original model. However, since the difference between t_{fluid_out} and t_{fluid_in} is usually less than 18°F (10 °C) and there is no significant change of C_{fluid} within such a small range, it is accurate enough to use C_{fluid} evaluated at t_{fluid_in} in the calculations. Therefore, there are only three unknowns in the three linearly independent equations and they can be solved explicitly. This significantly reduces the computational time. The explicit solution of the normalized ground load at the n^{th} time step (QN_n) has been derived and given in Equation (5-4). The corresponding solutions of t_{fluid_avg} and t_{fluid_out} can then be obtained by substituting QN_n into Equation (5-3) and (5-2) subsequently.

$$QN_n = \frac{t_{ground} - \sum_{i=1}^{n-1} \frac{(QN_i - QN_{i-1})}{2 \cdot \pi \cdot k} g\left(\frac{\theta_n - \theta_{i-1}}{\theta_s}, \frac{r_b}{H}\right) + \frac{QN_{n-1}}{2 \cdot \pi \cdot k} g\left(\frac{\theta_n - \theta_{n-1}}{\theta_s}, \frac{r_b}{H}\right) - t_{fluid\_in}}{R_{borehole} + \frac{1}{2 \cdot \pi \cdot k} g\left(\frac{\theta_n - \theta_{n-1}}{\theta_s}, \frac{r_b}{H}\right) + \frac{H \cdot N_{borehole}}{2 \cdot \dot{m} \cdot C_{fluid}}} \quad (5\text{-}4)$$

5.1.1.2. Hierarchical Load Aggregation

Because the effect of any given ground load on the performance of the GLHE decreases as time goes by, it is possible to aggregate the previous loads into average values over multi-time-step intervals. This improves computational efficiency by reducing the number of terms involved in the superposition. In the original model developed by Yavuzturk and Spitler (1999b), a monthly load aggregation algorithm was implemented. It aggregated hourly ground loads into a block every 730 hourly simulation

time steps (approximate equal to 1 month). In order to reduce the error from aggregating the hourly loads, a minimum “waiting period” of 192 hours was used in the monthly load aggregation algorithm so that the loads would not be aggregated until an additional 192 hours passed after the 730 hourly time steps. It thus ensured that at least 192 hourly loads would be superposed in the computation of the current average borehole wall temperature.

To further improve the computational efficiency, an algorithm of hierarchical load aggregation has been implemented. It can aggregate ground loads into blocks of different time intervals, hence the term “hierarchical”. Currently, there are three different aggregation blocks (“small”, “medium”, and “large”) employed in the hierarchical load aggregation algorithm. In order to reduce the error when aggregating individual loads (or, smaller load blocks) to a bigger load block, a “waiting period” is specified for each level of load aggregation. An operation of load aggregation can only be processed after enough loads (or, smaller load blocks) have been accumulated to compose a bigger load block, and the “waiting period” for this level of load aggregation has been passed. The hierarchical load aggregation procedure at a given simulation time step is as follows:

- Calculate the time difference between the current simulation time and the ending time of last “small” load block. If no loads have been aggregated, the time difference is just the current simulation time.
- Check whether the time difference exceeds the defined size of the “small” load block.

- If true, then
  - ✓ Calculate the average value of the individual loads (since the time step size could be varied during the simulation, the time-period-weighted average is used)
  - ✓ Reset the ending time of the last “small” load block
  - ✓ Signal that a new “small” load block is available

- Calculate the time difference between the current simulation time and the ending time of the last “small” load block. Check whether the time difference exceeds the specified waiting period and there is a new “small” load block available.
  - If true, then
    - ✓ Increase the number of the “small” load blocks
    - ✓ Update the history of the “small” load blocks, which is recorded by the time period and the aggregated load of each “small” load block
    - ✓ Update the number and history of the individual loads
- Count the accumulated number of the “small” load blocks. Check whether the accumulated number exceeds the required value for composing a “medium” load block.
  - If true, then
    - ✓ Calculate the time-period-weighted average value of the “small” aggregated loads
    - ✓ Reset the ending time of the last “medium” load block
    - ✓ Signal that a new “medium” load block is available

- Count the accumulated number of the “small” load blocks. Check whether the accumulated number exceeds the required value before aggregating a “medium” load block period and there is a new “medium” load block available.
    - If true, then
        - ✓ Increase the number of the “medium” load blocks
        - ✓ Update the history of the “medium” load blocks, which is recorded by the time period and the aggregated load of each “medium” load block
        - ✓ Update the history of the “small” load blocks
- Count the accumulated number of the “medium” load blocks. Check whether the accumulated number exceeds the required value for composing a “large” load block.
    - If true, then
        - ✓ Calculate the time-period-weighted average value of the “medium” aggregated loads
        - ✓ Reset the ending time of the last “large” load block
        - ✓ Signal that a new “large” load block is available
- Count the accumulated number of the “medium” load blocks. Check whether the accumulated number exceeds the required value before aggregating a “large” load block period and there is a new “large” load block available.
    - If true, then
        - ✓ Increase the number of the “large” load blocks

- ✓ Update the history of the "large" load blocks, which is recorded by the time period and the aggregated load of each "medium" load block
- ✓ Update the history of the "medium" load blocks

After hierarchically aggregating the preceding loads, Equation (5-3) becomes:

$$
\begin{aligned}
t_{fluid\_avg} = t_{ground} &+ \sum_{i=1}^{n} \frac{(QN_i - QN_{i-1})}{2 \cdot \pi \cdot k} g\left(\frac{\theta_n - \theta_{i-1}}{\theta_s}, \frac{r_b}{H}\right) \\
&+ \sum_{j=1}^{n\_small} \frac{(\overline{QN}_{small\ j} - \overline{QN}_{small\ j-1})}{2 \cdot \pi \cdot k} g\left(\frac{\theta_{small\ n\_small} - \theta_{small\ j-1}}{\theta_s}, \frac{r_b}{H}\right) \\
&+ \sum_{k=1}^{n\_medium} \frac{(\overline{QN}_{medium\ k} - \overline{QN}_{medium\ k-1})}{2 \cdot \pi \cdot k} g\left(\frac{\theta_{medium\ n\_medium} - \theta_{medium\ k-1}}{\theta_s}, \frac{r_b}{H}\right) \\
&+ \sum_{l=1}^{n\_large} \frac{(\overline{QN}_{large_l} - \overline{QN}_{large_{l-1}})}{2 \cdot \pi \cdot k} g\left(\frac{\theta_{large\ n\_large} - \theta_{large\ l-1}}{\theta_s}, \frac{r_b}{H}\right) + QN_n R_{borehole}
\end{aligned}
\tag{5-5}
$$

where,

QN_i : i^{th} individual ground load, Btu/ (hr-ft) or (W/m)

$\overline{QN}_{small\ j}$: average ground load in j^{th} "small" block, Btu/ (hr-ft) or (W/m)

$\overline{QN}_{medium\ k}$: average ground load in k^{th} "medium" block, Btu/ (hr-ft) or (W/m)

$\overline{QN}_{large_l}$: average ground load in l^{th} "large" block, Btu/ (hr-ft) or (W/m)

θ_i : beginning time of i^{th} individual ground load, (s)

$\theta_{small\ j}$: beginning time of j^{th} "small" block, (s)

$\theta_{medium\ k}$: beginning time of k^{th} "medium" block, (s)

θ_{large_l} : beginning time of l^{th} "large" block, (s)

n : number of individual ground loads

n_small : number of “small” blocks

n_medium : number of “medium” blocks

n_large : number of “large” blocks

The selection of the size and corresponding “waiting period” for each level of the aggregation block will affect the total number of loads involved in the superposition, and subsequently, the computational efficiency of the model. In the current hierarchical load aggregation algorithm, the size of a “small” load block is 24 hours and the “waiting period” is 12 hours. A “medium” load block is composed of 5 “small” load blocks and the “waiting period” is 3 “small” load blocks. A “large” load block is composed of 73 “medium” load blocks and the “waiting period” is 40 “medium” load blocks. Although this set of parameters is by no means the optimal combination, it leads to significant reduction in the total number of loads involved in the superposition and improvement in computational efficiency. As indicated in Table 5-1, at the end of a 20-year hourly simulation, the total number of load blocks involved in the superposition using the hierarchical load aggregation algorithm is only 12% of that using the monthly load aggregation algorithm, which results in a 20% reduction in computational time.

To evaluate the error resulting from load aggregation, the exiting fluid temperatures of a GLHE predicted with models using hierarchical and monthly load aggregation algorithms were compared with that predicted with the model that did not have any load aggregation. To eliminate the masking effects of time-varing loads imposed on the GLHE, constant loads over a period of 20 years but with hourly time

steps have been used in the simulations of GLHE. The temperature differences between simulation results using the two aggregation methods and a simulation result without load aggregation are shown in Figure 5-2. As can be seen in this figure, the temperature difference resulting from the hierarchical load aggregation is almost identical with that from the monthly load aggregation. The temperature differences do not exceed the bound of ±0.0027 ˚F (±0.0015 ˚C).

TABLE 5-1 Comparison of Total Number of Loads Involved in the Load Superposition at the End of 20 Years Hourly Simulation

	Number of hourly loads	Number of Small blocks	Number of Medium blocks	Number of large blocks	Total number of loads for superposition
Hierarchical load aggregation	24	4	72	19	119
Monthly load aggregation	730	239	0	0	969
Without load aggregation	175200				175200

It should be noted that load aggregation algorithms should not affect the predictions of exiting fluid temperature of GLHE if constant loads are imposed on the GLHE, which means the temperature difference should be zero. The temperature differences observed in the above figure are due to numerical error in the loop temperature calculation.

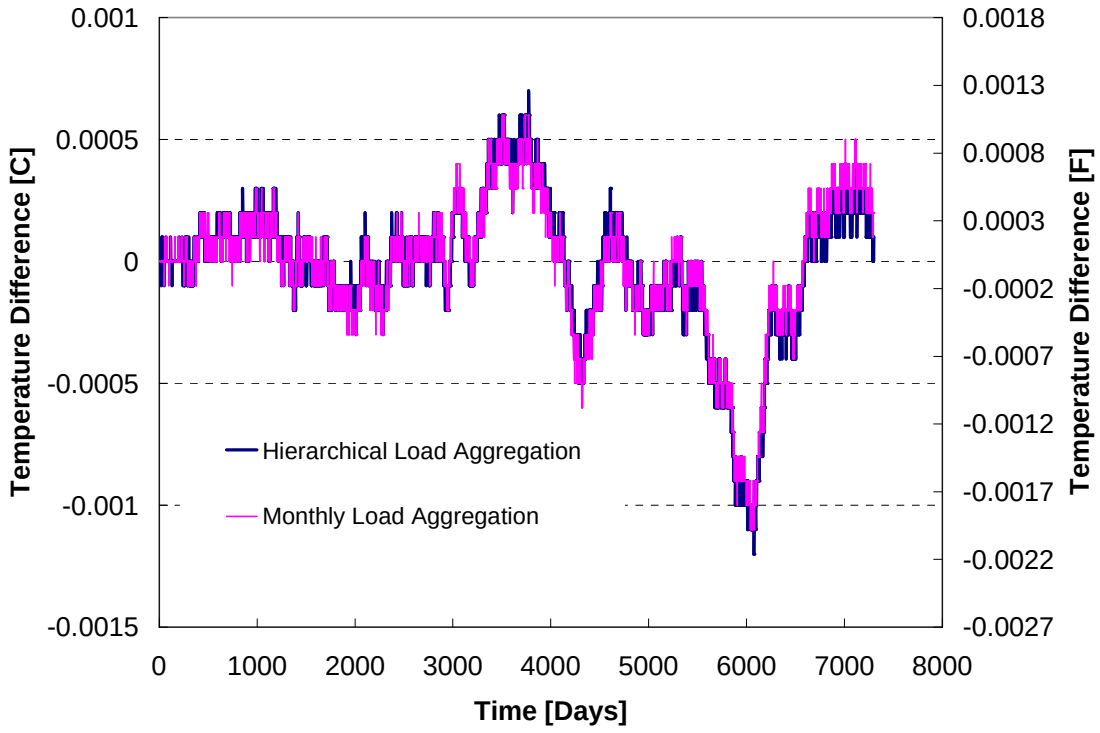

Figure 5-2 Temperature differences between the predicted GLHE exiting fluid temperature without using load aggregation and that using monthly load aggregation and hierarchical load aggregation.

5.1.2. Water-to-water Heat Pump

A parameter-estimation-based water-to-water heat pump model developed by Jin and Spitler (2002a and 2002b) has been revised and used in the system simulation. This model uses a thermodynamic analysis of the refrigeration cycle, simplified models for heat exchangers and compressor. This model can also account for the effects of antifreeze solutions being used as secondary heat transfer fluids. The parameters of the model are estimated from the manufacturers' catalog data by applying a multi-variable optimization algorithm. Once the optimal values of the parameters have been determined, the model

can accurately simulate the performance of the particular heat pump over its full operating range.

For a large bridge deck, a number of heat pumps may be necessary. To simplify the simulation of such a multiple heat pump system, the single water-to-water heat pump model was expanded to represents several pairs of serially connected heat pumps (Ramamoorthy 2001). As shown in Figure 5-3, the two heat pumps in a pair have their source sides in parallel and load sides in series. The number of operating heat pump pairs will be controlled following specified control strategies.

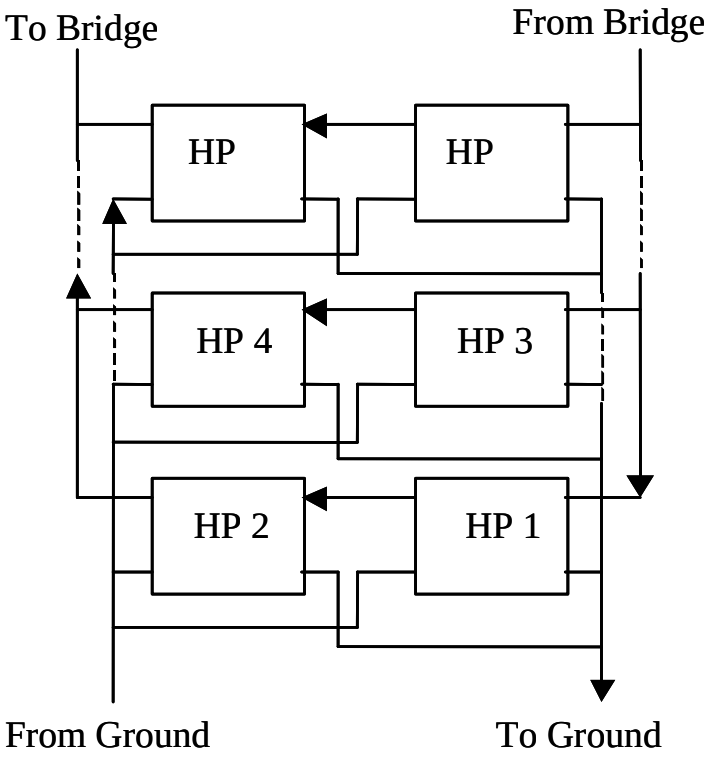

Figure 5-3 Schematic showing the arrangement of heat pump pairs.

5.1.3. System Controller

To effectively use energy in snow melting, the GSHP system needs to be properly controlled. Once the GSHP system is activated, the general approach of control is to measure the bridge deck surface temperature, and then modulate heat output of the GSHP system according to the measurements following specified control strategy. A model of a linear proportional controller has been implemented and used in the system simulation. This controller will turn on the GSHP system a certain number of hours in advance of the snowfall by looking ahead in the weather file[5]. Then, it will adjust the number of operating heat pump pairs according to the difference between the measured average bridge deck surface temperature (t_{surf_mea}) and the preset upper and lower limits (t_{surf_upper}, t_{surf_lower}) until the bridge surface is clear from snow and ice. If t_{surf_mea} is greater than t_{surf_upper}, only one pair of heat pumps will be operated; If t_{surf_mea} is less than t_{surf_lower}, all the heat pump pairs will be put into operation. For any value of t_{surf_mea} between the upper and lower limits, the number of operating heat pump pairs (N_HP) is determined by following linear interpolation:

$$N\_HP = \frac{N\_HP_{\max} \cdot \left(t_{surf\_upper} - t_{surf\_mea}\right)}{\left(t_{surf\_upper} - t_{surf\_lower}\right)} \tag{5-6}$$

where,

$N\_HP_{\max}$: total number of heat pump pairs in the GSHP system

[5] This is an ideal representation of a forecasting controller, which can turn on the system according to the forecast of freezing precipitations. Development of such a controller is the focus of another part of the Geothermal Smart Bridge project (Jenks, et al. 2003).

The result of N_HP will be rounded off to the next successive integer when it has a fractional value. Figure 5-4 shows an example of the relationship between the number of operating heat pump pairs and the average surface temperature.

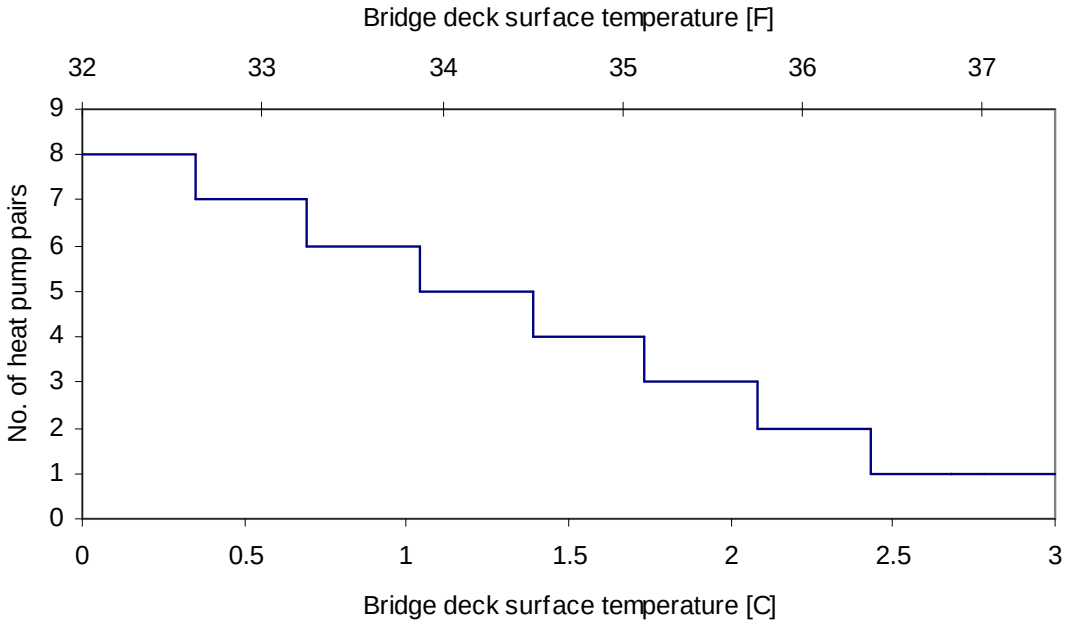

Figure 5-4 An example of the relationship between the number of operating heat pump pairs and the average surface temperature.

The controller also controls the recharge operation of the system following specified control strategies. Since the control strategy will affect both the benefits obtained from the recharge operation and the corresponding pumping power consumption, it needs to be optimized.

5.1.4. Circulating Pump

The circulating pump model used in the system simulation is a simple pump model. It computes power consumption for pumping and the fluid temperature rise using fluid mass flow rate, pressure rise across the pump, and the pump efficiency. The pump power consumption (P) and fluid temperature at the outlet of pump (t_{fluid_out}) are computed using relation (5-7) and (5-8), respectively.

$$P = \frac{\Delta P \cdot \dot{m}}{\rho \cdot \eta} \tag{5-7}$$

$$t_{fluid\_out} = t_{fluid\_in} + \Delta P \left(\frac{\frac{1}{\eta} - 1}{\rho \cdot C_p} \right) \tag{5-8}$$

where,

ΔP : pressure drop across the pump (kPa)

t_{fluid_in} : fluid temperature at the inlet of pump, °F or (°C)

$\dot{m}$: fluid mass flow rate, lb/s or (kg/s)

ρ : fluid density, lb/ft^3 or (kg/m^3)

C_p : fluid specific heat, Btu/(lb-°F) (J/kg-°C)

η : pump efficiency, (-)

5.2. Implementation of the System Simulation

A system simulation can be implemented by combining all the component models together and solving the systems of differential and algebraic equations (DAE) that represent the behavior of the system. There are several component based simulation environments, under which the system simulation might be implemented in this way. HVACSIM+ is one of the component based simulation environments. It provides not only tools to integrate pre-programmed component models into system models but also a solver to solve the systems of differential and algebraic equations. It has been selected for the simulation of the GSHP based hydronic snow melting system because of its attractive features, such as the advanced equation solving techniques, hierarchical structure, and variable time step approach.

In this section, a brief overview of HVACSIM+ will be given with emphasis on its features. Then, some issues related to implementing the system simulation under the environment of HVACSIM+ will be discussed. These include the method for handling the discrete controller and the algorithm for coupling the hydronic calculation with the thermal calculation.

5.2.1. Overview of HVACSIM+

HVACSIM+ is a public domain dynamic simulation program developed at the National Institute of Standards and Technology (NIST). Detailed information of

HVACSIM+ was documented primarily in three publications: a reference manual (Clark, 1985), a user guide (Clark and May, 1985), and a report on building loads calculation (Park et al. 1986). In this section, some important features of HVAVSIM+ will be reviewed in brief.

5.2.1.1. Advanced Equation Solving Techniques

The solver of HVACSIM+ is called MODSIM. It employs a simultaneous nonlinear equation-solving package called SNSQ, which is based on the Powell's hybrid method (Powell 1970), to solve the system of nonlinear algebraic equations. The Powell's hybrid method is a combination of the quasi-Newton method and the steepest method. By automatically adjusting the steps in the solution searching process, this method provides a good compromise between the speed of Newton's method and the guaranteed convergence of steepest descent. MODSIM uses a variable time step and variable order Gear algorithm (Brayton et al. 1972), which is an extension of the Gear (1971) algorithm, to solve the stiff ordinary differential equations. Using it to solve sets of ordinary differential equations can significantly reduce the computational time required for dynamic simulations.

5.2.1.2. Hierarchical Structure

HVACSIM+ is hierarchical in the sense that a system simulation can be constructed with UNITs, BLOCKs and SUPERBLOCKs. The UNIT is the lowest level in the hierarchical structure of HVACSIM+. It represents a component model of HVAC or control systems, or a building element. One or more units form a BLOCK. The connections between the units define a set of differential and algebraic equations that need to be solved simultaneously by MODSIM. One or more BLOCKs constitute a SUPERBLOCK, which is the highest level of the hierarchical structure provided by HVACSIM+. Connections between the blocks in a SUPERBLOCK also define a system of simultaneously solved equations. However, equations in different SUPERBLOCKs are not simultaneously solved. The coupling between SUPERBLOCKs is implemented by transferring information of the coupled variables from one SUPERBLOCK to another SUPERBLOCK sequentially at each time step. This hierarchical structure allows partitioning a large set of equations into several smaller subsets, and therefore reduces the number of simultaneously solved equations and improves the computational efficiency of the solver.

The BLOCK/SUPERBLOCK structure of a simulation will affect the convergence properties of the equation solver since it will determine the sets of equations to be solved simultaneously. This fact limits the flexibility of simulation constructions and thus special care must be taken when constructing a simulation, especially when control loops are involved. The partitioning of a system into blocks and superblocks is

left to the user and it depends upon the nature of the system and the type of interactions among its various components. The practice of constructing the simulation of the GSHP based hydronic snow melting system will be introduced in section 5.2.2 and 5.2.3.

5.2.1.3. Variable Time Step Approach

The MODSIM program incorporates two different types of time steps, namely, the fixed time step (FTS) and the variable time step (VTS). The variable time step approach is a unique feature of HVACSIM+. When an ordinary differential equation is integrated by MODSIM, the simulation time step will be dynamically changed between the preset minimum and maximum values during the integration process. The variable time step approach is intended to prevent numerical instabilities resulting from relatively large time steps when the system is unsteady, and to save computational time after the system becomes stabilized. To apply the variable time step approach, there must be at least one ordinary differential equation solved by MODSIM. If all the ordinary differential equations are solved inside the component models[6], the maximum time step will be used in the simulation.

The time steps for each SUPERBLOCK are determined independently (excluding the superblock for the building shell). To synchronize the time steps of each

[6] HVACSIM+ is designed to solve user-specified sets of differential-algebraic equations. Ordinary differential equations may be specified by the user and solved by HVACSIM+. However, it is possible, and probably necessary, to solve partial differential equations (e.g. temperature field in bridge deck slab) internally.

SUPERBLOCK, a SUPERBLOCK input scanning option (INSOPT) is provided by HVACSIM+. When this option is selected, all SUPERBLOCK inputs are scanned after each time step. If the variation of inputs to a SUPERBLOCK that was not called during the time step is beyond an error tolerance, this SUPERBLOCK will be called and its state will be updated using the new value of its input for this time step and will be used by other SUPERBLOCKs for next variable time step.

5.2.2. Dealing with Discrete Controller

Discrete control signals introduce sudden changes to the system simulation. For example, an output of the linear proportional controller introduced before is the number of operating heat pump pairs, which is an integer in the range between 1 and the maximum number of the heat pump pairs in the system. As shown in Figure 5-4, the relationship between the average surface temperature and the number of operating heat pump pair is only piece-wise continuous and discontinuity occurs when the number of operating heat pump pairs changes.

In system simulation, the discrete outputs of a controller model tend to introduce severe numerical problems to the DAE solver of HVACSIM+ if they are solved simultaneously with other continuous variables. This is caused by difficulties in calculating the system Jacobian (the matrix of the partial derivatives of residual functions with respect to each variable) when discontinuities are encountered during the solution searching process.

It is possible to explicitly update the discrete control signals in a system simulation instead of solving it simultaneously with other continuous variables. To do this, the system simulation needs to be partitioned by putting the model of the discrete controller into a SUPERBLOCK, which is separated from other SUPERBLOCK(s) containing the continuous component models. The discrete outputs of the controller are thereby separated from the other simultaneously solved continuous variables. If the fixed time step is used in the simulation, the controller model will update its outputs (the control signals) only once at each time step according to the solutions of its inputs, which are solved in other SUPERBLOCKs at last time step. The updated control signals will then be used as inputs in other SUPERBLOCKs to solve the continuous variables at current time step. This procedure requires short simulation time step to avoid delayed response of the controller. The ideal time step size for accurately simulating the behavior of a controller should be equal to the time interval at which the real controller updates its signals, which would typically be 1-5 seconds (Haves and Norford 1995). However, such small time step is not practical for multi-year simulation of the snow melting system. In addition, the system status will not change significantly within such short period because of the large thermal mass of the system. Therefore, it is reasonable to use a larger time step in the system simulation. A sensitivity analysis may be necessary to select a proper size of the simulation time step.

5.2.3. Decoupling Hydronic and Thermal Calculations

Flow rate, pressure, and temperature are the three categories of variables involved in the simulation of a hydronic heating system. If all these three categories of variables solved simultaneously with the solver of HVACSIM+, the variation of flow rates during the iterative solution searching process may result in discontinuities, especially when flow rate is close to zero. As with the discrete control signals, this can cause convergence problems.

Generally, the variation of the flow rates and pressure depend more strongly on the operation mode rather than the variation of temperatures. Therefore, the flow rates and pressures can be solved separately from the temperatures. It will not only improve the convergence ability of the simulation but also save computational time by reducing the number of simultaneously resolved equations.

If flow rates of a system will not change significantly when the system is in operation, it is possible to set the pre-determined flow rates as parameters of the controller, by which the flow rates used in each component model are assigned according to the operating mode. Since the controller model is in a separate SUPERBLOCK than other component models, the mass flow rates are not simultaneously solved with the fluid temperatures. In this case, calculation of the pressure drops will not be necessary in the simulation and the pre-calculated values of pressure drops in the pipe network of the system can be set as parameters in the circulating pump models.

If system flow rates will change significantly during operation, the calculations of flow rates and pressure drops can be processed in an individual SUPERBLOCK prior to the calculations of fluid temperatures at each time step. However, it will increase the complexity and computational time of the simulation.

5.3. Experimental Validation of System Simulation Results

To examine whether the predictions of the system simulation can match the actual behavior of a real system, simulation results have been validated with experimental data collected from the experimental hydronic bridge snow melting system described in Chapter 4. Since the performance of the system simulation depends on the performance of its component models, the first part of the validation work is to compare the predictions of the individual component models with the corresponding experimental measurements. The second part of the validation work is to validate the system simulation results against the experimental data. The experimental apparatus and validation results will be presented in the following sub-sections.

5.3.1. Experimental Apparatus

The experimental system consists of a bridge deck with embedded hydronic tubing, a single water-to-water heat pump, a six-borehole vertical ground loop heat exchanger (GLHE), circulating pumps and control system. Figure 5-5 is a schematic

diagram of this system. A detailed description of the hydronically-heated bridge deck has been given in Chapter 4 and will not be repeated here. The descriptions of the GLHE and the water-to-water heat pump are given in the following sub-sections along with the validation results for the individual component models.

A custom data acquisition system has been developed to measure and record experimental data from the snow melting system at 10-minute intervals. The instrumentation consists of 60 thermistors embedded in the bridge deck, six thermistor probes inserted in the pipe network, two flow meters, and three kWh meters. The following data are collected:

- Entering and exiting fluid temperatures in both the source and load sides of the heat pump;
- Temperatures at different locations in the heated pavement slab;
- Flow rates in both the source and load sides of the heat pump;
- Power consumption of the heat pump and circulating pumps

As described in Chapter 4, additional instrumentation has been added to measure some essential parameters of the bridge deck and weather elements, including solar absorptance of the bridge surface, longwave atmospheric radiation, and snowfall rate.

The experimental snow melting system is operated with an on-off controller to maintain the average bridge surface temperature in the range of 40-42°F (4.4-5.5°C) when there is a risk of icing or snowfall. To replenish the thermal energy stored in the

ground using the solar energy collected from the bridge, fluid will be circulated directly from the bridge to the ground heat exchangers when the surface temperature is higher than 90°F (32.2°C) and will be switched off when the temperature falls to 88 °F (31.1°C).

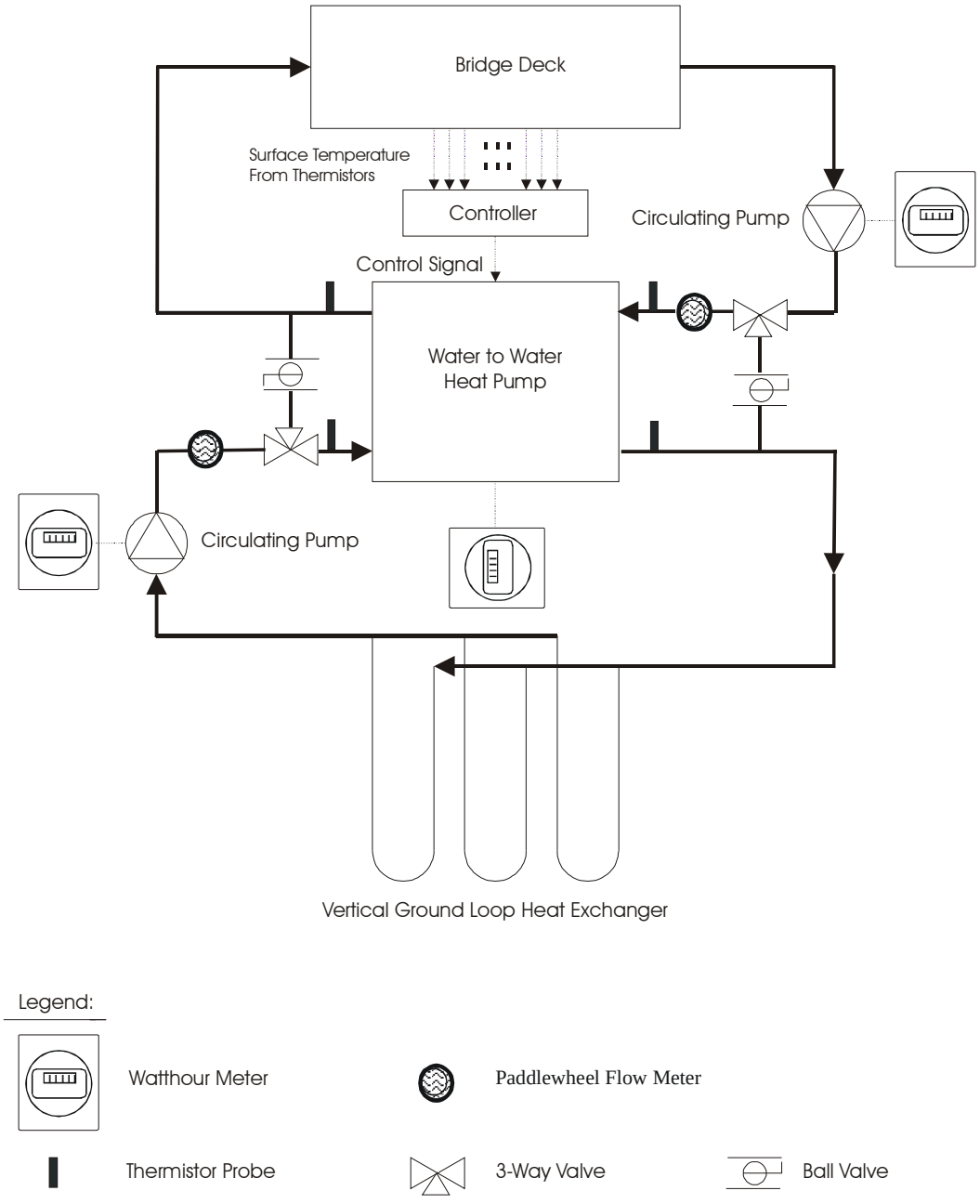

Figure 5-5 Schematic diagram of experimental GSHP-based snow-melting system.

5.3.2. Validation Results of Individual Component Models

Since the validation results of the hydronically-heated slab model have been reported in chapter 4, the validation work in this sub-section only focuses on the models of the vertical ground loop heat exchanger and the water-to-water heat pump.

5.3.2.1. Validation of Vertical Ground Loop Heat Exchanger Model

The vertical ground loop heat exchanger used in the experimental system is comprised of 6 boreholes with a diameter of 5.25 inch (0.13 m) that are in a 2 by 3 configuration with 25 ft (7.62 m) spacing. Each borehole contains an HDPE U-bend pipe loop with nominal diameter of 1 in (25 mm), and is grouted with a mixture of 4020 sand and bentonite. The effective thermal conductivity and temperature of the surrounding clay/sandstone formation has been estimated from *in situ* test data (Smith 1999). The parameters of the vertical ground loop heat exchanger are summarized in Table 5-2.

TABLE 5-2 Ground Loop Heat Exchanger Parameters

Design Parameters	Parameter Value (SI Units)	Parameter Value (IP Units)
Number Of Boreholes	6	
Borehole Depth	66.1 m	217 ft
Borehole Radius	67 mm	2.625 in
Ground Thermal Conductivity	2.34 W/m-K	1.351 Btu/hr-ft-^{o}F
Ground Volumetric Heat Capacity	2350 kJ/m^{3}-K	35.1 Btu/ft^{3}-^{o}F
Undisturbed Ground Temperature	17.2 ^{o}C	63 ^{o}F
Grout Thermal Conductivity	1.61 W/m-K	0.933 Btu/hr-ft-^{o}F
Pipe (U-Tube) Thermal Conductivity	0.39 W/m-K	0.226 Btu/hr-ft-^{o}F
Pipe (U-Tube) Wall Thickness	3 mm	0.119 in
Pipe (U-Tube) Outer Diameter	33 mm	1.31 in
Shank Spacing	67 mm	2.62 in

The short-term g-functions of the GLHE are generated with a computer program described by Yavuzturk and Spitler (1999a). The long-term g-functions are those calculated by Eskilson (1987) and obtained from GLHEPRO (Spitler 1999, 2000). The generated short-term and long-term g-functions of the 2 X 3 borehole field of the GLHE used in the experimental system are plotted in Figure 5-6. The g-functions are used as parameters of the GLHE model.

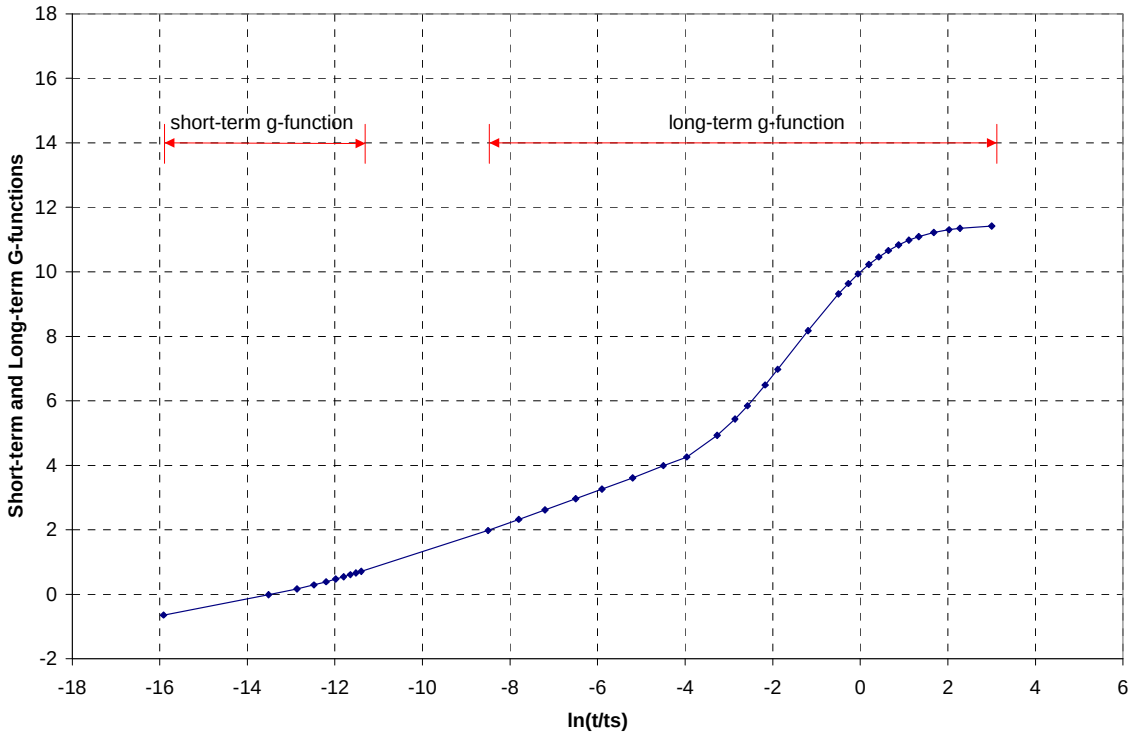

Figure 5-6 Short-term and long-term g-functions of the 2 X 3 borehole field of the GLHE used in the experimental GSHP based hydronic snow melting system.

The validation is conducted by providing the measured entering fluid temperatures (EFT) and flow rates as inputs to the GLHE model, and comparing the predicted exiting fluid temperature (ExFT) with the corresponding measured data. After the GLHE had been installed at the end of July 2000, the system recharged the ground

with heat collected from the bridge deck by circulating water between the bridge deck and the GLHE until it was switched to heating mode in November 2000. Experimental data from July 2000 to December 2002 are used to validate the GLHE model. As previously stated, the system is controlled with an ON-OFF strategy; therefore its operation is intermittent. Since the fluid temperatures are measured in the machine room where the heat pump and data acquisition system is installed, the measurements drift towards the room temperature if the system is not in operation and there is no circulation. Therefore, only the measured fluid temperatures when the system is in operation are used to validate the model predictions.

Figure 5-7 shows the comparison between the predicted and measured GLHE exiting fluid temperature (ExFT) for portions of the period from July 2000 to October 2000 when the system was operated in recharge mode. As shown in the figure, the predicted ExFT matches the measured data very well. The RMS error of the predicted ExFT is 0.5 ˚F (0.3 ˚C) during the whole period. It can also be observed that, in each operation cycle, the largest difference occurred at the beginning and the predicted ExFT is about 0.9˚F (0.5 ˚C) less than the measured data. The thermal mass of the water, which was at the room temperature before circulating in the GLHE, is thought to be the reason for it. As a result, the relative error in the predicted heat transfer rate is 35% higher than the measured data at the beginning of each operating cycle (see Figure 5-8). However, in most of the operating cycles, the error reduces quickly and it is less than 5% when the EFT reached its highest. The predicted cumulative heat rejected into the ground from July

to October in 2000 is 11% less than the measured data, which is 14.22 MBTU (4165 kW-hr).

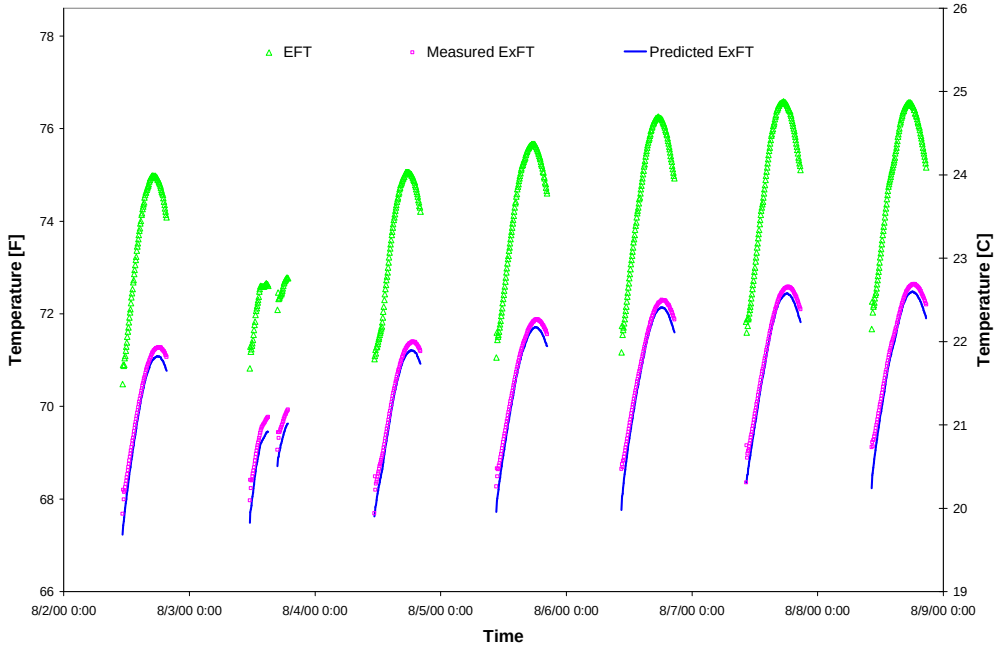

Figure 5-7 Measured and predicted exiting fluid temperatures of the ground loop heat exchanger – recharging mode.

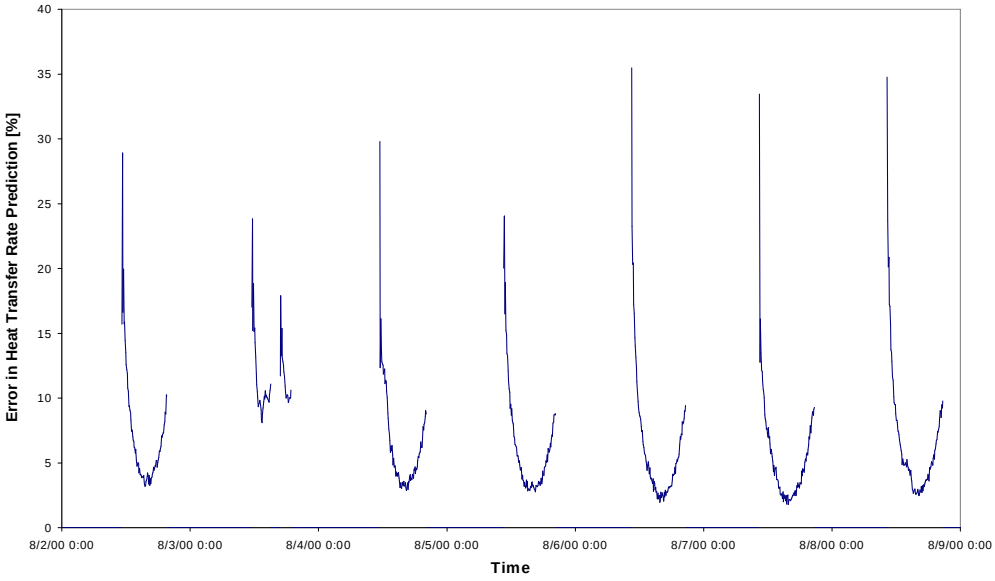

Figure 5-8 Relative errors in the predicted heat transfer rate – recharging mode.

The GLHE model has also been validated with the measured data when the system was operated in heating mode. The validation result using measured data from 12/23/02 to 12/25/02 when the GLHE was used to extract heat from the ground is shown in Figure 5-9. A mixture of propylene glycol and water at a weight concentration of 39%[7] was circulated in the GLHE during this period. As shown in the figure, the predicted ExFT is a little bit lower than the measured data and the RMS error during the periods when there was flow in the GLHE is 1 ˚F (0.58 ˚C). The predicted cumulative heat extracted from the ground during the whole period of operation is 9% less than the measured data, which is 2.07 MBTU (605 kW-hr).

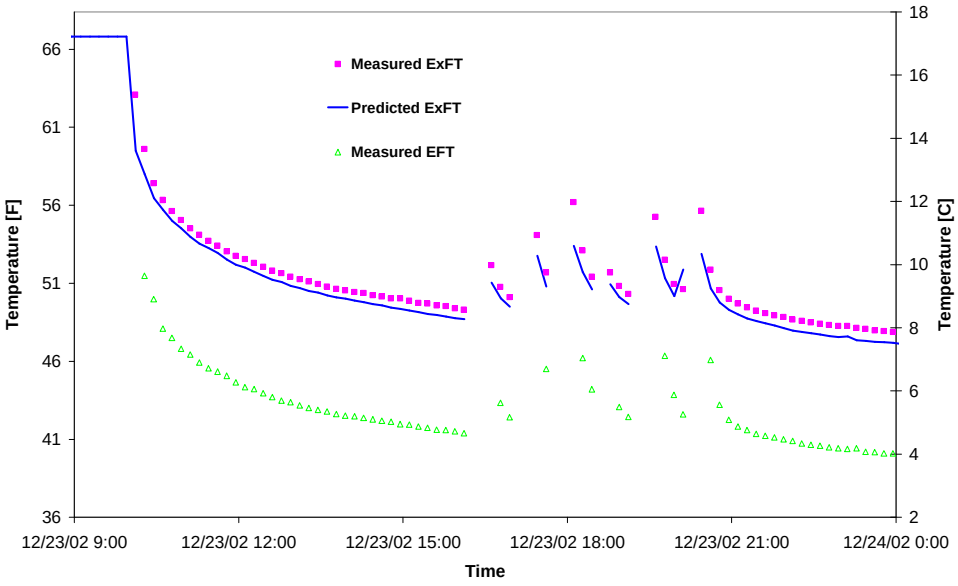

Figure 5-9 Measured and predicted exiting fluid temperatures for the ground loop heat exchanger – heating mode.

[7] It was determined by measuring the freezing point temperature of the propylene glycol solution (Spitler, et al. 2001).

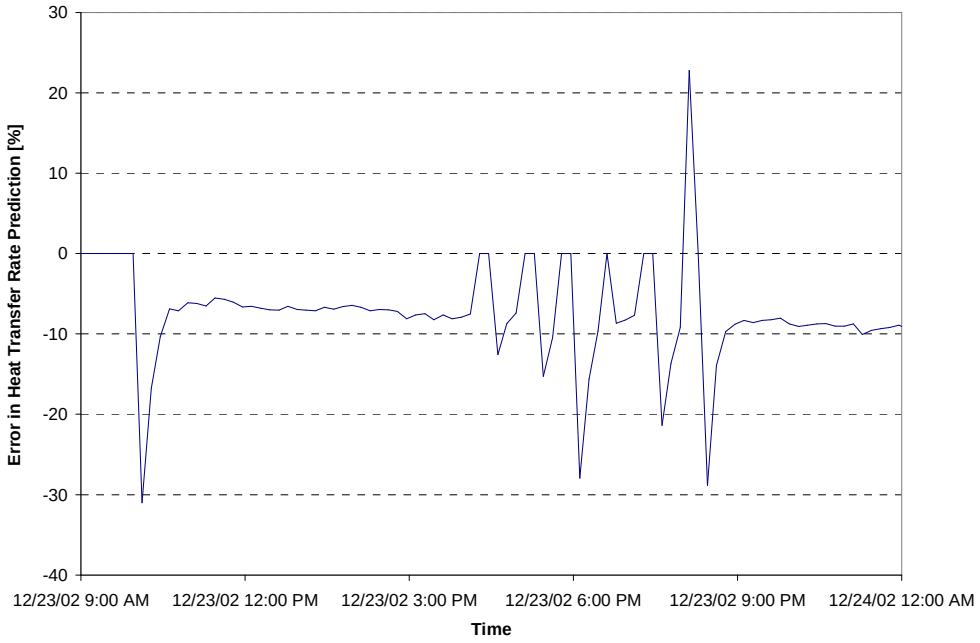

Figure 5-10 Relative errors in the predicted heat transfer rate – heating mode.

The predicted ExFT from simulation using the history of the GLHE loads (heat rejected into the ground or extracted from the ground) prior to the simulated period has been compared with the result from the simulation that does not use the loads history. The comparison shows that there is no significant difference resulting from using the loads history. It is not surprising since the system was only operated in recharge mode in 2000, from then on, only a few short periods of heating operations happened prior to the simulated period and the most recent operation occurred 18 days before.

5.3.2.2. Validation of Water to Water Heat Pump Model

A FHP model WP120 water-to-water heat pump with nominal cooling capacity of 10 tons (35 kW) is used in the system to heat the bridge deck. This heat pump utilizes a

scroll compressor and uses a mixture of propylene glycol and water at a weight concentration of 39% as coolant in both the condenser and evaporator of the heat pump[8]. The parameter-estimation-based water-to-water heat pump model introduced in section 5.1.2 is used in the system simulation. The coefficients of the heat pump model were estimated from the catalog data for the performance with pure water since they are the only available data from the heat pump manufacturer (Jin 2002).

The validation is conducted by providing the measured entering fluid temperature (EFT) and flow rates in the condenser and evaporator as inputs to the heat pump model, and comparing the predicted exiting fluid temperature (ExFT) of the condenser and evaporator with corresponding measured data. For convenience, in the context of this thesis, the condenser (connected with the bridge deck) and the evaporator (connected with the GLHE) are termed as the load and source sides of the heat pump, respectively.

Jin (2002) had validated this heat pump model with three sets of experimental data. It was reported that this model over-predicted the source side heat transfer rate by 19.2 % when the propylene glycol solution was used as coolant in the evaporator, although it can predict the heat pump performance reasonably well (the errors in predictions of the load and source side heat transfer rates are within 7.6 % and 11.7 %, respectively) when pure water was used in the evaporator.

[8] The coolant used in the evaporator was changed from pure water to the propylene glycol solution in August 2001.

The reason for the over-prediction of the source side heat transfer rate has been preliminarily investigated. The method that was used in the model to account for the effect of using antifreeze on the overall heat transfer coefficient of the heat exchangers appears the most likely reason. In this model, an "Antifreeze Degradation Factor (ADF)" is used to estimate the degradation of the coolant side convection heat transfer coefficient. It is derived from the Sieder-Tate correlation (Kern 1950), which is used to calculate Nusselt number (Nu) of turbulent flow inside tubes. Strictly speaking, the ADF is only applicable for turbulent flow. However, since the model never calculates Reynolds number (Re), it does not know if the flow is laminar or turbulent and therefore the same ADF is applied for both cases. Obviously, it will result in over-estimated coolant side convection heat transfer coefficient, and in turn, the overall heat transfer coefficient of the heat exchanger if the flow becomes laminar when antifreeze is used as the coolant instead of pure water. Because the load side fluid temperature is higher than that in the source side of the heat pump, it is possible that the flow of antifreeze is turbulent in condenser but laminar in the evaporator[9]. This may explain why the over-prediction of the heat transfer rate only occurs in the source side of the heat pump.

As discussed previously, the "Antifreeze Degradation Factor (ADF)" is only valid when the flow of antifreeze is turbulent. To properly account for the transition to laminar flow with this parameter-estimation-based model, it would be necessary to have a more complete data set than what currently available from manufacturers. Given the limited

[9] An interview with a senior engineer at a major water source heat pump manufacturer has confirmed that it is likely that laminar flow occurs in the coolant side of the evaporator of the heat pump if 39% Propylene Glycol is used as coolant.

availability of data, a heuristic approach is to correct the overall heat transfer coefficient of the evaporator with a correction factor since it is only in the evaporator that the laminar flow of antifreeze occurs. This approach has been adopted to improve the model performance. This additional correction factor is determined with a one-dimensional minimization procedure.

The measured heat pump performance data during the period from 12/23/02 to 12/24/02 were used in the minimization procedure. The minimization procedure finds a correction factor that reduces the errors in the predicted exiting fluid temperatures of the heat pump, and in turn, the errors in the predicted cumulative heat at both the load and source sides of the heat pump. The finally determined correction factor is 0.35, which reduces the errors of the predicted cumulative heat into the uncertainty band of the model when pure water is used as coolant. By applying the correction factor of 0.35, the overall heat transfer coefficient of the evaporator is reduced by 65%.

As shown in Figure 5-11, the differences between the predicted and measured ExFT of the evaporator are significantly reduced after applying this correction. Figure 5-12 shows that this correction also simultaneously results in decreasing the predicted ExFT of the condenser, but the differences between the predictions and the measured data are still within the uncertainty band of the model. Since the viscosity of Propylene Glycol solution varies significantly with its temperature, the correction factor of 0.35 may be only applicable for the temperature range encountered in the specified time period. It is highly desirable to further investigate the relationship between the anti-freeze thermal

properties and the resulting heat pump performance so that a general algorithm may be developed to properly account for the effects of anti-freeze on the heat pump performance.

The comparison of the errors in the heat pump model predictions before and after the correction is summarized in Table 5-3. It can be seen from the table that the errors in the predicted cumulative heat at the load and source sides of the heat pump are significantly reduced and they are all within the band of model uncertainties reported by Jin (2002). There is no significant difference in the prediction of heat pump power consumption since the errors in the fluid temperature prediction do not change the operating conditions of the compressor significantly.

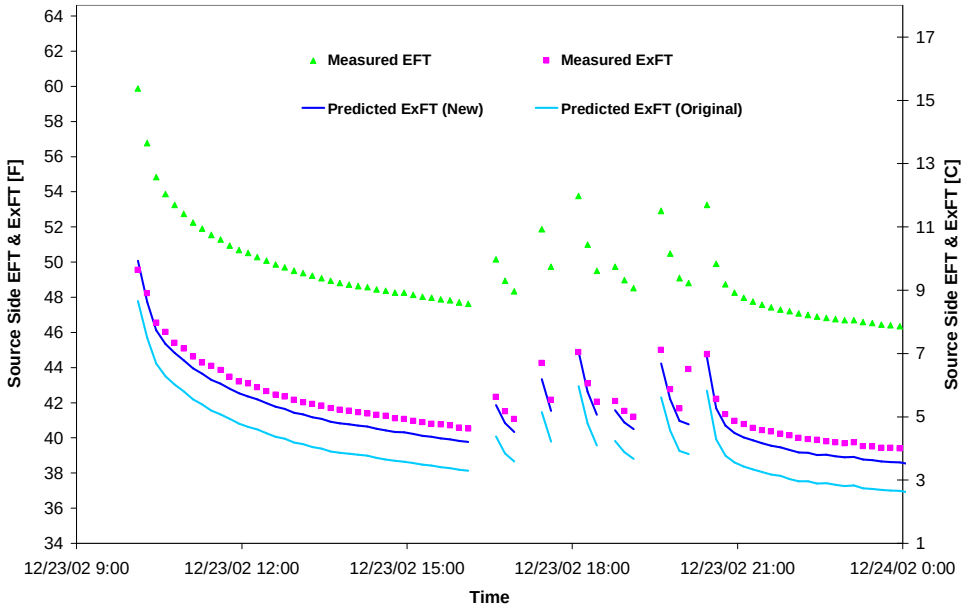

Figure 5-11 Measured and predicted Exiting fluid temperatures (ExFT) of the evaporator of the water-to-water heat pump.

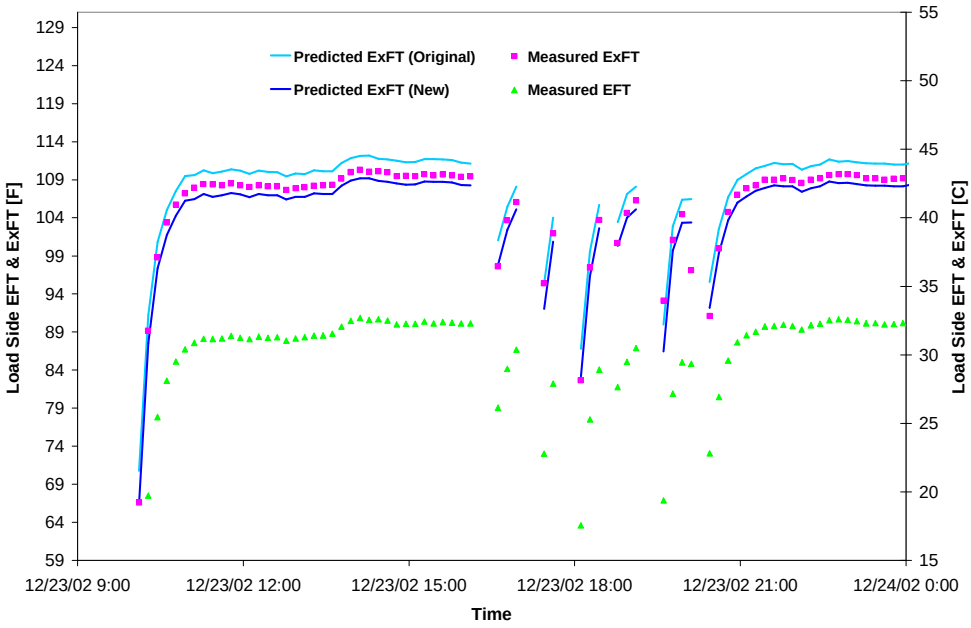

Figure 5-12 Measured and predicted Exiting fluid temperatures (ExFT) of the condenser of the water-to-water heat pump.

TABLE 5-3 Comparison of Errors in the Heat Pump Model Predictions Before and After the Correction of the Source Side Overall Heat Transfer Coefficient

	RMS error in load side ExFT	RMS error in source side ExFT	Error in cumulative load side heat	Error in cumulative source side heat	Error in cumulative power
Before correction	2.0 ˚F (1.1 ˚C)	2.3 ˚F (1.3 ˚C)	11.1%	32.7%	2.4%
After correction	1.2 ˚F (0.7 ˚C)	0.7 ˚F (0.4 ˚C)	-3.3%	11%	–1.7%
Model uncertainties			±8.9%	±11.2%	±8.7%

5.3.3. Validation Results of System Simulation

The validation of the system simulation results is conducted by providing only the local weather data as inputs to the system model and comparing the model predictions with the corresponding measured data. The weather data used for the validation are

obtained by combining the local cloud cover data (cloud fraction and height of cloud bases at low, medium, and high levels) from the National Climatic Data Center (NCDC) with the data from Oklahoma Mesonet (*meso*scale *net*work) and the snowfall rate and ambient air temperature measured in the site of the experimental bridge deck. Weather data from Mesonet are averaged value over 5-minute observation intervals.

5.3.3.1. System in Recharge Mode

The validation of the system simulation in recharge mode is conducted using measured data in the period from 8/01/00 to 8/14/00. In this period, pure water was used as heat transfer fluid in both the bridge deck and the GLHE. As shown in Figure 5-13, the flow rate during the recharge operation was kept at 19.6 GPM (1.24 L/s) with less than 1% variation. Therefore, a constant flow rate of 19.6 GPM (1.24 L/s) is used during recharge operation in the system simulation.

The required weather data includes solar radiation, ambient temperature, humidity ratio, wind speed, wind direction, precipitation rate, and the sky temperature. In the simulation of the system in recharge mode, the operating status of the system (recharging the ground or not) at current time step depends on the average surface temperature of bridge deck calculated at the end of last time step.

Figure 5-14 shows a comparison between the predicted and measured average surface temperature. As can be seen in the figure, while the predicted surface temperature

match the measured data very well over most of the time, it is higher than the measured data at about 4.00 pm in each day. The peak error in daytime is up to 7.2 ˚F (4 ˚C). The RMS error of the predicted average surface temperature over the entire simulated period is 1.6 ˚F (0.9 ˚C). Considering only daytime, the RMS error is 2.0 ˚F (1.1 ˚C); considering only nighttime, the RMS error is 0.9 ˚F (0.5 ˚C)[10].

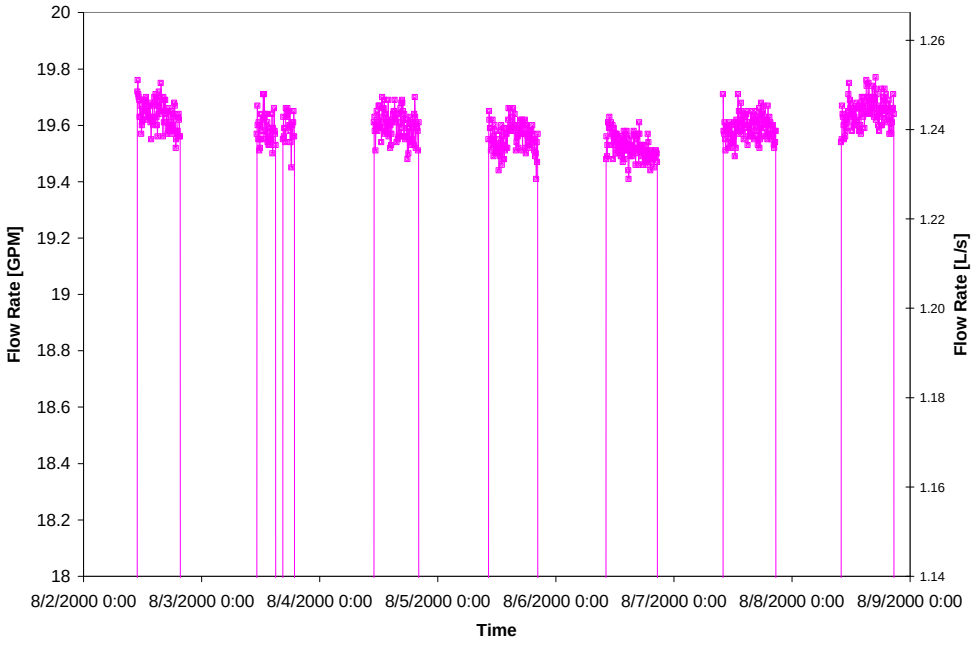

Figure 5-13 Measured flow rate in recharge operation.

The predicted and measured EFT and ExFT of the GLHE (which are the ExFT and EFT of the bridge loop) are compared in Figure 5-15. The RMS errors in the predicted EFT and ExFT over the simulated period are about 0.9 ˚F (0.5 ˚C) and 0.9 ˚F (0.5 ˚C), respectively.

[10] Daytime and nighttime are distinguished by whether there is solar radiation.

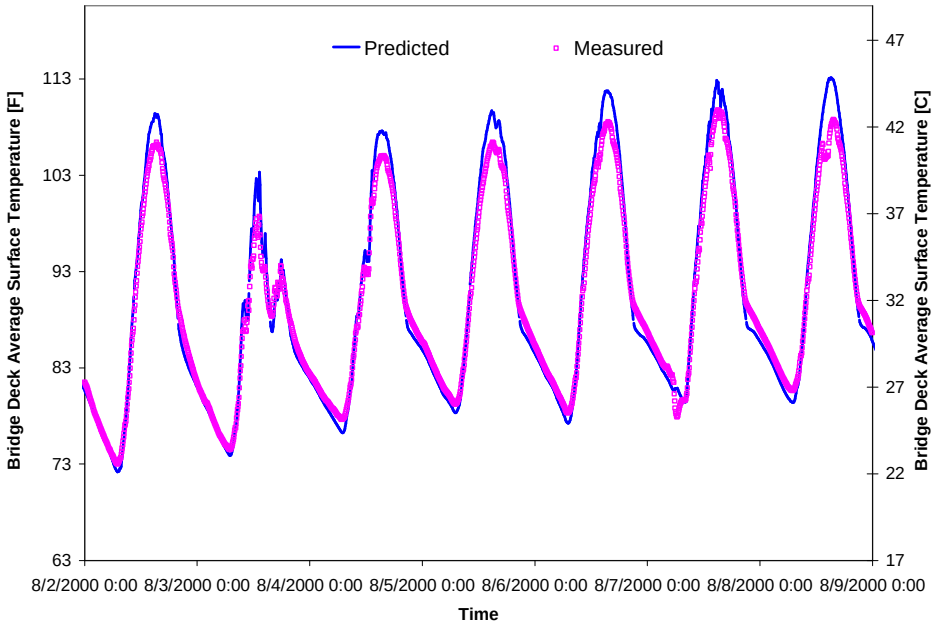

Figure 5-14 Measured and simulated average surface temperature – recharge mode.

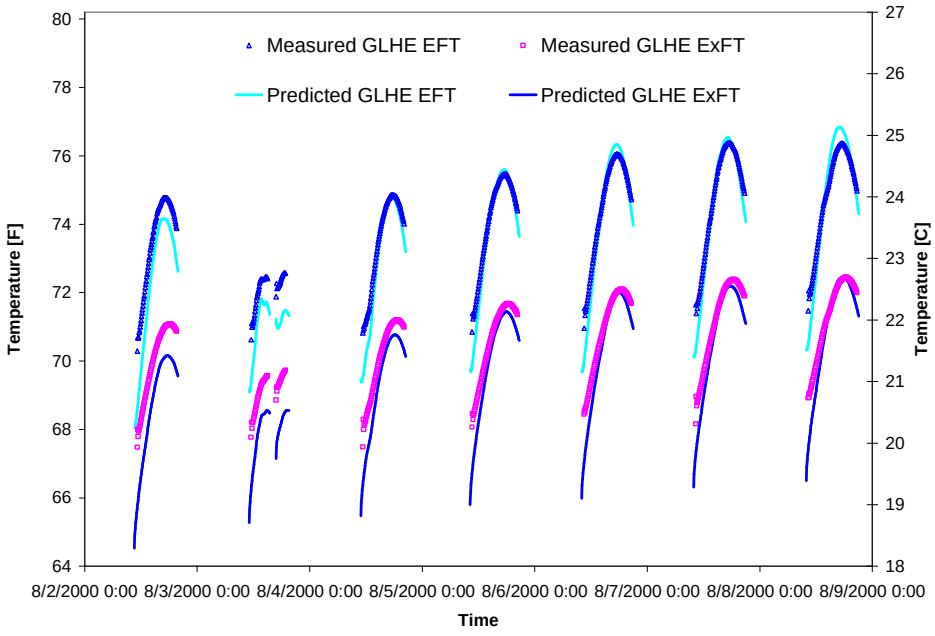

Figure 5-15 Measured and predicted EFT and ExFT of the GLHE – recharge mode.

The measured and predicted recharge (heat transfer to the ground) rates have been compared in Figure 5-16. The simulation predicted cumulative heat transferred to the ground over the entire simulated period has been calculated and it is 11% higher than that calculated from measured data. Since the uncertainty in the measurement of flow rate is 3% and the uncertainty of the temperature measurements is ±0.18 ˚F (0.1 ˚C) (Holloway 2000), the propagated uncertainty of the heat transfer rate measurement is ±7.6% given the average difference of 3.6 ˚F (2 ˚C) between the ExFT and EFT of the GLHE during the recharge operation. Therefore, the cumulative heat transfer is over-predicted by the simulation. It is consistent with the over-prediction of the surface temperature. As will be discussed later in this section, the uncertainties associated with the input parameters of the simulation are likely the reason for the over-predicted surface temperature and the cumulative heat transfer.

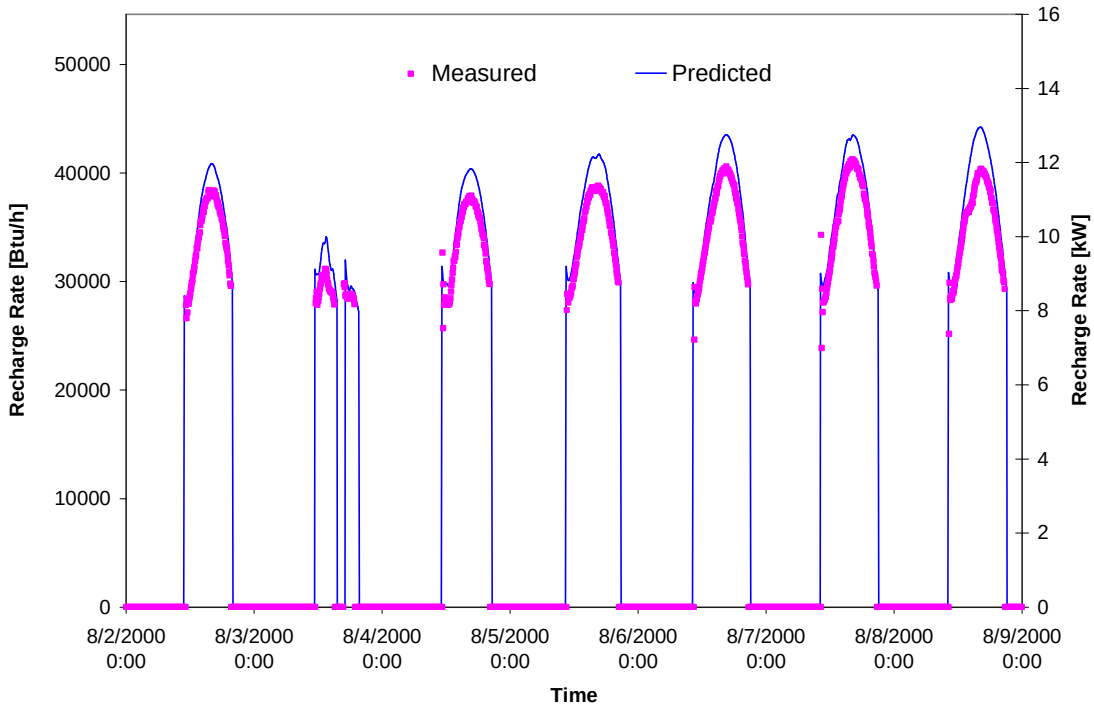

Figure 5-16 Measured and predicted recharge rates – recharge mode.

As shown in Figures 5-14 and 5-16, there are some differences between the predicted and measured average surface temperature and recharge rates. These errors may come from the following three sources:

(1) Uncertainty of the calculated sky temperature. Since there is no available measurement of sky temperature (t_{sky}) during the simulated period, the algorithm proposed by Martin and Berdahl (1984) has been used to calculate the sky temperature. Martin and Berdahl (1984) estimated the uncertainty of the sky temperature calculated using this algorithm as ±4.1 ºF (±2.3 ºC).

(2) Uncertainty of the measured/estimated bridge pavement parameters. As discussed in Section 4.2.2.2, there could be up to ±11% uncertainty in the measured solar absorptance. In addition, the predicted surface temperature is sensitive to the pavement thermal properties, which are affected by the embedded rebar and the moisture content of the concrete. The volume-weighted averages of the thermal properties of the concrete and rebar have been used as an approximation of the effective pavement thermal properties. As shown earlier in Figure 4-4 (a) and (b), using the volume-weighted averages of the thermal properties at saturated condition leads to a very good match between the predicted and measured surface temperature when the snow is melting on the pavement. However, there are some uncertainties in the moisture content of the concrete when the system is operated in recharge mode. In the simulation of system in recharge mode, the volume-weighted

averages of the thermal properties at normally dry condition have been used. But, it is possible that the actual moisture content is higher.

(3) Uncertainty in the calculation of the convective heat transfer coefficient (h_c) on the bridge deck surface. As presented in Chapter 4, the correlations described by Incropera and DeWitt (1996) are used in the bridge model to calculate the convective heat transfer coefficient. However, as stated by Incropera and DeWitt (1996), although the correlations are suitable for most engineering calculations, "in practice they rarely provide exact values for the convection coefficients. Conditions vary according to the free stream turbulence and surface roughness, and errors as large as 25% may be incurred by using the expressions."

In the following uncertainty analysis, each of the parameters of interest is changed to its estimated upper and lower bounds and simulations using the changed parameters are performed. The simulation results are compared with the measured data and presented in Figures 5-17 to 5-21.

Effects of sky temperature

As shown in Figure 5-17, increasing the sky temperature increases the predicted surface temperature both at the daytime and nighttime. It therefore increases the peak error at daytime but almost eliminates the errors at nighttime.

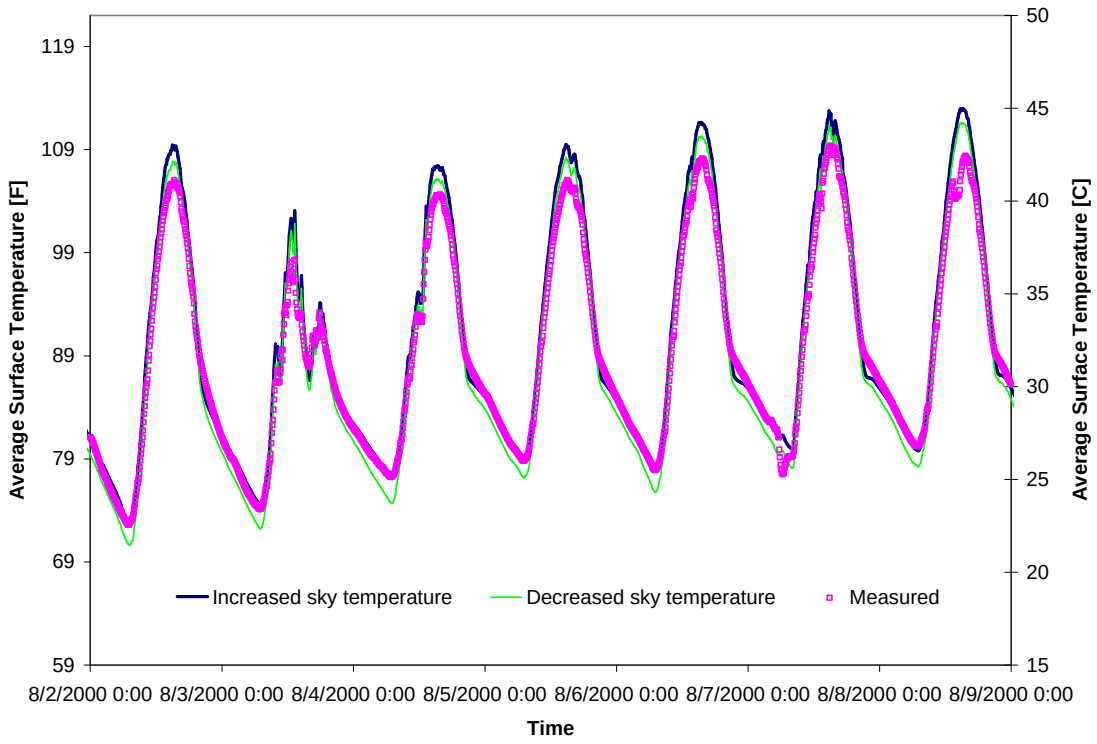

Figure 5-17 Effects of uncertainty of the calculated sky temperature on the predicted average surface temperature.

Effects of solar absorptance

As shown in Figure 5-18, the uncertainty of surface solar absorptance significantly affects the predicted average surface temperature at daytime, but obviously it does not make difference at nighttime. Using the estimated lower bound of the solar absorptance (0.53) leads to a very well match between the predicted and measured surface temperature during the daytime. Comparing with data measured by Levinson and Akbari (2001), which shows that the mature solar absorptance of concrete mixes could range from 0.23 to 0.59 (mean 0.41), it is very likely that the estimated lower bound of

the solar absorptance is closer to its real value and the error of the solar absorptance is the main reason for the errors of the predicted surface temperature during the daytime.

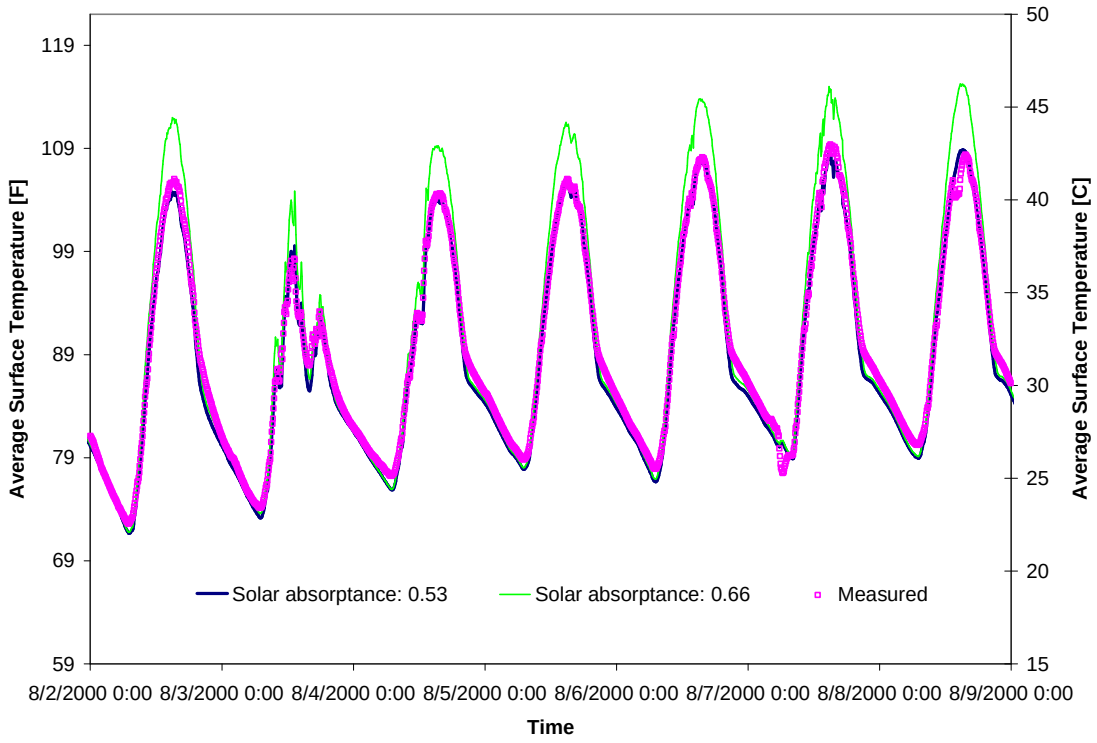

Figure 5-18 Effects of uncertainty of the measured solar absorptance on the predicted average surface temperature.

Effects of pavement thermal properties

As shown in the Figure 5-19, by considering the 50% moisture content in the concrete, the peak difference between the predicted and measured surface temperature during the daytime is reduced by 1.4 ºF (0.8 ºC). But, it only reduces the peak temperature difference by 0.4 ºF (0.2 ºC) in the night.

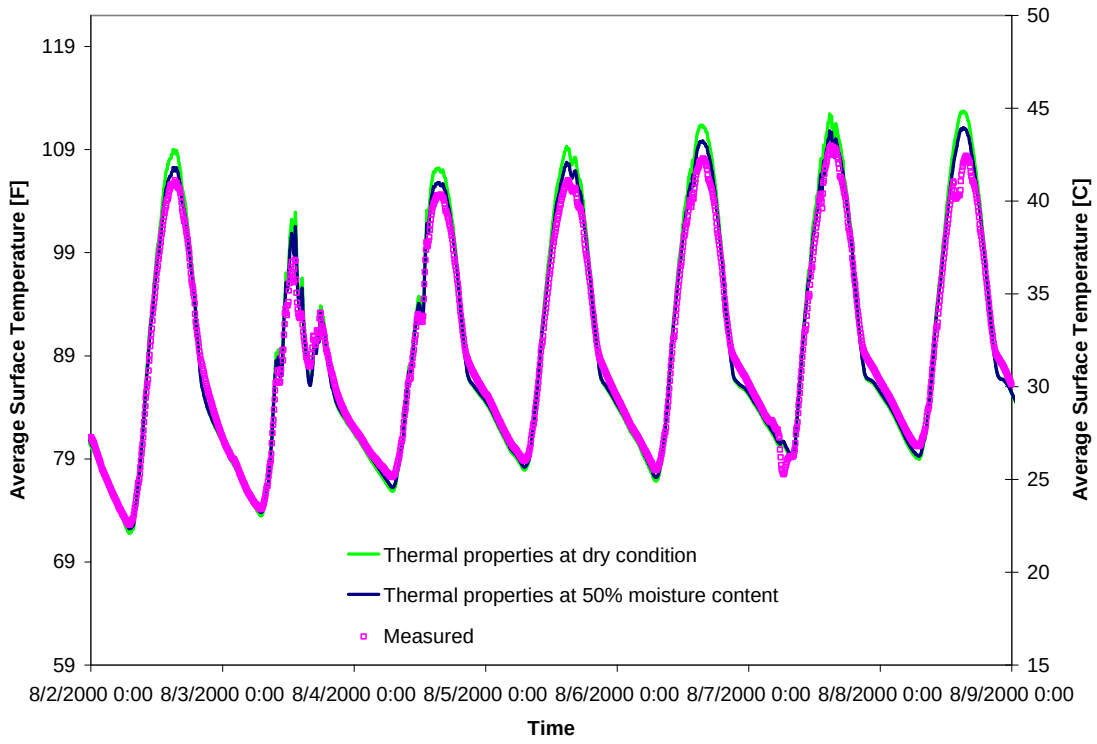

Figure 5-19 Effects of uncertainty of the pavement thermal properties on the predicted average surface temperature.

Effects of convective heat transfer coefficient

Likewise, as shown in Figure 5-20, the uncertainty of convective heat transfer coefficient also only changes the surface temperature significantly during the daytime because the difference between the surface and ambient temperature is very small in the night. This has been illustrated in Figure 5-21.

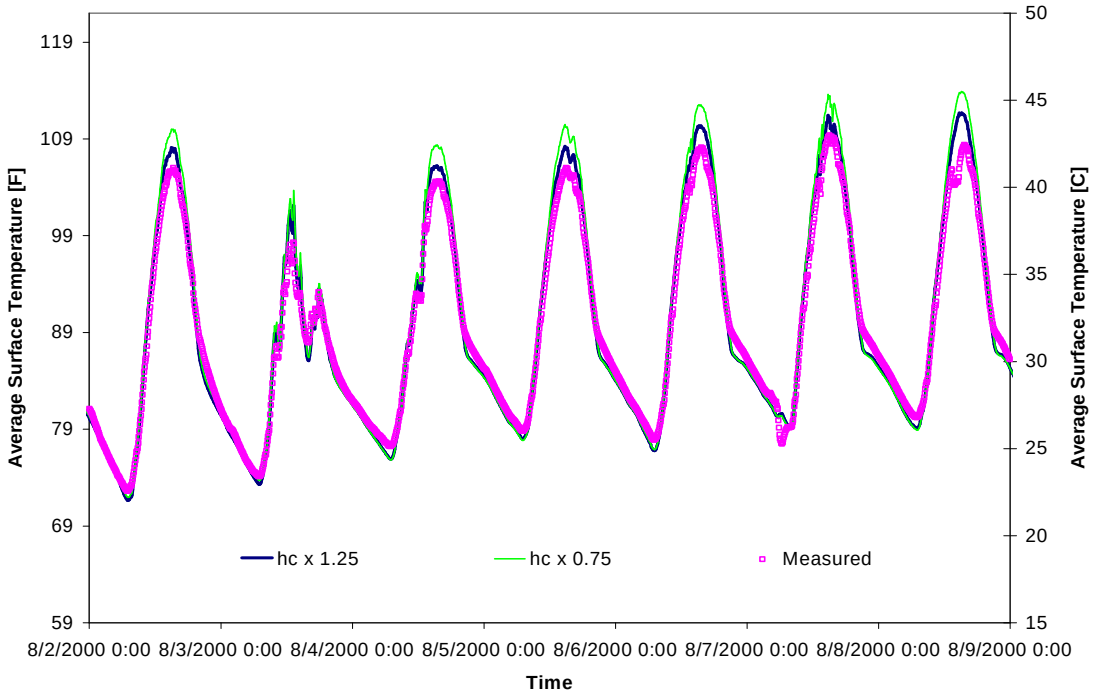

Figure 5-20 Effects of uncertainty of the convective heat transfer coefficient on the predicted average surface temperature.

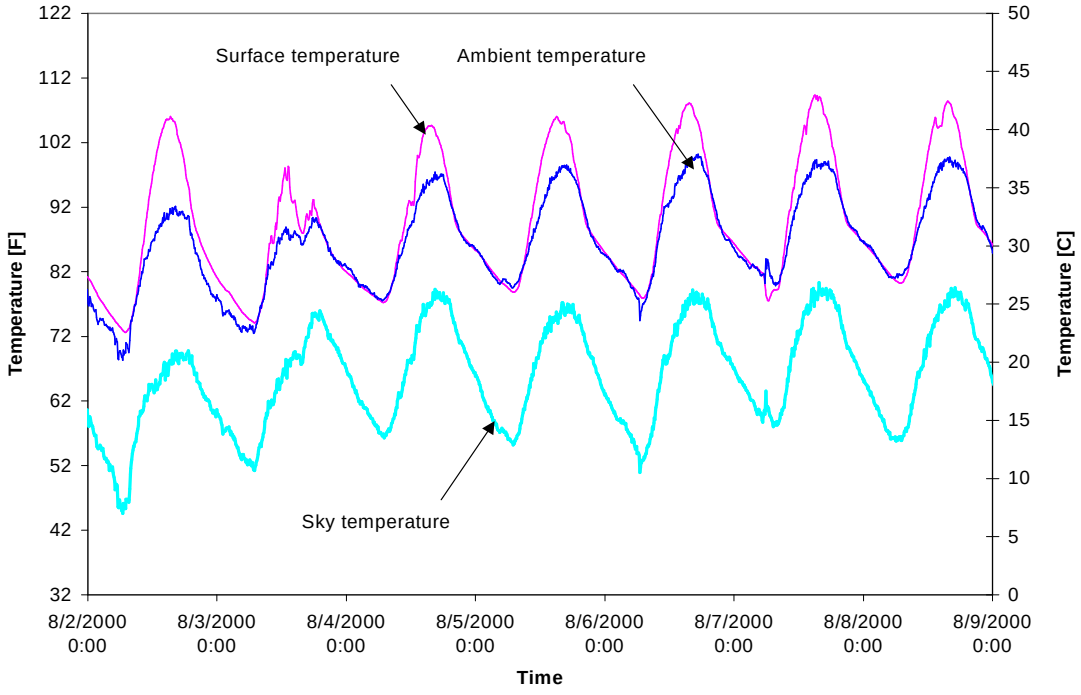

Figure 5-21 Comparison among the surface temperature, ambient temperature, and the calculated sky temperature.

The RMS errors of the predicted average surface temperature and the relative error of the predicted cumulative heat resulting from various uncertainties have been presented in Table 5-4. As illustrated in above figures, the influences of each parameter on the predicted average surface temperature are different at daytime and nighttime. Therefore, the RMS errors at daytime, nighttime, and overall the entire simulated period have been calculated and given in the table for comparison.

As can be seen in the table, the surface solar absorptance significantly affects not only the predicted surface temperature but also the cumulative heat transfer to ground. Changing the solar absorptance to its lower bound reduces the relative error of the predicted cumulative heat transfer to ground to 1%.

Effects of combined uncertainties

Figure 5-22 illustrates the effects of the combined uncertainties of the input parameters on the predicted surface temperature. The upper bound of the predicted surface temperature is from the simulation that uses all the varied parameters that increase the surface temperature at the daytime, and the lower bound is from the simulation that uses all the varied parameters that decrease the surface temperature at the daytime. As shown in Figure 5-22, the measured surface temperature is within the zone bounded by the upper and lower limits of the combined uncertainties.

TABLE 5-4 Uncertainties of Input Parameters and the Resulting RMS Errors of the predicted Average Surface Temperature

Parameters		Sky temperature t_{sky}		Surface solar absorptance		Pavement thermal properties		Convective heat transfer coefficient h_c	
Original value		Calculated with Martin and Berdahl's Model (see section 4.1.2)		0.6		At Normally-dry condition K = 1.2 Btu/(h-ft-ºF) [2.0 W/(m-K)] ρ =148 lb/ft^3) (2375 kg/m^3) c_p =0.22 Btu/(lb-ºF) [928 J/(kg-ºC)]		Calculated with the correlation described by Incropera and DeWitt (see section 4.1.2)	
Uncertainty		±3.6 ºF (±2 ºC)		±11%		With 50% moisture content		±25%	
New value		$t_{sky} + 2°C$	$t_{sky} - 2°C$	0.66	0.53	K = 1.3 Btu/(h-ft-ºF) [2.2 W/(m-K)] ρ =150 lb/ft^3) (2410 kg/m^3) c_p =0.23 Btu/(lb-ºF) [973 J/(kg-ºC)]		$h_v \times 1.25$	$h_v \times 0.75$
Original relative error in predicted cumulative heat transfer to ground		11%							
New relative error in predicted cumulative heat transfer to ground		15%	6%	18%	1%	14%	11% *	9%	13%
Original RMS Error	Daytime	2.0 ˚F (1.1 ˚C)							
	Nighttime	0.9 ˚F (0.5 ˚C)							
	Overall	1.6 ˚F (0.9 ˚C)							
New RMS Error	Daytime	2.3 ˚F (1.3 ˚C)	1.6 ˚F (0.9 ˚C)	3.5 ˚F (1.9 ˚C)	1.2˚F (0.7 ˚C)	1.2 ˚F (0.7 ˚C)	2.0 ˚F * (1.1 ˚C)	1.5 ˚F (0.8 ˚C)	2.6 ˚F (1.4 ˚C)
	Nighttime	0.7 ˚F (0.4 ˚C)	1.6 ˚F (0.9 ˚C)	0.9 ˚F (0.5 ˚C)	1.2˚F (0.7 ˚C)	0.9 ˚F (0.5 ˚C)	0.9 ˚F * (0.5 ˚C)	1.1 ˚F (0.6 ˚C)	0.9 ˚F (0.5 ˚C)
	Overall	1.8 ˚F (1.0 ˚C)	1.6 ˚F (0.9 ˚C)	2.7 ˚F (1.5 ˚C)	1.2˚F (0.7 ˚C)	1.1 ˚F (0.6 ˚C)	1.6 ˚F * (0.9 ˚C)	1.3 ˚F (0.7 ˚C)	2.1 ˚F (1.2 ˚C)

* The lower bounds of the pavement thermal properties are those at normally dry condition.

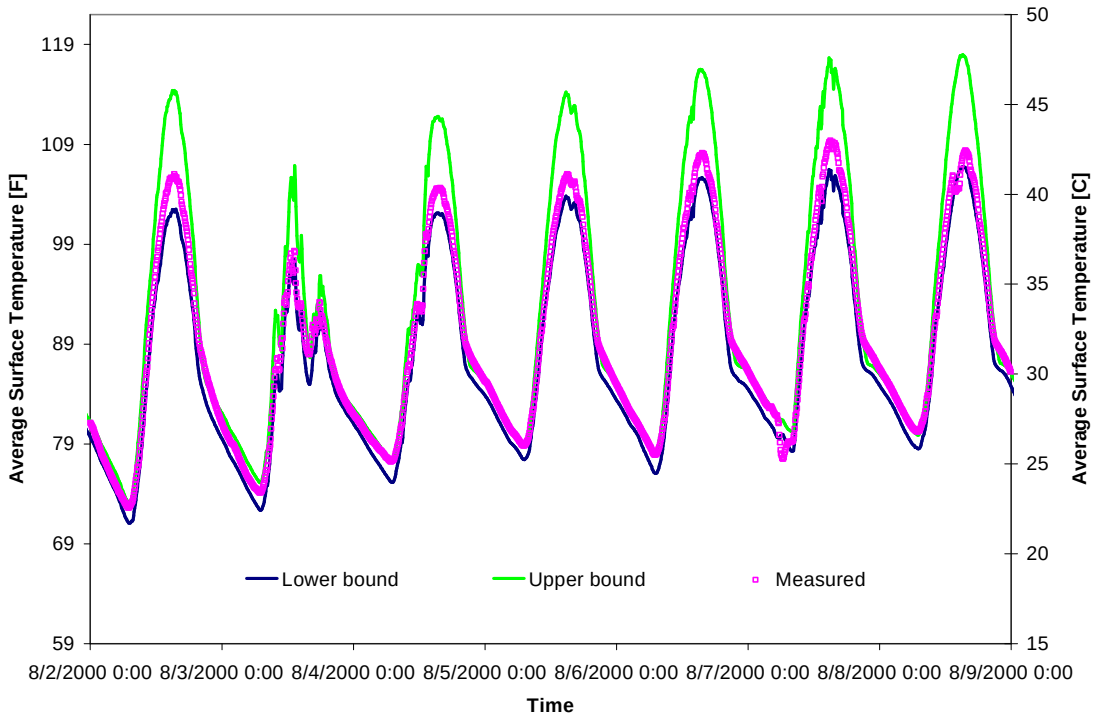

Figure 5-22 Effects of the combined uncertainties of the input parameters on the predicted average surface temperature.

The following conclusions may be drawn from the above uncertainty analysis:

- The difference between the predicted and measured surface temperature is within the estimated uncertainty level.
- While the uncertainties associated with the sky temperature, solar absorptance, convection heat transfer coefficient, and pavement thermal properties can significantly affect the predicted average surface temperature during the daytime, only the uncertainties in the sky temperature make significant difference in the predicted average surface temperature during the nighttime.

- Compared with data from a published source (Levinson and Akbari 2001), the measured solar absorptance used in the system simulation, which is 0.6, is very likely overestimated. Reducing the solar absorptance to the lower bound of uncertainty of the measurement (by 11% from 0.6 to 0.53) can almost eliminate the difference between the predicted and measured surface temperature. It also reduces the error in the cumulative heat transfer to the ground to 1%.

5.3.3.2. System in Heating Mode

The validation of the system simulation in heating mode is conducted using measured data during a heating operation from 12/23/02 to 12/25/02. As discussed in section 5.4.2.1, the loads history does not make significant difference in the performance of the GLHE. Therefore, the system simulation only covers the period from 12/20/02 to 12/25/02. The three days ahead of the heating operation is the initial period of the simulation. In the system simulation, the time step is fixed to be 10 minutes since the experimental data are recorded every 10 minutes. In this period, a mixture of propylene glycol and water at a weight concentration of 39% was used as heat transfer fluid in both the load and source sides of the heat pump. As shown in Figure 5-23, the source side flow rate was kept at 19.6 GPM (1.24 L/s) with less than 4% variation and the load side flow rate was kept at 12.0 GPM (0.76 L/s) with less than 3% variation. Therefore, constant flow rates of 19.6 GPM (1.24 L/s) and 12.0 GPM (0.76 L/s) are used in the system simulation.

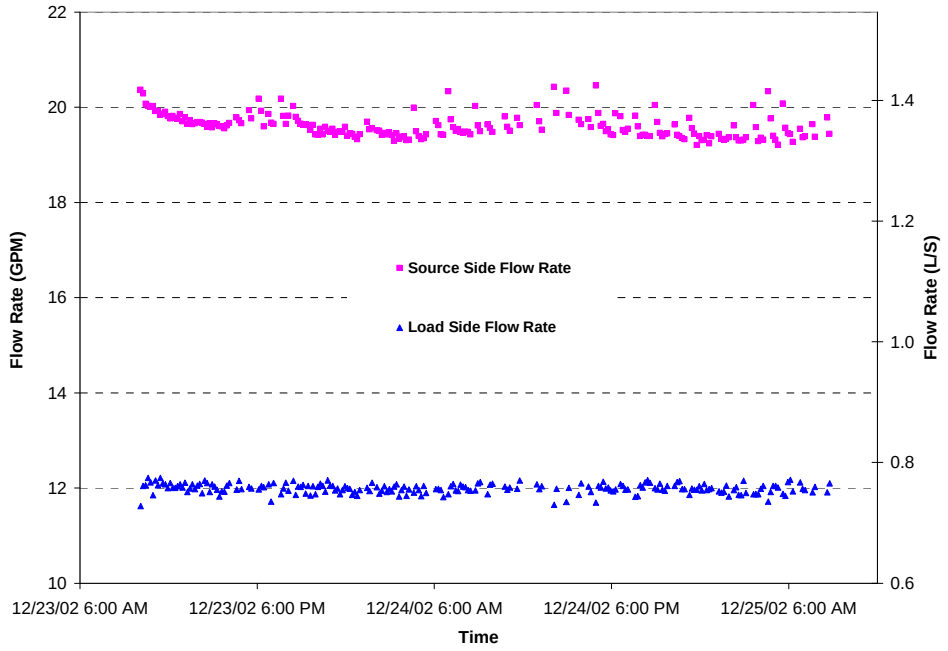

Figure 5-23 Measured flow rate in heating operation.

The measured and predicted average surface temperatures and snow free area ratio from 12/23/02 6.00 am to 12/24/02 12.00 am when a snow event occurred are compared in Figures 5-24 and 5-25, respectively. As can be observed in Figure 5-24, the predicted average surface temperature matches the measured data very well. The maximum difference is less than 1.8°F (1°C). Oscillation of the surface temperature after the surface clear from snow can be observed in Figure 5-24, which is due to the intermittent operation of the heat pump controlled by the On-Off controller. The peak predicted average surface temperatures are higher than the measured data. As discussed in Chapter 4, the residual water and drifting snow on the bridge deck surface after it is clear from the snow are not accounted for in the bridge model. The corresponding surface

heat losses are neglected in the model. This is believed to be the cause of the difference between the predicted and measured average surface temperature.

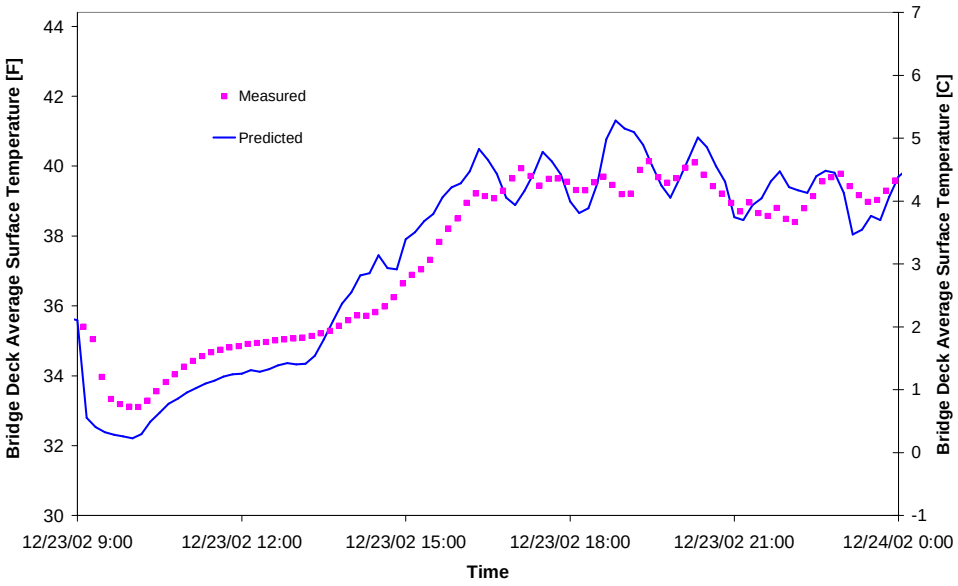

Figure 5-24 Measured and predicted bridge deck average surface temperature – heating mode.

Figure 5-25 shows that the predicted time for melting all the snow is about 1 hour longer than what was observed. Since the whole time period from the beginning of snowfall to the moment when the surface is clear of snow is about 8 hours, the relative error of the prediction is 13%. This is identical with the simulation result of the individual bridge model.

Figure 5-26 and 5-27 show the comparison between the predicted and measured entering and exiting fluid temperatures of the bridge loop and the GLHE. As previously stated, only the predicted and measured fluid temperature when there is flow circulated in

the system are presented in the figures. As a result, the curves for the predicted temperatures are not continuous.

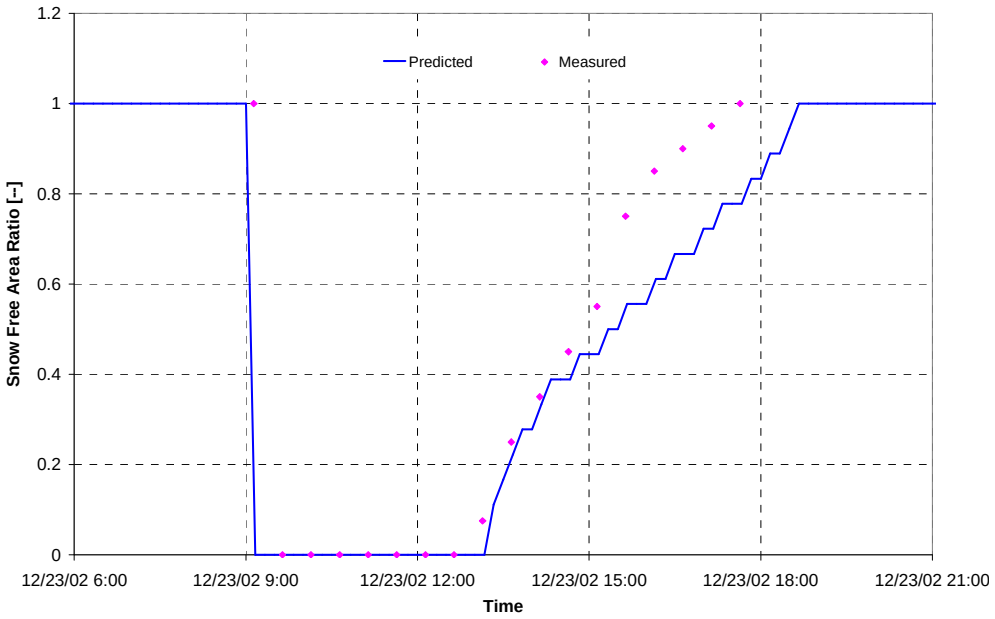

Figure 5-25 Measured and predicted snow free area ratio.

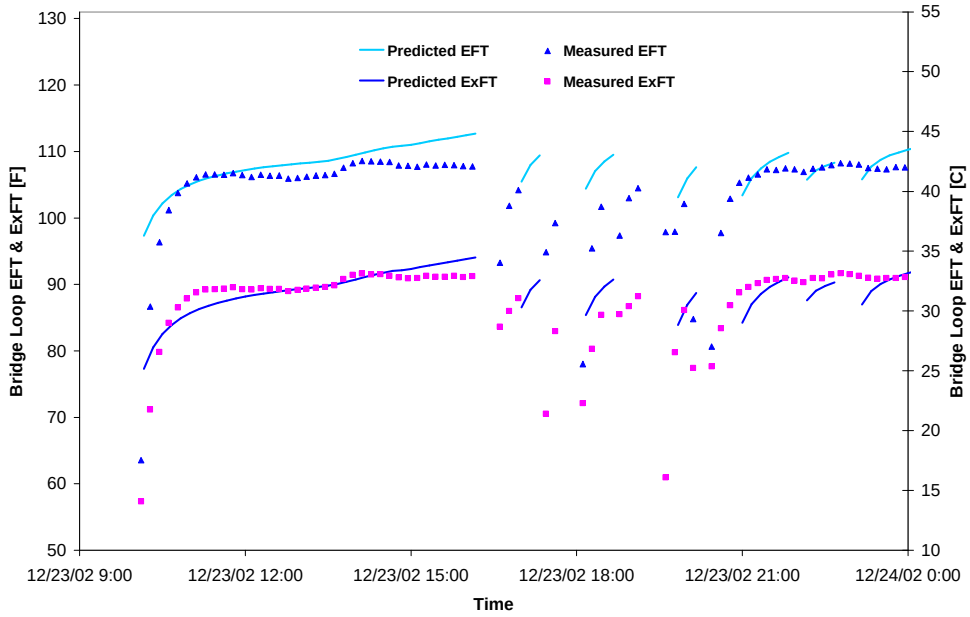

Figure 5-26 Measured and simulated entering and exiting fluid temperature to the bridge deck– heating mode.

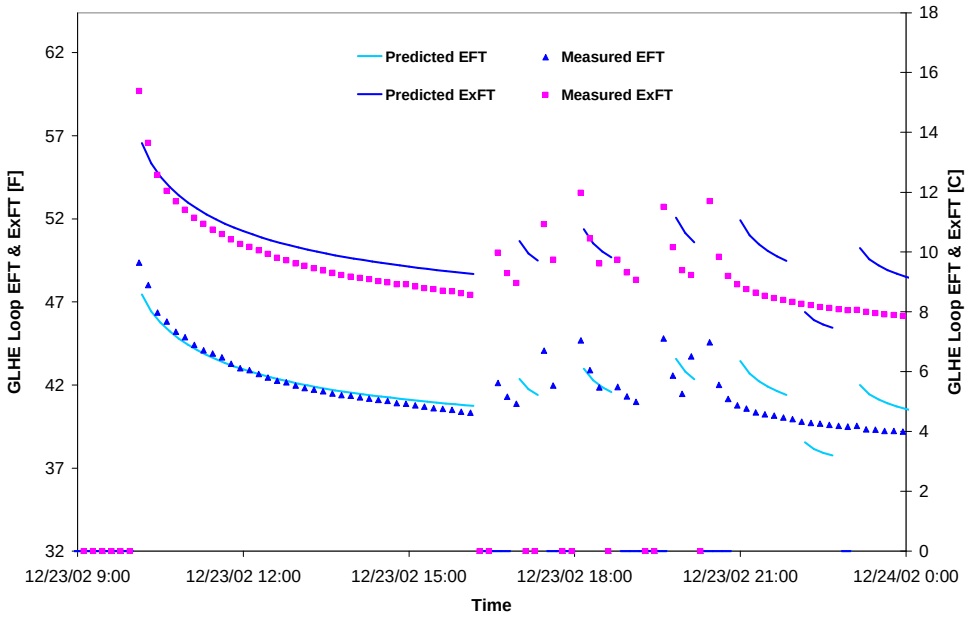

Figure 5-27 Measured and simulated entering and exiting fluid temperature to the GLHE– heating mode.

From the above two figures, it can be seen that larger differences between the predicted and measured temperature occur at the beginning of the heating operation. In addition, the predicted temperatures can more closely match the measured data when the system is continuously operated than when the system is turned on and off frequently. It can also be observed from the figures that the simulated operating time is shorter than what was shown by the measured data in the later time of the simulated period. It results from the error in the prediction of bridge average surface temperature as discussed in Chapter 4.

Figure 5-28 and 5-29 show the comparison between simulation results and the measured data for the heat transfer rate in the bridge loop and GLHE, respectively. Figure 5-30 shows the comparison for the heat pump power.

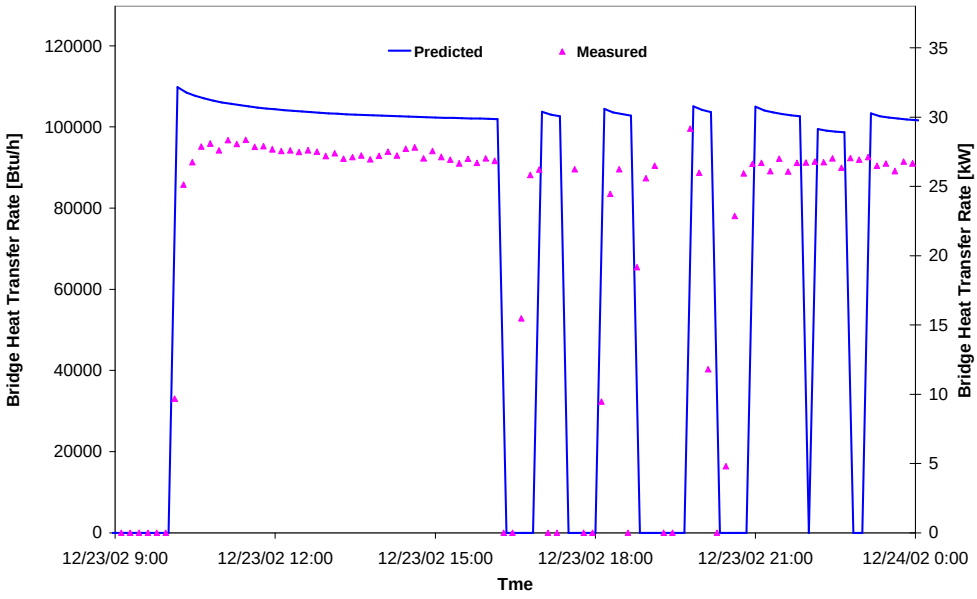

Figure 5-28 Comparison between measured and predicted bridge heat transfer rate - heating mode.

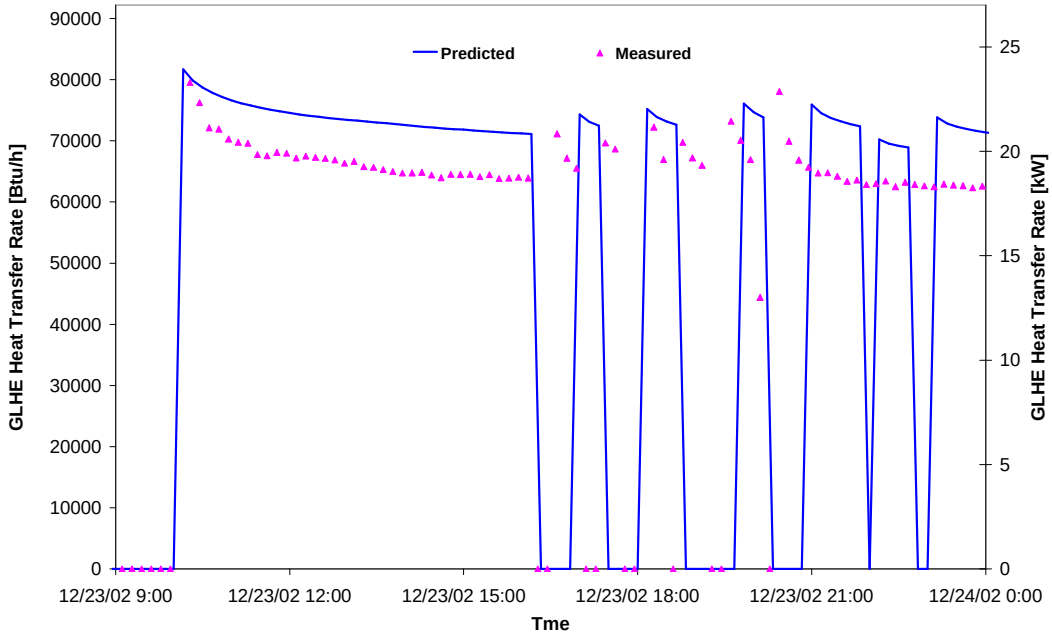

Figure 5-29 Comparison between measured and predicted GLHE heat transfer rate - heating mode.

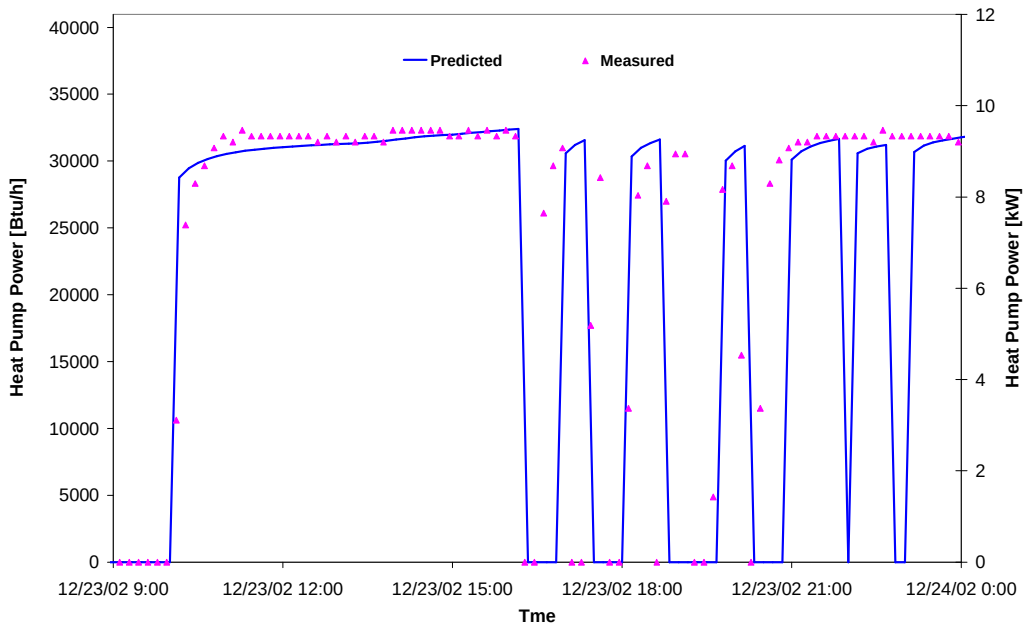

Figure 5-30 Comparison between measured and predicted heat pump power - heating mode.

The above three figures show consistently that the predicted heat transfer rates and heat pump power can more closely match the measured data when the system is continuously operated than when the system is turned on and off frequently. Average differences between the predicted and measured load and source side heat transfer rates and the heat pump power are 13.3 %, 9.1 %, and 0.9 % respectively when the system is continuously operated, but they go up to 17 %, 10.5 %, and 10.5 % when the system is turned on and off frequently.

5.4. Conclusions

A computer simulation program of the GSHP based hydronic snow melting system has been implemented under the component-based simulation environment of

HVACSIM+. Necessary modifications have been made in the previously developed component models in order to improve the accuracy, computational efficiency, and the reliability of the system simulation.

To avoid numerical problems resulting from discontinuity, the discrete controller has been treated specially in the system simulation by updating its outputs explicitly instead of solving them simultaneously with other continuous variables. This procedure has been implemented using the hierarchical structure of HVACSIM+.

The system simulation has been validated with measured data from an experimental GSHP-based hydronic snow melting system. Validation exercises that compare measured data with simulation predictions from both the individual component models and whole system simulation have been conducted. Validation results have shown that the system simulation is able to predict the surface conditions during the snow melting process with reasonable accuracy. The predictions of fluid temperatures, heat transfer rates, and the power consumption match the measured data fairly well when the system is operated continuously. However, increased discrepancies between simulation predictions and measured data occur when the system is turned on and off frequently.

It appears that the “Antifreeze Degradation Factor (ADF)” approach adopted in the heat pump model is not valid for the case where the model coefficients have been estimated based on turbulent flow in the evaporator, but where the flow is actually laminar. Although the model performance has been improved by applying an additional

correction to the overall heat transfer coefficient of the evaporator, it is desirable to develop a more general algorithm that can be implemented in the model to distinguish laminar flow and apply a proper correction.

CHAPTER 6. SIMULATION BASED INVESTIGATION ON THE DESIGN OF HYDRONIC SNOW MELTING SYSTEMS

Determining the heating capacity is the first important task in the design of the hydronic snow melting system. Current guidance in the ASHRAE HVAC Applications Handbook (2003) for required surface heat fluxes is based on a one-dimensional steady-state heat balance (Ramsey et al. 1999) of the snow-melting surface. For 46 North American locations, the required heat flux to maintain a specified snow free area ratio for a statistically determined percentage of hours with snowfall has been tabulated. Required heat fluxes are given for snow free area ratios of 0, 0.5, and 1, and for percentage-of-snowfall-hours-not-exceeded of 75%, 90%, 95%, 98%, 99% and 100%.

This approach is limited by the fact that real systems are almost never operated continuously through the winter due to the energy cost implications. Rather, the systems are turned on when a pavement sensor detects the presence of snow or ice. It is also possible that the systems might be turned on a few hours in advance of a snowfall event. While not common practice, such a control system is the topic of an ongoing research project (Jenks et al. 2003). In addition, two-dimensional effects, such as pipe spacing and bottom losses are clearly important, but neglected by the procedure used to develop the design heat fluxes. Furthermore, the required heat fluxes were all computed without

considering the contribution from solar radiation. This is a conservative approximation but its effect is not well understood.

Given the transient, two-dimensional and solar effects, it is unclear how an actual snow melting system performance might compare to the tabulated values. To answer this question, a simulation-based investigation has been conducted. The system simulation utilized in this investigation employs the transient and two-dimensional model of the hydronically-heated slab, which has been introduced in Chapter 4, and uses multi-year actual weather data. The primary objective of this investigation is to evaluate the performance, under realistic transient operating conditions, of snow melting systems designed with the heat fluxes given in the ASHRAE handbook. In addition, the impact of idling time, heating capacity, pipe spacing, bottom insulation and control strategies on snow melting performance will also be investigated.

6.1. ASHRAE Snow-melting Loads

Tabulated surface heat flux requirements for 46 North American cities in the ASHRAE Handbook of HVAC Applications (2003) are based on the results from an ASHRAE research project (Ramsey et al. 1999). The algorithm for calculating the surface heat flux requirements was based on the one dimensional steady-state energy balance for required total heat flux (heat flow rate per unit surface area) q_o at the upper surface of a snow-melting slab during snowfall:

$$q_o = q_s + q_m + A_r(q_h + q_e) \tag{6-1}$$

where,

q_o : total required heat flux, Btu/hr-ft^2 (W/m^2)

q_s : heat flux required to raise the temperature of snow falling on the slab to the melting temperature plus, after the snow has melted, to raise the temperature of the liquid to the assigned temperature of the liquid film, Btu/hr-ft^2 (W/m^2)

q_m : heat flux required to melt the snow, Btu/hr-ft^2 (W/m^2)

q_h : combined convective heat losses to the ambient air and radiative heat losses to the surroundings, Btu/hr-ft^2 (W/m^2)

q_e : heat flux for evaporating the melted snow, Btu/hr-ft^2 (W/m^2)

A_r : equivalent snow-free area ratio, which is defined as the ratio of the snow free area of a surface to the total area of the surface, dimensionless

The procedures for evaluating each of the terms are described in the ASHRAE Handbook of HVAC Applications (2003) and the paper of Ramsey et al. (1999). In the calculations, the slab surface temperature was assumed uniform at 33°F (0.6°C). Based upon the frequency distribution of hourly heat fluxes, which were calculated with weather data for the years 1982 through 1993, the design heat flux was chosen to maintain certain surface snow-free area ratios for a percentage of snowfall hours.

"Idling" operation was described in the same ASHRAE Handbook as supplying heat to the slab anytime the ambient temperature is below 32°F (0°C) and it is not

snowing. The purpose of such idling operation is to maintain the slab surface temperature above the freezing point of water, so that snow can be melted immediately at the beginning of snowfall with the steady-state heat flux. However, as illustrated by the data presented in the same handbook, the annual energy requirement for idling can be more than 20 times greater than that for snow melting. Obviously, such idling operation is not energy efficient and is seldom done in practice.

As reviewed previously, there are two primary limitations on the surface heat fluxes presented in the ASHRAE handbook: the first is that the calculations were based on steady state heat balance on the surface of a slab, and therefore, the transient effects of weather and operation were not taken into account; the second is that the slab surface temperature was assumed to be uniform, and therefore, the effect of the arrangement of the pipes was not considered. Furthermore, the solar radiation was not taken into account in the calculations. Since snow-melting systems generally have heating elements embedded in material of significant thermal mass, transient effects should not be neglected in determining the required surface heat flux. A two-dimensional transient analysis of the snow melting system (Rees et al. 2002) has shown that, for particular storm conditions, heat fluxes up to five times greater than those indicated by steady-state analysis need to be delivered to the slab in order to keep its surface clear from snow during the early hours of the snowfall when the heating system is just starting to operate. On the other hand, continuous idling of the system as described in the handbook can eliminate the transient effect but will consume too much energy to be practical. Utilizing weather forecasts and local weather data, it may be possible to predict snow events

several hours in advance with reasonable accuracy (Jenks et al. 2003). This will significantly reduce the idling operation but may also require higher heating capacity than that calculated from the steady-state heat fluxes to achieve the desired snow melting performance. Therefore, the relationship between the idling duration and the snow melting performance is important to reach the optimal balance between the system heating capacity and the operating costs.

6.2. Simulation Approach

A simple hydronic snow melting system is simulated in this work. This system consists of a hydronically-heated slab, a circulating pump, a heater and a controller. Figure 6-1 shows a schematic of this system.

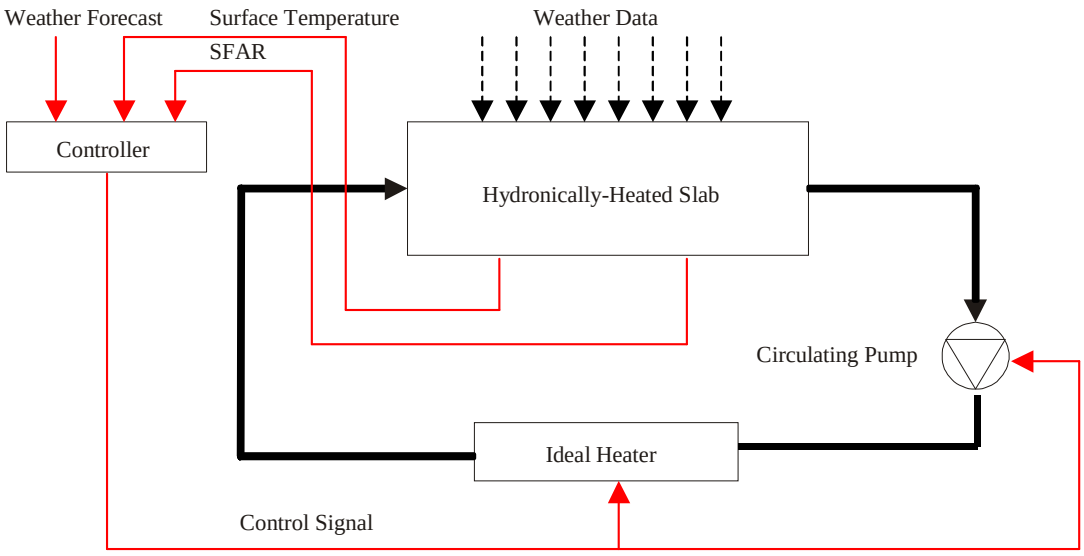

Figure 6-1 Schematic of the simulated hydronic snow melting system.

The parameters of the hydronically-heated slab are intended to be typical for a heated bridge deck application and are summarized in Table 6-1. The heater, when operating, provides a constant heat input to the slab. The fluid temperature will rise to the necessary level to provide the specified heat input, although this may sometimes result in unfeasibly high fluid temperatures. Since the purpose of this simulation is to evaluate the heat input to the slab, neither thermal mass nor transport delay are considered in the heater model.

TABLE 6-1 Parameters of the Hydronically-Heated Slab

Design Parameters	Parameter Value (SI Units)	Parameter Value (IP Units)
Slab Thickness *	203 mm	8 in
Slab Thermal Conductivity *	1.4 W/m.K	0.81 Btu/hr.ft.^{o}F
Slab Volumetric Heat Capacity *	2200 kJ/m^{3}-C	32.8 Btu/ft^{3}-^{o}F
Slab Surface Solar Absorptance	0.6	
Pipe Spacing *	152 mm	0.5 ft
Pipe Depth Below Surface	76 mm	3 in
Pipe Diameter	25mm	1 in
Pipe Wall Thickness	2 mm	0.0625 in
Pipe Wall Thermal Conductivity	0.39 W/m-K	0.23 Btu/hr-ft-^{o}F
Bottom Insulation *	Adiabatic	
Heat Carrier Fluid	Propylene Glycol (42% concentration by mass)	

* Varied parameters in the parametric study; values given are for the base case.

The controller is assumed to be perfect – it will turn on the heating system a certain number of hours in advance of the snowfall, and will turn it off at the end of the snowfall or when the slab surface is clear from snow. This number of hours is referred to as the idling time. This perfect control is accomplished by looking ahead in the weather

file. In practice, an imperfect forecasting tool would be used. The work described here will be useful in determining the requirements for a successful forecasting controller. For example, how many hours in advance does the system need to be turned on?

The system simulation was implemented in the HVACSIM+ (Clark 1985) environment, using component models of a hydronically-heated slab, a circulating pump, a heater and a controller, connected together in a graphical user interface (Varanasi 2002).

6.3. Weather Data

Since the weather conditions associated with snow events vary widely, it is desirable to investigate the snow melting performance with a number of years of weather data in order to draw a more reliable conclusion on the effect of transient weather/operation conditions on the snow melting performance. Ten different North American locations have been chosen to represent a range of climates. In the calculations which led to the tabulated ASHRAE design heat fluxes, the weather data for the years 1982 to 1990 were taken from the Solar and Meteorological Surface Observation Network (SAMSON)(NCDC 1993), while the data for 1991 through 1993 were taken from DATSAV2 (NSSL/NCDC 2003). Since the DATSAV2 data were not available for current study, SAMSON data from 1981-1990 were used in the simulations. The average hours of snowfall were compared for the two periods, which are 1981-1990 vs. 1981-

1993; they are close (within 6 %) for six of the ten locations. For Minneapolis, OKC, Spokane and Reno, the differences are 8%, 9%, 10% and 11% respectively.

The following measurements were extracted from the SAMSON data:

- Hourly values of the precipitation amount in equivalent depth of liquid water
- Precipitation type
- Ambient air dry-bulb temperature
- Dew-point temperature
- Wind speed
- Total solar radiation incident on a horizontal surface
- Cloud cover fraction
- Cloud height

In addition to the data used in the calculation of the ASHRAE design loads, two additional measurements, total horizontal solar radiation and cloud height, are utilized in the current research in order to account for solar radiation and more accurately compute the thermal radiative exchange between the slab top surface and the sky.

6.4. Organization and Methodology of Parametric Study

The immediate goal of the parametric study is to find the actual snow melting performance of systems with given heating capacity, idling time and slab design at

particular locations. Following the ASHRAE design procedure, the snow melting performance is expressed here by the percentage of hours when the system can keep the slab surface clear from snow during snowfall. In this study, the heating capacity of the system is specified as a parameter of the heater and determined by multiplying the heated area with the surface heat fluxes tabulated in the ASHRAE Handbook, corresponding to percentage of snowfall hours not to be exceeded (75%, 90%, 95%, 98%, 99% and 100%). In addition to the location and heating capacity, other parameters to be varied include the idling time (0,1,3,5 hours), pipe spacing, and bottom boundary condition.

One of the aims of the current study is to investigate the performance of snow melting systems designed with the heat fluxes given in the ASHRAE handbook. Specifically, to what degree will a system designed with the tabulated heat fluxes be able to give the indicated snow melting performance? Therefore, most of the work has been done with a simple control strategy, referred to as "snow only." This control strategy turns the system on at its full design capacity during snowfall and during the idling period. This strategy may not be energy efficient and will often result in excessively high fluid and surface temperatures when the system is operated in relatively mild weather conditions.

In addition, a more practical control strategy, referred to as "snow and surface temperature" has been evaluated. This control strategy turns the system on during the same times (during snowfall and idling) as the "snow only" control strategy. However, the system output is modulated so that the temperature on the surface midway between

pipes is not higher than 37°F (3°C). This is implemented with a dead band control strategy. During idling or snowfall, the controller will turn on the heater if the surface temperature between the two adjacent pipes is lower than 36°F (2.5°C); and turn off it if the temperature is higher than 37°F (3°C). In addition, if any snow remains after the snowfall is over, the controller will continue to maintain the surface temperature within the specified range.

As discussed in Chapter 4, one of the limitations of the bridge model is that it does not account for the variation of pavement thermal properties during the snow melting process. In fact, due to the penetration of snowmelt into the pavement, moisture content of the pavement is increased and in turn the thermal properties of the pavement will be changed. It is of interest to know to what degree this limitation will affect the results of predicted snow melting performance. As a result, simulations of bridges that use the thermal properties of limestone concrete at saturated condition are used for some cases in this parametric study.

Pavement thickness given in Table 6-1 is 8” (203 mm), which is actually the lower limit of the typical thickness of pavement used in bridges. In practice, the pavement can be as thick as 11” (279 mm). Since thickness affects the thermal mass of the pavement, which affects the transient response of the pavement, it is also of interest to investigate the sensitivity of snow melting performance to the pavement thickness.

The parametric studies are divided into six sets of cases, as shown in Table 6-2. In the first two sets of cases, the bottom of the slab is assumed perfectly insulated (adiabatic). The first and second sets are identical, except that the pipe spacing is 6" (150 mm) in the first set and 12" (300 mm) in the second set. (Also, only five locations are simulated.) In the third set of cases, the bottom of the slab is fully exposed to the environment without any insulation. The pipe spacing of 6" (150 mm) is specified in this set of cases. In the first three sets of parametric studies, the "snow only" control strategy is used. The fourth set, which uses the "snow and surface temperature" control strategy, is for two locations -- Chicago and SLC. The last two sets of simulations are also for Chicago and SLC. In the fifth set, the thermal properties of limestone concrete at saturated condition are used; in the sixth set, pavement thickness is 11" (279 mm). In total, there are 624 different cases in the parametric study. The computational time for each case (10 year simulation) is around 40 minutes on a personal computer with a CPU of Pentium 4, 2.8G HZ. Batch files are used to automate the parametric study.

TABLE 6-2 Organization of Parametric Study for Ar = 1

	Parameter	Number of Variations
Set 1	Location: Spokane, Reno, SLC, Colorado Springs, Chicago, OKC, Minneapolis, Buffalo, Boston and Philadelphia	10
	Heating capacity *: 75%, 90%, 95%, 98%, 99%, 100%	6
	Idling duration: 0,1,3,5 hours	4
	Pipe spacing: 6 inches (150 mm)	1
	Bottom condition: Adiabatic	1
	Control strategy: "Snow only"	1
	Pavement thermal properties: at dry condition	1
	Pavement thickness: 8 inches (203 mm)	1
Set 2	Location: Chicago, Minneapolis, Philadelphia Reno and SLC	5
	Heating capacity *: 75%, 90%, 95%, 98%, 99%, 100%	6
	Idling duration: 0,1,3,5 hours	4
	Pipe spacing: 12 inches (300 mm)	1
	Bottom condition: Adiabatic	1
	Control strategy: "Snow only"	1
	Pavement thermal properties: at dry condition	1

	Pavement thickness: 8 inches (203 mm)	1
Set 3	Location: Chicago, Minneapolis, Philadelphia Reno and SLC	5
	Heating capacity *: 75%, 90%, 95%, 98%, 99%, 100%	6
	Idling duration: 0,1,3,5 hours	4
	Pipe spacing: 6 inches (150 mm)	1
	Bottom condition: Exposed	1
	Control strategy: "Snow only"	1
	Pavement thermal properties: at dry condition	1
	Pavement thickness: 8 inches (203 mm)	1
Set 4	Location: Chicago and SLC	2
	Heating capacity *: 75%, 90% and 99%	3
	Idling duration: 0,1,3,5 hours	4
	Pipe spacing: 6 inches (150 mm) and 12 inches (300 mm)	2
	Bottom condition: Exposed	1
	Control strategy: "Snow and surface temperature"	1
	Pavement thermal properties: at dry condition	1
	Pavement thickness: 8 inches (203 mm)	1
Set 5	Location: Chicago and SLC	2
	Heating capacity *: 75%, 90%, 95%, 98%, 99%, 100%	6
	Idling duration: 0,1,3,5 hours	4
	Pipe spacing: 6 inches (150 mm)	1
	Bottom condition: Adiabatic	1
	Control strategy: "Snow only"	1
	Pavement thermal properties: at saturated condition	1
	Pavement thickness: 8 inches (203 mm)	1
Set 6	Location: Chicago and SLC	2
	Heating capacity *: 75%, 90%, 95%, 98%, 99%, 100%	6
	Idling duration: 0,1,3,5 hours	4
	Pipe spacing: 6 inches (150 mm)	1
	Bottom condition: Adiabatic	1
	Control strategy: "Snow only"	1
	Pavement thermal properties: at dry condition	1
	Pavement thickness: 11 inches (279 mm)	1

* The heating capacity is calculated by multiplying the heated area with the ASHRAE surface heat fluxes, which are loads that was not be exceeded during certain percentage of snowfall hours from 1982 through 1993 according to the steady state analysis.

6.5. Results and Discussion

The simulation results were analyzed to characterize the relationship between the idling time, heating capacity and snow melting performance of a hydronic snow melting system. In addition, the effects of the arrangement of the pipes, bottom insulation and control strategies on this relationship are also investigated.

6.5.1. Idling Time, Heating Capacity, and Snow Melting Performance

Figure 6-2 is an attempt to show the results of the first set of parametric study cases all on one plot. The horizontal axis represents the percentage of snowfall hours where the surface would be snow free, based on the tabulated ASHRAE surface heat flux values, which vary with location. The vertical axis represents the percentage of snowfall hours where the surface would be snow free, based on transient simulation results of the systems with heating capacity corresponding to the ASHRAE surface heat flux. The diagonal line represents a one-to-one match between the performance of the system calculated with the transient simulation and the performance calculated based on a steady state heat balance. A point on this line would represent a case where the actual performance is as good as that predicted with the ASHRAE steady state heat balance analysis. In the plot, different symbols refers to cases with different idling times; individual data points with same symbol show the system performance at different locations.

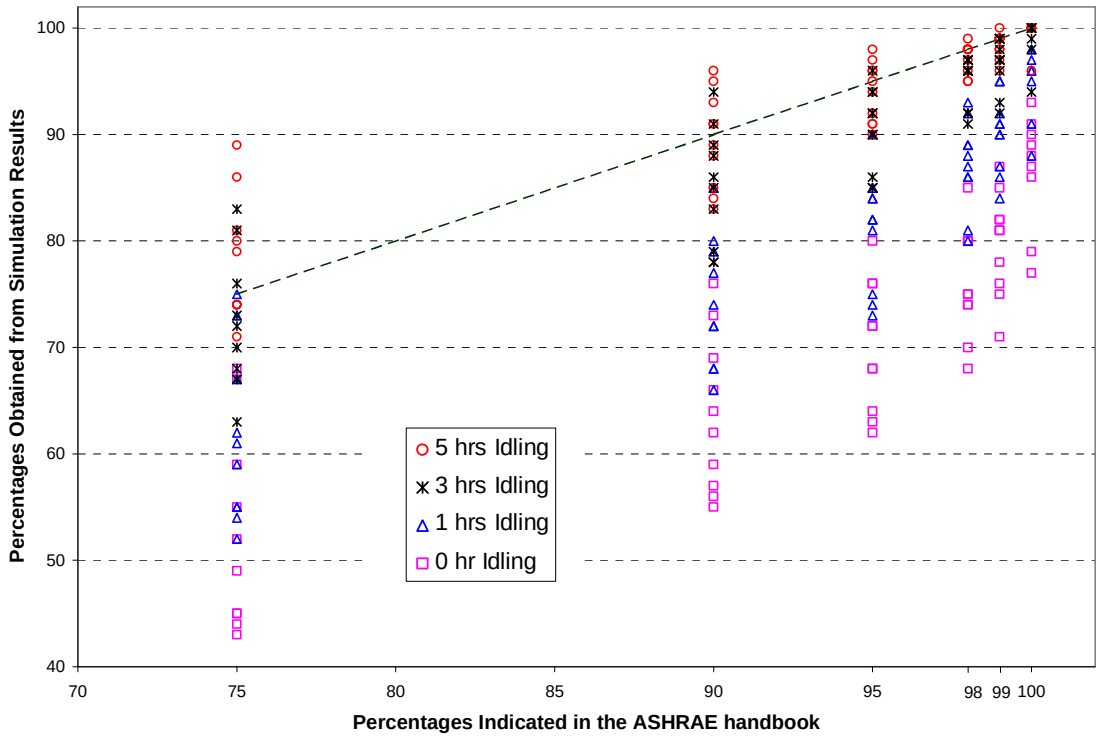

Figure 6-2 Snow melting performances obtained from the simulation results of the first set of parametric study (Adiabatic bottom and edges with 6" (150 mm) pipe spacing).

As expected, the performance increases with increasing idling times. For zero hours idling, i.e. the system is turned on when snowfall starts, the performance for all locations falls substantially below that predicted with a steady state heat balance. For most locations, approximately 5 hours of idling will give system performance similar to that expected from the steady state analysis. However, it may be noted that a few data points show good performance for even one hour of idling, and performance exceeding that expected from the steady state heat balance with three hours of idling. These data points correspond to Reno and Salt Lake City.

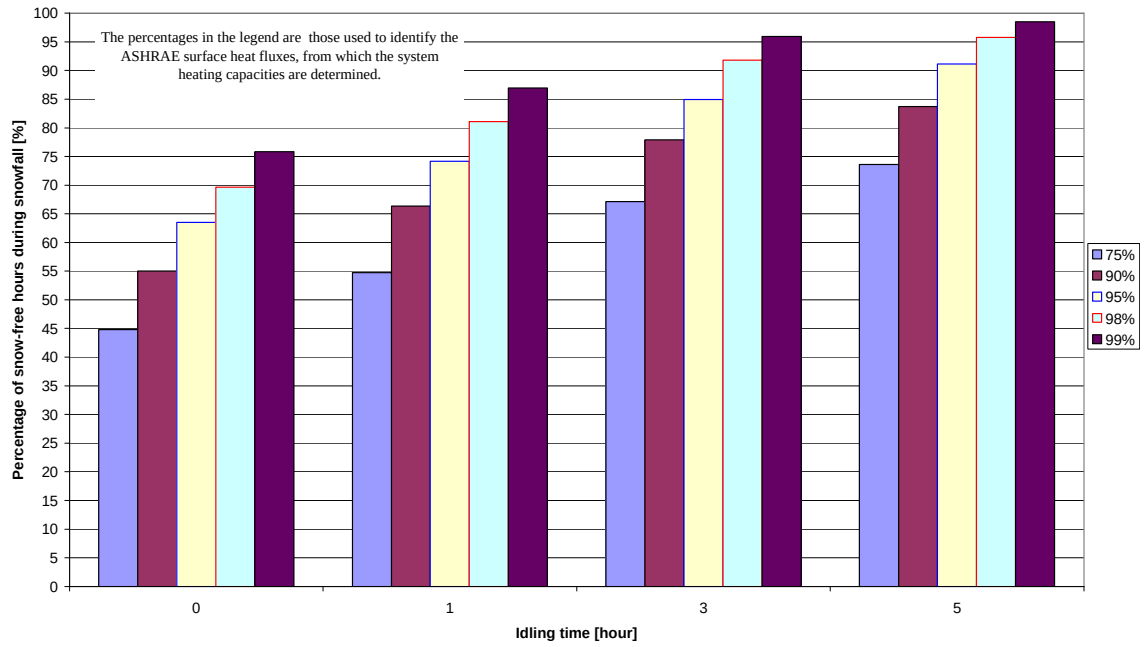

Figure 6-3 Relationship among the idling time, heating capacity and snow melting performance at Chicago.

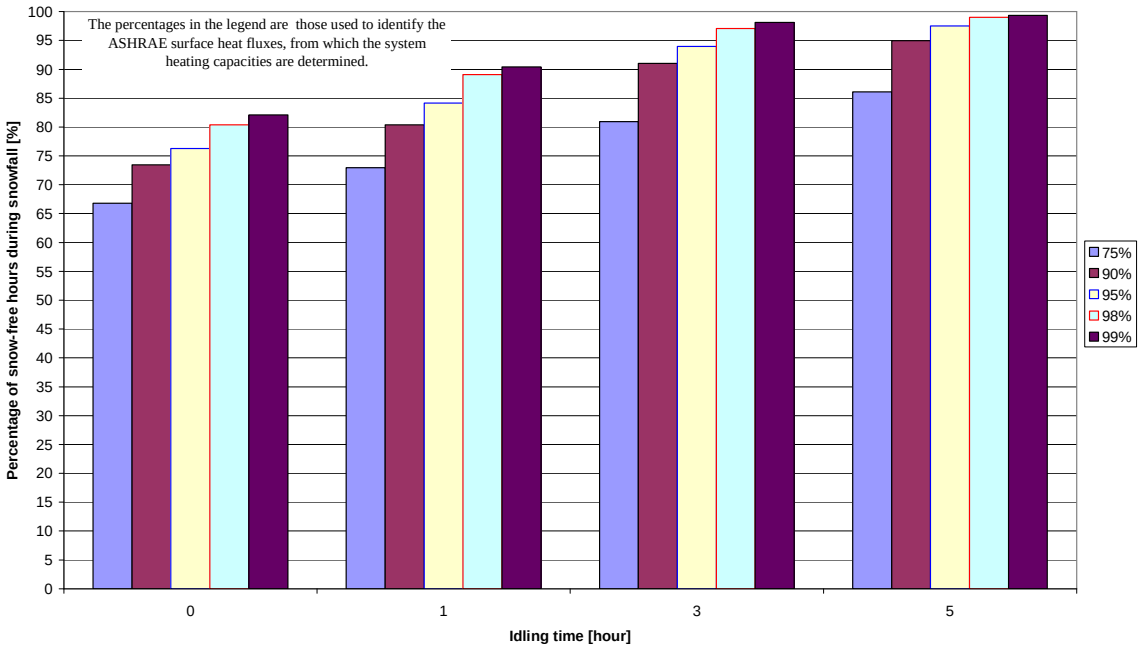

Figure 6-4 Relationship among the idling time, heating capacity and snow melting performance at Salt Lake City.

This difference can be seen more clearly in Figures 6-3 and 6-4, which show results for Chicago and Salt Lake City. The bars in these figures indicate the snow melting performance predicted by the simulation. For Chicago, five hours of idling gives performance similar (but not quite equal) to that expected from the steady state heat balance. However, for Salt Lake City, three hours of idling gives results that are close to or exceed that expected from the steady state analysis. To try to understand this phenomenon, a number of measures of the weather data were calculated. For hours coincident with snowfall, average values of dry bulb temperature, solar radiation flux, wind speed and snowfall rate were considered. At present, the best explanation seems to be that the average dry bulb temperature coincident with snowfall is comparatively high at Salt Lake City and Reno. This can be seen in Figure 6-5. Given the higher dry bulb temperature it is likely that the slab temperatures are also naturally higher, on average, at the start of each snowfall event. Therefore, less energy is required to raise the slab temperature above freezing. The higher dry bulb temperature also means less convective and radiative heat loss from the top surface of the slab. As a result, the surface heat flux requirements at Salt Lake City and Reno are significantly lower than those at other locations as can be seen in the ASHRAE Handbook of HVAC Applications (2003).

The simulations results illustrate that, for the system investigated in this parametric study, preheating the slab 3-5 hours before snowfall with the full heating capacity obtained from the ASHRAE surface heat flux requirement is necessary to achieve the desired snow melting performance.

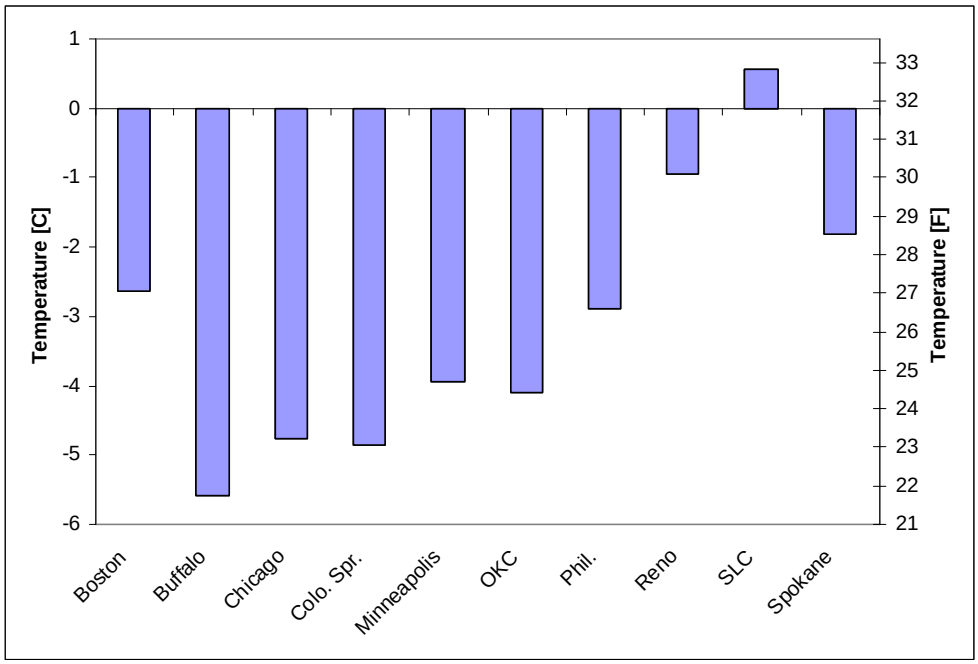

Figure 6-5 Average coincident ambient dry-bulb temperature during snowfall.

6.5.2. Effects of Pipe Spacing and Bottom Condition

Three combinations of pipe spacing and bottom condition have been simulated for a range of locations, heating capacities, and idling times in the first three sets of parametric studies, which use the "snow only" control strategy. However, due to space limitations, only the results of Chicago and Salt Lake City are shown in Figure 6-6 and Figure 6-7 respectively. Each figure gives the actual performance vs. the design performance for four different idling times and 6" (150 mm) and 12" (300 mm) pipe spacing with adiabatic bottom condition, and 6" (150 mm) pipe spacing with exposed bottom condition.

As can be seen, either increasing the pipe spacing or eliminating the bottom-side insulation degrades the performance of the system. Increasing the pipe spacing makes it more difficult to uniformly heat the top surface of the slab. Furthermore, this analysis assumes that the same heat flux is achieved with either spacing. However, increasing the pipe spacing requires higher fluid temperatures, some of which are infeasible.

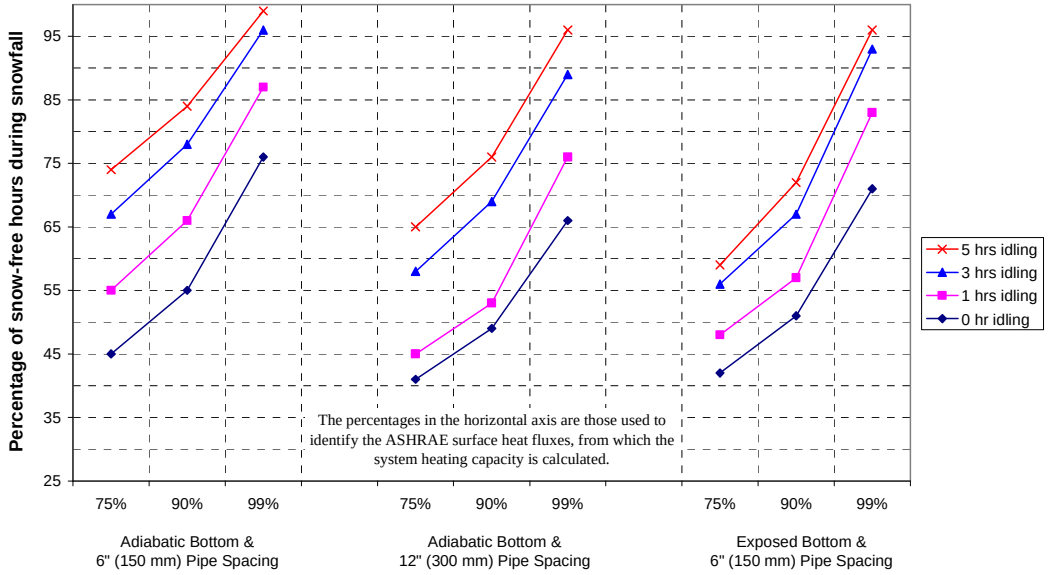

Figure 6-6 Parametric study results (with "snow only" control strategy) - Chicago.

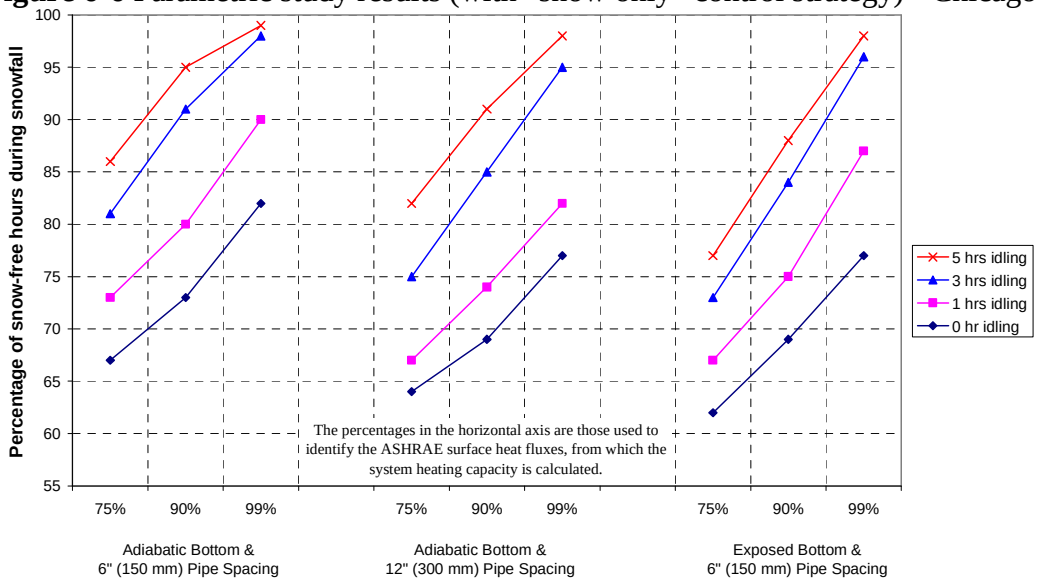

Figure 6-7 Parametric study results (with "snow only" control strategy) – SLC.

6.5.3. Effects of Control Strategies

In the fourth set of simulations, the "snow and surface temperature" control strategy is used instead of the "snow only" control strategy used in the first three sets of simulations. Figure 6-8 shows the snow melting performance of the systems at Chicago with different combinations of control strategy and pipe spacing. It can be seen in this figure that using the "snow and surface temperature" control strategy degrades the snow melting performance compared with the "snow only" control. The degradation is 3% when the system is not idled and it goes up to 10% when the system is idled 5 hours before snowfall. The decrease in performance is due to the lower surface temperatures maintained with the "snow and surface temperature" control strategy. Increasing the pipe spacing from 6" (150 mm) to 12" (300 mm) further degrades the performance.

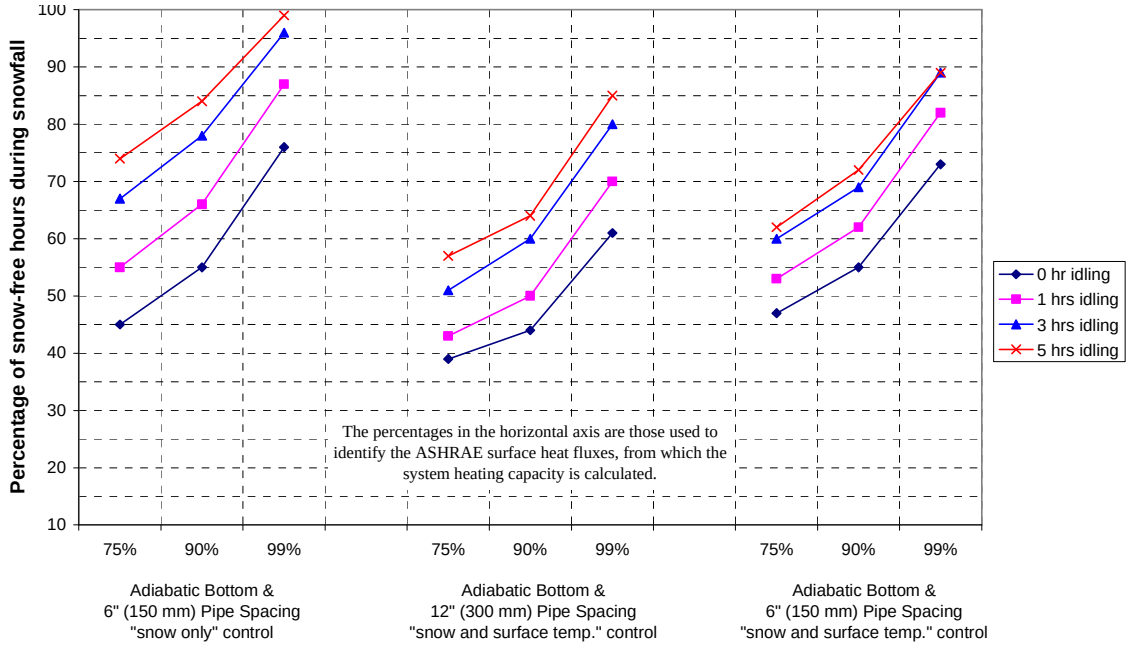

Figure 6-8 Comparison of snow melting performance resulting from different combinations of control strategy and pipe spacing - Chicago.

However, the reduction of heating energy consumption resulting from the "snow and surface temperature" control strategy is much more significant. Figure 6-9 shows a comparison of the cumulative heating energy consumed from 1981 to 1990 by the systems at Chicago with different control strategies. The system heating capacity is determined with 99% steady state snow melting loads, which is 235 Btu/h-ft^2 (740 W/m^2). In the simulation, 6" (150 mm) pipe spacing is used and the lower surface of the slab is perfectly insulated. As shown in Figure 6-9, the system controlled with "snow and surface temperature" strategy consumes much less energy than the system controlled with the "snow only" strategy, especially when longer idling operation is used.

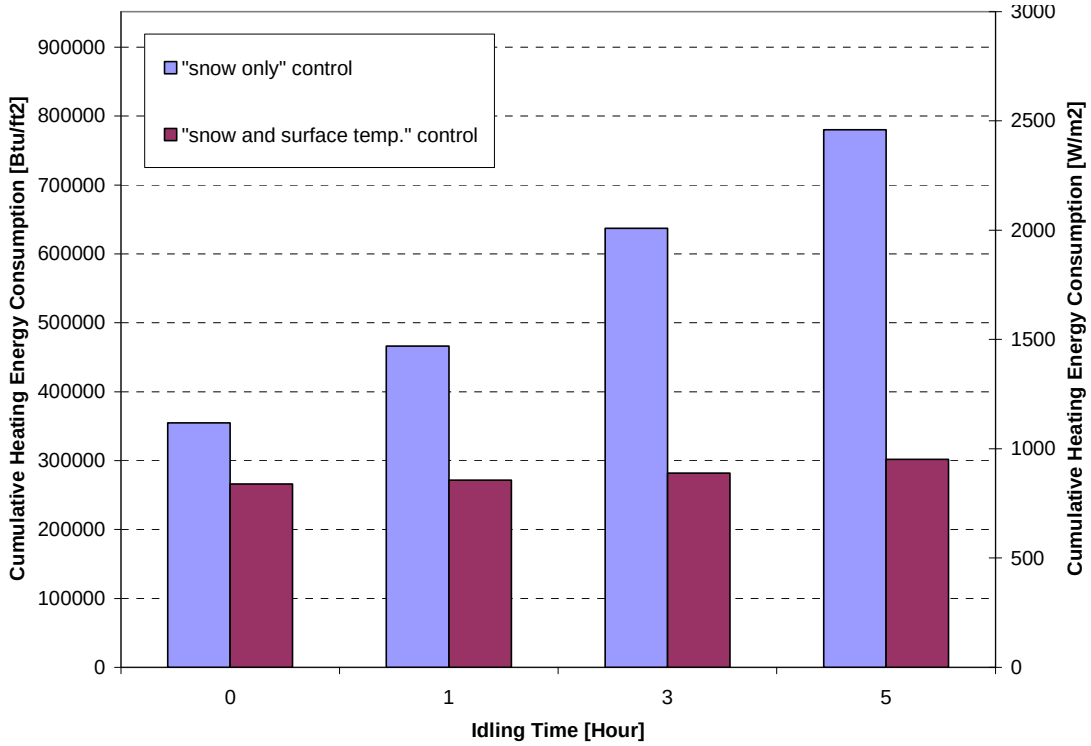

Figure 6-9 Comparison of the 10-year (from 1981 to 1990) cumulative heating energy consumed by the systems with different control strategies - Chicago.

Further simulations of the systems controlled with the "snow and surface temperature" strategy have been performed to get the data of annual heating energy consumption. These data are compared with the data calculated using the steady state analysis and tabulated in the ASHRAE Handbook (2003)[11]. To be consistent with the condition described in the ASHRAE Handbook, the simulated systems are designed with the 99% steady state snow melting loads. Different from the continuous idling used in the steady state analysis, the systems are idled only 5 hours ahead of the snowfall in the simulations. As shown in Figure 6-10, the annual heating energy consumptions of systems controlled with the "snow and surface temperature" strategy and idled only 5 hours before snowfall are significantly less than those resulting from the continuous idling operation. For the simulated 10 locations, the savings in the annual heating energy consumptions are in the range from 49% (at Buffalo) to 89% (at Reno). However, as shown in Figure 6-11, the snow melting performances that achieved by systems controlled with the "snow and surface temperature" strategy and idled only 5 hours before snowfall are about 10% lower than the designed snow melting performance.

[11] The annual heating energy consumption is a sum of the heating energy consumed for melting and idling over the year. Continuous idling is assumed in the steady state analysis. The melting loads are based on systems designed to satisfy the loads 99% of the time for achieving a snow-free surface ($A_r = 1$).

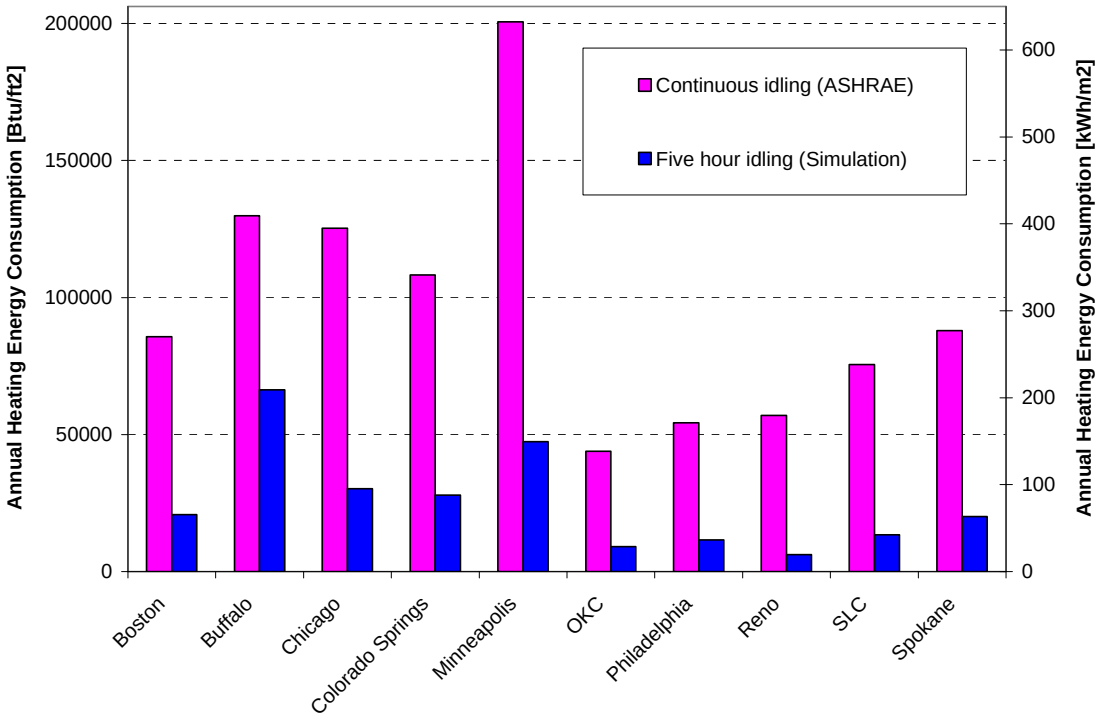

Figure 6-10 Comparison of annual heating energy consumption between continuous idling (ASHRAE) and five hour idling (simulation results).

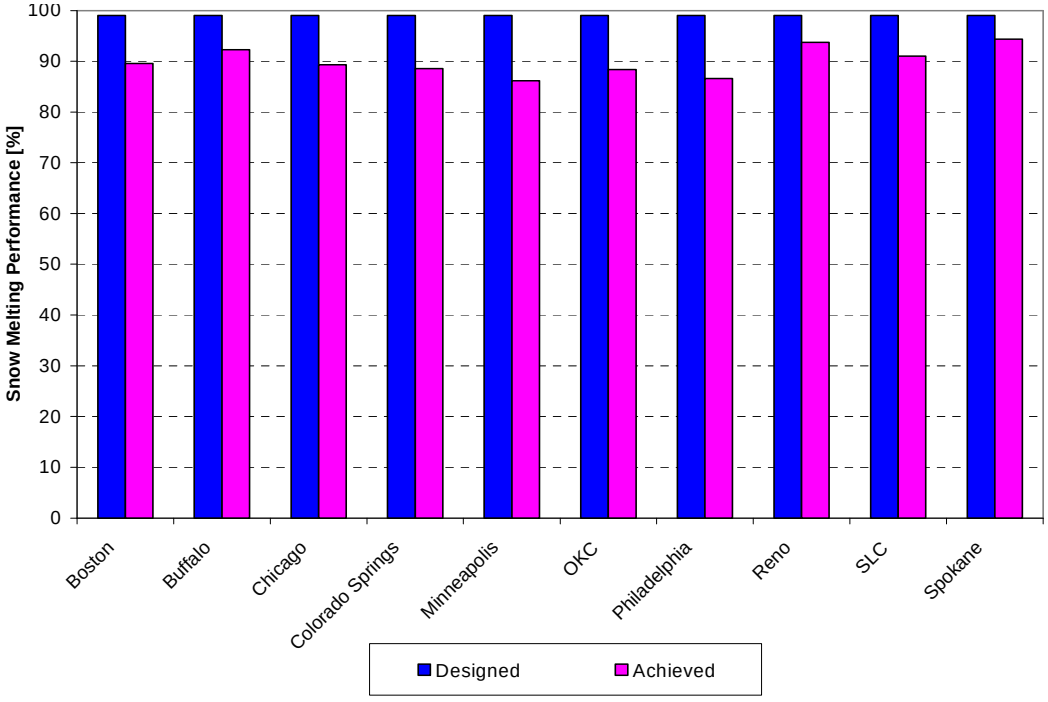

Figure 6-11 Comparison between the designed and achieved snow melting performance.

Although the “snow only” control strategy would seem to result in better snow melting performance, it often requires impractically high fluid temperatures, as can be seen in Figure 6-12. Likewise, even with the “snow and surface temperature” control strategy, a 12” (300 mm) spacing requires very high fluid temperatures to deliver the design heat fluxes. The heat source, piping material, and working fluid place limitations on the maximum fluid temperature. For example, a heat pump system typically cannot exceed 55°C (131 °F). Cross-linked polyethylene piping used in radiant heating systems typically has an upper temperature limit of 82°C (180 °F). Water/anti-freeze solutions may be able to exceed 100°C (212°F), but it is not clear that using such high temperatures is advisable.

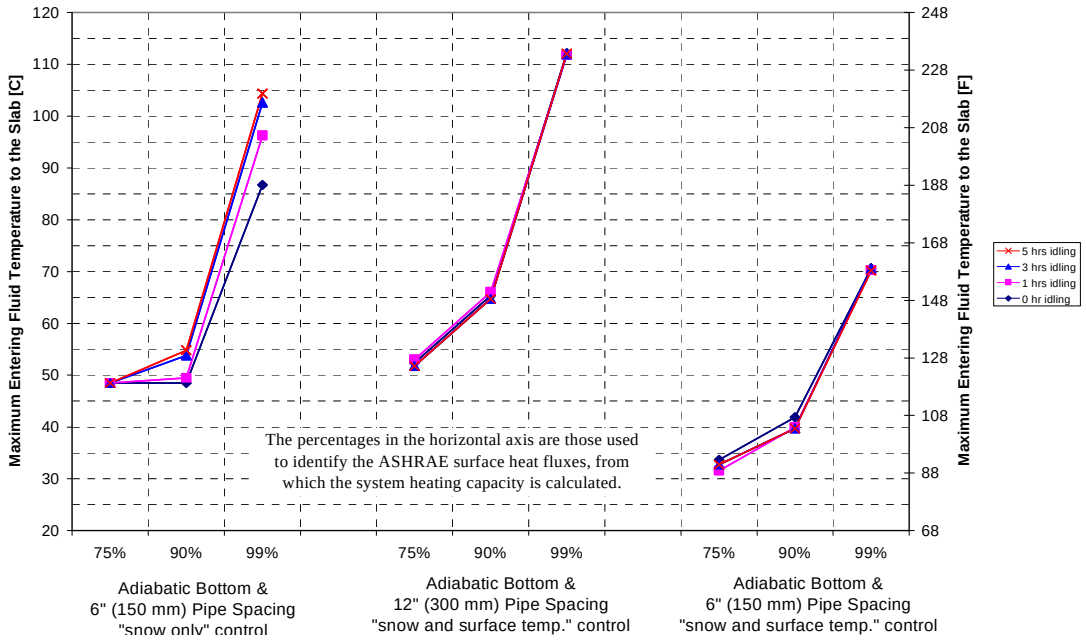

Figure 6-12 Comparison of the maximum entering fluid temperature to the slab resulting from different combinations of control strategy and pipe spacing - Chicago.

This raises the question of whether or not the system performance can be satisfactory if a reasonable maximum fluid temperature is a constraint to the design. As can be seen in Figure 6-8, with 6" (150 mm) pipe spacing, five hours of idling and the "snow and surface temperature" control strategy, the 99% design requires a maximum fluid temperature of 70°C (163°F), but yields snow-free surface conditions for only 89% of the snowfall hours. However, it should be kept in mind that "snow-free" means no ice crystals at all, whether they are in snow or slush. Presumably, conditions that are not snow-free, but mostly snow-free are safer than conditions where the bridge/roadway is completely snow-covered.

Therefore, if the slight degradation of the snow melting performance is acceptable, forecasting-based control with the "snow and surface temperature" control strategy should be utilized in the snow melting systems to improve the energy efficiency.

6.5.4. Effects of Pavement Properties

The effects of thermal properties and thickness of the pavement to the snow melting performance of a hydronic snow melting system have been investigated through the last two sets of simulations in the parametric study. The pavement thermal properties and thickness used in the simulations are summarized in Table 6-3. As can be seen in the table, the thermal diffusivity of the pavement is increased when the pavement is saturated with water.

TABLE 6-3 Varied Slab Parameters Used in the Sensitivity Analysis

Set Index	Concrete Condition	Slab Thickness mm (inch)	Concrete Thermal Properties		
			Thermal Conductivity W/(m-K) [Btu/(h-ft-°F)]	Volumetric Specific Heat kJ/(K-m^3) [Btu/(°F- m^3)]	Thermal Diffusivity m^2/s (ft^2/s)
1	Dry	203 (8)	1.4 (9.7)	2200 (32.8)	6.36E-7 (6.85E-6)
5	Saturated	203 (8)	2.2 (15.3)	2520 (37.6)	8.73E-7 (9.40E-6)
6	Dry	279 (11)	1.4 (9.7)	2200 (32.8)	6.36E-7 (6.85E-6)

The predicted snow melting performance of the fifth and sixth set of simulations has been compared with the results of the baseline case (first set of simulations). Figure 6-13 and 6-14 show the comparisons for bridges at Chicago and Salt Lake City, respectively. Each figure gives the actual performance vs. the design performance for four different idling times and three combinations of concrete condition and thickness.

As shown in Figure 6-13 and 6-14, using thermal properties of concrete at saturated condition results in about a 5% increase in the predicted snow melting performance due to the increased thermal diffusivity. However, since the moisture content of pavement during snow melting process is most likely between dry and saturated condition, the actual increase of the predicted snow melting performance should be less than 5%. Similarly, increasing pavement thickness degrades the performance of the system, but the decrease is less than 3%. Therefore, although the variation of pavement thermal properties and thickness can make a difference in the snow melting performance of a hydronic snow melting system, 3-5 hours idling is still necessary to let a system designed with the ASHRAE steady state snow melting loads achieve the desired snow melting performance.

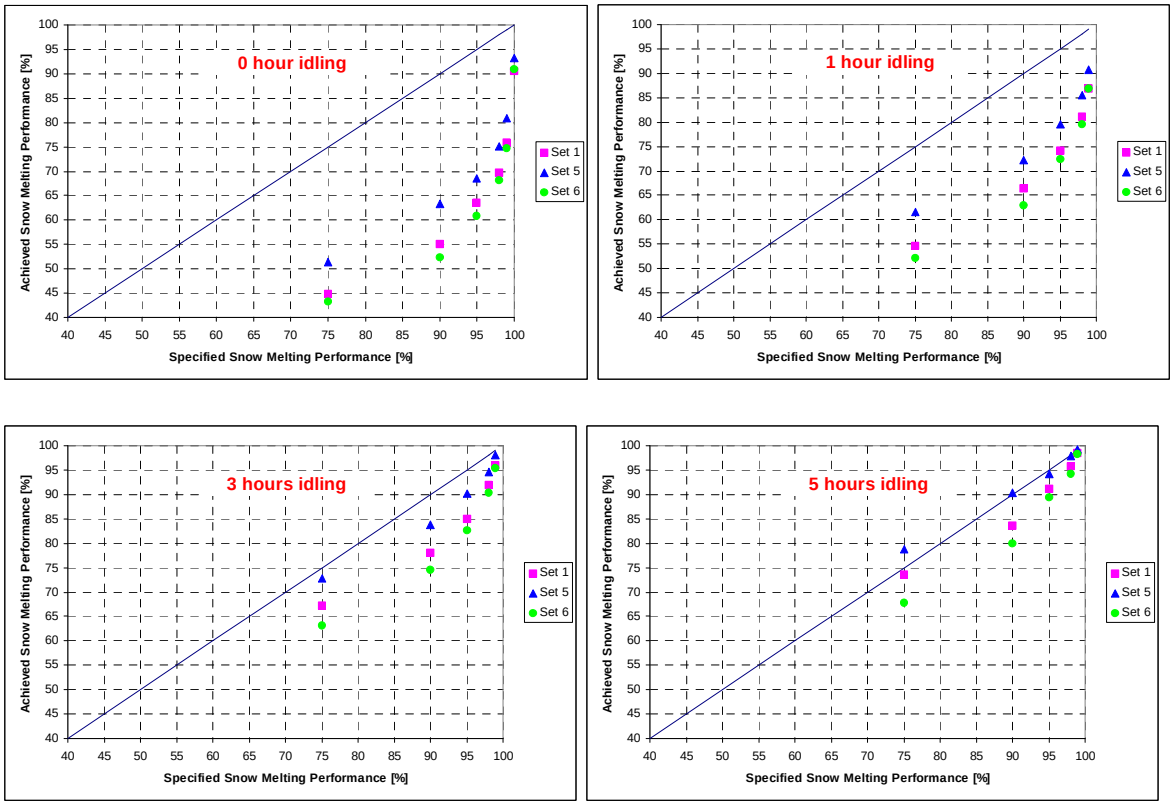

Figure 6-13 Sensitivity of the statistic snow melting performance to the idling time and the slab parameters – for bridges at Chicago.

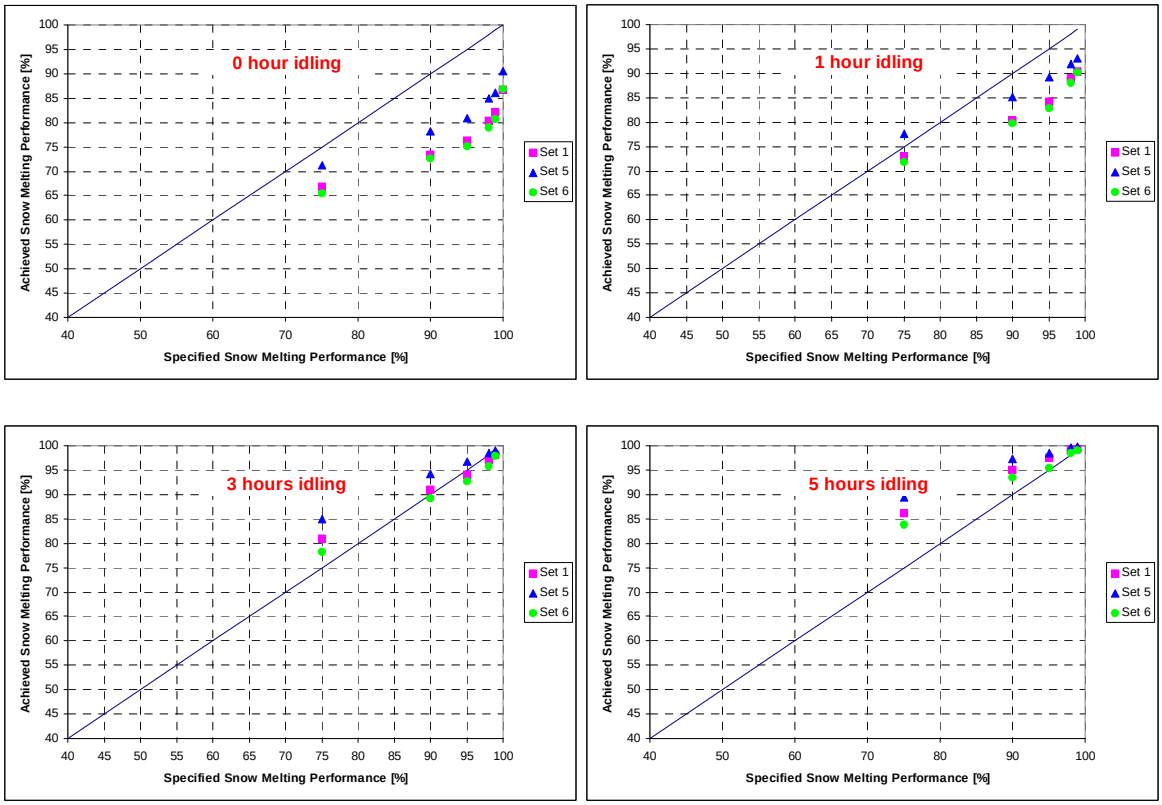

Figure 6-14 Sensitivity of the statistic snow melting performance to the idling time and the slab parameters – for bridges at SLC.

6.6. Snow Melting Loads for Ar=0.5

In the previous section, the snow melting performance has been expressed by the percentage of hours when the surface is completely clear from snow ($A_r = 1$) during snow fall hours. However, it might be much more important to know the performance based on times when the surface is mostly clear of snow. Williams (1973) suggested that a 50% snow-free condition would be “reasonable for most traffic conditions.” Therefore, a parametric study has also been conducted with the ASHRAE steady state loads for achieving partially clear surface ($A_r = 0.5$). Table 6-4 shows the organization of this

parametric study. Following the sequence of the parametric studies described in the previous section, the index of parametric studies in this section starts from 7.

TABLE 6-4 Organization of Parametric Study for Ar = 0.5

	Parameter	Number of Variations
Set 7	Location: Spokane, Reno, SLC, Colorado Springs, Chicago, OKC, Minneapolis, Buffalo, Boston and Philadelphia	10
	Heating capacity *: 75%, 90%, 95%, 98%, 99%, 100%	6
	Idling duration: 0,1,3,5 hours	4
	Pipe spacing: 6 inches (150 mm)	1
	Bottom condition: Adiabatic	1
	Control strategy: “Snow only”	1
Set 8	Location: Spokane, Reno, SLC, Colorado Springs, Chicago, OKC, Minneapolis, Buffalo, Boston and Philadelphia	10
	Heating capacity *: 75%, 90%, 95%, 98%, 99%, 100%	6
	Idling duration: 0,1,3,5 hours	4
	Pipe spacing: 12 inches (300 mm)	1
	Bottom condition: Adiabatic	1
	Control strategy: “Snow only”	1
Set 9	Location: Spokane, Reno, SLC, Colorado Springs, Chicago, OKC, Minneapolis, Buffalo, Boston and Philadelphia	10
	Heating capacity *: 75%, 90%, 95%, 98%, 99%, 100%	6
	Idling duration: 0,1,3,5 hours	4
	Pipe spacing: 6 inches (150 mm)	1
	Bottom condition: Exposed	1
	Control strategy: “Snow only”	1

* The heating capacity is calculated by multiplying the heated area with the ASHRAE surface heat fluxes, which are loads that was not be exceeded during certain percentage of snowfall hours from 1982 through 1993 according to the steady state analysis.

Figures 6-15 to 6-17 show the results of the three sets of simulations. The meaning of each axis and symbols of data points in these figures are exactly the same as that in Figure 6-2. Conclusions drawn from this parametric study are following:

- As shown in Figure 6-15, without idling, systems designed with the ASHRAE steady snow melting loads cannot achieve the desired snow melting performance, which is indicated by the percentage of snowfall hours during which the system can keep at least 50% surface area is clear from snow.

- It can also be seen in Figure 6-15 that, for locations except SLC and Reno, the snow melting performances predicted by the transient simulation are worse than those indicated with the ASHRAE steady state loads even if the systems have been operated at their full heating capacity 5 hours prior to the snowfall. The reason is that slush was not considered in the ASHRAE steady state heat balance analysis for a partially snow-covered surface (Ar = 0.5). In the ASHRAE analysis, it is assumed that the snow-covered area is perfectly insulated and has no evaporation. As a result, evaporation and convection were only accounted for on the half surface clear from snow, but actually more than half of the surface has evaporation and convection since the snow-covered surface may have slush on it. As described in Chapter 4, the slush has been accounted for in the simulation.
- Comparing Figure 6-15 with Figure 6-16, it can be seen that increasing pipe spacing from 6" (150 mm) to 12 "(300 mm) can slightly improve the snow melting performance. This is due to the relatively higher surface temperature at the area above the pipes, which is resulted from the higher fluid temperature required by the wider pipe spacing for providing same amount of heat to the slab.
- Comparing Figure 6-15 with Figure 6-17, it can be seen that the snow-melting performance is degraded by about 5 percent if the lower bridge surface is exposed to ambient conditions and there is no insulation at the bottom of the bridge pavement.

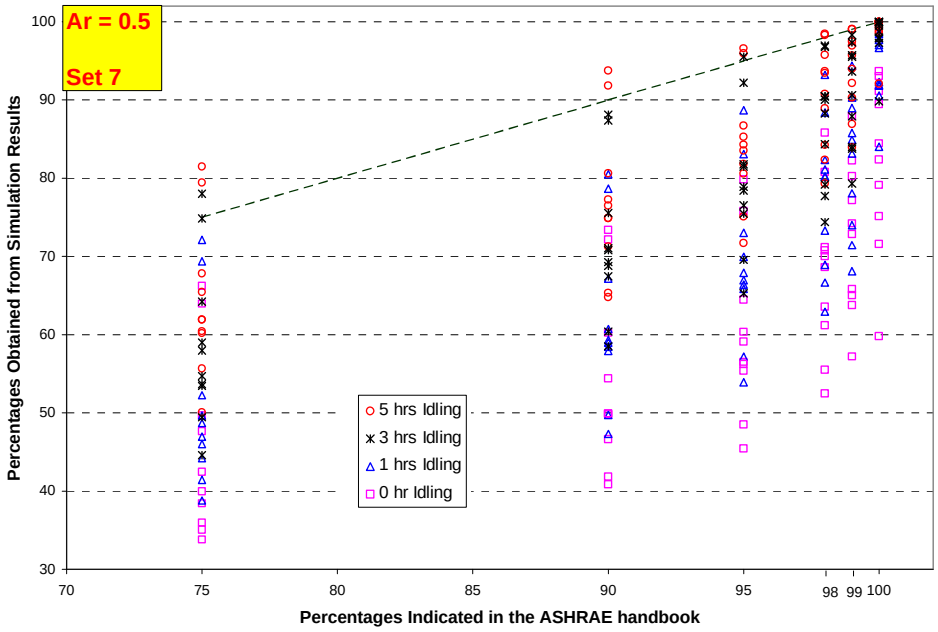

Figure 6-15 Relationship between idling time and snow melting performance – Set 7: Adiabatic bottom and edges with 6” (150 mm) pipe spacing.

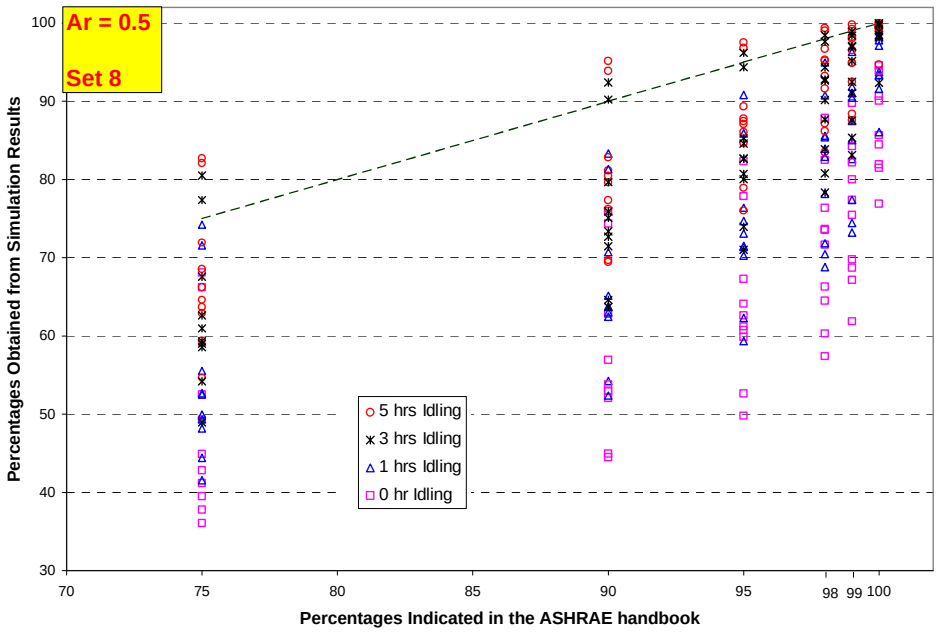

Figure 6-16 Relationship between idling time and snow melting performance – Set 8: Adiabatic bottom and edges with 12” (300 mm) pipe spacing.

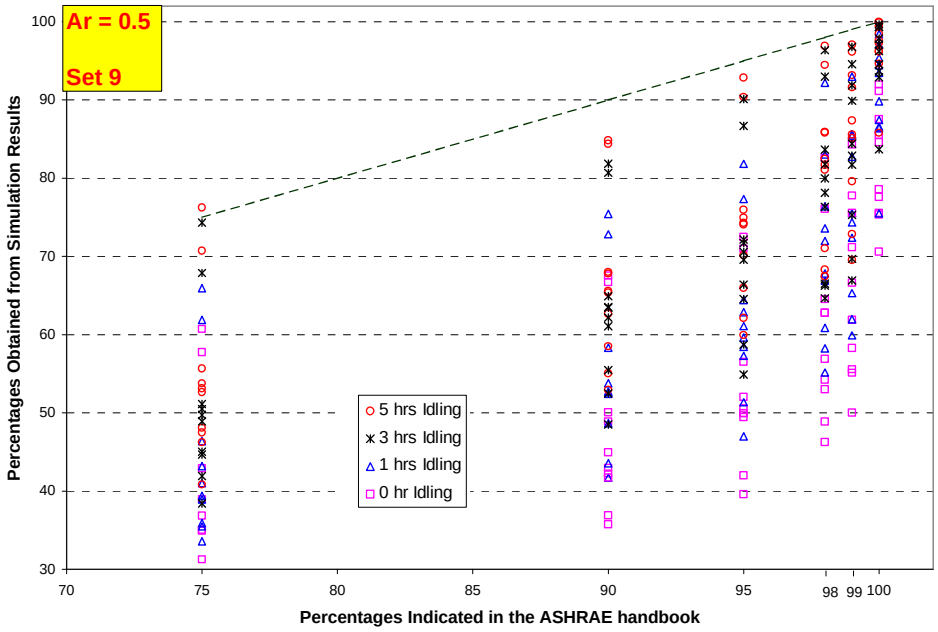

Figure 6-17 Relationship between idling time and snow melting performance – Set 9: Convective bottom and edges with 6" (150 mm) pipe spacing.

6.7. Updated Snow Melting Loads

As shown in the above parametric study results, many factors can affect the heating capacity required to achieve a desired snow melting performance. Although the required heating capacity can be determined through system simulation, it is desirable to generate a set of tables distilled from the simulation results so that the designer can conveniently select the proper heating capacity[12] for a snow melting system from the tabulated data.

[12] To be independent of surface area, the required heating capacities are expressed in the form of heat flux in the unit of Btu/h-ft^2 (W/m^2).

In the table (Table 1 “Frequencies of Snow-Melting Loads”) presented in Chapter 50 of the ASHRAE Handbook of HVAC Applications (2003), the required heat fluxes are given for snow free area ratios of 0, 0.5, and 1, and for percentage-of-snowfall-hours-not-exceeded of 75%, 90%, 95%, 98%, 99%, and 100%. However, the concept of maintaining a “snow free area ratio of 0” only has a meaning with a steady-state analysis that ignores previous history. Therefore, only the required heat fluxes for snow free area ratios of 0.5 and 1 are determined through the transient simulations.

To determine the required heat fluxes, the ideal approach is to set the design objective (maintain a specified snow free area ratio for a statistically determined percentage of hours with snowfall) and run transient simulations of the snow melting system iteratively with various heating capacities until the design objective can be achieved. The required heat flux can then be determined from the final heating capacity and area of heated surface. However, this approach may need many iterations to get the final results and therefore requires a considerable amount of computational time to get a single data point in the table. For instance, if 12 simulations are performed to get a required heat flux and each 10-year simulation takes about 1 hour to run on a Pentium 4, 2.8G HZ PC, it will take 36.8 months (1104 days) to get all the required heat fluxes for 46 locations, 6 percentage-of-snowfall-hours-not-exceeded, 2 snow free area ratios, and 4 idling times. Furthermore, the required computational time will be multiplied if the required heat fluxes for various pipe spacings and bottom conditions are calculated. Accordingly, a simplified approach has been adopted to determine the required heat fluxes for only 10 US locations as a sample of the complete data set.

This simplified approach determines the required heat fluxes by linear interpolation or extrapolation (when necessary) based on the data pairs of heat flux vs. snow melting performance obtained in the parametric study described in the last two sections. For each of the 10 locations, there are 6 pairs of data for a given idling time. For cases where the systems are idled prior to the snowfall, the data pairs pretty much cover the range from 75% to 100% and hence the required heat fluxes are mainly obtained by interpolation. However, for the non-idling cases, the data pairs are far below 100% and extrapolation is necessary. In order to reduce the error from extrapolation, additional simulations of systems with higher heating capacities have been conducted to obtain additional data. Due to the temperature limitation of the heating equipment and pavement, very high heat fluxes are unrealistic. Therefore, the heat fluxes used in the additional simulations have been limited to a maximum of 634 Btu/h-ft^2 (2000 W/m^2).

As an example, Figure 6-18 shows the interpolated/extrapolated heat fluxes along with the data pairs obtained from simulation results for the snow melting system at Boston. In the legend of this figure, “SR” means simulation results and “Interp” means the heat fluxes obtained from interpolation/extrapolation. The numbers following “SR” or “Interp” are the idling time. As can be seen in the figure, the required heat fluxes are all obtained by interpolation for cases where the systems are idled 3 or 5 hours prior to the snowfall. However, for the case where the system is idled for only 1 hour ahead of snowfall, the required heat fluxes for achieving 99% and 100% snow melting performance are extrapolated from the available simulation results. For the case where

the system is not idled, the steady state snow melting load for 100% snow melting performance can actually only maintain the surface clear from snow for 93% of the snowfall time. As a result, additional heat fluxes from 539 Btu/h-ft^2 (1700 W/m^2) to 634 Btu/h-ft^2 (2000 W/m^2)[13] have been used in the simulation and the resulted maximum snow melting performance is 98%.

The required heat fluxes for achieving complete snow-free surface (A_r = 1) and half snow-free surface (A_r = 0.5) for 10 US locations are tabulated in Table 6-5 and 6-6, respectively. Parameters of the simulated pavement are summarized in Table 6-1. To illustrate the effect of idling time, the required heat fluxes for 4 different idling times (0, 1, 3, and 5 hours) are presented in same row along with the ASHRAE steady state loads.

As can be seen in the tables, the required heat fluxes for achieving a percentage-of-snowfall-hours-not-exceeded higher than 95% are greater than 634 Btu/h-ft^2 (2000 W/m^2) for most of the locations if the system is not idled before snowfall. It can also be observed that the required heat fluxes for achieving complete snow-free surface (A_r = 1) are close to the steady state snow melting loads if the system is idled for more than 3 hours ahead of the snowfall.

[13] In this example, the heat fluxes of 634 Btu/h-ft^2 (2000 W/m^2) and 602 Btu/h-ft^2 (1900 W/m^2) lead to same snow melting performance. Therefore, only data of 602 Btu/h-ft^2 (1900 W/m^2) is shown in the figure.

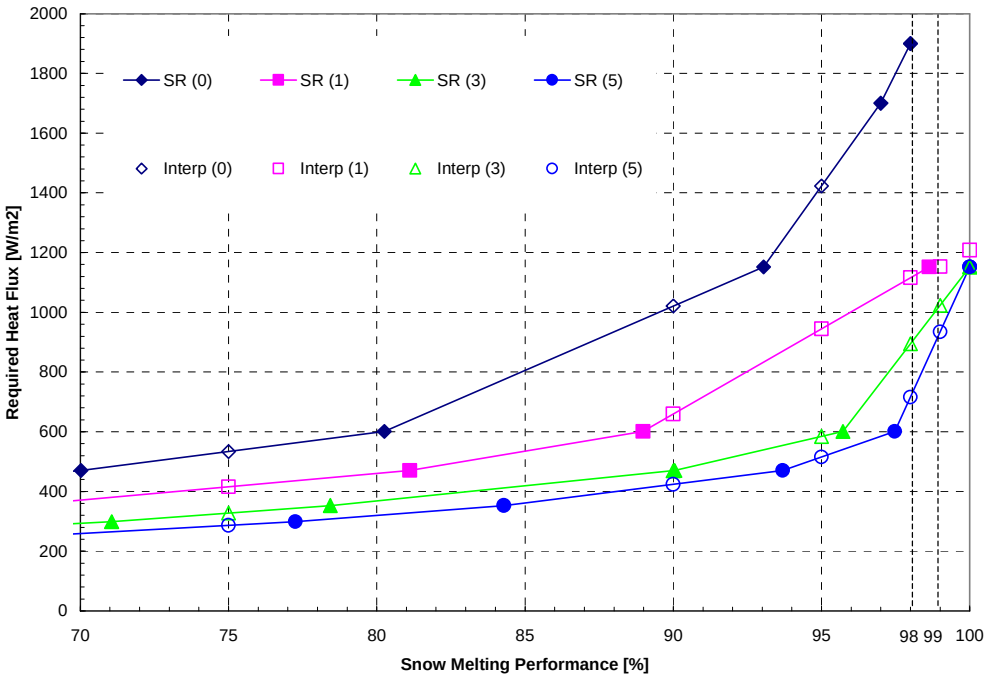

Figure 6-18 Interpolated/extrapolated heat fluxes along with the data pairs obtained from simulation results for the snow melting system at Boston.

TABLE 6-5 Required Heat Fluxes (Ar = 1)

Location	Snow Melting Performance [%]	ASHRAE Loads [W/m2]	Required Heat Fluxes [W/m2]			
			0 hr idling	1 hr idling	3 hrs idling	5 hrs idling
Boston	**75**	303	636	460	367	312
	90	431	1243	724	519	449
	95	519	1700	1030	617	558
	98	636	> 2000	1213	867	724
	99	724	> 2000	1274	1009	938
	100	1152	> 2000	1335	1152	1152
Buffalo	**75**	364	742	502	384	303
	90	522	1462	813	550	486
	95	664	> 2000	1040	734	617
	98	873	> 2000	1207	957	873
	99	1040	> 2000	1263	1040	1040
	100	1799	> 2000	1318	1124	1207
Chicago	**75**	303	714	497	371	312
	90	396	1583	817	556	470
	95	482	> 2000	945	702	565
	98	586	> 2000	1022	817	689
	99	740	> 2000	1048	856	740
	100	1643	> 2000	1074	894	791
Colo. Spr.	**75**	281	511	377	269	195
	90	425	1299	665	475	411
	95	525	1900	963	609	525
	98	637	> 2000	1167	862	637
	99	692	> 2000	1234	1031	862
	100	1031	> 2000	1302	1201	1031
Minneapolis	**75**	376	925	641	493	421
	90	532	1900	1013	703	608
	95	608	> 2000	1189	900	722
	98	722	> 2000	1295	1048	883
	99	801	> 2000	1330	1097	966
	100	1048	> 2000	1366	1147	1048
OKC	**75**	370	820	573	423	381
	90	529	1642	944	677	603
	95	677	> 2000	1099	913	781
	98	781	> 2000	1192	1006	944
	99	820	> 2000	1223	1037	1006
	100	882	> 2000	1254	1068	1068
Phil.	**75**	296	655	487	373	308
	90	406	1038	736	554	477
	95	487	1700	908	638	583
	98	655	> 2000	1038	736	655
	99	777	> 2000	1082	777	777
	100	1038	> 2000	1125	1038	1038
Reno	**75**	158	218	158	108	20
	90	227	518	280	202	168
	95	280	1152	431	254	217
	98	365	1800	604	398	365
	99	431	> 2000	662	431	398
	100	604	> 2000	719	604	431
SLC	**75**	165	269	187	118	70
	90	243	889	379	235	200
	95	282	1468	541	303	243
	98	346	2000	638	379	282
	99	379	> 2000	671	460	346
	100	541	> 2000	703	541	541
Spokane	**75**	210	458	315	231	177
	90	308	1153	481	347	300
	95	366	1700	673	425	354
	98	444	> 2000	802	572	444
	99	500	> 2000	846	644	500
	100	716	> 2000	889	716	716

TABLE 6-6 Required Heat Fluxes (Ar = 0.5)

Location	Snow Melting Performance [%]	ASHRAE Loads [W/m2]	Required Heat Fluxes [W/m2]			
			0 hr idling	1 hr idling	3 hrs idling	5 hrs idling
Boston	**75**	207	534	416	328	287
	90	299	1021	659	469	424
	95	353	1423	945	584	515
	98	470	1900	1116	895	716
	99	601	> 2000	1153	1023	934
	100	1152	> 2000	1208	1152	1152
Buffalo	**75**	214	669	457	348	306
	90	305	1188	860	511	457
	95	399	1700	1121	740	570
	98	517	> 2000	1285	1064	963
	99	594	> 2000	1337	1171	1124
	100	1227	> 2000	1390	1265	1273
Chicago	**75**	184	674	454	338	296
	90	242	1455	792	595	428
	95	297	> 2000	902	732	643
	98	358	> 2000	970	814	778
	99	431	> 2000	992	835	823
	100	835	> 2000	1015	862	866
Colo. Spr.	**75**	178	460	333	254	223
	90	258	1220	626	429	380
	95	311	1700	764	590	497
	98	392	> 2000	846	700	659
	99	442	> 2000	873	735	688
	100	687	> 2000	900	770	737
Minneapolis	**75**	230	827	613	440	392
	90	312	1578	893	725	647
	95	360	> 2000	997	837	781
	98	434	> 2000	1054	897	861
	99	485	> 2000	1073	919	888
	100	904	> 2000	1092	941	905
OKC	**75**	226	651	510	385	344
	90	320	1478	741	663	573
	95	389	> 2000	819	831	778
	98	419	> 2000	865	932	900
	99	453	> 2000	881	966	940
	100	655	> 2000	897	999	980
Phil.	**75**	204	556	436	339	283
	90	282	985	674	505	451
	95	353	1700	784	575	503
	98	511	> 2000	847	726	671
	99	582	> 2000	868	784	757
	100	842	> 2000	890	842	842
Reno	**75**	115	189	135	97	84
	90	174	427	263	189	156
	95	235	899	391	231	201
	98	331	1700	524	356	314
	99	363	> 2000	571	437	360
	100	543	> 2000	616	543	543
SLC	**75**	122	230	167	123	95
	90	196	655	324	220	185
	95	240	1700	486	277	230
	98	301	> 2000	600	385	290
	99	329	> 2000	635	471	328
	100	541	> 2000	671	610	541
Spokane	**75**	141	412	278	211	184
	90	191	1259	438	335	277
	95	229	1626	492	420	368
	98	266	> 2000	526	478	439
	99	300	> 2000	538	496	455
	100	459	> 2000	549	514	478

6.8. Conclusions

A computer simulation of the hydronic snow melting system has been used to evaluate the performance, under realistic transient operating conditions, of snow melting systems designed with the heat fluxes given in the ASHRAE handbook. In addition, the impact of idling time, heating capacity, pipe spacing, bottom insulation, and control strategies on snow melting performance has been investigated. Conclusions drawn from this study include:

- Due to the limitation of the steady state analysis and neglecting the effects of pipe layout on the surface temperature, the tabulated surface heat fluxes in ASHRAE handbook (ASHRAE 2003) are not high enough to achieve the expected snow-melting performance without idling, even if the heat loss from back and edges of the slab are eliminated;
- Preheating the slab with full heating capacity before snowfall can significantly improve the snow melting performance. For a typical hydronic snow melting system designed with the current ASHRAE snow melting loads, preheating the slab several hours before snowfall with the full heating capacity of the system is necessary to achieve the specified snow melting performance. Depending on weather conditions of a particular location, the required preheating time may vary from 3 to 5 hours given 6" pipe spacing and thermally insulated bottom of the slab. However, preheating the slab with full heating capacity may result in excessively high fluid temperatures in mild

weather conditions. These high fluid temperatures may not be achievable with typical system design constraints.

- Although the variation of pavement thermal properties and thickness makes difference in the snow melting performance of a hydronic snow melting system, it does not change the required preheating time.
- Using the “snow and surface temperature” control strategy and idling snow melting systems only several hours in advance of the snow event can significantly reduce the heating energy consumption comparing with idling system continuously as described in the ASHRAE Handbook. In the mean while, the achieved snow melting performances are only slightly lower than those resulting from the continuous idling. Therefore, forecasting-based control with the “snow and surface temperature” control strategy should be utilized in the snow melting systems to improve the energy efficiency.
- For a typical pavement, the required heat fluxes for achieving certain snow melting performance at 10 US locations are updated with data obtained from transient simulations. The updated loads have been tabulated in two tables (Tables 6-5 and 6-6) to facilitate the design of snow melting systems.

CHAPTER 7. CONCLUSIONS AND RECOMMENDATIONS

This thesis is organized so that conclusions are given for each aspect of the work in Chapter 2 and Chapters 4-6. Therefore, this chapter provides a brief summary of the work and the most important conclusions and recommendations.

A detailed literature survey was conducted of modeling approaches for hydronic/electric snow melting systems. The literature survey also included design objectives and current guidance for the heating capacity of hydronic/electric snow melting systems (Chapter 2). The conclusion drawn from the literature review is that the previously developed models are either insufficiently accurate or unacceptably time-consuming. As a result, the current design snow melting loads published by ASHRAE (2003) are based on a one-dimensional steady state analysis, which neglects the effects of the transient characteristic of the storm and the dynamic response of the heated slab. Therefore, it is highly desirable to develop a more computationally efficient model while retaining reasonable accuracy and to update the current design snow melting loads using the transient simulation results.

A transient, two-dimensional numerical model was developed for modeling the temperature response of the hydronically-heated slab and the snow melting process occurring on its surface. Given entering fluid temperature, flow rate, and weather data,

this model can predict exiting fluid temperature, snow cover condition and temperature distribution over the slab surface. The predictions of this model have been validated against corresponding measured data from an experimental hydronic bridge snow melting system (Chapter 4). Major conclusions drawn from this chapter are as follows:

- The model developed in this study can predict the average bridge surface temperature, exiting fluid temperature, and the conditions over the bridge surface with reasonable accuracy. Compared with previously developed models, this model achieves a balance between accuracy and required computational effort. It therefore can be used in the design and optimization of the hydronic snow melting system, which requires multi-year simulations of the hydronic snow melting system.
- The thermal conductivity of the pavement is an important parameter that affects the heat transfer rate from the heated fluid to the bridge surface. It is significantly affected by the moisture content of the concrete and the embedded reinforcement steel. Therefore, the thermal conductivity should be adjusted accordingly. The volume-weighted-average of the thermal properties of the concrete and the rebar can adequately account for this effect.
- Comparison between predictions of various sky temperature models (Clark and Allen 1978; Martin and Berdahl 1984; Brown 1997; Ramsey, et al. 1999; Crawford and Duchon 1999) and measured data shows that the model proposed by Martin and Berdahl (1984) most closely matches the measured data during various seasons and sky conditions. Therefore, it is recommended for use in calculating the sky temperature.

Combining this model with other component models, system simulation of a hydronic bridge snow melting system that utilizes a GSHP as a heat source has been implemented in the component-based simulation environment of HVACSIM+. In order to improve the computational efficiency of the system simulation, the previously developed GLHE model (Yavuzturk and Spitler 1999b) has been updated by employing an explicit solution and hierarchical load aggregation algorithm. In addition, a parameter-estimation-based water-to-water heat pump model developed by Jin and Spitler (2002a and 2002b) has been heuristically adjusted to account for the laminar flow in the evaporator when anti-freeze is used as coolant. Predictions of both the standalone component models and the system simulation have been validated against measured data from an experimental GSHP-based hydronic bridge snow melting system (Chapter 5). Major conclusions drawn from this chapter are summarized as follows:

- The hierarchical load aggregation algorithm implemented in the GLHE model reduces computational time by 20% for a 20-year system simulation while retaining almost the same accuracy.
- The "Antifreeze Degradation Factor (ADF)" approach adopted in the heat pump model (Jin and Spitler 2002b), which uses coefficients estimated based on turbulent flow, is not valid when the flow is laminar, which may occur at the evaporator when propylene glycol solution with high concentration is used as coolant. As a result, a heuristic correction to the overall heat transfer coefficient of the evaporator has been applied and it improves the accuracy of the results.

- Simulation results for the system in recharge mode match the experimental data fairly well except there are some noticeable difference in the peak surface temperature, which is mainly due to the uncertainty of the surface solar absorptance.
- When the system is in heating mode, larger differences between the simulation results and measured data may be observed, particularly with respect to the timing of the on/off cycles. This is due to the increased complexity of the simulation and the uncertainties associated with each component model. However, the predicted snow melting performance and the heat pump power consumption are of sufficient accuracy for the purposes of system design and performance analysis.

A simulation-based investigation has been conducted to investigate the validity of the snow melting loads (required heat intensity for achieving designed snow melting performance) presented in the ASHRAE Handbook – HVAC Applications Volume (ASHRAE 2003). In addition, the impacts of idling time, heating capacity, pipe spacing, bottom insulation, and control strategies on snow melting performance have also been investigated. Based on the transient simulation results, the snow melting loads for 10 locations in US have been updated and tabulated in two tables to facilitate the design of snow melting systems (Chapter 6). Conclusions drawn from this study include:

- The snow melting loads tabulated in the ASHRAE handbook (ASHRAE 2003), which are obtained from a one-dimensional steady state heat balance

analysis, are not sufficient to achieve the specified snow melting performance if the slab is not preheated prior to snow events.

- For a typical hydronic snow melting system designed with the current ASHRAE snow melting loads, depending on the weather conditions of a particular location, preheating the slab 3 to 5 hours before the snowfall with the full heating capacity of the system is necessary to achieve the specified snow melting performance.
- Varying the pavement thermal properties from dry to saturated condition or changing the pavement thickness in the typical range from 8” (203 mm) to 11” (279 mm) can make a difference in the snow melting performance. However, it does not change the required preheating time to achieve the desired snow melting performance.
- Compared with continuous idling of the system as described in the ASHRAE Handbook-HVAC Applications Volume (ASHRAE 2003), preheating the bridge only several hours in advance of a snow event and modulating the heat output according to the bridge surface temperature can significantly reduce the heating energy consumption. The achieved snow melting performance is only slightly worse than that resulting from the continuous idling. Therefore, forecasting-based control should be used in the snow melting system to improve its energy efficiency.

The recommendations for future research are as follows:

- Investigate traffic effects on the snow melting process and account for these effects in the snow-melting model in a reasonably simple way. The snow-melting model described in Chapter 4 focuses on the analysis of heat and mass balance involved in the snow melting process and does not account for any effects of traffic on the bridge. However, the traffic on a real bridge may affect the actual snow melting performance in many ways, such as by discharging waste heat to the snow, compressing the snow (and therefore changing its properties and distribution over the bridge surface), and changing the wind speed on the bridge surface. It is therefore of interest to investigate to what degree the traffic changes the snow melting performance on a heated bridge, and in turn, the required heat fluxes to achieve certain snow melting performance.
- Similarly, some heated bridge deck systems may be assisted by snow plowing and it would be useful to have a model that could incorporate snow plowing procedures.
- Investigate the modeling of moisture transport in the pavement during the snow melting process and the resulting variations in thermal properties. As discussed in Chapters 4 and 6, the thermal diffusivity of pavement could be increased significantly when the pavement is wetted by rainfall or snowmelt. It will considerably enhance the heat transfer in the pavement and in turn improve the snow melting performance. In order to more accurately design a snow melting system, it is desirable to model the moisture transport in the pavement and account for the variation of pavement thermal properties.

- Improve the parameter-estimation-based model of the water-to-water heat pump by accounting for the case of laminar flow in the coolant side of the heat exchanger. As discussed in Chapter 5, it appears that the “Antifreeze Degradation Factor (ADF)” approach adopted in the heat pump model is not valid for the case when the flow has transitioned to laminar in the heat exchanger. Although re-estimating the parameters of the model using the performance data when laminar flow occurs is an approach to solve this problem, it is desirable to develop a more general algorithm that can be implemented in the model to distinguish laminar flow and apply a proper correction.
- Field test of the road/bridge surface friction factors associated with various degrees and distribution of snow/ice cover over the surface. This study may lead to a recommendation for reasonable design objectives of the hydronic snow melting system in terms of permissible snow/ice cover degree over a heated road/bridge. This study may provide guidance for the layout of the hydronic piping. For instance, it may be able to determine which kind of pipe layout can most efficiently melt snow on the track of transportation.
- In the parametric study described in Chapter 6, the lower surface of the heated slab is either perfectly insulated (adiabatic) or exposed to ambient condition without any insulation, which are two extreme conditions for a bridge deck. However, in order to extend the current study to roadway snow melting systems, it is necessary to model the heat and mass transfer between the heated slab and the soil underneath. Furthermore, it may also be necessary to

develop a three-dimensional model to account for the heat and mass transfer at the edges of the heated slab.

- Due to the significant computational effort demanded, it is not possible to complete the data set of required heat fluxes for all the 46 locations and various pipe spacing and bottom conditions in this study. Tables 6-5 and 6-6 are only samples of a complete set of design tables. However, the results and methodology presented here could be the starting point of a new project, which is to update the design guidance of snow melting systems using transient simulation. In order to reduce the computational time, it is necessary to find an efficient algorithm to search for the required heat flux and shorten the weather data used in the simulation.

BIBLIOGRAPHY

Aase, J.K., S.B. Idso. 1978. *A Comparison of Two Formula Types for Calculating Long-Wave Radiation From the Atmosphere*. Water Resources Research, 14 (4): 623-625.

ASHRAE. Handbook of HVAC Applications 2003 (SI). Chapter 50. American Society of Heating, Refrigerating and Air-Conditioning Engineers, Inc.

ASHRAE. Handbook of Fundamental 2001 (SI). Chapter 3. American Society of Heating, Refrigerating and Air-Conditioning Engineers, Inc.

ASTM. 1978. *Significance of Tests and Properties of Concrete and Concrete-Making Materials*. STP 169B. American Society for Testing and Materials.

Bourdouxhe, J, M. Grodent and J. Lebrun. 1998. *Reference Guide for Dynamic Models of HVAC Equipment*. American Society of Heating, Refrigerating and Air-Conditioning Engineers, Inc.

Boyd, T, 2003. *New snow melt projects in Klamath falls*, OR, Geo-heat center quarterly bulletin, Sep. 2003.

Brayton, R.K., Gustavson, F.G., and Hachtel, G.D., *A New Efficient Algorithm for Solving Differential – Algebraic Systems Using Implicit Backward Differential Formulas.* Proc. IEEE, 60(1): 98-108.

Brown, D.F. 1997. *An Improved Methodology For Characterizing Atmospheric Boundary Layer Turbulence And Dispersion*. Ph. D. Thesis. UIUC, IL.

CECW-EH, 1998. Engineering and design: runoff from snowmelt, Department of the Army, U.S. Army Corps of Engineers, Washington, DC.

Chapman, W.P. 1952a. *Design of snow melting system*. Heating and Ventilating, (49) 4: 95-102.

Chapman, W.P. 1952b. *Calculating the heat requirements of a snow melting system*. Heating and Ventilating, November, P. 88-91.

Chapman, W.P. 1956a. *Calculating the heat requirements of a snow melting system*. Air Conditioning, Heating and Ventilating, September, P. 67-71.

Chapman, W.P. and S. Katunich. 1956b. *Heat Requirements of Snow Melting*. Heating, Piping and Air Conditioning, February, P. 149-153.

Chen, A., Y. Zhu, N. Nakahara. 1999. *Improvement Of The Fluid Network's Module Construction For HVACSIM+*. Proceedings of Building Simulation '99, 3: 1229-1236.

Chiasson, A. 1999. *Advances in Modeling of Ground-Source Heat Pump Systems*. M.S. Thesis. Oklahoma State University. Stillwater, OK.
(Also available at http://www.mae.okstate.edu/Faculty/spitler/chiasson_thesis.pdf)

Chiasson, A.D., J.D. Spitler, S.J. Rees, M.D. Smith. 2000a. *A Model for Simulating the Performance of a Pavement Heating System as a Supplemental Heat Rejecter with Closed-loop Ground-Source Heat Pump Systems*. ASME Journal of Solar Energy Engineering, 122:183-191.

Chiasson, A.C., S.J. Rees, J.D. Spitler. 2000b. *A Preliminary Assessment Of The Effects Of Ground-Water Flow On Closed-Loop Ground-Source Heat Pump Systems*. ASHRAE Transactions, 106(1): 380-393.

Chiasson, A. J. and Spitler J. D. 2000c. *A Modeling Approach to Design of Ground Source Heat Pump Bridge Deck Heating System*. Proceedings of the Fifth International Symposium on Snow Removal and Ice Control Technology, Raonoke, VA. September 5-8, 2000.

Clark, C and C. Allen. 1978. *The Estimation of Atmospheric Radiation for Clear and Cloudy Skies*. Proceedings of the 2nd National passive Solar Conference (AS/ISES, 1978), 2: 675-678.

Clark, D. R., C. W. Hurley, and C. R. Hill. 1985. *Dynamic models for HVAC System Components*. ASHRAE Transactions, 91(1): 737-751.

Clark, D.R. 1985. *HVACSim+ Building Systems and Equipment Simulation Program: Reference Manual.* NBSIR 84-2996. National Bureau of Standards.

Clark, D.R. and W. B. May. 1985. *HVACSim+ Building Systems and Equipment Simulation Program: Users Guide.* NBSIR 85-3243. National Bureau of Standards.

Crawford, T.M. and C.E. Duchon. 1999. *An Improved Parameterization for Estimating Effective Atmospheric Emissivity for Use in Calculating Daytime Downwelling Longwave Radiation*. Journal of Applied Meteorology, 38: 474-480.

Duffie, J.A. and W.A. Beckman, 1991. Solar Engineering of Thermal Processes, 2nd Edition. John Wiley and Sons.

Elliot, R.L., F.V. Brock, M.L. Stone, and S.L. Sharp. 1994. *Configuration Decisions for an Automated Weather Station Network.* Applied Engineering in Agriculture, 10(1): 45-51.

Eskilson, P. 1987. *Thermal Analysis of Heat Extraction Boreholes*. Doctoral Thesis, University of Lund, Department of Mathematical Physics. Lund, Sweden.

Ferrara, A. A. and Haslett, R. 1975. *Prevention of Preferential Bridge Icing using Heat Pipes*. Report No. FHWA-RD-75-111, Federal Highway Administration.

Gear, C. W. 1971. *The Automatic Integration of Ordinary Differential Equations.* Comm. ACM, 14:176-179.

Haves, P. and L. K. Norford. 1995. *A Standard Simulation Test Bed for the Evaluation of Control Algorithms and Strategies.* ASHRAE 825- RP Final Report.

Hockersmith, S.L. 2002. *Experimental and Computational Investigation of Snow Melting on Heated Horizontal Surfaces*. M.S. Thesis: Oklahoma State University. Stillwater, OK. (Also available at http://www.hvac.okstate.edu/pdfs/Hockersmith%20Thesis.pdf)

Holloway, B. 2000. Personal Communications.

Hoppe, E.J., *Evaluation of Virginia's First Heated Bridge (Final report)*, Dec. 2000, VTRC 01-R8, Virginia Transportation Research Council, Charlottesville, Virginia.

Hunter, J.E. 1998. "Winter 1998" issue, The Source. Society of Accident Reconstructionists (SOAR)
(Obtained from http://www.enteract.com/~icebike/Articles/howslippery.htm)

Incropera, F.P. and D.P. Dewitt. 1996. Introduction to Heat Transfer, P. 332-334. New York: Wiley & Sons.

Iwamoto, K., Nagasaka, S., Hamada, Y., Nakamura, M., Ochifuji, K. and K. Nagano. 1998. *Prospects of Snow Melting System (SMS) Using Underground Thermal Energy Storage (UTES) in Japan*. Proceedings of the Second Stockton International Geothermal Conference, Pomona, New Jersey. March 16 – 17, 1998.

Jenks, S.C., J.R. Whiteley, K.N. Pandit, D.S. Arndt, M.L. Stone, R.L. Elliott, J.D. Spitler, M.D. Smith. 2003. *Smart Control of a Geothermally Heated Bridge Deck*, Proceedings of the Transportation Research Board 82nd Annual Meeting, Washington, D.C. January 12-16, 2003.

Jin, H. and J.D. Spitler. 2002a. *A Parameter Estimation Based Model of Water-To-Water Heat Pumps for use in Energy Calculation Programs*. ASHRAE Transactions, 108(1): 3-17.

Jin, H. 2002. *Parameter Estimation Based Models of Water Source Heat Pumps*. Ph. D. Thesis: Oklahoma State University. Stillwater, Oklahoma.

(Also available at http://www.hvac.okstate.edu/pdfs/Hui_Jin_Thesis.pdf)

Jin, H. and J.D. Spitler. 2003. *Parameter Estimation Based Model of Water-to-Water Heat Pumps with Scroll Compressors and Water/Glycol Solutions*. Building Services Engineering Research and Technology, 24(3): 203-219.

Taylor, J. R.1997. An Introduction to Error Analysis, 2nd edition, University Science Books, Sausalito, California.

Ketcham, S.A., L.D. Minsk, R.R. Blackburn, E.J. Fleege. 1996 *Manual of Practice for an Effective Anti-icing Program: A Guide for Highway Winter Maintenance Personnel*. US Army Cold Regions Research and Engineering Laboratory. 1996.
(Also available at http://www.fhwa.dot.gov/reports/mopeap/mop0296a.htm)

Kilkis, I.B., 1992. *Enhancement of heat pump performance using radiant floor heating systems*. ASME AES, 28: 119-127.

Kilkis, I.B., 1994a. *Design of Embedded Snow Melting Systems: Part 1, Heat Requirements – An Overall Assessment and Recommendations*. ASHRAE Transaction, 100(1): 423-433.

Kilkis, I.B., 1994b. *Design of Embedded Snow Melting Systems: Part 2, Heat Transfer in the Slab – A Simplified Model*. ASHRAE Transactions, 100(1): 434-441.

Kipp & Zonen, 2000. Instruction Manual – CNR1 Net Radiometer. (Available at http://www.kippzonen.com/download/kipp_manual_cnr1_1413.pdf)

Levinson, R. and H. Akbari, 2001. Eeffects of composition and exposure on the solar reflectance of portland cement concrete, LBNL-48334, Heat Island Group, Environmental Energy Technologies Division, Lawrence Berkeley National Laboratory, University of California, Berkeley, CA.

Leal, M. and P.L. Miller. 1972. *An Analysis of the Transient Temperature Distribution in Pavement Heating Installations*. ASHRAE Transactions, 78(2): 61-66.

Liu, X., S.J. Rees, J.D. Spitler. 2003. *Simulation of a Geothermal Bridge Deck Anti-icing System and Experimental Validation.* Proceedings of the Transportation Research Board 82nd Annual Meeting, Washington, D.C. January 12-16, 2003.

Martin, M., P. Berdahl, 1984. Characteristics of infrared sky radiation in the United States, Solar Energy 33(3/4): 321-336.

McAdams, W. H. 1954. Heat Transmittion, New York: McGraw-Hill.

Minsk, L.D. 1999. *Heated Bridge Technology.* Report on ISTEA Sec. 6005 Program. Report no.: FHWA-RD-99-158. July, 1999.

Nydahl, J., K. Pell, R. Lee, J. Sackos. 1984. *Evaluation of an Earth Heated Bridge Deck*. Report No. FHWA-WY-84-001. April 1984.

Nakamura, H., T. Tanimoto and S. Hamada. *Study of a Snow-Melting and Antifreeze system for prevention of Auto Accidents on Slippery Bridge Decks*. Snow Engineering: Recent Advances: Proceedings of the Third International Conference on Snow Engineering, Sendai, Japan, 26-31. May, 1996.

Park, C., Clark D. R., Kelly G. E. 1985. *An Overview of HVACSIM+, a Dynamic Building/HVAC/Control Systems Simulation Program*. Building Energy Simulation Conference, Seattle, Washington. August 21-22, 1985.

Park, C., D.R. Clark, G.E. Kelly 1986. *HVACSIM+ Building Systems and Equipment Simulation Program: Building Loads Calculation.* NBSIR 86-3331. National Bureau of Standards. February 1986.

Paul, N. D. 1996. The Effect of Grout Thermal Conductivity on Vertical Geothermal Heat Exchanger Design and Performance. M.S. Thesis. South Dakota State University.

Powell, M. J. D. 1970. A Hybrid Method for Nonlinear Equations in Numerical Methods. London : P. Rbinowitz, Ed., Gordon and Breach.

Ramamoorthy, M.H. 2001. *Application of Hybrid Ground Source Heat Pump Systems To Buildings and Bridge Decks*. M.S. Thesis. Oklahoma State University. Stillwater, OK. (Also available at http://www.mae.okstate.edu/Faculty/spitler/ Ramamoorthy_thesis.pdf)

Ramsey, J.W, H.D. Chiang, and R.J. Goldstein. 1982. *A Study of the Incoming Longwave Atmospheric Radiation from a Clear Sky*. Journal of Applied meteorology, 21: 566- 578.

Ramsey, J.W, M.J. Hewett, T.H. Kuehn, and S.D. Petersen. 1999. *Updated Design Guidelines for Snow Melting Systems*. ASHRAE Transactions, 105(1): 1055-1065.

Ramsey, J.W, M.J. Hewett, T.H. Kuehn, and S.D. Petersen. 1999. *Updated Design Guidelines for Snow Melting Systems*. ASHRAE 926-RP Final Report.

Rauber, M. 1995. *Energy from Road Surface*, Caddet Renewable Energy Newletter, issue 1/95, harwell, UK, P. 25-27.

Rees, S.J., J.D. Spitler, X. Xiao and M. Chulliparambil. 2001. *Development of a Two-Dimensional Transient Model of Snow-Melting System, and Use of the Model for Analysis of Design Alternatives*. ASHRAE 1090-RP Final Report, August, 2001.

Rees, S.J., J.D. Spitler and X. Xiao. 2002. *Transient Analysis of Snow-melting System Performance*. ASHRAE Transactions, 108(2): 406-423.

Sahlin, P. 1996. *Modeling and Simulation Methods for Modular Continuous Systems in Buildings*. Doctoral Thesis, Royal Institute of Technology, Department of Building Sciences. Stockholm, Sweden.

Schnurr, N.M. and D.B. Rogers. 1970. *Heat Transfer Design Data for Optimization of Snow Melting Systems*. ASHRAE Transactions, 76(1): 257-263.

Schnurr, N.M. and M.W. Falk. 1973. *Transient Analysis of Snow Melting Systems*. ASHRAE Transactions, 79(2): 159-166.

Smith, D. *Quarterly Progress Report of the Oklahoma State University Smart Bridge Project*. (1999-2002). Oklahoma State University. Stillwater, OK.

SEL. 1996. TRNSYS Manual - a Transient Simulation Program. Madison: Solar Engineering Laboratory, University of Wisconsin.

Spitler, J.D. and M. Ramamoorthy. 2000. *Bridge Deck Deicing using Geothermal Heat Pump*. Proceedings of the Fourth International Heat Pumps in Cold Climates Conference, Aylmer, Quebec. August 17-18, 2000.

Spitler, J. D., S. J. Rees and X. Liu. *Quarterly Progress Report of the Oklahoma State University Smart Bridge Project*. (2001). Oklahoma State University. Stillwater, OK.

U.S. Army Corps of Engineers. 1973. *Method of Test for Specific Heat of Aggregates, Concrete, and other Materials (Method of Mixtures)*. Specification CRD-C124-73.

U.S. Army Corps of Engineers. 1998. *Engineering and Design: RUNOFF FROM SNOWMELT*. Engineer Manual 1110-2-1406. Department of the Army, Washington, DC.

Varanasi, A. 2002. *Development of a Visual Tool for HVACSIM+*. M.S. Thesis. Oklahoma State University, Stillwater, OK.
(Also available at http://www.hvac.okstate.edu/pdfs/Hui_Jin_Thesis.pdf)

Williams, G.P. 1976. *Design heat requirements for embedded snow-melting systems in cold climates*. Transportation Research Record, 576: 20-32.

Williams, G.P. 1973. *Heat Requirements of Snow Melting Systems in Canada*. Proc., National Conference on Snow and Ice Control. Roads and Transportation Association of Canada, Ottawa, April 1973, P. 179-197.

Williamson, P.J. 1967. *The estimation of heat outputs for road heating installations*. Road Res. Lab. Report No. RRL-LR77. Crowthorne, UK.

Whiting, D., A. Litvin and S. E. Goodwin, *Specific Heat of Selected Concrete*, Journal of the American Concrete Institute, July 1978, P. 299-305.

Yavuzturk, C. 1999. *Modeling of Vertical Ground Loop Heat Exchangers for Ground Source Heat Pump Systems*. Ph. D. Thesis. Oklahoma State University. Stillwater, OK. (Also available at http://www.mae.okstate.edu/Faculty/spitler/Yavuzturk_thesis.pdf)

Yavuzturk, C., J. D. Spitler. 1999a. *A Transient Two-Dimensional Finite Volume Model for the Simulation of vertical U-tube Ground Heat Exchangers*. ASHRAE Transaction, 105(2): 465-474.

Yavuzturk, C., J. D. Spitler. 1999b. *A Short Time Step Response Factor Model for Vertical Ground Loop Heat Exchangers*. ASHRAE Transactions, 105(2): 475-485.

Yavuzturk, C., J.D. Spitler. 2001. *Field Validation of a Short Time-Step Model for Vertical Ground Loop Heat Exchangers*. ASHRAE Transactions, 107(1): 617-625.

APPENDIX A: MODEL DOCUMENTATION

A.1. TYPE 700: Hydronically-Heated Bridge Deck Model

General Description

This component model simulates heat transfer mechanisms within a hydronically-heated bridge deck. The heat transfer mechanisms within the bridge deck slab include several environmental factors as well as convection due to the heat transfer fluid. The heat transfer fluid in this model can be either pure water or an antifreeze solution. The fluid is carried by a series of pipes positioned in parallel circuits, which are embedded in the slab and perpendicular to the length direction of the bridge. This model was developed to simulate the performance of a bridge deck snow melting or de-icing system.

The different modes of heat transfer include at the top surface of the bridge include the effects of solar radiation heat gain, convection heat transfer to the atmosphere, thermal or long-wave radiation heat transfer, sensible heat transfer to snow, heat of fusion required to melt snow, and heat of evaporation lost to evaporating rain or melted snow. Heat transfer at the bottom surface of the bridge includes convection heat transfer to the atmosphere and heat transfer due to radiation to the ground. Weather data are supplied by the user at a desired time interval and read from the boundary file. Heat transfer mechanisms within the pavement slab include conduction through the pavement material and convection due to flow of the heat transfer fluid through the embedded pipes.

Because of symmetry and small temperature differences between adjacent pipes (and neglecting edge effects), the model domain is reduced to a width equivalent to one-half of the pipe spacing as shown in Figure A.1.1. The half of the round pipe was approximated by a rectangular (the two missing cells on the left hand side of the solution domain) in the square grid system. It is assumed that the average top surface temperature for the cross-section approximates the average top surface temperature for the entire pavement area.

As shown in Figure 1, boundary conditions are of two types:

- A flux boundary at top surface and bottom surface (if exposed) nodes and at nodes surrounding the pipe location
- An adiabatic boundary at all other boundary nodes

The finite-difference equation for all nodes is obtained by the energy balance method for a control volume about the nodal region (i.e. using a “node-centered” approach) assuming all heat flow is into the node.

In order to predict the snow free area ratio, which is the ratio of the area free of snow to the total area of a surface, the snow accumulation on each surface node is calculated.

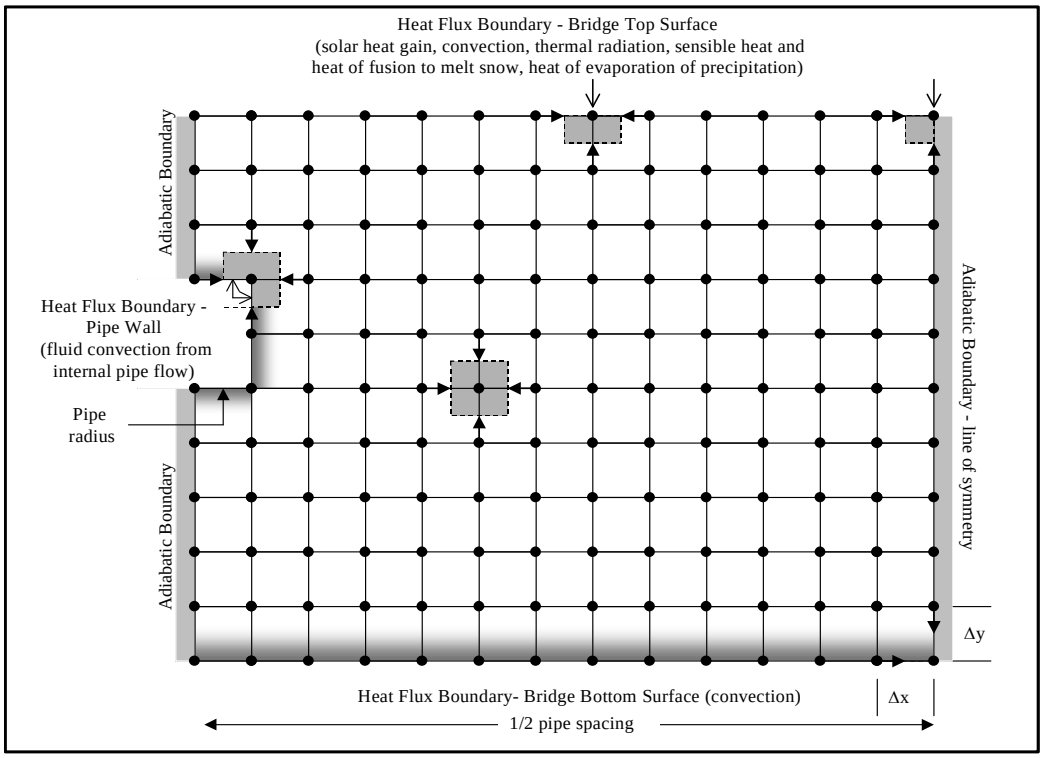

Figure A.1.1 Model domain showing the finite-difference grid and boundary conditions. Shaded squares show example control volumes for different types of grid node geometries. Arrows show the direction of heat flow used to derive the finite-difference equations for each node type; open arrowheads denote an exterior flux and closed arrowheads denote conduction between adjacent nodes. y is positive downward and x is positive to the right. Note $\Delta x = \Delta y$. (Adopted from Chiasson 2000)

Nomenclature

α	= thermal diffusivity of pavement material	(m^2/s)
α_{solar}	= solar absorptance of pavement	(--)
Δt	= size of time step	(s)
Δx	= grid size in x direction	(m)
Δy	= grid size in y direction	(m)
ε	= emissivity coefficient	(--)
ρ	= density	(kg/m^3)
σ	= Stephan-Boltzmann constant = 5.67×10^{-8}	(W/m^2-K^4)
c_p	= specific heat	(J/(kg-°C))
Delta	= x and y grid spacing	(m)
D_{AB}	= Binary mass diffusion coefficient	(m^2/s)
D_{pipe}	= Pipe diameter	(m)
Fo	= Fourier Number	(--)
h_c	= convection heat transfer coefficient at pavement top surface	(W/m^2-°C)
h_d	= mass transfer coefficient	(kg/m^2-s)
h_{fg}	= heat of evaporation	(J/kg)

h_{if}	= latent heat of fusion of water	(J/kg)
h_{fluid}	= convection heat transfer coefficient for fluid	(W/m^2-°C)
I	= solar radiation incident on the pavement surface	(W/m^2)
k	= thermal conductivity	(W/(m-°C))
l	= length	(m)
Le	= Lewis number	(--)
m''	= accumulated snow or ice per unit area	(kg/ m^2)
$\dot{m}''$	= mass flux	(kg/ s-m^2)
mdot	= fluid mass flow rate	(kg/s)
mdott	= fluid mass flow rate per flow circuit	(kg/s)
Nu	= Nusselt Number	(--)
P	= pressure	(atmospheres)
Pr	= Prandtl Number	(--)
$q''_{cond,surface}$	= conductive heat flux at the pavement top surface	(W/m^2)
q''_{conv}	= convective heat flux from pavement surface	(W/m^2)
q''_{evap}	= heat flux due to evaporation	(W/m^2)
q''_{fluid}	= heat flux from heat carrier fluid	(W/m^2)
q_{fluid}	= heat transfer rate per unit length of pipe	(W/m)
q''_{melt}	= heat flux for melting snow	(W/m)
q''_{rad}	= solar radiation heat flux	(W/m^2)
q''_{sen}	= sensible heat for melting snow	(W/m^2)
$q''_{thermal}$	= thermal radiation heat flux from pavement surface	(W/m^2)
Re	= Reynold's Number	(--)
Snowfall	= snowfall rate	(mm of water equivalent per hr)
t	= time	(s)
T	= temperature	(°C or K)
$T_{(m,1)}$	= surface node temperature	(°C)
$T_{(x,y)}$	= non-surface node temperature	(°C)
U	= overall heat transfer coefficient for fluid	(W/m^2-°C)
w	= humidity ratio	(kg water /kg d.a.)
wallt	= pipe wall thickness	(m)

Subscript

amb	= ambient air
avg	= average
circuit	= per circuit of flow
evap	= evaporation
fl	= fluid
in	= inlet
out	= outlet
pipe	= pipe
pv	= pavement
r	= thermal radiation

sky = sky
snow = snow
wt = water

Mathematical Description

1. Numerical Stability Criterion

The governing equation of model is the two-dimensional form of the transient heat diffusion equation:

$$\frac{\partial^2 T}{\partial x^2} + \frac{\partial^2 T}{\partial y^2} = \frac{1}{\alpha}\frac{\partial T}{\partial t} \tag{A.1.1}$$

Appearing in all nodal equations is the finite-difference form of the Fourier number as given in Equation (A.1.2). Since the model employs uniform grid spacing, Δx is equal to Δy. In this model, Δx is set to be the multiplication of the pipe radius and $\frac{\pi}{4}$ so that the approximated "rectangular" pipe has the same perimeter as that of the real round tube.

$$Fo = \frac{\alpha \Delta t}{(\Delta x)^2} \tag{A.1.2}$$

One disadvantage of the fully explicit finite difference method employed in this model is that the solution is not unconditionally stable. For a 2-D grid, the stability criterion is:

$$Fo \leq \frac{1}{4} \tag{A.1.3}$$

For the prescribed values of α and Δx, the appropriate time step can be determined with Equation (A.1.3).

2. Classification and Definition of Surface Conditions

Following the classification described by Rees, *et al.* (2002), seven surface conditions are identified. The classification and definition of the seven surface conditions are summarized in Table A.1.1.

TABLE A.1.1 Classification and Definition of Surface Conditions

Surface condition	Definition
Hoarfrost	The surface is covered with frost, which is due to sublimation of water vapor in the ambient air on a cold surface. The pavement surface temperature must be below freezing.
Dry	The surface is free of liquid and ice. The pavement surface temperature may be above or below freezing.

Wet	The surface temperature is above freezing and has some liquid water retained on it, but no ice. The liquid water can come from rainfall, condensed vapor, or the melted snow.
Dry snow	The surface is covered with dry snow without liquid. The snow can be regarded as a porous matrix of ice. The pavement surface temperature is below freezing so that snow is not currently being melted.
Slush only	The surface contains ice crystals that are fully saturated with water. Water penetrates the porous matrix of ice from bottom to the upper surface. The pavement surface temperature is at freezing point.
Snow and slush	The surface contains snow that is partly melted. The lower part of the snow is saturated with water and the upper is as dry snow. The pavement surface temperature is at freezing point.
Solid ice	The ice on the surface is in solid form rather than porous like snow. The pavement surface temperature must be below freezing.

These surface conditions are identified by taking a rules-based approach and the heat and mass balance on the surface is formed with appropriate terms. To identify a surface condition, it needs to consider previous surface temperature, present mass of ice, heating flux, and weather boundary conditions. Weather boundary conditions used in the model have been restricted to those found in standard weather records (data files), which include: rate and type of precipitation (rain, snow or hail); ambient wet and dry bulb temperature; wind speed and solar fluxes. The procedure for identifying surface conditions and calculating corresponding heat and mass balance is shown in Figure A.1.2.

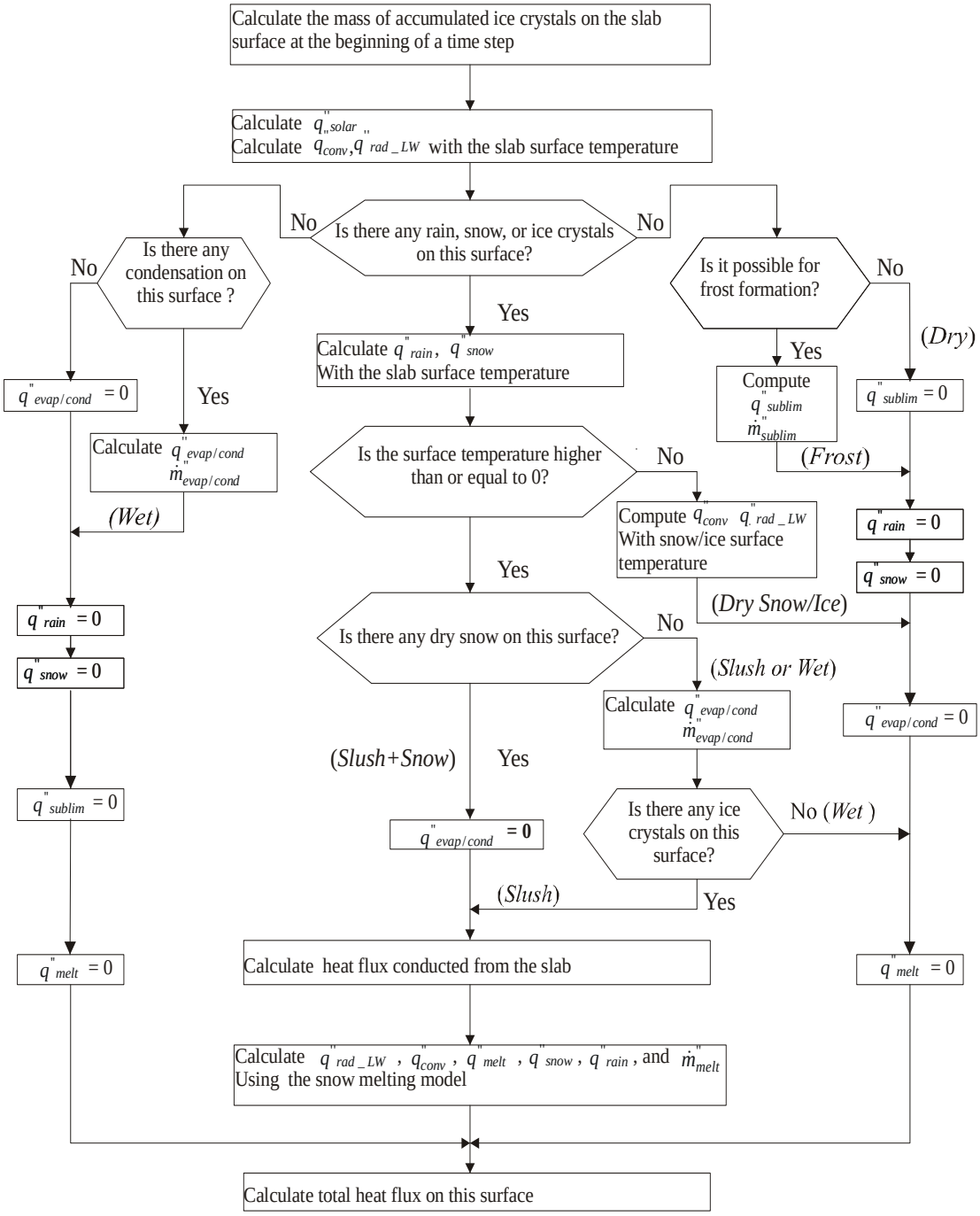

Figure A.1.2 Procedure for identifying various surface conditions and calculating corresponding heat and mass balance.

3. Heat Flux Calculation Algorithm

To provide the finite-difference equations with the appropriate heat flux term at the boundaries, several heat fluxes are considered in the model. They are:

- Solar radiation heat flux
- Convection heat flux at the pavement surfaces
- Thermal radiation heat flux
- Heat flux due to evaporation of rain and melted snow
- Heat flux due to melting of snow
- Convection heat transfer due to internal pipe flow

(1). Solar Radiation Heat Flux

Solar radiation heat gain is the amount of solar radiation absorbed by the pavement of the bridge. The solar radiation mentioned here is the sum of the beam and diffuse solar radiation incident upon the (horizontal) bridge top surface:

$$q''_{solar} = \alpha_{solar} I \tag{A.1.4}$$

The surface solar absorptance (α) is the balance of the surface albedo, which will vary under different surface conditions. Research conducted by Levinson and Akbari (2001) at LBNL showed that the mature solar absorptance of concrete mixes could range from 0.23 to 0.59 (mean 0.41). Wetting strongly increases the solar absorptance of concretes (mean increase 0.23). The solar absorptance of snow is generally a minimum after a fresh snowfall and increases with time due to growth in grain sizes, melt water near the snow surface and the accumulation of dust and debris on the snow surface. Values for solar absorptance can range from less than 0.2 for freshly fallen snow to as much as 0.6 for melting, late-season, ripe snow (CECW-EH 1998). In this model, the solar absorptance at dry condition (α_{solar_dry}) is a required parameter and the variation of solar absorptance at different surface conditions is considered. For wet surface, the solar absorptance (α_{solar_wet}) will be increased by 0.23 according to Levinson and Akbari (2001); for snow surface, the solar absorptance (α_{solar_snow}) will be 0.2; for surface covered only with slush, the solar absorptance (α_{solar_slush}) is approximated by linear interpolation between the values of wet and dry snow surface according to the accumulated mass flux of ice crystals in the snow (m''_{ice}).

(2). Convection Heat Flux at the pavement Surface

This mechanism accounts for heat transfer at the pavement top and bottom surfaces (if exposed) due to free and forced convection.

$$q''_{convection} = h_c (T_{amb} - T_{surf}) \tag{A.1.5}$$

where, h_c is taken as the maximum of the free convection coefficient and the forced convection coefficient. The convection coefficient (h_c) is a function of the Nusselt Number (Nu).

For free convection heat transfer, Nu is a function of the Rayleigh Number (Ra), and it is calculated with the correlations described by Incropera and DeWitt (1996) for free convection from the upper surface of a heated plate or the lower surface of a cooled plate:

$$Nu = 0.54Ra^{\frac{1}{4}} \qquad (10^4 < \text{Ra} < 10^7 - \text{laminar flow}) \qquad \text{(A.1.6)}$$

$$Nu = 0.15Ra^{\frac{1}{3}} \qquad (10^7 > \text{Ra} > 10^{11} - \text{turbulent flow}) \qquad \text{(A.1.7)}$$

For forced convection heat transfer, Nu is a function of the Reynolds Number (Re), and it is calculated with the empirical relations described by Incropera and DeWitt (1996) as shown following:

$$Nu = 0.664\,\text{Re}^{\frac{1}{2}}\,\text{Pr}^{\frac{1}{3}} \quad \text{(laminar flow)} \qquad \text{(A.1.8)}$$

$$Nu = 0.037\,\text{Re}^{\frac{4}{5}}\,\text{Pr}^{\frac{1}{3}} \quad \text{(mixed and turbulent flow)} \qquad \text{(A.1.9)}$$

The convection coefficient (h_c) is then computed by following equation:

$$h_c = \frac{Nu \cdot K}{L} \qquad \text{(A.1.10)}$$

where, k is the thermal conductivity of air at pavement surface - air film temperature and the characteristic length (L) is set to be the smaller between the length and width of the bridge.

The larger of the free and forced convection coefficients is used as h_c in Equation (A.1.5).

The surface temperature (T_{surf}) can be the temperature at the pavement surface or the temperature at the dry snow surface, or at the freezing point if there is only a slush layer on the pavement surface. The procedure of determining the surface temperature of a dry snow layer is described in Liu (2005).

(3). Thermal Radiation Heat Flux

This heat transfer mechanism accounts for heat flux at the pavement top surface and bottom surface (if exposed) due to thermal or long-wave radiation. The thermal radiation heat flux ($q"_{thermal}$) is then computed by:

$$q"_{thermal} = \varepsilon\sigma[(T_2 + 273.15)^4 - (T_{surf} + 273.15)^4] \qquad \text{(A.1.11)}$$

where, T_2 represents either the sky temperature (for top surface) or the ground surface temperature (for bottom surface). In this model, the ground temperature is approximated by the ambient temperature. The surface temperature (T_{surf}) can be the temperature at the pavement surface or the temperature at the dry snow surface, or at the freezing point if

there is only a slush layer on the pavement surface. The procedure of determining the surface temperature of a dry snow layer is described in Liu (2005).

The sky temperature (T_{sky}) needs to be pre-calculated and provided as a time dependent variable in the boundary condition file. The model proposed by Martin and Berdahl (1984) is recommended in the calculation of T_{sky}. Martin and Berdahl (1984) developed an algorithm for calculating the thermal radiant temperature of the sky. It is based on a simple empirical and theoretical model of clouds, together with a correlation between clear sky emissivity and the surface dew point temperature. The monthly average clear sky emissivity (ε_{clear}) is obtained by the following relationship:

$$\varepsilon_{clear} = 0.711 + 0.56(\frac{t_{dp}}{100}) + 0.73(\frac{t_{dp}}{100})^2 + 0.013\cos[2\pi\frac{\theta_h}{24}] + 0.00012(P - 1000) \quad \text{(A.1.12)}$$

where,

t_{dp} is the dew point temperature, °C;

θ_h is hour of the day;

P is the station pressure in millibar.

The cloudy sky emissivity (ε_{cloud}) is obtained by the following relationship:

$$\varepsilon_{cloud} = \varepsilon_{clear} + (1 - \varepsilon_{clear})\sum_i n_i \varepsilon_{c,i} \Gamma_i \quad \text{(A.1.13)}$$

The cloud fractions n_i are those visible to an observer on the ground. Low and mid-level clouds tend to be opaque ($\varepsilon_{c,i} \approx 1.0$), while the emissivity of high-altitude cloud is recommended by the authors to be 0.4. The cloud factor Γ_i is a function of cloud base height:

$$\Gamma_i = e^{-h_i / h_0} \quad \text{(A.1.14)}$$

where,

h_i is the base height of cloud at different level, km;

h_0 is 8.2 km.

The sky temperature (T_{sky} , K) is finally determined by:

$$T_{sky} = T_{air}\,\varepsilon_{cloud}^{1/4} \quad \text{(A.1.15)}$$

A computer program has been developed to facilitate the work of calculating the required time dependent variables with the meteorological data and preparing the boundary condition file for the simulation.

(4). Heat Flux Due to Evaporation of Rain and Melted Snow

Heat flux due to evaporation is considered only if the temperature of a specified top surface node is not less than 32 °F (0 °C) and there is no snow layer covered on the surface. In other words, only when a surface node is wet or merely covered with "slush" layer (mixture of ice and water), the heat flux of evaporation will be taken into account. Accumulation of rain is not considered; rainfall is assumed to drain instantaneously from the pavement surface, forming a thin film from which evaporation occurs.

This model uses the j-factor analogy to compute the mass flux of evaporating water at each pavement top surface node ($\dot{m}''_{evap}(m,1)$):

$$\dot{m}''_{evap}(m,1) = h_d (w_{air} - w_{(m,1)}) \tag{A.1.16}$$

where, w_{air} is the humidity ratio of the ambient air, and $w_{(m,1)}$ represents the humidity ratio of saturated air at the top surface node, which is calculated with the psychrometric chart subroutine PSYCH companied with HVACSIM+ package. The mass transfer coefficient (h_d) is defined using the Chilton-Colburn analogy by following equation:

$$h_d = \frac{h_c}{c_p Le^{\frac{2}{3}}} \tag{A.1.17}$$

where, h_c is the convection coefficient defined above, c_p is the specific heat capacity of the air evaluated at the pavement node - air film temperature (T_{film}), and Le is the Lewis number described by following equation:

$$Le = \frac{\alpha_{air}}{D_{AB}} \tag{A.1.18}$$

where, α_{air} and D_{AB} are each evaluated at the pavement node - air film temperature (T_{film}). α_{air} is calculated with a internal subroutine of AIR_PROPS, and D_{AB} is computed after Mills (1995) who references Marrero and Mason (1972):

$$D_{AB} = \frac{1.87 \times 10^{-10} (T_{film} + 273.15)^{2.072}}{P_{air}} \tag{A.1.19}$$

The heat flux due to evaporation ($q''_{evap}(m,1)$) is then given by:

$$q''_{evap}(m,1) = h_{fg} \dot{m}''_{evap} \tag{A.1.20}$$

(5). Heat Flux Due to Melting of Snow

The heat required to melt snow includes two parts: one is the amount of sensible heat needed to raise the temperature of the snow to 0 °C, the other is the heat of fusion. The temperature of freshly fallen snow is assumed to be the air temperature T_{air} in this model.

The heat flux for melting snow q''_{melt} is determined with heat and mass balance on a specified top surface node. In this model, snow is treated as an equivalent ice layer. The heat available for melting the snow on a specific node can come from the conductive heat flux from its neighbor nodes and the heat stored in the cell represented by the node. The procedure for determining surface heat flux due to melting snow is given as following:

At the beginning of each time step, the mass of accumulated ice on the surface cell of (m,1) is calculated as:

$$m''_{ice\_Accumulated\_Current}(m,1) = m''_{ice\_Accumulated\_Previous}(m,1) + (\dot{m}''_{snow} + \dot{m}''_{FreezingRain}) \cdot \Delta t \quad \text{(A.1.21)}$$

where,

$m''_{ice\_Accumulated\_Previous}(m,1)$: mass of ice accumulated in the previous time steps, [kg/m^2]

$(\dot{m}''_{snow} + \dot{m}''_{FreezingRain})$: sum of the freezing rainfall and snowfall rate in current simulation time step, [kg/(s-m^2)]

Determine the maximum snow-melting rate $\dot{m}''_{melt\_max}(m,1)$ on the surface cell of (m,1) in this time step, which can be determined by the accumulated snow at current time step $m''_{ice\_Accumulated\_Current}(m,1)$ and the time step size Δt:

$$\dot{m}''_{melt\_max}(m,1) = \frac{m''_{ice\_Accumulated\_Current}(m,1)}{\Delta t} \quad \text{(A.1.22)}$$

Determine the maximum required heat flux for melting snow q''_{melt_max} with following Equation:

$$q''_{melt\_max} = \dot{m}''_{melt\_max}(m,1) \cdot (h_{if} + c_{p\_snow}(0 - T_{air})) \quad \text{(A.1.23)}$$

where,

h_{if} : Latent heat of fusion of water, [J/kg]

c_{p_snow} : specific heat of snow, [J/(kg-°C)]

Determine the first part of snow melting heat flux q''_{melt}_1, which is transferred from its neighbors by conduction, with following equation:

$$q''_{melt\_1} = \min((q''_{solar} + q''_{thermal} + q''_{conv} + q''_{evap} + q''_{cond,surface}), q''_{melt\_max}) \quad \text{(A.1.24)}$$

where,

q''_{solar} : solar radiation heat flux, [W/m^2]

$q''_{thermal}$: thermal radiation heat flux from top surface, [W/m^2]

q''_{conv} : convective heat flux from top surface, [W/m^2]

q''_{evap} : heat flux due to evaporation, [W/m^2]

$q''_{cond,surface}$: conductive heat flux at the pavement top surface, [W/m^2]

Determine heat required to melt all the left snow ($q''_{melt\_2\_max}$) with following equation:

$$q''_{melt\_2\_max} = q''_{melt\_max} - q''_{melt\_1} \quad \text{(A.1.25)}$$

Determine the maximum heat from cell itself available for melting snow (q''_{cell_max}) with following Equation.

$$q''_{cell\_max} = \frac{\pi(\rho c_p)_{\_pv} D_{pipe}[t_{(m,1)} - 0]}{16 \cdot \Delta t} \quad \text{(A.1.26)}$$

where,

$(\rho c_p)_{\_pv}$: volumetric heat capacity of bridge pavement material, [kJ/m^{3}C]

D_{pipe} : pipe diameter, [m]

Δt : size of time step, [s]

$t_{(m,1)}$: average temperature of the surface cell (m,1) at last numerical time step, [C]

Determine the second part of snow melting heat flux (q''_{melt_2}), which is obtained from the cell itself, with following Equation:

$$q''_{melt\_2} = \min(q''_{cell\_max}, q''_{melt\_2\_max}) \quad \text{(A.1.27)}$$

Determine the total snow melting heat flux (q''_{melt}) with following equation:

$$q''_{melt} = -(q''_{melt\_1} + q''_{melt\_2}) \quad \text{(A.1.28)}$$

Determine mass flux of the melted snow on the node ($\dot{m}''_{melt}(m,1)$) with following equation:

$$\dot{m}''_{melt}(m,1) = -q''_{melt} / (h_{if} + c_{p\_snow}(0 - T_{air})) \quad \text{(A.1.29)}$$

The latent heat for melting snow (q''_{melt_lat}) is then calculated with following Equation:

$$q''_{melt\_lat} = -\dot{m}''_{melt}(m,1)h_{if} \quad \text{(A.1.30)}$$

The sensible heat for melting snow (q''_{melt_sen}) is then calculated with following Equation:

$$q''_{melt\_sen} = \dot{m}''_{melt}(m,1)c_{p\_snow}(T_{air} - 0) \quad \text{(A.1.31)}$$

At the end of each time step, $m''_{ice\_Accumulated\_Previous}(m,1)$ is updated by:

$$m''_{ice\_Accumulated\_Previous}(m,1) = m''_{ice\_Accumulated\_Current}(m,1) - \dot{m}''_{melt}(m,1)\cdot\Delta t \quad \text{(A.1.32)}$$

In Equation (A.1.24), q''_{evap} is taken into account only when the pavement surface is wet or merely covered with a "slush" layer. If the pavement surface is covered with a layer of dry snow, $q''_{thermal}$ and q''_{conv} should be evaluated with the surface temperature of the dry snow layer. However, if there is only "slush" layer (a thin saturated water-ice mixture) on the pavement surface, $q''_{thermal}$ and q''_{conv} will be evaluated with the freezing point temperature.

Distinguishing whether a surface is covered with 'slush only' or 'slush and snow' is important in this approach and it is necessary to define a set of criteria that can be applied as a rule in the model algorithm. Experimental investigations have shown that, due to capillary forces, water will rise to an equilibrium height in about 10 seconds if there is enough water at the bottom of the snow cover. It was also reported that the capillary rise level was dependent on the snow characteristics (e.g. porosity and grain size). The height of capillary rise of water in freshly fallen snow (density is 7.3 lb_m/ft^3 or 117 kg/m3) was reported by Jordan, et al. (1999) to be approximately 1" (2.5 cm). Given the two layer conceptual model used in this work, the total height of the snow/ice matrix can be estimated from the layer's mass. The existence of a 'slush only' condition can then be tested by comparing the predicted mass of the snow/ice with a mass equivalent to a 1" (2.5 cm) layer of slush. Detailed description of modeling the surface conditions of 'slush only' and 'slush and snow' is presented in Liu (2005).

(6). Convection Heat Transfer Due to Internal Pipe Flow

Either water or aqueous solution of Propylene Glycol and Ethylene Glycol can be modeled as the heat carrier fluid. The thermal properties of the specified heat carrier fluid are computed at each time step with the subroutine of UTILSECC, which was developed with the data from ASHRAE Handbook of Fundamentals (SI) 1997. Since the outlet temperature at any current time step is unknown, it is determined in an iterative manner.

The heat flux transferred from the heat carrier fluid through the pipe wall (q''_{fluid}) is computed as:

$$q''_{fluid} = U(T_{fl\_avg} - T_{(x,y)}) \quad \text{(A.1.33)}$$

where, U is the overall heat transfer coefficient between the heat carrier fluid and pipe wall, which is expressed as:

$$U = \frac{1}{\frac{1}{h_{fluid}} + \frac{l}{k_{pipe}}} \tag{A.1.34}$$

The convection coefficient (h_{fluid}) is determined from correlations for the Nusselt Number. For laminar flow in the pipe (Re<2300), the Nusselt Number is constantly equal to 4.36. For transition and turbulent flow, the Gnielinski correlation described by Hellstrom (1991) is used to compute the Nusselt Number as shown in the following equation:

$$Nu_{TranTurb} = \frac{(f/2)(\mathrm{Re}-1000)\,\mathrm{Pr}}{1+1.27(f/2)^{\frac{1}{2}}(\mathrm{Pr}^{\frac{2}{3}}-1)} \tag{A.1.35}$$

where, the friction factor f is given by:

$$f = \left[1.58\ln(\mathrm{Re}) - 3.28\right]^{-2} \tag{A.1.36}$$

The gap between 4.36 (the Nu number for laminar flow) and the value calculated from the Gnielinski correlation for transition flow could result in discontinuities in the value of convection coefficient. It will introduce numerical problem in finding a converged solution for the outlet temperature. In order to avoid this problem, the gap of the Nu number is "smoothed" by following equation:

$$Nu = \sqrt{4.36^2 + Nu_{TranTurb}{}^2} \tag{A.1.37}$$

Finally, the convection coefficient (h_{fluid}) is given by following equation:

$$h_{fluid} = \frac{Nu \cdot k_{fl}}{L} \tag{A.1.38}$$

where, the characteristic length (L) is defined as the inner diameter of the pipe.

References

CECW-EH, 1998. Engineering and design: runoff from snowmelt, Department of the Army, U.S. Army Corps of Engineers, Washington, DC.

Chiasson, A.D., J.D. Spitler, S.J. Rees, M.D. Smith. 2000. A Model for Simulating the Performance of a Pavement Heating System as a Supplemental Heat Rejecter with Closed-loop Ground-Source Heat Pump Systems. ASME Journal of Solar Energy Engineering, 122:183-191.

Jordan, R.E., J.P. Hardy, F.E. Perron, and D.J. Fisk, 1999. Air permeability and capillary rise as measures of the pore structure in snow: an experimental and theoretical study, Hydrological Processes, 13:1733-1753.

Incropera, F.P. and D.P. Dewitt. 1996. Introduction to Heat Transfer, P. 332-334. New York: Wiley & Sons.

Levinson, R. and H. Akbari, 2001. Eeffects of composition and exposure on the solar reflectance of portland cement concrete, LBNL-48334, Heat Island Group, Environmental Energy Technologies Division, Lawrence Berkeley National Laboratory, University of California, Berkeley, CA.

Liu, X. 2005. Development and Experimental Validation of Simulation of Hydronic Snow Melting Systems for Bridges. Ph.D. Thesis. Oklahoma State University. Stillwater, OK.

Martin, M., P. Berdahl, 1984. Characteristics of infrared sky radiation in the United States, Solar Energy 33(3/4): 321-336.

Rees, S.J., J.D. Spitler and X. Xiao. 2002. Transient Analysis of Snow-melting System Performance. ASHRAE Transactions, 108(2): 406-423.

Component Configuration

Inputs

XIN(1)	Ambient air temperature	(°C)
XIN(2)	Humidity ratio of air	(kg water /kg dry air)
XIN(3)	Sky temperature	(°C)
XIN(4)	Wind speed	(m/s)
XIN(5)	Wind direction	(degrees from north 0-90)
XIN(6)	Solar radiation	(W/m^2)
XIN(7)	Solar angle of incidence	(radians)
XIN(8)	Snowfall rate in water equivalent per hour	(mm/hr)
XIN(9)	Rainfall rate in water equivalent per hour	(mm/hr)
XIN(10)	Inlet fluid temperature	(°C)
XIN(11)	Total mass flow rate of heat carrier fluid	(kg/s)

Outputs

OUT(1)	Average top surface temperature	(°C)
OUT(2)	Outlet fluid temperature	(°C)
OUT(3)	Heat provided to bridge	(kW)
OUT(4)	Snow free area ratio	(--)

Parameters

PAR(1)	Bridge length	(m)
PAR(2)	Bridge width	(m)
PAR(3)	Bridge length azimuth in terms of 0 –90 degree from north	(degrees)
PAR(4)	Bridge pavement thickness	(m)
PAR(5)	Distance between adjacent pipes	(m)
PAR(6)	outer diameter of pipe	(m)
PAR(7)	Pipe depth below surface	(m)
PAR(8)	Depth to interface of material 1 ,2	(m)
PAR(9)	Thermal conductivity of layer 1 of pavement material	(W/(m-°C))
PAR(10)	Thermal conductivity of layer 2 of pavement material	(W/(m-°C))
PAR(11)	emissivity coefficient	(--)
PAR(12)	Solar absorptance of pavement	(--)
PAR(13	Volumetric heat capacity of layer 1 pavement material	($J/(m^3$-°C))
PAR(14)	Volumetric heat capacity of layer 2 pavement material	($J/(m^3$-°C))
PAR(15)	Thermal conductivity of pipe material	(W/(m-°C))
PAR(16)	Wall thickness of the pipe	(m)
PAR(17)	Type of heat carrier fluid: (0 For Water; 1 For Propylene Glycol; 2 For Ethylene Glycol; 3 For Methyl Alcohol; 4 For Ethyl Alcohol)	(--)
PAR(18)	Antifreeze concentration	(%)
PAR(19)	Number of flow circuit	(--)
PAR(20)	Pipe length per circuit	(m)
PAR(21)	Flag for bottom condition (0=Adiabatic; 1=Convection type)	(--)

A.2. TYPE 713: WATER-TO-WATER HEAT PUMP (SINGLE)

General Description

This model simulates the performance of a single water-to-water heat pump with scroll compressor and water/glycol solutions. Inputs to the model are condenser and evaporator entering fluid temperature and fluid mass flow rates. Outputs provided by the model include power consumption, condenser and evaporator exiting fluid temperature.

This parameter-estimation-based model uses a thermodynamic analysis of the refrigeration cycle, simplified models for heat exchangers and the compressor. The various parameters of the model are estimated from the manufacturers' catalog data by applying a multi-variable optimization algorithm. A procedure for adjusting the model parameters to account for the change in working fluid has beem implemented in this model. A detailed description of this model and experimental validation can be found in Jin (2002, 2003).

References

Jin, H. 2002. Parameter Estimation Based Models of Water Source Heat Pumps. Ph. D. Thesis: Oklahoma State University. Stillwater, Oklahoma.
(Also available at
http://www.hvac.okstate.edu/pdfs/Hui_Jin_Thesis.pdf)
Jin, H. and J.D. Spitler. 2003. Parameter Estimation Based Model of Water-to-Water Heat Pumps with Scroll Compressors and Water/Glycol Solutions. Building Services Engineering Research and Technology, 24(3): 203-219.

Component Configuration

Inputs

XIN(1)	Load side entering fluid temperature	(°C)
XIN(2)	Source side entering fluid temperature	(°C)
XIN(3)	Load side mass flow rate	(kg/s)
XIN(4)	Source side mass flow rate	(kg/s)
XIN(5)	Heat pump control signal (0: OFF; 1: ON)	(--)

Outputs

OUT(1)	Load side leaving fluid temperature	(°C)
OUT(2)	Source side leaving fluid temperature	(°C)
OUT(3)	Heat pump power consumption	(kW)
OUT(4)	Load side heat transfer rate	(kW)
OUT(5)	Source side heat transfer rate	(kW)

Parameters

PAR(1)	Intake volumetric flow rate	(m3/s)
PAR(2)	Built-in Compression Ratio	(--)
PAR(3)	Constant for calculating load side heat transfer coefficient	(--)
PAR(4)	Constant for calculating load side heat transfer coefficient	(--)
PAR(5)	Constant for calculating source side heat transfer coefficient	(--)
PAR(6)	Constant for calculating source side heat transfer coefficient	(--)
PAR(7)	Electromechanical loss factor for compressor	(--)
PAR(8)	Constant part of electromechanical loss	(kW)
PAR(9)	Superheat	(°C)
PAR(10)	Minimum source side entering fluid temperature	(°C)
PAR(11)	Maximum load side entering fluid temperature	(°C)
PAR(12)	Initial guess of load side heat transfer rate	(kW)
PAR(13)	Initial guess of load side heat transfer rate	(kW)
PAR(14)	Load side fluid type (0 For Water; 1 For Propylene Glycol; 2 For Ethylene Glycol; 3 For Methyl Alcohol; 4 For Ethyl Alcohol)	(--)
PAR(15)	Weight concentration of anti-freeze in load side	(%)
PAR(16)	Source side fluid type (0 For Water; 1 For Propylene Glycol; 2 For Ethylene Glycol; 3 For Methyl Alcohol; 4 For Ethyl Alcohol)	(--)
PAR(17)	Weight concentration of anti-freeze in source side	(%)

A.3. TYPE 711: GANG OF WATER-TO-WATER HEAT PUMPS

General Description

This model simulates the performance of "N" pairs of serially connected water-to-water heat pumps. The two heat pumps in a pair have their source side in parallel and load side in series. The model inputs are entering fluid temperatures and mass flow rates to the gang of heat pumps on the load and source side, and a control signal dictating the number of heat pump pairs in operation at any given time during the simulation.

A positive integer N denotes the maximum number of heat pump pairs in the gang. Depending upon the control signal input to the heat pump, the model computes the exit fluid temperatures of the gang on the load and source sides accounting for the mixing of fluid streams from the heat pump in operation and those that are not in use. The other outputs of the model are cumulative heat pump power consumption, and the entering fluid temperature to the second heat pump in the pair. The second heat pump in the pair will be shut off when the entering fluid temperature to the second heat pump, which is the exiting fluid temperature from the first heat pump, exceeds the permitted operation limit.

To simplify the simulation of smart bridge system, modifications has been implemented in the model to bypass the heat pump when the system is operated in recharge mode, in which fluid is circulated directly from the bridge to the ground heat exchangers and back to the bridge.

To approximately represent the transient behavior of the system, two first order low pass filters (first order ordinary differential equations) are applied to the outputs of the steady state heat pump model.

Nomenclature

C	= Clearance factor	(--)
Cp	= specific heat of fluid	(kJ/(kg-°C))
$Flow_1$	= mass flow rate through heat pump pairs in use on load side	(kg/s)
$Flow_2$	= mass flow rate through heat pump pairs not in use on load side	(kg/s)
$Flow_3$	= mass flow rate through heat pumps in use on source side	(kg/s)
$Flow_4$	= mass flow rate through heat pumps not in use on source side	(kg/s)
h	= enthalpy	(kJ/kg)
$\dot{m}_l$	= load side mass flow rate	(kg/s)
$\dot{m}_r$	= refrigerant mass flow rate	(kg/s)
$\dot{m}_s$	= source side mass flow rate	(kg/s)
$\dot{m}total_l$	= total load side mass flow rate to the gang of heat pumps	(kg/s)
$\dot{m}total_s$	= total source side mass flow rate to the gang of heat pumps	(kg/s)
N	= number of heat pump pairs in use	(--)
N_{max}	= maximum number of heat pump pairs in the gang	(--)
$P_{suction}$	= suction pressure	(kPa)

$P_{discharge}$	= discharge pressure	(kPa)
Q_l	= load side heat transfer rate	(kW)
Q_s	= source side heat transfer rate	(kW)
T_{SH}	= superheat	(°C)
T_c	= condensing temperature	(°C)
T_{con}_L	= time constant in load side	(s)
T_{con}_S	= time constant in source side	(s)
T_{min}	= minimum source side entering fluid temperatures	(°C)
T_{max}	= maximum load side entering fluid temperatures	(°C)
TL_{i_2nd}	= load side entering fluid temperature to 2nd heat pump in a pair	(°C)
TL_i	= load side entering fluid temperature	(°C)
TL_o	= load side exiting fluid temperature of gang of heat pump pairs	(°C)
TL_{o_pair}	= load side exiting fluid temperature of one heat pump pair	(°C)
TS_i	= source side entering fluid temperature	(°C)
TS_o	= source side exiting fluid temperature of gang of heat pump pairs	(°C)
TS_{o_pair}	= source side exiting fluid temperature of heat pump pair	(°C)
V_{cd}	= specific volume of saturated vapor at condensing pressure	(m^3/kg)
V_{ev}	= specific volume of saturated vapor at evaporating pressure	(m^3/kg)
V_{sh}	= specific volume of superheated vapor from evaporator	(m^3/kg)
W	= total power consumption of the gang of heat pump	(kW)
W_{loss}	= constant part of the electromechanical losses	(kW)
$W_{\_pair}$	= power consumption of a single heat pump pairs	(kW)
ε_l	= thermal effectiveness of the heat exchanger on load side	(-)
ε_s	= thermal effectiveness of the heat exchanger on source side	(-)
η	= electromechanical loss factor proportional to power consumption	(-)
ΔP	= pressure drop across suction and discharge valves	(kPa)

Mathematical Description

1. **Steady State Heat Pump Model**
   (for water-to-water heat pump with reciprocating compressor and operated in heating mode)

The model computes the heat transfer in the condenser and evaporator, power consumption, exit fluid temperatures on the condenser and evaporator using the mass flow rates and entering fluid temperatures on the load and source sides and the user supplied parameters as described below.

The model described below is for heating mode operation. Hence, the evaporator acts as the source side and the condenser acts as the load side. The load and source sides of the heat pump are reversed during the cooling cycle. Therefore, parameters obtained for cooling mode should be used to simulate the performance of the heat pump in cooling mode.

The load side and source side effectiveness of the heat exchanger is determined using the Equation (A.3.1) and (A.3.2):

$$\varepsilon_s = 1 - e^{(\frac{-UA_s}{\dot{m}_s Cp})} \quad \text{(A.3.1)}$$

$$\varepsilon_l = 1 - e^{(\frac{-UA_l}{\dot{m}_l Cp})} \quad \text{(A.3.2)}$$

where, UA_s and UA_l represent the overall heat transfer coefficient of the source and load sides respectively and $\dot{m}_l$ and $\dot{m}_s$ are the mass flow rate of the fluid on the load and source sides and Cp is specific heat capacity of the fluid.

The evaporating and condensing temperatures of the heat pump are computed using the effectiveness calculated using equations (A.3.1) and (A.3.2). The evaporating temperature T_e and condensing temperature T_c are computed using equation (A.3.3) and (A.3.4):

$$T_e = TS_i - \frac{Q_s}{\varepsilon_s \dot{m}_s Cp} \quad \text{(A.3.3)}$$

$$T_c = TL_i + \frac{Q_l}{\varepsilon_l \dot{m}_l Cp} \quad \text{(A.3.4)}$$

TS_i and TL_i represent the source side and load side entering fluid temperatures. And, Q_s and Q_l are source side and load side heat transfer rates. Guess values of Q_s and Q_l are used during the first iteration. The heat transfer rates are updated after every iteration until the convergence criteria are met. The suction pressure $P_{suction}$ and discharge pressure $P_{discharge}$ of the compressor is computed from the evaporator and condenser temperatures as shown in equations (A.3.5) and (A.3.6):

$$P_{suction} = P_e - \Delta P \quad \text{(A.3.5)}$$

$$P_{discharge} = P_c + \Delta P \quad \text{(A.3.6)}$$

where, ΔP represents the pressure drops across the suction and discharge valves of the compressor respectively. The pressure drop is again a predetermined parameter for specific model of heat pump.

The refrigerant mass flow rate is found using the relation given by (A.3.7):

$$\dot{m}_r = \frac{PD}{Vsuc}\left[1 + C + C\left(\frac{P_{discharge}}{P_{suction}}\right)^{1/\gamma}\right] \quad \text{(A.3.7)}$$

where γ is the isentropic exponent and V_{suc} is the specific volume of at suction pressure.

The power consumption of the compressor for an isentropic process is computed. The actual power consumption is the sum of electromechanical losses W_{loss} and the isentropic work times the loss factor η. The condenser side heat transfer rate Q_l is then the sum of power consumption W and the heat transfer rate in the evaporator Q_s.

For a given set of inputs, the computation is repeated with the updated heat transfer rates until the heat transfer rate of the evaporator and condenser converge within a specified tolerance.

2. Calculation of exiting fluid temperature in load and source side

Flow through each heat pump on the load side is given by (A.3.8)

$$\dot{m}_l = \frac{\dot{m}total_l}{N_{\max}} \tag{A.3.8}$$

Where N_{max} is the maximum number of heat pump pairs that constitute the gang. Flow through each heat pump on the source side is given by (A.3.9) (since the source sides are arranged in parallel, the total flow is divided equally between the two):

$$\dot{m}_l = \frac{\dot{m}total_l}{2N_{\max}} \tag{A.3.9}$$

If none of the heat pump pair are operational or if the entering fluid temperatures do not lie within the limits supplied by the manufactory specification, the heat pump power consumption is set to zero and the exit fluid temperatures set at the same value as the inlet temperatures. Otherwise, heat pump power consumption and exit fluid temperatures on the load and source sides are computed using $\dot{m}_l$ and $\dot{m}_s$. If the exit fluid temperatures on the load side from the first heat pump exceed T_{max}, then the second heat pump is bypassed. Else, the computation is repeated to find the exit fluid temperatures from the second heat pump and its power consumption. The source side entering fluid temperature to the second heat pump is the same as that of first one in the pair since their source sides are in parallel.

The power consumed by the gang of heat pumps is the cumulative power consumption of the heat pumps in use as given by (A.3.10):

$$W = N \times W_{\_\,\text{pair}} \tag{A.3.10}$$

Flow through the operational heat pump pairs is computed as follows:

$$\text{Flow}_1 = \dot{m}_l \times \text{N} \tag{A.3.11}$$

$$\text{Flow}_2 = \dot{m}total_l - \text{Flow}_1 \tag{A.3.12}$$

The load side exit fluid temperature computed after mixing streams is then given by equation (A.3.13):

$$TL_o = (Flow_1 \times TL_{o\_pair} + Flow_2 \times TL_i) / \dot{m}total_l \quad \text{(A.3.13)}$$

The source side exit fluid temperature for the gang of heat pumps is computed in a similar manner using equations (A.3.14), (A.3.15), and (A.3.16):

$$Flow_3 = \dot{m}_l \times 2N \quad \text{(A.3.14)}$$

$$Flow_4 = \dot{m}total_l - Flow_3 \quad \text{(A.3.15)}$$

$$TS_o = (Flow_3 \times TS_{o\_pair} + Flow_4 \times TS_i) / \dot{m}total_s \quad \text{(A.3.16)}$$

3. Bypass heat pumps in recharge mode

If system is operated in recharge mode, the heat pump will be bypassed by fixing the source side outlet temperature TS_o equal to the load side inlet temperature TL_i; and load side outlet temperature TL_o equal to the source side inlet temperature TS_i internally in the model. Operation of the heat pump during heating and recharge mode can be easily understood by looking at the schematic diagram of the heat pump during the two modes of operation given below.

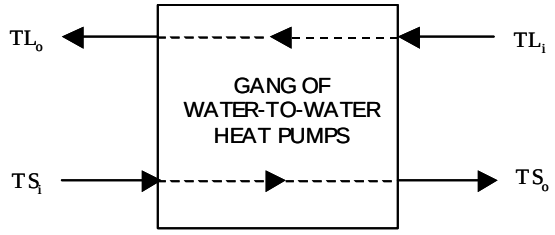

Figure A.3.1 Heating mode

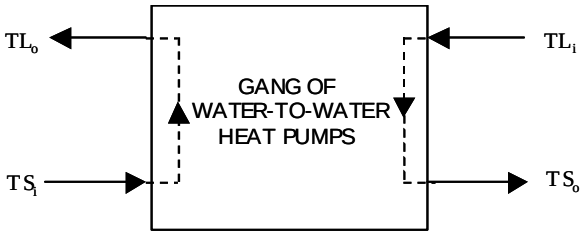

Figure A.3.2 Recharge mode

4. Approximate the dynamic behavior of heat pump

Two first order ordinary differential equations, which needed to be solved externally by the non-linear differential equation solver of HVACSIM+, were added into the original steady state heat pump model to account for the dynamics due to thermal capacitance of the system when the number of operating heat pump is shifted up or down.

Equation (A.3.17) is the expression of differential equations added in the heat pump model.

$$\frac{dT_{Out\_D}}{dt} = \frac{T_{Out\_S} - T_{Out\_D}}{\tau} \qquad \text{(A.3.17)}$$

where,

T_{Out_D} = approximated dynamic fluid temperature at the outlet of load or source side of heat pump;

T_{Out_S} = steady state fluid temperature at the outlet of load or source side of heat pump, which is calculated with the original steady state heat pump model;

t = time;

τ = time constant, which is the ratio of the effective thermal mass of the system (MC_p) to the thermal mass of the heat carrier fluid in the heat pump ($\dot{m}C_p$). The value of the time constant needs to be calibrated with the experimental data or with more detailed models.

The effect of the ODE filter can be considered as a result of a well-insulated "tank", which has the effective thermal mass of the piping system. The fluid in this "tank" is assumed to well mixed so that the fluid temperature is identical in the "tank".

References

Jin, H. 2002. Parameter Estimation Based Models of Water Source Heat Pumps. Ph. D. Thesis: Oklahoma State University. Stillwater, Oklahoma.

(Also available at http://www.hvac.okstate.edu/pdfs/Hui_Jin_Thesis.pdf)

Ramamoorthy, M.H. 2001. Application of Hybrid Ground Source Heat Pump Systems To Buildings and Bridge Decks. M.S. Thesis. Oklahoma State University. Stillwater, OK.

(Also available at http://www.mae.okstate.edu/Faculty/spitler/ Ramamoorthy_thesis.pdf)

Component Configuration

Inputs

XIN(1)	Load side entering fluid temperature	(°C)
XIN(2)	Source side entering fluid temperature	(°C)
XIN(3)	Load side mass flow rate	(kg/s)
XIN(4)	Source side mass flow rate	(kg/s)
XIN(5)	Number of operating heat pump pairs	(--)
XIN(6)	Transient load side leaving fluid temperature	(°C)
XIN(7)	Transient source side leaving fluid temperature	(°C)

Outputs

OUT(1)	Derivative of load side leaving fluid temperature	(°C/s)
OUT(2)	Derivative of source side leaving fluid temperature	(°C/s)
OUT(3)	Load side EFT to the second heat pump in series	(°C)
OUT(4)	Heat pump power consumption	(kW)

Parameters

PAR(1)	Piston displacement	(m3/s)
PAR(2)	Clearance factor	(--)
PAR(3)	Load side heat transfer coefficient	(kW/K)
PAR(4)	Source side heat transfer coefficient	(kW/K)
PAR(5)	Electromechanical loss factor for compressor	(--)
PAR(6)	Constant part of electromechanical loss	(kW)
PAR(7)	Pressure drop across the suction valve	(kPa)
PAR(8)	Superheat	(°C)
PAR(9)	Maximum number of heat pump pairs in the system	(--)
PAR(10)	Minimum source side entering fluid temperature	(°C)
PAR(11)	Maximum load side entering fluid temperature	(°C)
PAR(12)	Initial guess of load side heat transfer rate	(kW)
PAR(13)	Initial guess of load side heat transfer rate	(kW)
PAR(14)	Load side time constant	(s)
PAR(15)	Source side time constant	(s)
PAR(16)	Load side fluid type (0 For Water; 1 For Propylene Glycol; 2 For Ethylene Glycol; 3 For Methyl Alcohol; 4 For Ethyl Alcohol)	(--)
PAR(17)	Weight concentration of anti-freeze in load side	(%)
PAR(18)	Source side fluid type (0 For Water; 1 For Propylene Glycol; 2 For Ethylene Glycol; 3 For Methyl Alcohol; 4 For Ethyl Alcohol)	(--)
PAR(19)	Weight concentration of anti-freeze in source side	(%)

A.4. TYPE 721: GROUND LOOP HEAT EXCHANGER (1)

General Description

The ground loop heat exchanger (GLHE) model is an updated version of that described by Yavuzturk and Spitler (1999), which is an extension of the long-time step temperature response factor model of Eskilson (1987). It is based on dimensionless, time-dependent temperature response factors known as "g-functions", which are unique for various borehole field geometries. This updated model includes a hierarchical load aggregation algorithm that significantly improves the computational efficiency of the model.

Inputs to the model are the mass flow rate and entering fluid temperature. The outputs from the model include exiting fluid temperature, average fluid temperature, and heat transfer rate to the ground, which is normalized to borehole depth.

Since the borehole thermal resistance is calculated using a subroutine BORERES in this model, it can be used for situations when the mass flow rate is not constant through out the simulation period.

Nomenclature

C_{ground}	= volumetric heat capacity of ground	(J/(m^{3}K))
C_{fluid}	= specific heat capacity of fluid	(J/(kgK))
d_i	= inner diameter of the U-tube pipe	(m)
$g(\ )$	= g-function	(--)
H	= borehole length over which heat extraction takes place	(m)
$h_{c,i}$	= convection coefficient	(W/m^2 °K)
k_{pipe}	= pipe thermal conductivity	(W/m °K)
k_{grout}	= grout thermal conductivity	(W/m °K)
k_{fluid}	= fluid thermal conductivity	(W/m °K)
K	= thermal conductivity of the ground	(W/m °K)
$\dot{m}$	= mass flow rate of fluid	(kg/s)
$N_{borehole}$	= number of boreholes	(--)
$Pipe_t$	= wall thickness of the U-tube	(m)
Pr	= Prandtl number	(--)
QN_n	= normalized heat extraction rate for nth hour	(W/m)
r_o	= outer radius of the U-tube pipe	(m)
r_i	= inner radius of the U-tube pipe	(m)
Re	= Reynolds number	(--)
R_b	= borehole thermal resistance	(^{o}K per W/m)
$R_{borehole}$	= borehole radius	(m)
R_{cond}	= conductive resistance	(^{o}K per W/m)
R_{conv}	= convective resistance	(^{o}K per W/m)
R_{grout}	= resistance of the grout	(^{o}K per W/m)

t	= current simulation time	(s)
T_{fluid_avg}	= average fluid temperature	(^{o}C)
T_{fluid_in}	= inlet fluid temperature	(^{o}C)
T_{om}	= undisturbed ground temperature	(^{o}C)
T_{fluid_out}	= outlet fluid temperature	(^{o}C)
t_s	= steady-state time	(s)
X_{tube}	= distance between t legs of the U-tube	(m)
β_1, β_0	= shape factors	(--)

Mathematical Description

1. Basic equations

The g-function value for each time step is pre-computed and stored in an array for later use. The initial ground load, which has been normalized to the active borehole length, is given by (A.4.1):

$$QN_n = \frac{\dot{m} \cdot C_{fluid} \cdot (t_{fluid\_out} - t_{fluid\_in})}{H \cdot N_{borehole}} \tag{A.4.1}$$

The outlet fluid temperature is computed from average fluid temperature using equation (A.4.2):

$$t_{fluid\_out} = t_{fluid\_avg} + \frac{QN_n \cdot H \cdot N_{borehole}}{2 \cdot \dot{m} \cdot C_{fluid}} \tag{A.4.2}$$

The average fluid temperature T_{fluid_avg} is computed using the relation:

$$t_{fluid\_avg} = t_{ground} - \sum_{i=1}^{n} \frac{(QN_i - QN_{i-1})}{2 \cdot \pi \cdot k} g\left(\frac{\theta_n - \theta_{i-1}}{\theta_s}, \frac{r_b}{H}\right) - QN_n \cdot R_{borehole} \tag{A.4.3}$$

There are totally 3 unknowns: T_{fluid_out}, QN_n and T_{fluid_avg} in three un-equivalent equations, so, they can be solved simultaneously. The explicit solution of the normalized ground load at the n^{th} time step (QN_n) has been derived and given in Equation (A.4.4). The corresponding solutions of t_{fluid_avg} and t_{fluid_out} can then be obtained by substituting QN_n into Equation (A.4.3) and (A.4.2) subsequently.

$$QN_n = \frac{t_{ground} - \sum_{i=1}^{n-1} \frac{(QN_i - QN_{i-1})}{2 \cdot \pi \cdot k} g\left(\frac{\theta_n - \theta_{i-1}}{\theta_s}, \frac{r_b}{H}\right) + \frac{QN_{n-1}}{2 \cdot \pi \cdot k} g\left(\frac{\theta_n - \theta_{n-1}}{\theta_s}, \frac{r_b}{H}\right) - t_{fluid\_in}}{R_{borehole} + \frac{1}{2 \cdot \pi \cdot k} g\left(\frac{\theta_n - \theta_{n-1}}{\theta_s}, \frac{r_b}{H}\right) + \frac{H \cdot N_{borehole}}{2 \cdot \dot{m} \cdot C_{fluid}}} \tag{A.4.4}$$

2. Hierarchical load aggregation

To reduce the computation time and burden, the superposition of ground loads from the earlier time steps is aggregated into 'blocks' using a load aggregation algorithm. An algorithm of hierarchical load aggregation has been implemented in this model. Currently, there are three different aggregation blocks ("small", "medium", and "large") employed in the hierarchical load aggregation algorithm. In order to reduce the error when aggregating individual loads (or, smaller load blocks) to a bigger load block, a "waiting period" is specified for each level of load aggregation. An operation of load aggregation can only be processed after enough loads (or, smaller load blocks) have been accumulated to compose a bigger load block, and the "waiting period" for this level of load aggregation has been passed. Liu (2005) presents detailed information of the procedure and parameters used in the hierarchical load aggregation.

3. Calculation of Borehole Thermal Resistance

The procedure for computing the borehole thermal resistance is explained below. The borehole thermal resistance is calculated using equation (A.4.4):

$$R_b = R_{cond} + R_{conv} + R_{grout} \tag{A.4.5}$$

R_{cond} is the conductive resistance is computed using Equation (A.4.5):

$$R_{cond} = \frac{\log\left(\frac{r_o}{r_i}\right)}{4\pi\ k_{pipe}} \tag{A.4.6}$$

Where, r_o is the outer radius of the pipe, r_i is the pipe inner radius, and k_{pipe} is the pipe thermal conductivity. The convective resistance R_{conv} is computed as follows:

$$R_{conv} = \frac{1}{2\pi\ d_i\ h_{c,i}} \tag{A.4.7}$$

Where, d_i is the pipe inner diameter, and $h_{c,i}$ is the convection coefficient inside the pipe computed using Dittus-Boelter correlation:

$$h_{c,i} = Nu\ K_{fluid} \big/ d_i \tag{A.4.8}$$

For laminar flow in the pipe (Re<2300), the Nusselt Number is constantly equal to 4.36. For transition and turbulent flow, the Gnielinski correlation described by Hellstrom (1991) is used to compute the Nusselt Number as shown in the following equation:

$$Nu_{TranTurb} = \frac{(f/2)(\mathrm{Re}-1000)\,\mathrm{Pr}}{1+1.27(f/2)^{\frac{1}{2}}(\mathrm{Pr}^{\frac{2}{3}}-1)} \tag{A.4.9}$$

where, the friction factor f is given by:

$$f = \left[1.58\ln(\mathrm{Re}) - 3.28\right]^{-2} \tag{A.4.10}$$

The gap between 4.36 (the Nu number for laminar flow) and the value calculated from the Gnielinski correlation for transition flow could result in discontinuities in the value of convection coefficient. It will introduce numerical problem in finding a converged solution for the outlet temperature. In order to avoid this problem, the gap of the Nu number is "smoothed" by following equation:

$$Nu = \sqrt{4.36^2 + Nu_{TranTurb}{}^2} \tag{A.4.11}$$

Resistance due to the grout, R_{grout} is calculated using the following relation:

$$R_{grout} = \frac{1.}{k_{grout}\,\beta_0\left(R_{borehole}/r_o\right)^{\beta_1}} \tag{A.4.12}$$

Where, β_1 and β_0 are the resistance shape factor coefficients (Paul 1996) whose value depends on the U-tube shank spacing inside the borehole.

References

Liu, X. 2005. Development and Experimental Validation of Simulation of Hydronic Snow Melting Systems for Bridges. Ph.D. Thesis. Oklahoma State University. Stillwater, OK.

Paul, N. D. 1996. The Effect of Grout Thermal Conductivity on Vertical Geothermal Heat Exchanger Design and Performance. M.S. Thesis. South Dakota State University.

Per Eskilson, 1987. Thermal Analysis of Heat Extraction Boreholes. Ph.D. Thesis. Dept. of Mathematical Physics, University of Lund, Sweden.

Yavuzturk, C., J. D. Spitler. 1999b. A Short Time Step Response Factor Model for Vertical Ground Loop Heat Exchangers. ASHRAE Transactions, 105(2): 475-485.

Component Configuration

Inputs

XIN(1)	Inlet fluid temperature	(°C)
XIN(2)	Mass flow rate in GLHE	(kg/S)

Outputs

OUT(1)	Outlet fluid temperature	(°C)
OUT(2)	Average fluid temperature	(°C)
OUT(3)	Normalised heat extraction rate	(W/m)

Parameters

PAR(1)	Number of boreholes)	(--)
PAR(2)	Borehole length	(m)
PAR(3)	Borehole radius	(m)
PAR(4)	Thermal conductivity of the ground	(W/(mK))
PAR(5)	Volumetric heat capacity of ground	(J/(m3K))
PAR(6)	Undisturbed ground temperature	(°C)
PAR(7	Grout thermal conductivity	(W/(mK))
PAR(8)	Pipe thermal conductivity	(W/(mK))
PAR(9)	Outer diameter of the pipe	(m)
PAR(10)	Distance between the two legs of the U Tube	(m)
PAR(11)	Wall thickness of the pipe)	(m)
PAR(12)	Type of heat carrier fluid (0 For Water; 1 For Propylene Glycol; 2 For Ethylene Glycol; 3 For Methyl Alcohol; 4 For Ethyl Alcohol)	(--)
PAR(13)	WT. of anti-freeze in the heat carrier fluid	(%)

A.5. TYPE 724: GROUND LOOP HEAT EXCHANGER (2)

General Description

This model is a revised version of Type 721. The revisions include:

- Instead of calculating the borehole thermal resistance (R_b) using the subroutine of BORERES, it is pre-calculated with other program (i.e. GLHEPRO®) and read by the model as a parameter.
- All the data pairs of the g-function are read as parameters instead of being read from the input file of "GFILE.dat" as it does in Type 721.
- Since the "ratio correction"[14] for the g-function has been done in generating the g-function with GLHEPRO®, it is not necessary to correct it again when interpolating or extrapolating g-functions. Therefore, a subroutine of INTERP_NRC is used in Type 724.

Component Configuration

Inputs

XIN(1)	Inlet fluid temperature	(°C)
XIN(2)	Mass flow rate in GLHE	(kg/S)

Outputs

OUT(1)	Outlet fluid temperature	(°C)
OUT(2)	Average fluid temperature	(°C)
OUT(3)	Normalised heat extraction rate	(W/m)

Parameters

PAR(1)	Number of boreholes	(--)
PAR(2)	Borehole length	(m)
PAR(3)	Borehole radius	(m)
PAR(4)	Thermal conductivity of the ground	(W/(mK))
PAR(5)	Volumetric heat capacity of ground	(J/(m3K))
PAR(6)	Undisturbed ground temperature	(°C)
PAR(7)	Type of heat carrier fluid (0 For Water; 1 For Propylene Glycol; 2 For Ethylene Glycol; 3 For Methyl Alcohol; 4 For Ethyl Alcohol)	(--)
PAR(8)	WT. of anti-freeze in the heat carrier fluid	(%)

[14] When the ratio of the borehole radius to the active borehole length is not equal to 0.0005, a correction factor for the long-term g-function must be used.

PAR(9)	Borehole thermal resistance	(K/(W/m))
PAR(10)	Number of data pairs of the g-functions	(--)
PAR(11)-PAR(210)	Data of the g-functions	(--)

A.6. TYPE 731: SNOW MELTING SYSTEM CONTROLLER (TD)

General Description

This model is for a controller specifically designed for the hydronic bridge deck snow melting system. When system is operated in heating mode, it controls the number of operating heat pump pairs (see TYPE 711) according to the bridge deck surface temperature. A temperature differential (TD) control strategy is used in this model to control the recharge operation.

The inputs to the model are average bridge deck surface temperature, SFAR (Snow Free Area Ratio) of the bridge deck surface, average fluid temperature in the GLHE, and a control signal that is used to startup the system in heating mode operation. The outputs are control signal for the number of operating heat pump pairs and mass flow rates in both load and source sides of the system.

In order to avoid numerical problems due to the discrete characteristics of the controller outputs, this component model should be included in a superblock other than the superblock(s) that contain(s) continuous component models.

Nomenclature

Con_HP	= number of heat pump units to be used (The unit could be single heat pump or heat pump pairs depending upon the heat pump model used in the simulation)	(--)
T_{diff}	= difference between T_{surf} and T_{GLHE_avg}	(°C)
T_{GLHE_avg}	= bridge deck surface temperature	(°C)
T_{rech_upper}	= upper limit of the temperature difference	(°C)
T_{rech_lower}	= lower limit of the temperature difference	(°C)
T_{surf}	= bridge deck surface temperature	(°C)
T_{surf_upper}	= surface temperature upper limit	(°C)
T_{surf_lower}	= surface temperature lower limit	(°C)
N_{max}	= maximum number of heat pump units in the system	(--)

Mathematical Description

1. Heating mode control

When the control signal is equal to 1 or the snow free area ratio is less than 1 (a parameter could be added in the future for the user specified acceptable value of SFAR), the model will send the value of mass flow rates to the component models in both the load and source sides of the system to startup the heating operation.

If the average bridge deck surface temperature T_{surf} is greater than T_{surf_upper} when system is in heating mode, *Con_HP* is set to be 1; If T_{surf} 1ess than the lower limit temperature T_{surf_lower}, *Con_HP* equal is set to be N_{max} . For any value of T_{surf} between the two set point temperatures, *Con_HP* is calculated using the relation given below:

$$Con\_HP = \frac{N_{\max}\left(T_{surf\_upper} - T_{surf}\right)}{\left(T_{surf\_upper} - T_{surf\_lower}\right)} \quad \text{(A.6.1)}$$

The result of *Con_HP* will be rounded off to the next successive integer when it has a fractional value.

2. Recharge mode control

When T_{diff} exceeds T_{rech_upper}, the model will send the user specified recharge mass flow rates to all the component models to startup the recharge operation. When T_{diff} is lower than T_{rech_lower}, the mass flow rates are set to be 0 and sent to all the component models to stop the recharge operation. When T_{diff} is between T_{rech_upper} and T_{rech_lower}, the model will keep the previous outputs.

Component Configuration

Inputs

XIN(1)	Flag to start the system	(--)
XIN(2)	Average bridge deck surface temperature	(°C)
XIN(3)	Average fluid temperature in GLHE	(°C)
XIN(4)	Snow Free Area Ratio	(--)

Outputs

OUT(1)	Mass flow rate for components in load side	(kg/s)
OUT(2)	Mass flow rate for components in source side	(kg/s)
OUT(3)	number of operating heat pump pairs	(--)

Parameters

PAR(1)	Lower set point in heating mode	(°C)
PAR(2)	Upper set point in heating mode	(°C)
PAR(3)	Max. number of heat pump pairs in the system	(--)
PAR(4)	Upper set point in recharge mode	(°C)
PAR(5)	Lower set point in recharge mode	(°C)
PAR(6)	Load side mass flow rate in heating mode	(kg/s)
PAR(7)	Source side mass flow rate in heating mode	(kg/s)
PAR(8)	Mass flow rate in recharge mode	(kg/s)

A.7. TYPE 732: SNOW MELTING SYSTEM CONTROLLER (ON-OFF)

General Description

This model is for a controller specifically designed for the hydronic bridge deck snow melting system. When system is operated in heating mode, it turns on and off the heat pump (see TYPE 713) according to the bridge deck surface temperature. A set point (SP) control strategy is used in this model to control the recharge operation.

In order to avoid numerical problems due to the discrete characteristics of the controller outputs, this component model should be included in a superblock other than the superblock(s) that contain(s) continuous component models.

Component Configuration

Inputs

XIN(1)	Average bridge deck surface temperature	(°C)
XIN(2)	Signal to start or shut off the system	(--)

Outputs

OUT(1)	Mass flow rate for components in load side	(kg/s)
OUT(2)	Mass flow rate for components in source side	(kg/s)
OUT(3)	Number of heat pump in operation	(--)

Parameters

PAR(1)	Lower set point in heating mode	(°C)
PAR(2)	Upper set point in heating mode	(°C)
PAR(3)	Max. number of heat pump in the system	(--)
PAR(4)	Lower set point in recharge mode	(°C)
PAR(5)	Upper set point in recharge mode	(°C)
PAR(6)	Load side mass flow rate in heating mode	(kg/s)
PAR(7)	Source side mass flow rate in heating mode	(kg/s)
PAR(8)	Mass flow rate in recharge mode	(kg/s)

A.8. TYPE 740: Ideal Steady State Electrical Heater

General Description

The ideal steady state heater model is designed to provide specialized heat input condition to the hydronically-heated bridge model, by which the procedure of determining the heating capacity of the snow melting system can be simplified. The model has two modes, determined by the first parameter (MODE). If the value of MODE is 1, the model will calculate the outlet temperature of the heat carrier fluid for given mass flow rate and inlet temperature with a user specified constant power input. If the value of MODE is 2, the model will provide constant outlet temperature and calculate the required power input for given mass flow rate and inlet temperature.

The inputs to the model include mass flow rate and inlet temperature of the heat carrier fluid. The outputs from the model are outlet fluid temperature and the power input to the heater.

Nomenclature

C_{p_fl}	= heat capacity of the heat carrier fluid	(kJ/(kg-°C))
$\dot{m}_{\_fl}$	= fluid mass flow rate	(kg/s)
Q_{input_const}	= constant power input to the heater	(kW)
$Q_{input\_required}$	= required power input to the heater	(kW)
T_{in}	= inlet fluid temperature	(°C)
T_{out}	= outlet fluid temperature	(°C)
T_{out_const}	= user specified outlet fluid temperature	(°C)

Mathematical Description

In this model, it is assumed that the thermal mass of the heater and the transient process of heated transfer can be neglected, thus, the steady state outlet temperature can be achieved instantaneously.

If the value of MODE is 1, the required power input is the constant of Q_{input_const}, and the outlet fluid temperature T_{out} is calculated as following.

$$T_{out} = T_{in} + \frac{Q_{input\_const}}{C_{p\_fl}\dot{m}_{\_fl}} \tag{A.8.1}$$

If the value of MODE is 2, the outlet fluid temperature T_{out} is fixed to be the user specified value T_{out_const}, and the required power input $Q_{input\_required}$ is determined as following:

$$Q_{input\_required} = C_{p\_fl}\dot{m}_{\_fl}(T_{out\_const} - T_{in}) \quad \text{(A.8.2)}$$

Component Configuration

Inputs

XIN(1)	Input temperature	(°C)
XIN(2)	Mass flow rate of the fluid	(kg/s)

Outputs

OUT(1)	Output temperature	(°C)
OUT(2)	Heat flux supplied by the heater	(kW)

Parameters

PAR(1)	Heater operation mode	(--)
PAR(2)	Maximum outlet temperature	(°C)
PAR(3)	Maximum heat flux supplied by the heater	(kW)
PAR(4)	Type of heat carrier fluid (0 For Water; 1 For Propylene Glycol; 2 For Ethylene Glycol; 3 For Methyl Alcohol; 4 For Ethyl Alcohol)	(--)
PAR(5)	Weight concentration of antifreeze in fluid	(%)

A.9. TYPE 750: PUMP

General Description

This pump model computes the power consumption and the temperature rise of the fluid using the parameters of fluid mass flow rate, pressure rise across the pump, and the pump efficiency.

The inputs to the model include inlet fluid temperature and fluid mass flow rate. The outputs from the model are outlet fluid temperature and the pump power consumption.

Nomenclature

C_p	= heat capacity of the heat carrier fluid	(kJ/(kg-°C))
$\dot{m}_{\_fl}$	= actual fluid mass flow rate	(kg/s)
P	= pump power consumption	(kW)
T_{in}	= inlet fluid temperature	(°C)
T_{out}	= outlet fluid temperature	(°C)
ΔP	= pressure drop across the pump	(kPa)
η	= pump efficiency	(--)
ρ	= density of the fluid	(kg/m^3)

Mathematical Description

The pump power consumption P and the outlet fluid temperature T_{out} are computed using relation (A.9.1) and (A.9.2) respectively.

$$P = \frac{\Delta P \dot{m}_{\_fl}}{\rho \cdot \eta} \tag{A.9.1}$$

$$T_{out} = T_{in} + \Delta P \left(\frac{\frac{1}{\eta} - 1}{\rho \cdot C_p} \right) \tag{A.9.2}$$

Component Configuration

Inputs

XIN(1)	Inlet temperature	(°C)
XIN(2)	Mass flow rate	(kg/s)

Outputs

OUT(1)	Outlet temperature	(°C)

OUT(2)	Pump power consumption	(kW)

Parameters

PAR(1)	Nominal pump efficiency	(--)
PAR(2)	Nominal mass flow rate	(kg/s)
PAR(3)	Nominal pressure rise across the pump	(kPa)
PAR(4)	Type of heat carrier fluid (0 For Water; 1 For Propylene Glycol; 2 For Ethylene Glycol; 3 For Methyl Alcohol; 4 For Ethyl Alcohol)	(--)
PAR(5)	Weight concentration of antifreeze in fluid	(%)

VITA

Xiaobing Liu

Candidate for the Degree of

Doctor of Philosophy

Thesis: DEVELOPMENT AND EXPERIMENTAL VALIDATION OF SIMULATION OF HYDRONIC SNOW MELTING SYSTEMS FOR BRIDGES

Major Field: Mechanical and Aerospace Engineering

Biographical:

Personal Data: Born in Wuzhong, Ningxia, On June 21, 1973, the son of Changming Liu and Yulan Ye.

Education: Received the degree of Bachelor of Engineering from Tongji University at Shanghai, P. R. China in July 1995. Received the degree of Master of Science from Tongji University at Shanghai, P. R. China in April 1998. Completed the requirements for the Doctor of Philosophy degree with a major in Mechanical and Aerospace Engineering at Oklahoma State University in May 2005.

Experience: Worked for China Haisum Engineering Co., Ltd. (previously Shanghai Design Institute of Light Industry of China), Shanghai, P. R. China from 1998 to 2000 as HVAC design engineer. Employed by Oklahoma State University from 2000 to 2005 as research associate. Currently work for ClimateMaster, OK as system engineering manager.

Professional Membership: American Society of Heating, Refrigerating and Air Conditioning Engineers (ASHRAE), International Building Performance Simulation Association, Affiliate in the United States (IBPSA-USA), American Society of Mechanical Engineers (ASME).